Overview of Scenarios of Transition to Chaos in Nonideal Dynamic Systems

Aleksandr Shvets

National Technical University of Ukraine "Igor Sikorsky Kyiv Polytechnic Institue", Kyiv, Ukraine
(E-mail: alex.shvets@bigmir.net, aleksandrshvetskpi@gmail.com)

Abstract. A number of deterministic dynamic systems that are nonideal according to the Sommerfeld-Kononenko classification are considered. In particular, pendulum, hydrodynamic, and electroelastic systems with limited excitation are considered. The scenarios of transitions to chaos that are possible in the above systems are analyzed. We study both the transitions "regular attractor - chaotic attractor" and the transitions "chaotic attractor of one type - chaotic attractor of another type". In particular, the "chaos - hyperhaos" and "hyperhaos - hyperhaos" transitions are studied. Ten scenarios of transition to chaos are analyzed in detail. Some of the scenarios were widely known, while others are very unusual and are revealed only in nonideal dynamic systems.
Keywords: nonideal dynamic system, scenario of transition to chaos, chaotic attractor.

1 Introduction

A prominent place among dynamical systems is occupied by so-called nonideal systems or systems with limited excitation. For the first time such systems originated in the experiments of A. Sommerfeld in the early twentieth century [1,2]. But as a established scientific direction, the theory of systems with limited excitation was formed after the publication V. Kononenko [3] in which he introduced a clear axiomatics and constructed mathematical models for a wide range of problems. The theory of systems with limited excitation explores the interaction of vibrational systems with excitation sources of their oscillations. Within the framework of this theory, it is assumed that oscillation excitation sources have a power comparable to the power consumed by the oscillatory load. In this case, the operation of the energy source depends on the regime of oscillation load and influenceof the source cannot be expressed as a predetermined explicit time function. Whereas in the traditional mathematical modeling of the oscillatory system, idealized sources of excitation of unlimited power are considered. In many cases, the ideal approach is fundamentally wrong, which in practice leads to gross errors in describing the dynamics of both the oscillatory system and the source of excitation [4–7]. The use of limited excitation models becomes even more relevant in our time, when humanity faces the problems of global energy conservation, which requires the maximum minimization of the power of the applied excitation sources.

The discovery of deterministic chaos stimulated the emergence of a new direction in theory of systems with limited excitation associated with the search

for chaotic modes of interaction of oscillatory systems with sources of excitation. Of particular interest are those chaotic regimes whose appearance is associated with a nonlinear interaction between the oscillatory system and the excitation source, and not with their autonomous properties.

In the papers [8–11] describe the occurrence of chaotic attractors in a number of deterministic nonideal dynamical systems whose chaotization is fundamentally impossible when considering cases of ideal (unlimited) excitation.

2 Mathematical models of considered nonideal systems

In studying the occurrence of deterministic chaos in dynamical systems, it is of great interest to identify and describe scenarios of transition to chaos. Moreover, both scenarios of transitions from regular attractors to chaotic, and scenarios of transitions between chaotic attractors of different types. Some of these scenarios are widespread and implemented in many dynamic systems. Such scenarios include, for example, the Feigenbaum's scenario and the Manneville-Pomeau scenario. Other scenarios were described relatively recently and the question of their prevalence requires further study.

In this paper, we analyze the scenarios of transition to chaos identified and described in a number of nonideal dynamical systems. The implementation of transitions to chaos considered in such systems: a pendulum - an excitation source,

$$\begin{aligned}
\frac{dy_1}{d\tau} &= Cy_1 - y_2y_3 - \frac{1}{8}(y_1^2y_2 + y_2^3),\\
\frac{dy_2}{d\tau} &= Cy_2 + y_1y_3 + \frac{1}{8}(y_1^3 + y_1y_2^2) + 1,\\
\frac{dy_3}{d\tau} &= Dy_2 + Ey_3 + F,
\end{aligned} \tag{1}$$

a spherical pendulum - an excitation source,

$$\begin{aligned}
\frac{dy_1}{d\tau} &= Cy_1 - [y_3 + \frac{1}{8}(y_1^2 + y_2^2 + y_4^2 + y_5^2)]y_2 - \frac{3}{4}(y_1y_5 - y_2y_4)y_4 + 2y_2,\\
\frac{dy_2}{d\tau} &= Cy_2 + [y_3 + \frac{1}{8}(y_1^2 + y_2^2 + y_4^2 + y_5^2)]y_1 - \frac{3}{4}(y_1y_5 - y_2y_4)y_5 + 2y_1,\\
\frac{dy_3}{d\tau} &= D(y_1y_2 + y_4y_5) + Ey_3 + F,\\
\frac{dy_4}{d\tau} &= Cy_4 - [y_3 + \frac{1}{8}(y_1^2 + y_2^2 + y_4^2 + y_5^2)]y_5 + \frac{3}{4}(y_1y_5 - y_2y_4)y_1 + 2y_5,\\
\frac{dy_5}{d\tau} &= Cy_5 + [y_3 + \frac{1}{8}(y_1^2 + y_2^2 + y_4^2 + y_5^2)]y_4 + \frac{3}{4}(y_1y_5 - y_2y_4)y_2 + 2y_4,
\end{aligned} \tag{2}$$

an analog generator - a piezoceramic transducer,

$$\begin{aligned}
\frac{d\xi}{d\tau} &= \zeta, \\
\frac{d\zeta}{d\tau} &= -\xi + \alpha_1\zeta + \alpha_2\zeta^2 - \alpha_3\zeta^3 + \alpha_4\beta, \\
\frac{d\beta}{d\tau} &= \gamma, \\
\frac{d\gamma}{d\tau} &= \alpha_5\xi + \alpha_6\zeta - \alpha_0\beta - \alpha_7\gamma,
\end{aligned} \tag{3}$$

a tank with a liquid - an excitation source,

$$\begin{aligned}
\frac{dp_1}{d\tau} &= \alpha p_1 - \left[\beta + \frac{A}{2}(p_1^2 + q_1^2 + p_2^2 + q_2^2)\right]q_1 + B(p_1q_2 - p_2q_1)p_2, \\
\frac{dq_1}{d\tau} &= \alpha q_1 + \left[\beta + \frac{A}{2}(p_1^2 + q_1^2 + p_2^2 + q_2^2)\right]p_1 + B(p_1q_2 - p_2q_1)q_2 + 1, \\
\frac{d\beta}{d\tau} &= N_3 + N_1\beta - \mu_1 q_1, \\
\frac{dp_2}{d\tau} &= \alpha p_2 - \left[\beta + \frac{A}{2}(p_1^2 + q_1^2 + p_2^2 + q_2^2)\right])q_2 - B(p_1q_2 - p_2q_1)p_1, \\
\frac{dq_2}{d\tau} &= \alpha q_2 + \left[\beta + \frac{A}{2}(p_1^2 + q_1^2 + p_2^2 + q_2^2)\right]p_2 - B(p_1q_2 - p_2q_1)q_1.
\end{aligned} \tag{4}$$

The derivation of systems of equations (1)–(4) is given in monograph [12], in which phase variables and parameters of these systems are described in detail. Note that the techniques for detecting, classifying, and investigating the properties of attractors of systems (1)–(4) are described in [13,14].

3 Scenarios of transition to chaos

Further we enumerate and describe the scenarios for the transition to chaos in systems (1)–(4):

3.1. **Feigenbaum's scenario**.

The most widespread scenario of transition to chaos through an infinite cascade of bifurcations of doubling the period of limit cycles [15–17]. The transition to chaos in the Feigenbaum scenario is observed in almost all dynamic systems. In particular, the appearance of chaotic attractors according to the Feigenbaum's scenario takes place in all systems (1)–(4).

3.2. **Intermittency by Manneville–Pomeau**.

Another widespread scenario of transition to chaos was first described in papers [18–20]. The transition from the limit cycle to the chaotic attractor occurs in one bifurcation. As a result of this bifurcation, the limit cycle disappears

and a chaotic attractor arises in the system. The motion of trajectories along the attractor consists of two phases - laminar and turbulent. In the laminar phase, the trajectory makes quasiperiodic movements in a small neighborhood of the disappeared limit cycle, and in the turbulent phase, it moves away to distant (relatively the disappeared cycle) regions of the phase space. Note that the transition from the laminar phase to the turbulent one and vice versa is unpredictable. The described transition to chaos through intermittency is also observed in all systems (1)–(4).

Next, we consider scenarios that are generalizations and combinations of a cascade of bifurcations of period doubling and intermittency.

3.3. **Generalized intermittency "chaos–chaos"**.

The Manneville–Pomeau's scenario describes the transition "limit cycle – chaotic attractor". A natural complication of this scenario is the scenario of transition "a chaotic attractor of one type – a chaotic attractor of another type". This scenario was first described in [13] and later called generalized intermittency. In further publications [14,21], this scenario was analyzed and substantiated in more details.

Briefly, this scenario can be described as follows. A some chaotic attractor exists in the system, which disappears when the bifurcation parameter reaches a certain value and a chaotic attractor of another type of is born in the system. The motion of the trajectories along the new attractor consists of two alternating phases. At one of these phases, the trajectory makes chaotic walks in a small neighborhood of the trajectories of the disappeared attractor. Then, at an unpredictable point in time, the trajectory leaves the region of localization of the disappeared attractor and leaves in the remote regions of the phase space. After some time, the movement of the trajectory again begins to resemble movement near of trajectories the disappeared chaotic attractor. The first of these phases was called coarse-grained (rough) laminar phase. The second is as before called turbulent phase. Note the duration of both the coarse-grained (rough) laminar and turbulent phases is unpredictable as are the moments of times of transition from one phase to another. An illustration of such a scenario is Fig.1. Here in Fig.1a shows the projection of the phase portrait before the bifurcation point, and in Fig.1b after the bifurcation point. The densely black part of the projection in the central region of Fig. 1b is the laminar phase of intermittency, and the more sparse part of this figure is the turbulent phase.

In fact, in this scenario a disappearing chaotic attractor plays the role of a disappearing limit cycle from the classical intermittency scenario.

3.4. **Generalized intermittency "hyperchaos–hyperchaos"**.

Recall that an attractor is called hyperchaotic if it has at least two positive Lyapunov's characteristic exponents. That is, in the phase space there are at least two directions along which the trajectories belonging to the hyperchaotic attractor diverge. Hyperchaotic attractors can exist only in dynamical systems whose phase space dimension is at least four.

This scenario was discovered and described in detail in the papers [22–24]. This scenario is similar of the scenario described in item 3.3. The only dif-

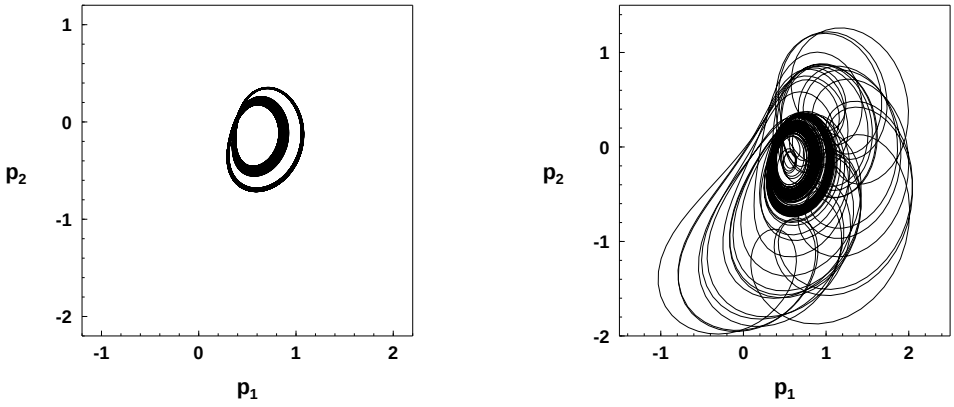

a b

Fig. 1.

ference is that the transitions from a hyperchaotic attractor of one type to a hyperchaotic attractor of another type are considered. Also, in such scenarios, transitions of the "chaos–hyperhaos" type are possible.

3.5. **Symmetry and intermittency in Feigenbaum's scenario**

This scenario is an unusual combination of Feigenbaum's scenario and intermittency. We briefly describe this scenario based on the results of the papers [21,22].

First, there are two stable limit cycles in the system. These cycles are symmetric with respect to one or another coordinate axis. Each of the limit cycles has its own basin of attraction. Then, with a change of the bifurcation parameter, infinite cascades of bifurcations of doubling the periods of these cycles simultaneously begin. Moreover, all bifurcations of doubling of each of the cycles occur at the same value of the bifurcation parameter. This cascade of doubling bifurcations ends with the simultaneous appearance of two symmetric chaotic attractors. Each of these attractors has its own basin of attraction.

With a further change of the parameter of bifurcation, phase portraits are glued together and only one chaotic attractor remains in the system. The arising chaotic attractor has a symmetric structure of the phase portrait. The motion of a typical trajectory of a chaotic attractor can be conditionally divided into two phases. In the first of these phases, the trajectory is located in the localization region of one of the disappeared chaotic attractors from time to time approaching the boundary of such a region. That is, in this phase, the trajectory is in one of the symmetric parts of the arising chaotic attractor. Then, at an unpredictable moment of time, the trajectory passes into the localization region of the second of the disappeared chaotic attractors, that is, into another

symmetric region of the arising chaotic attractor. This is the second phase of the trajectory. At an unpredictable moment of time, the trajectory again returns to the first symmetric region of the chaotic attractor. This process of transition from one symmetric region of the attractor to another is repeated an infinite number of times. Note that the duration of stay the trajectory in one of the symmetric regions of the attractor is unpredictable.

Thus, an unusual combination of the Feigenbaum's scenario (an infinite cascade of bifurcations of doubling of limit cycles) and intermittency (unpredictable intermittency between symmetric parts of the phase portrait of the arising chaotic attractor) takes place.

3.6. **Intermittency with two laminar phases**

We will describe such a scenario schematically. A necessary condition for the implementation of this scenario of transition to chaos is the simultaneous existence in the system of two symmetric stable limit cycles. Further changes in any parameter of bifurcation lead to the disappearance of both limit cycles and the birth of a chaotic attractor. In this case, the contours of the arising chaotic attractor in their form are two united symmetric limit cycles. The onset of chaos has many features typical of intermittency. However, in this case, moving the trajectory in the attractor includes three phases, two laminar and one turbulent. In the first laminar phase, the trajectory makes quasiperiodic movements in a small neighborhood of one of the stuck together limit cycles. At an unpredictable moment of time, a turbulent surge occurs and the trajectory leaves for a region of the phase space that is distant from the neighborhood of the disappeared cycle. Moreover, after the completion of the turbulent phase, the trajectory can either return to the first laminar phase of motion or go to the second laminar phase, which corresponds to quasiperiodic movements in a small neighborhood of the second of the disappeared limit cycles. Such a process of motion of a trajectory along an attractor of the form one of the laminar phases the turbulent phase one of the laminar phases is repeated an infinite number of times. Moreover, both the time moments of the transition of the trajectory into the turbulent phase and the switching between two laminar phases are unpredictable. Thus, the transition to chaos resembles the classic scenario of Manneville-Pomeau. However, unlike the classical scenario, we have not one, but two laminar phases of trajectory moving.

A graphic illustration of this scenario is shown in Fig.2. In Fig.2a–b show projections of symmetric limit cycles. In Fig.2c shows the distribution of the invariant measure in the projection of the phase portrait of a chaotic attractor. Bold sections Fig.2c correspond to two laminar phases of the trajectory motion. The paler areas in Fig.2c correspond to the turbulent phase.

Note that for the first time such a scenario was described in paper [22].

3.7. **Generalized intermittency with two coarse-grained (rough) laminar phases**

This scenario is in many ways similar to the scenario described in item "3.5. Symmetry and intermittency in Feigenbaum's scenario". For describe the beginning of this scenario, we can simply repeat the description of the scenario

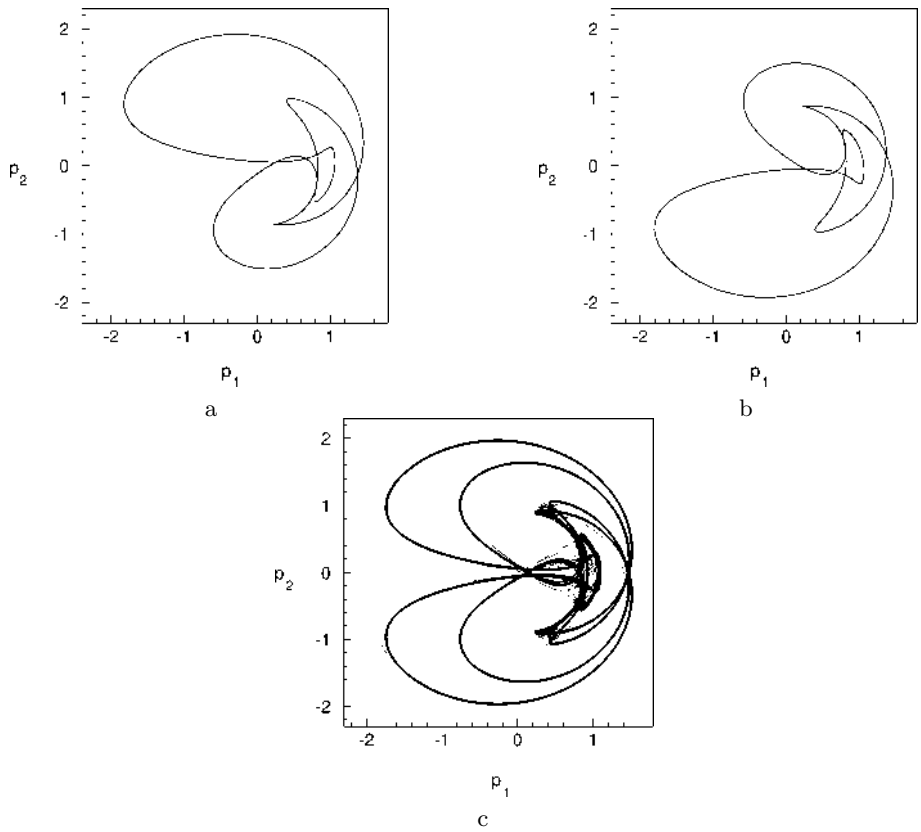

Fig. 2.

adduced in item 3.5. The differences begin from the moment of arising two symmetric chaotic attractors, which arise at the same value of the bifurcation parameter and have different attraction basins. With a further change in the bifurcation parameter, two symmetric chaotic attractors are combined into one chaotic attractor. The most significant difference from the scenario from item 3.5. is that the motion of the trajectory along the attractor consists of three phases. At two of these phases, the trajectory makes chaotic walks in a small neighborhood of the trajectories of the disappeared symmetric chaotic attractors. Such phases of movement are called coarse-grained (rough) laminar. The third phase of the movement is the departure of the trajectory into remote areas – this is the turbulent phase. The description of the sequence of transitions from one phase to another almost literally repeats such a description given in item "3.6. Intermittency with two laminar phases" . Only everywhere should the word "laminar" be replaced by "coarse-grained (rough) laminar".

A graphic illustration of ending this scenario is shown in Fig.3a-c. In Fig.3a-b are shown projections of phase portraits of symmetric chaotic attractors. Figure 3c is shown a chaotic attractor, which occurs after the disappearance of a pair of symmetric chaotic attractors. Three phases of the trajectory of

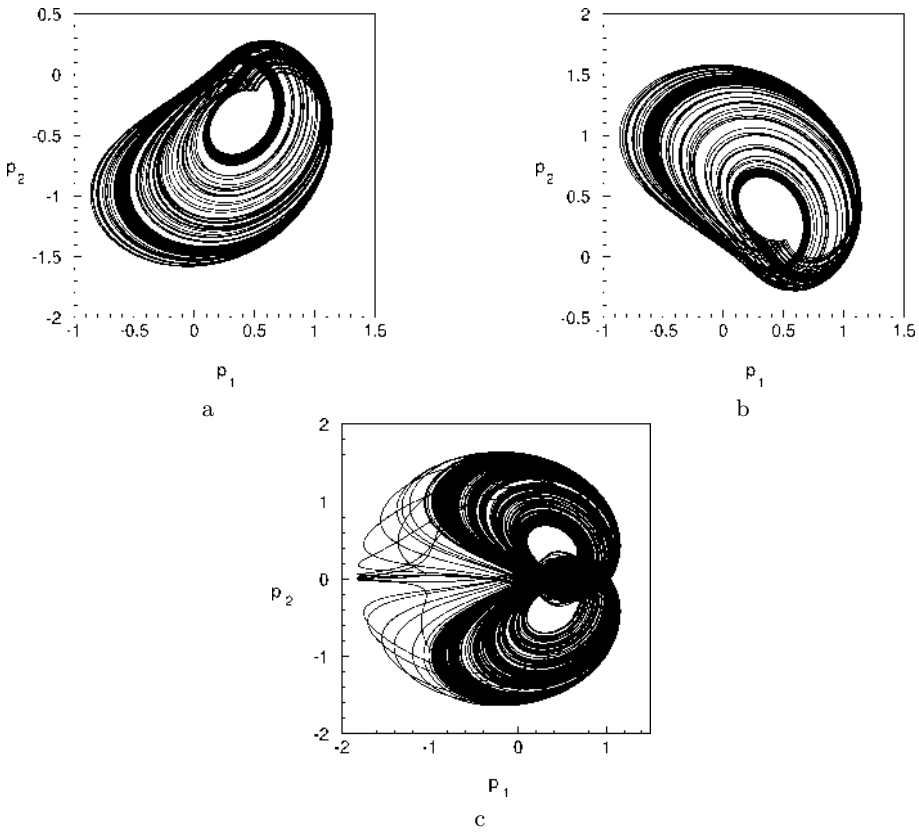

Fig. 3.

the attractor are clearly visible. These are two coarse-grained (rough) laminar phases (two dark regions in the upper right and lower parts of the figure) and a turbulent phase (the lighter region in the left part of the figure).

3.8. **Generalized intermittency "hyperchaos–hyperchaos" with two coarse-grained (rough) laminar phases**

This scenario has been discovered and described relatively recently and published in [23,24]. Qualitatively, this scenario is similar to the scenario given in the previous item "3.7. Generalized intermittency with two coarse-grained (rough) laminar phases". It begins with the appearance of two symmetric stable limit cycles. As a result of further changes in the bifurcation parameter, two hyperchaotic symmetric attractors arise, which then disappear and a combined hyperchaotic attractor is born in the system. The disappearing symmetric hyperchaotic attractors form two coarse-grained (rough) laminar phases of the final hyperchaotic attractor of this scenario.

Probably two more varieties of such a scenario are possible. The arising symmetric attractors will be chaotic, and the final attractor will be hyper-

chaotic. Conversely, symmetric attractors will be hyperchaotic, the final attractor will be chaotic.

We emphasize that the implementation of the scenarios described in items $3-8$ was found only for systems with a five-dimensional phase space.

3.9. **Atypical change of sequences scenarios**

The Feigenbaum's scenario and intermittency by Manneville-Pomeau are the main scenarios of the transition to chaos in dynamical systems. Moreover, in majority of dynamic systems, both of these scenarios are observed. As a rule, with an increase (decrease) in the value of the bifurcation parameter, the following sequence of transitions to chaos takes place. Cascade of bifurcations of period doubling – chaos – window of periodicity – cascadeof bifurcations of period doubling – chaos – window of periodicity and so on. On the other hand, with a decrease (increase) in the value of the bifurcation parameter, the following sequence takes place: window of periodicity – chaos through intermittency – window of periodicity – chaos through intermittency – window of periodicity and so on [25,26]. In systems (1), (3), (4) the situation was observed when, with an increase (decrease) in the value of the bifurcation parameter, transition to chaos is possible both according to the Feigenbaum's scenario and through intermittency.

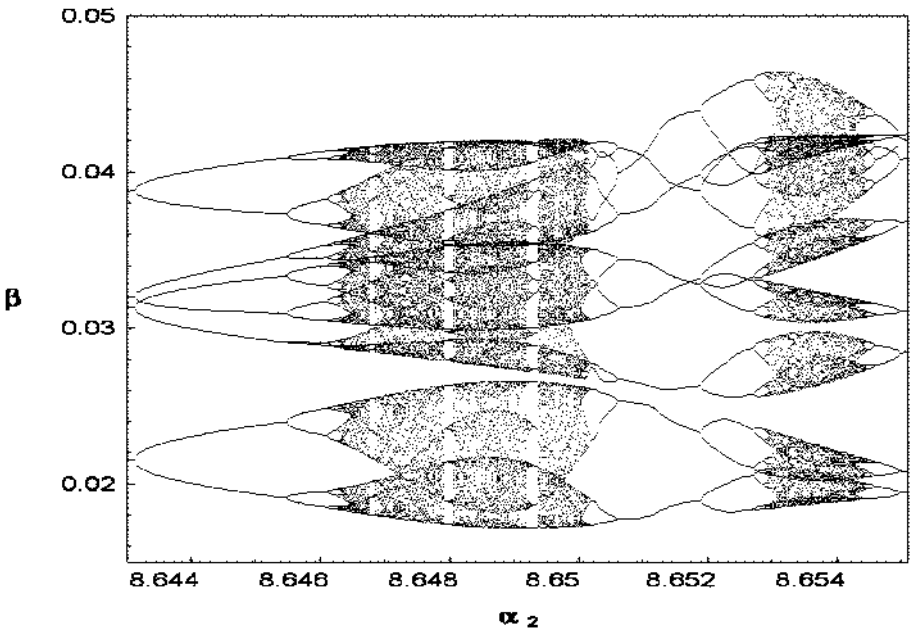

Fig. 4.

We illustrate this with help of the phase-parametric characteristic of system (3) is shown in Fig. 4. In system (3) there are numerous transitions from limit cycles to chaotic attractors, as well as the destruction of chaotic attractors

and the occurrence of limit cycles. All such transitions are clearly visible on the built bifurcation tree. Separate "branches" of this tree correspond to limit cycles, and densely dark areas correspond to chaotic attractors. The splitting points of the branches of the bifurcation tree are clearly visible in Fig. 4. In these points the bifurcations of the period doubling of the limit cycle occur. The threshold points are also clearly visible, during the passage of which an endless cascade of period doubling bifurcations ends with the appearance of a chaotic attractor, that is, a transition to chaos occurs according to the Feigenbaum's scenario. In turn, here is also possible a hard transition to chaos, in only one bifurcation, through Manneville-Pomeau intermittency. As can be seen from Fig. 4, the transition to chaos according to the Feigenbaum's scenario occurs both with increasing and decreasing values of the bifurcation parameter. A similar situation occurs for the transition to chaos through intermittency. Thus, there is some symmetry in the alternation of scenarios of transition to chaos. Such symmetry is atypical for dynamical systems.

Note that a similar symmetry effect of the scenarios of transition to chaos was established for nonideal systems (1), (4) in papers [27], [28].

4 Conclusion

The considered nonideal dynamic systems (1)–(4) are characterized by extremely diverse dynamic behavior. In these systems, there are possible all types of regular attractors: equilibrium positions, limit cycles, invariant tori. Also, various types of chaotic attractors were found in these systems, and various types of hyperchaotic attractors were revealed in systems (3), (4). In addition to all the scenarios of transition to chaos inherent in nonlinear dynamics as a whole, a number of unusual scenarios of transition to chaos were discovered and described in these systems. In further studies, the construction and study of the attraction basins of attractors of such systems can be of great interest. No less interesting will be an attempt to discover the described unusual scenarios of the transition to chaos in other dynamical systems.

References

1. Sommerfeld A. Beitrage zum dynamischen Ausbau der Festigkeitslehre, *Physikalische Zeitschrift*, 3, 266–271, 1902.
2. Sommerfeld A. Beitrage zum dynamischen ausbau der festigkeislehre, *Zeitschrift des Vereins Deutscher Ingenieure*, 46, 391–394, 1902.
3. Kononenko V.O. *Vibrating system with a limited power-supply*, Iliffe, London, 1969.
4. T.S Krasnopol'skaya. *Self-excitation of mechanical oscillations by an electrodynamic vibrator*. Sov. Appl. Mech., **13**, 187–191, 1977.
5. K.V. Frolov, T.S. Krasnopol'skaya. *Sommerfeld effect in systems without internal damping*. Sov. Appl. Mech., **23**, 1122–1126, 1987.
6. T.S. Krasnopolskaya. *Acoustic chaos caused by the Sommerfeld effect*. J. Fluids Struct., **8**(7), 803–815, 1994.
7. T.S. Krasnopolskaya. *Chaos in acoustic subspace raised by the Sommerfeld-Kononenko effect*. Meccanica, **41**(3), 299–310, 2006.

8. Krasnopol'skaya T.S., Shvets A.Yu. Prorerties of chaotic oscillations of the liquid in cylindrical tanks, *Prikladnaya Mekhanika*, **28**(6), 52–61, 1992.
9. Krasnopol'skaya T.S., Shvets A.Yu. Chaotic oscillations of a spherical pendulum as an example of interaction with energy source, *Int. Appl. Mech.*, **28**, 669–674, 1992.
10. Shvets A.Yu. Deterministic chaos of a spherical pendulum under limited excitation, *Ukr. Math. J.*, **59**, 602–614, 2007.
11. Balthazar J.M., Palacios Felix J.L. et al. Nonlinear interactions in a piezoceramic bar transducer powered by a vacuum tube generated by a nonideal source, J. Comput. Nonlinear Dyn., **4**(1), 1–7, 011013, 2009.
12. Krasnopolskaya T.S., Shvets A.Yu. *Regular and chaotical dynamics of systems with limited excitation*, R&C Dynamics, Moscow, 2008.
13. Krasnopolskaya T.S., Shvets A.Yu. Chaotic surface waves in limited power-supply cylindrical tank vibrations, *J. Fluids Struct.*, **8**(1), 1–18, 1994.
14. Krasnopolskaya T.S., Shvets A.Yu. Dynamical chaos for a limited power supply for fluid oscillations in cylindrical tanks, *J. Sound Vibr.*, **322**(3), 532–553 2009.
15. Feigenbaum M.J. Quantative universality for a class of nonlinear transformations, *J. Stat. Phys.* **19**(1), 25–52, 1978.
16. Feigenbaum M.J. The universal metric properties of nonlinear transformations, *J. Stat. Phys.* **21**(6), 669–706, 1979.
17. Feigenbaum M.J. The transition to aperiodic behavior in turbulent systems, *Comm. Math. Phys.* **77**(1), 65—86, 1980.
18. Manneville P., Pomeau Y. Different ways to turbulence in dissipative dynamical systems, *Physica D. Nonlinear Phenom.* **1**(2), 219-226 ,1980.
19. Pomeau Y., Manneville P. Intermittent transition to turbulence in dissipative dynamical systems, *Comm. Math. Phys.* **74**(2), 189-197 ,1980.
20. Berge P., Pomeau Y., Vidal C.H. *Order within chaos*,New York:John Wiley & Sons, 1984.
21. Shvets A.Yu., Sirenko V.O. Peculiarities of Transition to Chaos in Nonideal Hydrodynamics Systems, *Chaotic Modeling and Simulation (CMSIM) Journal*, 2, 303–310, 2012.
22. Shvets A., Sirenko V. Complicated Scenarios of Transitions to Deterministic Chaos in Non-Ideal Dynamic Systems , *Nonlinear Dynamics-2016 (ND-KhPI2016): proceedings of 5th International Conference, dedicated to the 90th anniversary of Academician V. L. Rvachev*, 222–229, 2016.
23. Shvets A., Sirenko V. Hyperchaos in Oscillating Systems with Limited Excitation, bf In: Skiadas C., Lubashevsky I. (eds) 11th Chaotic Modeling and Simulation International Conference. CHAOS 2018. Springer Proceedings in Complexity. Springer, Cham, 265–273, 2019.
24. Shvets A.Yu., Sirenko V.A., Scenarios of Transitions to hyperchaos in Nonideal Oscillating Systems, *J. Math. Sci.*, **243**(2), 338–346, 2019.
25. Afraimovich V, Hsu S.B. Lectures on chaotic dynamical sestems, *Sommerville, International Press*, 2003.
26. Kouznetsov, S.P. Dynamic chaos. P̂hysmatlit, Moscow, 2006.
27. Shvets A.Yu., Makaseyev A. Delay factors and chaotization of non-ideal pendulum systems, *CHAOS 2012 - 5th Chaotic Modeling and Simulation International Conference, Proceedings*, 2012.
28. Shvets A., Donetskyi. Transition to Deterministic Chaos in Some Electroelastic Systems, bf In: Skiadas C., Lubashevsky I. (eds) 11th Chaotic Modeling and Simulation International Conference. CHAOS 2018. Springer Proceedings in Complexity. Springer, Cham, 257–264, 2019.

Identification of Hidden and Rare Attractors in Some Electroelastic Systems with Limited Excitation

Aleksandr Shvets[1] and Serhii Donetskyi[2]

[1] National Technical University of Ukraine "Igor Sikorsky Kyiv Polytechnic Institue", Kyiv, Ukraine
(E-mail: Alex.Shvets@bigmir.net)
[2] National Technical University of Ukraine "Igor Sikorsky Kyiv Polytechnic Institue", Kyiv, Ukraine
(E-mail: dsvshka@gmail.com)

Abstract. Mathematical models of a deterministic dynamic system of the type analog generator–piezoelectric transducer are considered taking into account the influence of delay. A technique for searching for hidden and rare attractors of such system is proposed. Two approaches to the study of systems with delay are analyzed. The transformations of hidden attractors into self-excited ones, and rare attractors into non rare ones and vice versa are studied. The pairs of regular attractor – chaotic attractor are studied in point of view of their qualifications in terms of "hidden" and "rare". Symmetry was revealed in the scenarios of the transition from regular attractors to chaotic attractors. The effect of delay on the regular and chaotic dynamics of the system is investigated.
Keywords: hidden attractor, rare attractor, scenario of transition to chaos, delay.

1 Introduction

A dynamic system consisting of a piezoceramic transducer excited by an vacuum tube generator of limited power is considered. Such systems are widely used in various technical devices. Many aspects of the dynamic behavior of such systems were studied in papers [1–4,6–9]. The existence of various types of steady-state modes of interaction between the generator and the converter was revealed. In particular, chaotic and hyperchaotic regimes of interaction were discovered and the features of transitions from regular regimes to chaotic one were described. It was shown that dynamic chaos in that systems arise solely due to the interaction between the generator and the converter, and their individual characteristics.

However, earlier studies almost did not take into account such an important factor as the delay in the impact of the generator on transducer and delay of the inverse effect of the transducer on generator. Note that delay may be present in real systems due to limited speed signals: waves of compression, tension, bending, current and electrical voltage, as well as many other factors. In some cases influence of delay does not lead to significant changes in the dynamic behavior of researched systems. In other cases delay leads not only to significant quantitative changes of characteristics steady-state movement, but to completely qualitatively changes in the type of steady-state regimes.

2 The mathematical model

Consider a system consisting of a piezoceramic transducer, the source of excitation of which is an analog vacuum tube generator. Assume that a piezoceramic transducer has the shape of a circular cylinder and placed in an acoustic environment. Transducer and generator form an electrical circuit through a transmitting transformer. Let e_g and E_g be the variable and constant components of the grid generator lamp voltage, accordingly. Denote by $V(t)$ the electric voltage applied to the electrodes of the transducer. Introduce variable $\psi(t)$ by the formula

$$\psi(t) = \int_0^t (e_g + E_g)dt$$

Then, the equation describing the electrical oscillations of the generator has the form [6–8]:

$$\ddot{\psi}(t) + \omega_0^2\psi(t) = a_1\dot{\psi}(t) + a_2\dot{\psi}^2(t) - a_3\dot{\psi}^3(t) - a_4V(t-\rho), \tag{1}$$

here

$$\begin{gathered}\omega_0^2 = \frac{R_a + R_c}{R_cL_cC_c};\ a_0 = a_1 - \frac{M^2R_c}{L_cC_cLR_a^2};\ a_2 = \frac{3M_cI_3E_g}{L_cC_c}; a_3 = \frac{M_cI_3}{L_cC_c};\\ a_4 = \frac{2MM_c}{LR_aL_cC_c}; a_1 = \frac{M_c}{L_cC_c}(I_1 - \frac{R_aR_cC_c - L_c}{R_a(M_c - DL_c)} + \frac{R_cL_1}{R_a^2M_c} - 3I_3E_g^2).\end{gathered} \tag{2}$$

A detailed description of all the electromagnetic parameters of the generator, contained in the equation (2) is given in [7,8,10]. Constant non-negative parameter ρ introduced for accounting delay of influence the impact of the transducer on the generator.

In turn, the equation describing the voltage oscillations $V(t)$, taking into account the delay of the signal of the generator on transducer, can be written as [6–8]:

$$\ddot{V}(t) + \omega_1^2V(t) = a_5\psi(t-\rho) + a_6\dot{\psi}(t) - a_7\dot{V}(t), \tag{3}$$

here,

$$\begin{gathered}\omega_1^2 = \frac{2h}{LS\epsilon_{33}(1-k^2)};\ a_5 = -\frac{M\omega_1^2R_c(R_a + R_c)}{2M_cR_aL_c};\ a_6 = -\frac{M\omega_1^2R_c}{2M_cR_a};\\ a_7 = \frac{k^2}{\eta_0hS(1-k^2)};\ k = \frac{d_{33}}{\sqrt{\epsilon_{33}s_{33}}},.\end{gathered} \tag{4}$$

The parameters d_{33}, s_{33} and ϵ_{33} are constant coefficients of the theory of longitudinal deformations of a piezoelectric element described in [10]. Note that the presence of delay in real devices "generator–piezoceramic transducer" may be associated with territorial remoteness, sometimes quite significant, subsystems of the specified device. This leads to a delay feedback from one subsystem to another for the reasons stated in the Introduction.

Thus, the system of equations with retarded argument (1, 3) describes the interaction process a piezoceramic transducer with a source of its excitation, an

analog generator. We pass to the new system with the dimensionless variables according to the following formulas:

$$\xi(\tau) = \frac{\psi(\tau)\omega_0}{E_g},\ \frac{d\xi(\tau)}{d\tau} = \zeta(\tau),\ \beta(\tau) = \frac{V(\tau)}{E_g};$$
$$\frac{d\beta(\tau)}{d\tau} = \gamma(\tau),\ \tau = \omega_0 t. \tag{5}$$

Then we get the following system of equations

$$\begin{aligned}
\frac{d\xi(\tau)}{d\tau} &= \zeta(\tau);\\
\frac{d\zeta(\tau)}{d\tau} &= -\xi(\tau) + \alpha_1\zeta(\tau) + \alpha_2\zeta^2(\tau) - \alpha_3\zeta^3(\tau) - \alpha_4\beta(\tau-\delta);\\
\frac{d\beta(\tau)}{d\tau} &= \gamma(\tau);\\
\frac{d\gamma(\tau)}{d\tau} &= -\alpha_0\beta(\tau) + \alpha_5\xi(\tau-\delta) + \alpha_6\zeta(\tau) - \alpha_7\gamma(\tau).
\end{aligned} \tag{6}$$

here

$$\alpha_0 = \frac{\omega_1^2}{\omega_0^2},\ \alpha_1 = \frac{a_0}{\omega_0},\ \alpha_2 = \frac{a_2 E_g}{\omega_0},\ \alpha_3 = \frac{a_3 E_g^2}{\omega_0},$$
$$\alpha_4 = \frac{a_4}{\omega_0},\ \alpha_5 = \frac{a_5}{\omega_0^3},\ \alpha_6 = \frac{a_6}{\omega_0^2},\ \alpha_7 = \frac{a_7}{\omega_0},\ \delta = \omega_0\rho. \tag{7}$$

The function $\beta(\tau)$ corresponds to the signal propagated transducer into the acoustic medium, and the function $\xi(\tau)$ describes internal processes in the generator. Delays that are present in the system of equations (6) may lead qualitative changes of the steady-state regimes of interaction. Particularly, delay can lead, as to emergence of new regular and chaotic attractors, or lead to disappearance of such attractors, existing in the system in the absence of delay. Consider these processes in some concrete examples.

3 Simulation at absence of delay

Firstly, consider the case of absence of delay in system (6), i.e. $\delta = 0$. In such case the system (6) is a nonlinear system of differential equations of fourth order, so all its researches were carried out by means of various numerical methods. The technique for such calculations was developed and described in detail in [5,6,11–13].

Recently, new classification of attractors of dynamic systems has been proposed, which give the definition of self-excited, hidden and rare attractors [14–16]. We briefly recall the definitions of such types of attractors. An attractor is called self-exciting if there is an equilibrium position such that any neighborhood of it intersects with basin of attraction of the attractor. An attractor is called hidden if it is not self-excited.

For most dynamic systems, the main focus is the study of self-excited attractors. This is due to the fact that currently detection of the existence of hidden attractors is, generally speaking, extremely challenging. However, attractors of dynamical systems are not limited by self-excited attractors. Occurrence in specific dynamic system (device, structural element) of a hidden attractor can completely change the expected behavior of the system and make it impossible to perform its intended operational functions. Moreover, developers of a particular system may not guess that the functioning of the system occurs in the regime of a hidden attractor.

The attractor is called rare if it is located in the phase space nearby with other attractor herewith phase volume (measure) of its basin of attraction significantly less compared to the basin of attraction of attractor near which it is located. Or simply rare attractor is attractor that has an extremely small basin of attraction. It is clear that the probability of a trajectory entering this attractor is small.

The main goal of this work is to detect attractors of the system (6) and to identify their types, taking into account the classification proposed in [14–16]. Note that the study of rare attractors of system (6) was started in paper [17].

For revealing hidden attractors of the system (6), following algorithm can be proposed. Firstly, the trajectory of system is calculated using the Runge-Kutta method with correction of a variable step of numerical integration according to Dormand-Prince [18], at that is selected relatively large local error $O(10^{-4}) - O(10^{-5})$ for Dormand-Prince procedure and any initial conditions for the system (6) are specified. Next, for chosen trajectory, after ending of transition process, Lyapunov's characteristic exponents (LCEs) are calculated [19]. On the basis of LCEs identification of type of attractor are made. However, a paradoxical situation may arise. In our case such situation is absence of zero exponent in LCE spectrum for an attractor, which is not an equilibrium position. This situation may happen due to presence in the system hidden (rare) attractor. After decreasing the local error up to $O(10^{-7}) - O(10^{-8})$ the problem with absence of non zero LCE goes away and trajectories of system over time may be belong to hidden (rare) attractors.

Let parameters of the system be equal $\alpha_0 = 0.995$, $\alpha_1 = 0.0535$, $\alpha_3 = 9.95$, $\alpha_4 = 0.103$, $\alpha_5 = -0.0604$, $\alpha_6 = -0.12$, $\alpha_7 = 0.01$ and leave parameter α_2 as bifurcation one. For so chosen values the parameters, system (6) has a single unstable equilibrium position

$$\xi = 0, \zeta = 0, \beta = 0, \gamma = 0,$$

so-called zero equilibrium position [6,8,17].

At $\alpha_2 = 8.925$ chaotic attractor is the only attractor of the system in the neighborhood of the zero equilibrium position. This attractor is self-excited attractor. At increasing value of bifurcation parameter up to $\alpha_2 = 8.94$ another attractor arises, namely, the limit cycle. In system (6), in the neighborhood of the zero equilibrium position, two attractors begin to exist simultaneously. One of them is a chaotic attractor, and the second is a limit cycle. Phase portrait projections of coexisting attractor are presented in fig. 1a. Moreover, the chaotic attractor (black attractor) is still a self-excited attractor. In turn,

the limit cycle (red attractor) is both a hidden attractor and a rare attractor. The limit cycle is a hidden attractor because it is not a self-excited attractor. And it is rare attractor, because it has very small basin of attraction.

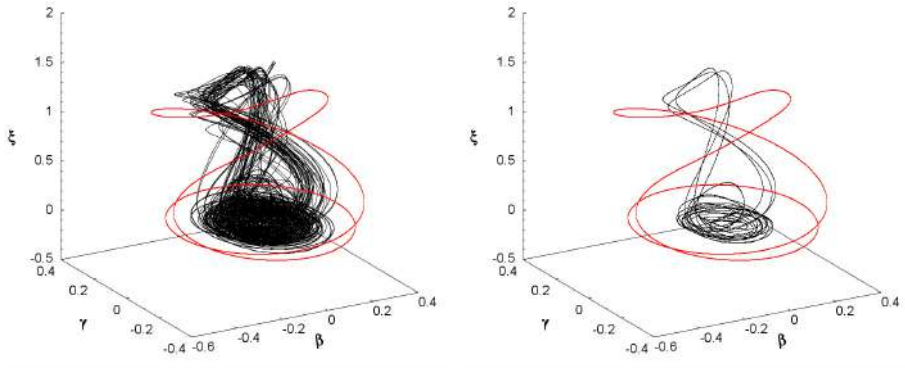

(a) (b)

Fig. 1. Phase portrait projections at: $\alpha_2 = 8.958$ (a); $\alpha_2 = 8.959$ (b).

In the future, one of the attractors of a pair of simultaneously existing attractors will be conventionally called black attractor, and the other - red. A part of the phase-parametric characteristics of the coexisting pair of attractors (black and red) is shown in fig. 2. For both attractors, as for black attractor as for red attractor, separate "branches" of this trees correspond to limit cycles. The densely black regions correspond to chaos of the black attractor, and the densely red regions correspond to the quasiperiodic regimes of the red attractor. In fig. 3 an enlarged fragment of the middle part of the phase-parametric characteristics is shown. The fig. 2 and the fig. 3 give a clear view of bifurcations in system (6) in a selected region of the space of its parameters. So there are numerous bifurcations of the black attractor of the type "cycle - chaos - cycle - chaos", etc. However, in such transitions, the black attractor will always be a self-excited attractor. In turn, for the red attractor, in fact, there is only one rigid bifurcation "cycle - invariant torus". Moreover, the red attractor, both being a limit cycle and an invariant torus, also constantly remains a hidden attractor and a rare attractor.

Another interesting feature of the alternation of scenarios of transition to the chaos of the black attractor is visible in Fig. 3. The transition to chaos according to the Feigenbaum's scenario through the endless cascade of periods doubling of limit cycles, occurs at increasing of bifurcation parameter α_2 and at decreasing of bifurcation parameter α_2. The same feature is inherent in the transition to chaos through intermittency. That is, there is some symmetry in the alternation of scenarios of transition to chaos. This situation, in general, is atypical for dynamical systems [19], however it seems to be natural for the system (6), since similar symmetry were already found before in paper [17].

We also illustrate these bifurcations using phase portraits of attractors. At $\alpha_2 = 9.02$ the black chaotic attractor turns into limit cycle through one rigid

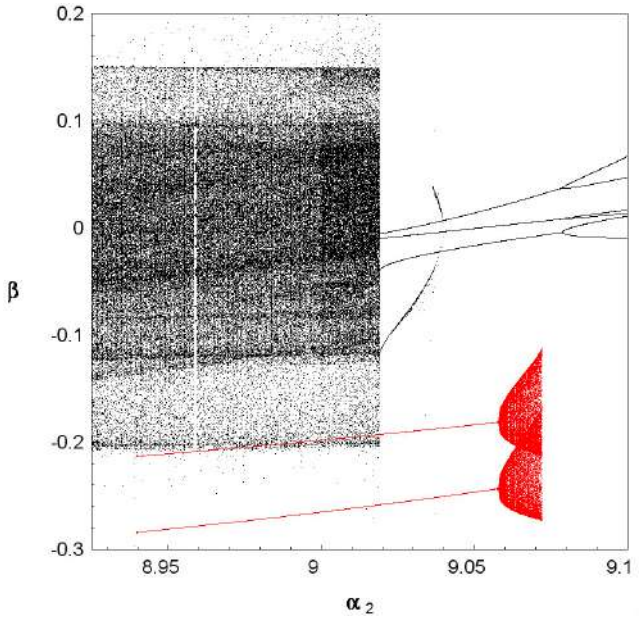

Fig. 2. Phase-parametric characteristic for $\alpha_2 \in [8.925; 9.1]$.

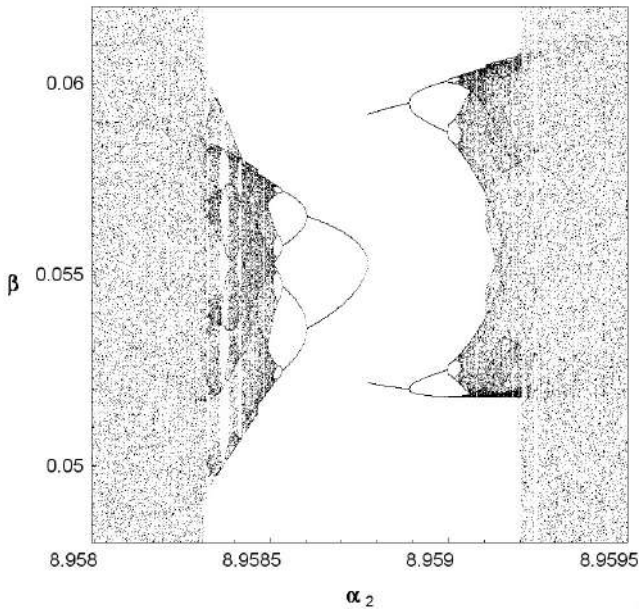

Fig. 3. Phase-parametric characteristic in window of periodicity at $\alpha_2 \in [8.958; 8.9595]$.

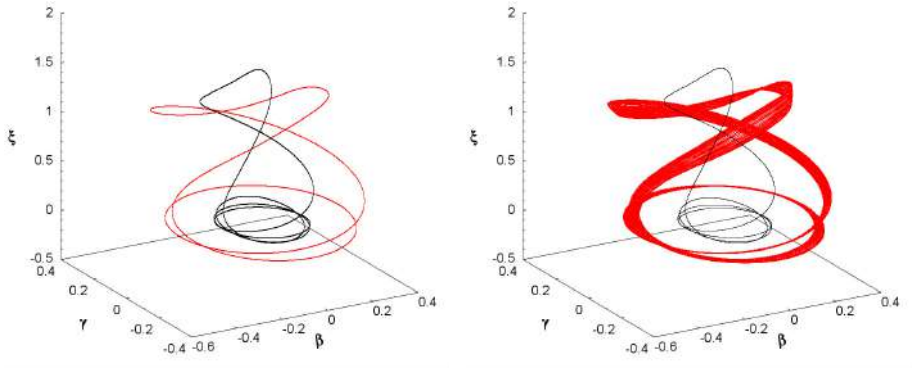

(a) (b)

Fig. 4. Phase portrait projections at: $\alpha_2 = 9.04$ (a); $\alpha_2 = 9.07$ (b).

bifurcation. In turn red attractor remains periodic. This situation holds until $\alpha_2 = 9.06$ when new bifurcation occurs with red limit cycle which turns it into invariant torus and remains up so to its disappearance at $\alpha_2 = 9.072$. As we have already noted, a black attractor will always be a self-excited attractor. The red attractor will always be a hidden attractor and at the same time will be a rare attractor. Projections of phase portraits of pairs "self-exited limit cycle – hidden and rare limit cycle" and "self-exited limit cycle – hidden and rare invariant torus" are pictured in fig. 4a–b correspondingly.

4 Methods of transformation systems with delay

We consider methods for transforming systems with a delayed argument into systems of ordinary differential equations. First one is based on assumption that delay factor δ is sufficiently small, so that we can write

$$\beta(\tau - \delta) \approx \beta(\tau) - \delta \cdot \frac{d\beta(\tau)}{d\tau} = \beta(\tau) - \delta \cdot \gamma(\tau);$$
$$\xi(\tau - \delta) \approx \xi(\tau) - \delta \cdot \frac{d\xi(\tau)}{d\tau} = \xi(\tau) - \delta \cdot \zeta(\tau).$$

Substituting the obtained expressions into the system of equations (6), we obtain

$$\begin{aligned}
\frac{d\xi(\tau)}{d\tau} &= \zeta(\tau);\\
\frac{d\zeta(\tau)}{d\tau} &= -\xi(\tau) + \alpha_1\zeta(\tau) + \alpha_2\zeta^2(\tau) - \alpha_3\zeta^3(\tau) - \alpha_4\beta(\tau) + \alpha_4\delta \cdot \gamma(\tau);\\
\frac{d\beta(\tau)}{d\tau} &= \gamma(\tau);\\
\frac{d\gamma(\tau)}{d\tau} &= -\alpha_0\beta(\tau) + \alpha_5\xi(\tau) - \alpha_5\delta \cdot \zeta(\tau) + \alpha_6\zeta(\tau) - \alpha_7\gamma(\tau).
\end{aligned} \tag{8}$$

The system of equation (8) is transformed in a system of ordinary differential equations. Delay δ is in the system (8) as additional parameter. This approach is applicable for systems with constant delay and with variable delay.

A more accurate approximation method is applicable only to systems with a constant delay of δ. Let us divide segment $[-\delta; 0]$ into m equal parts and introduce such new functions.

$$\beta(\tau - \frac{i\delta}{m}) = \beta_i(\tau), \qquad \xi(\tau - \frac{i\delta}{m}) = \xi_i(\tau), \qquad i \in \{0, \dots, m\}.$$

Then, using difference approximation of derivative, we turn system (6) into system

$$\begin{aligned}
&\frac{d\xi_0(\tau)}{d\tau} = \zeta_0(\tau);\\
&\frac{d\zeta_0(\tau)}{d\tau} = -\xi_0(\tau) + \alpha_1\zeta_0(\tau) + \alpha_2\zeta_0^2(\tau) - \alpha_3\zeta_0^3(\tau) - \alpha_4\beta_m(\tau);\\
&\frac{d\beta_0(\tau)}{d\tau} = \gamma_0(\tau);\\
&\frac{d\gamma_0(\tau)}{d\tau} = -\alpha_0\beta_0(\tau) + \alpha_5\xi_m(\tau) + \alpha_6\zeta_0(\tau) - \alpha_7\gamma_0(\tau);\\
&\frac{d\xi_i(\tau)}{d\tau} = \frac{m}{\delta}\cdot\Big(\xi_{i-1}(\tau) - \xi_i(\tau)\Big), \qquad i \in \{1, \dots, m\};\\
&\frac{d\beta_i(\tau)}{d\tau} = \frac{m}{\delta}\cdot\Big(\beta_{i-1}(\tau) - \beta_i(\tau)\Big), \qquad i \in \{1, \dots, m\}.
\end{aligned} \tag{9}$$

System (9) is a system of ordinary differential equations of $(2m + 4)$-th order. The delay δ is introduced as additional parameter of this system.

It should be noted that solutions $\xi, \zeta, \beta, \gamma$ of the system (6) are approximated by solutions $\xi_0, \zeta_0, \beta_0, \gamma_0$ of the system (9) respectively. And $\xi_0 \to \xi,\ \zeta_0 \to \zeta,\ \beta_0 \to \beta,\ \gamma_0 \to \gamma$ as $m \to \infty$.

Thus, we can study the influence of delay on the dynamic behavior of the generator-transducer system using either a system of equations (8) or a system of equations (9). Such studies are carried out using a number of numerical methods according to the technique described in [6,11,13]. The application of the second approach to reduce the system of differential equations with delay to the system of differential equations without delay allows, generally speaking, to obtain more accurate results at studying the dynamics of the "generator-transducer" system. However, this significantly increases the duration of computer calculations and complicates the procedure for creating the appropriate computer programs. So there must be a balance between computational speed and accuracy.

We will find such balance for a number of concrete cases. Assume that $\alpha_0 = 0.995$, $\alpha_1 = 0.0535$, $\alpha_3 = 9.95$, $\alpha_4 = 0.103$, $\alpha_5 = -0.0604$, $\alpha_6 = -0.12$, $\alpha_7 = 0.01$. As bifurcation parameters we use the parameters α_2, δ.

Comparison results for the two used methods are shown in fig. 5.

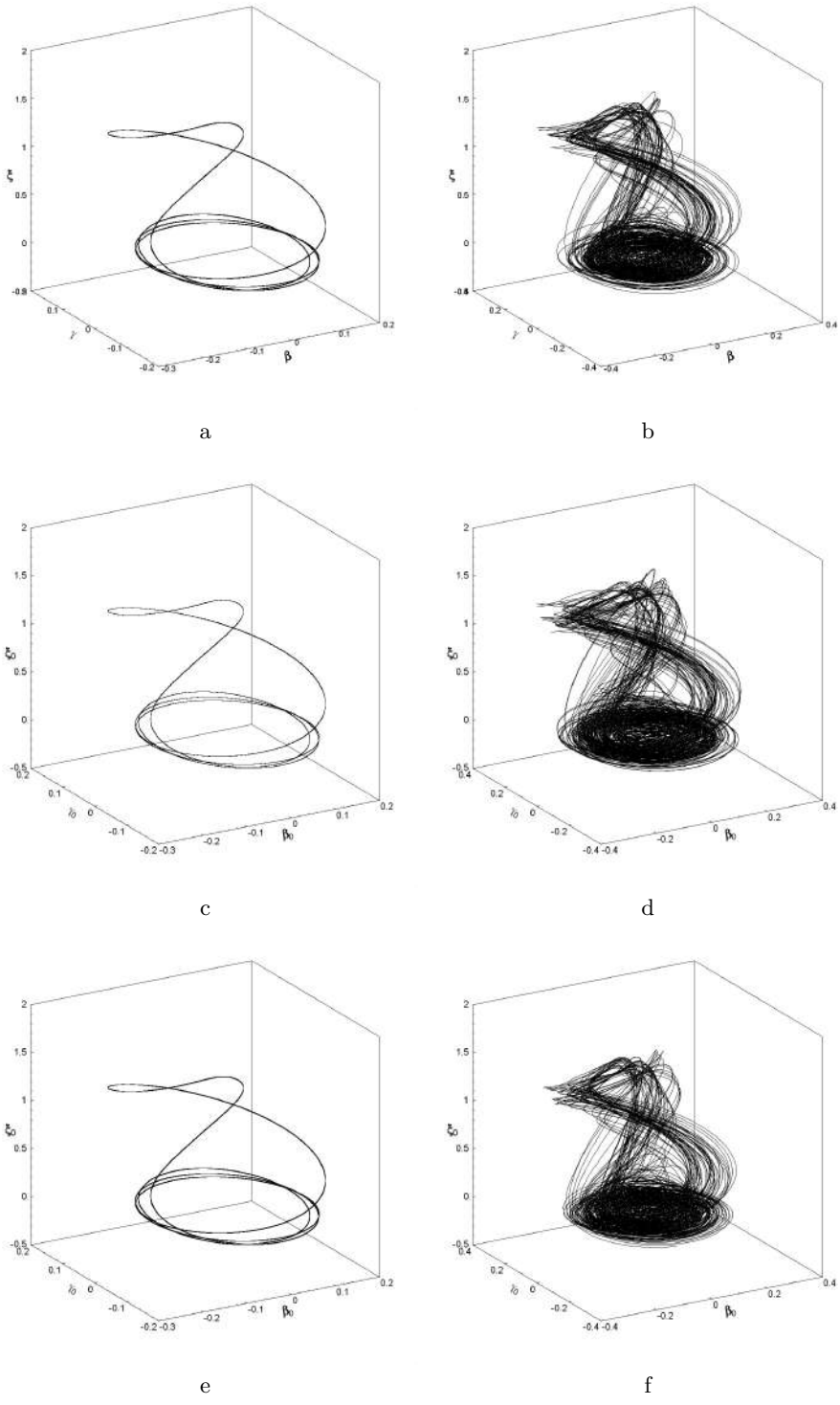

Fig. 5.

In fig. 5a the projection of the phase portrait of the limit cycle of system (8), constructed at $\alpha_2 = 9.075$, $\delta = 0.01$ is shown. Accordingly, in fig. 5c, e the projection of the phase portrait of the limit cycle of system (9), constructed at the same values of α_2, δ are shown. The fig. 5c is constructed at $m = 3$ and the fig. 5e is constructed at $m = 30$. In fig. 5b, d, f the projections of the phase portrait of the chaotic attractor constructed at $\alpha_2 = 9.075$, $\delta = 0.04$ are shown. In fig. 5b the chaotic attractor of system (8) is shown. Accordingly in fig. 5d the chaotic attractor of system (9) ($m = 3$) is shown and in fig. 5f the chaotic attractor of system (9) ($m = 30$) is shown.

Note that the identification of the type of attractor (limit cycle or chaotic attractor) was carried out on the basis of calculation and analysis of the LCE spectrum. As can be seen in fig. 5, all constructed phase portraits almost coincide. However, the duration of computer calculations increases significantly when applying the second method of transformation a system with delay (6) to a system without delay (9). At m = 30, the duration of computer calculations by the second method is more than 5000 times the duration of computer calculations by the first method. Moreover, the constructed phase portraits and Lyapunov's characteristic exponents practically coincide. Therefore all further analysis of influence of the delay was carried out by the first method.

5 Influence of the delay on the type of attractor

We investigate the influence of delay on the appearance and disappearance of various attractors of the "generator-transducer" system. As in the previous section, we assume that $\alpha_0 = 0.995$, $\alpha_1 = 0.0535$, α_2=9.075, $\alpha_3 = 9.95$, $\alpha_4 = 0.103$, $\alpha_5 = -0.0604$, $\alpha_6 = -0.12$, $\alpha_7 = 0.01$. As bifurcation parameters we use the delay δ.

In fig. 6, phase parametric characteristics of a pair of attractors coexisting in the system (6) are constructed. As previously conditionally we will call them black and red attractor.

In the absence of delay in the system, there is only one black attractor. This attractor is a stable limit cycle. In addition, this attractor will be the self-excited attractor. However, even at a negligible value of the delay $\delta = 0.0015$, another attractor is born in the system, namely, the invariant torus (red region in fig. 6). This invariant torus is both a hidden attractor and a rare attractor. At increasing delay, at $\delta = 0.005$ for red attractor the bifurcation "torus–cycle" is taken place. The invariant torus is destroyed and a resonant limit cycle is born in the system. With a further increase of the delay, in the selected interval of the change of the delay, no red attractor bifurcations occur anymore. The new resonant limit cycle will continue to be both a hidden attractor and a rare attractor.

Next, we consider the bifurcations of the black attractor. As can be seen from fig. 6 at $\delta = 0.032$ through one rigid bifurcation the limit cycle disappears and a chaotic attractor arises in the system. Such a chaotic attractor exists at the vast majority of $\delta > 0.032$. To this chaotic attractor corresponds the densely black region in fig. 6 and this attractor is self-excited attractor in this region. In addition, small slots are visible in this thickly black area. As

a rule, such slots correspond to periodicity windows in chaos. However, here the situation is much more interesting. At the values of delay corresponding to such slots, the chaotic attractor does not disappear and does not turn into a limit cycle. It will still be chaotic attractor, but not self-excited attractor. This attractor turns into hidden attractor, since trajectory that starts in the neighborhood of equilibrium position skips black attractor and approach to red limit cycle. Moreover, the phase portrait of such hidden attractor is not practically distinguishable from the phase portraits of self-excited chaotic attractor. Thus, at the values of delay corresponding to the "slots" in fig. 6, a rare and self-excited limit cycle and a hidden chaotic attractor simultaneously exist in the system.

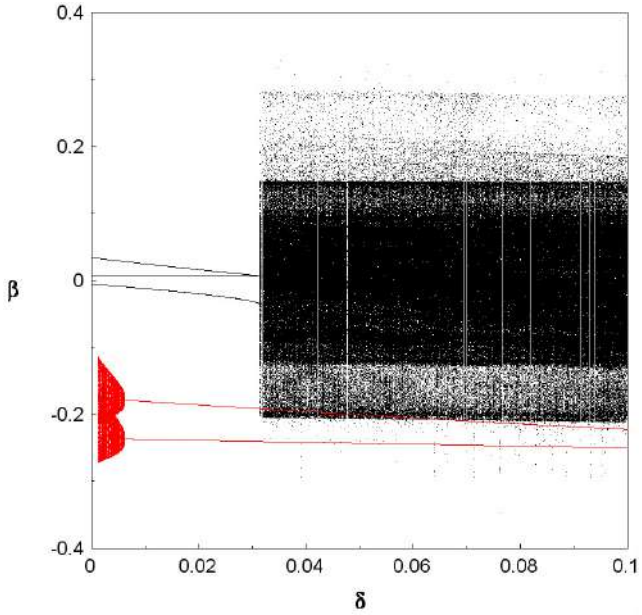

Fig. 6. Phase-parametric characteristic at $\alpha_2 = 9.075$ for $\delta \in [0; 0.1]$.

Projections of phase portrait of mentioned pairs of attractor ("limit cycle – torus", "limit cycle – limit cycle", "limit cycle – chaos") are shown in fig.7.

6 Conclusion

In the space of parameters of the "generator-piezoceramic transducer" system, regions were discovered in which two attractors coexist simultaneously. Moreover, these attractors can be both regular and chaotic. These attractors are located in close proximity to one another. At absence of delay one of the coexisting attractors is always a self-excited attractor, and the second attractor is always hidden and rare. It is shown that the presence of delay in the system can contribute to the appearance and disappearance of attractors of various

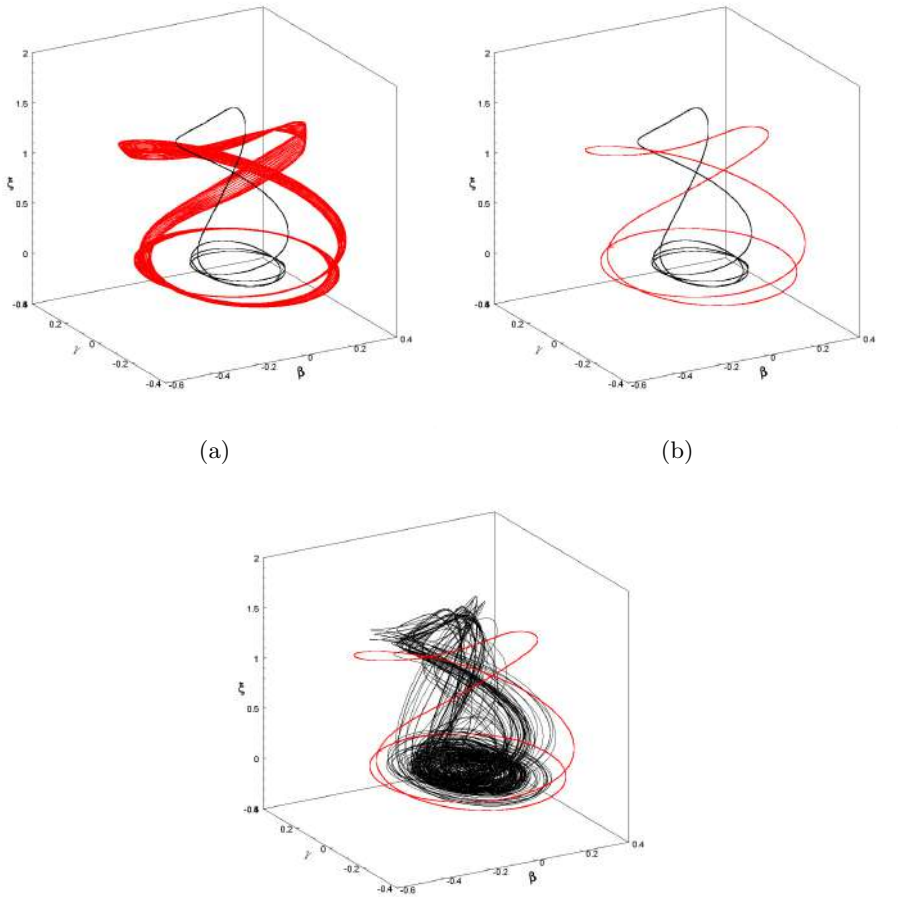

(a) (b)

(c)

Fig. 7. Phase portrait projections at: $\delta = 0.0015$ (a); $\delta = 0.01$ (b); $\delta = 0.035$ (c).

types. The possibility of simultaneous coexistence in the system of a hidden chaotic attractor and a rare and self-excited limit cycle is established.

References

1. T.S Krasnopol'skaya. *Self-excitation of mechanical oscillations by an electrodynamic vibrator*. Sov. Appl. Mech., **13**, 187–191, 1977.
2. K.V. Frolov, T.S. Krasnopol'skaya. *Sommerfeld effect in systems without internal damping*. Sov. Appl. Mech., **23**, 1122–1126, 1987.
3. T.S. Krasnopolskaya. *Acoustic chaos caused by the Sommerfeld effect*. J. Fluids Struct., **8**(7), 803–815, 1994.
4. T.S. Krasnopolskaya. *Chaos in acoustic subspace raised by the Sommerfeld-Kononenko effect*. Meccanica, **41**(3), 299–310, 2006.

5. Krasnopol'skaya T.S., Shvets A.Yu. Chaotic oscillations of a spherical pendulum as an example of interaction with energy source, *Int. Appl. Mech.*, **28**, 669–674, 1992.
6. T.S. Krasnopolskaya, A.Yu. Shvets. *Deterministic chaos in a system generator - piezoceramic transducer*. Nonlinear Dyn. Syst. Theor., **6**(4), 367–387, 2006.
7. T.S. Krasnopolskaya, A.Yu. Shvets. *Regular and chaotical dynamics of systems with limited excitation*. R&C Dynamics, Moscow, 2008.
8. A.Y. Shvets, T.S. Krasnopolskaya. *Hyperchaos in Piezoceramic Systems with Limited Power Supply*. In: Borisov A.V., Kozlov V.V., Mamaev I.S., Sokolovskiy M.A. (eds) IUTAM Symposium on Hamiltonian Dynamics, Vortex Structures, Turbulence. IUTAM Bookseries, Springer, Dordrecht, 6, 313–322, 2008.
9. J.M. Balthazar, J.L. Palacios Felix et al. *Nonlinear interactions in a piezoceramic bar transducer powered by a vacuum tube generated by a nonideal source*. J. Comput. Nonlinear Dyn., **4**(1), 1–7, 011013, 2009.
10. B.A. Auld. *Acoustic Fields and Waves in Solids*. New York: John Wiley & Sons, 1973.
11. Shvets A.Yu. Deterministic chaos of a spherical pendulum under limited excitation, *Ukr. Math. J.*, **59**, 602–614, 2007.
12. Krasnopolskaya T.S., Shvets A.Yu. Dynamical chaos for a limited power supply for fluid oscillations in cylindrical tanks, *J. Sound Vibr.*, **322**(3), 532–553 2009.
13. Shvets A.Yu., Sirenko V.A., Scenarios of Transitions to hyperchaos in Nonideal Oscillating Systems, *J. Math. Sci.*, **243**(2), 338–346, 2019.
14. G. Leonov, N. Kuznetsov et al. *Localization of hidden Chua's attractors*. Physics Letters A, **375**(23), 2230–2233, 2011.
15. G. Leonov, N. Kuznetsov. *Hidden attractors in dynamical systems*. Int. J. Bifurcat. Chaos, **23**(1), 1330002, 2013.
16. A. Chudzik, P. Perlikowski et al. *Multistability and rare attractors in van der Pol-Duffing oscillator*. Int. J. Bifurcat. Chaos, **21**(7), 1907–1912, 2011.
17. A. Shvets, S. Donetskyi. *Transition to Deterministic Chaos in Some Electroelastic Systems*. In: Skiadas C., Lubashevsky I. (eds) 11th Chaotic Modeling and Simulation International Conference. CHAOS 2018. Springer Proceedings in Complexity. Springer, Cham, 257–264, 2019.
18. E. Hairer, S.P. Norsett, G. Wanner G. *Solving ordinary differential equations. Nonstiff problems*. SpringerVerlag, Berlin, 1987.
19. Kouznetsov, S.P. Dynamic chaos. Physmatlit, Moscow, 2006.
20. N.A. Magnizkiy, S.V. Sidorov. *New methods of chaotic dynamics*. Editorial URSS, 2004.
21. A.A. Samarskii, A.V. Gulin. *Computational methods*. Moscow: Nauka, 430, 1989.

Bifurcation and Chaos in a Discrete Prey-Predator Model

Anuraj Singh[1] and Pradeep Malik[2]

[1] ABV-Indian Institute of Information Technology and Management Gwalior, M.P.,India
(E-mail: anuraj@iiitm.ac.in)
[2] Department of Mathematics, University of Petroleum and Energy Studies, Dehradun, Uttarakhand, India
(E-mail: pradeepmaths@gmail.com)

Abstract. In this paper, a modified Leslie-Gower predator-prey discrete model with Michaelis-Menten type prey harvesting is investigated. It is shown that the model exhibits several bifurcations of codimension 1 viz. Neimark-Sacker bifurcation, transcritical bifurcation and flip bifurcation on varying one parameter. The extensive numerical simulation is performed to demonstrate the analytical findings. The system exhibits periodic solution including flip bifurcation, Neimark-Sacker bifurcation followed by the wide range of dense chaos. .

Keywords: Discrete model, Codimension 1, Flip bifurcation, Neimark-Sacker bifurcation .

1 Introduction

The resource-consumer species interaction is one of the most common and focal research area in the field of mathematical biology. The dynamics of population models is concerned with population size, age distribution and many other natural factors. In biological systems, there are a number of models in which time is taken as a continuous function [1–3]. For population model this could be seen as a overlapping situation which implies a continuous series of birth and death processes and these models are usually performed by ordinary differential equations.
The discrete time population models are pertinent for non-overlapping generation models [4–6] and thus seems to be more realistic than continuous one. Many researchers investigated discrete-time models and gave interesting dynamics of the system by exploring several type of bifurcations [7–11].
The Lotka-Volterra prey-predator model with discrete time was firstly introduced by Maynard Smith [12] and studied by Levine [13] and Liu and Xiao [14]. It has been shown that these discrete time models undergo several bifurcations such as fold bifurcation, flip bifurcation and Neimark-Sacker bifurcation. Moreover, Hadelar and Gerstmann [15] were the first who derives a discrete time model involving Holling type-II functional response using continuous time model. Also the complete discussion for the bifurcations of codimension 1 and parametric restriction for non-hyperbolicity has been done by Li and Zhang [16]. In another study, the authors discussed the chaotic dynamics of a discrete

prey-predator model with Holling type-II functional response [6]. Singh and Deolia investigated a discrete-time the prey-predator model with Leslie-Gower functional response [11]. In their study the system exhibited Neimark-Sacker bifurcation, flip bifurcation and fold bifurcation under certain conditions.

2 Mathematical Model

Aziz-Alaoui and Daher Okiye [17] proposed the following two-dimensional prey-predator model with modified version of Leslie-Gower and Holling type II functional response:

$$\begin{aligned}\frac{dx}{dt} &= \left(r_1 - b_1 x - \frac{a_1 y}{k_1 + x}\right) x \\ \frac{dy}{dt} &= \left(r_2 - \frac{a_2 y}{k_2 + x}\right) y \end{aligned} \tag{1}$$

with positive initial conditions $x(0) \geq 0$ and $y(0) \geq 0$, when $x(t)$ and $y(t)$ represent the population densities at time t. Here r_1 denotes growth rate of prey and b_1 represents strength of competition among individuals in prey. The parameter $k_1(k_2)$ signifies the extent of protection provided by environment to the prey (predator) and r_2 describes the growth rate of y. $a_1(a_2)$ measures the maximum value per capita reduction rate of prey x (predator y). All the parameters are assumed to be positive.
The model (1) with Michaelis-Menten type harvesting under the assumption that same extent ($k_1 = k_2 = k$) to which environment provided protection to both the predator and prey [18,19] is given by:

$$\begin{aligned}\frac{dx}{dt} &= \left(r_1 - b_1 x - \frac{a_1 y}{k + x}\right) x - \frac{cEx}{m_1 E + m_2 x} \\ \frac{dy}{dt} &= \left(r_2 - \frac{a_2 y}{k + x}\right) y \end{aligned} \tag{2}$$

Here c signifies catchability coefficient and E denotes harvesting effort in prey species. Where m_1 and m_2 are suitable constants. All the parameters are assumed to be positive and similar meaning as of (1).
To investigate the dynamics of the system (2), the following non-dimensional scheme is taken:

$$x = \frac{r_1 x}{b_1}, \quad t = \frac{t}{r_1}, \quad y = \frac{r_1^2 y}{a b_1^2}$$

$$p = \frac{1}{b_1}, \quad \alpha = \frac{cEb_1}{m_2 r_1^2}, \quad \gamma = \frac{b_1 k}{r_1}, \quad \delta = \frac{m_1 E b_1}{m_2 r_1}, \quad \beta = \frac{r_2}{r_1}, \; q = \frac{a_2}{a_1 b_1}$$

Using the above scheme, we get the following non-dimensional system:

$$\begin{aligned}\frac{dx}{dt} &= x\left(1 - x - \frac{py}{\gamma + x} - \frac{\alpha}{\delta + x}\right) \\ \frac{dy}{dt} &= \beta y\left(1 - \frac{qy}{\gamma + x}\right) \end{aligned} \tag{3}$$

with the initial conditions $x(0) = x_0 \geq 0, \quad y(0) = y_0 \geq 0$.

Gupta and Chandra [20] investigated the continuous-time model (3) and determined several local bifurcations viz. Hopf bifurcation, saddle-node, transcritical bifurcation and Bogdanov-Takens bifurcation.
In order to derive discrete time model from the system (3) employing forward Euler scheme and taking ϵ is the step size. Letting $\epsilon \to 1$ then $(n+1)^{th}$ generation of the prey-predator population is governed by following set of equations:, it is obtained

$$\begin{aligned} x_{n+1} &= x_n + x_n\left(1 - x_n - \frac{py_n}{\gamma + x_n} - \frac{\alpha}{\delta + x_n}\right) \\ y_{n+1} &= y_n + \beta y_n\left(1 - \frac{qy_n}{\gamma + x_n}\right) \end{aligned} \tag{4}$$

with initial conditions $x(0) = x_0$, and $y(0) = y_0$.
Now, the discrete time prey-predator model can be defined by a mapping

$$G : \begin{pmatrix} x \\ y \end{pmatrix} \to \begin{pmatrix} x + x\left(1 - x - \frac{py}{\gamma+x} - \frac{\alpha}{\delta+x}\right) \\ y + \beta y\left(1 - \frac{qy}{\gamma+x}\right) \end{pmatrix} \tag{5}$$

The map (5) is considered for the region $\Omega = {\mathbb{R}_+}^2 = \{(x, y) : x \geq 0, y \geq 0\}$.

3 Existence and stability of fixed points

This section illustrates the existence and stability of the fixed points of the map (5).
The fixed points of the map (5) are summarized as follows:

1. The trivial fixed point is $E_0(0, 0)$.
2. The semitrivial fixed points are $E_{x_{1,2}}(x_{1,2}, 0)$, where

$$x_{1,2} = \frac{1}{2}\left(1 - \delta \pm \sqrt{(1-\delta)^2 - 4(\alpha - \delta)}\right),$$

   $\delta < 1$ and $(\delta + 1)^2 > 4\alpha$.
   - If $\alpha > \delta$, then $E_{x_{1,2}}(x_{1,2}, 0)$ both exits provided $(\delta + 1)^2 > 4\alpha$, $\delta < 1$.
   - If $\alpha < \delta$, then E_{x_1} exists only.
3. Another semitrivial fixed points is $E_y(0, \frac{\gamma}{q})$.
4. The positive fixed points are $E_{(xy)_{1,2}} = (x^*_{1,2}, y^*_{1,2})$, where $y^*_{1,2} = \frac{\gamma + x^*_{1,2}}{q}$ and $x^*_{1,2} = \frac{1}{2}\left((1 - \delta - \frac{p}{q}) \pm \sqrt{(1 - \delta - \frac{p}{q})^2 - 4\delta(\frac{p}{q} + \frac{\alpha}{\delta} - 1)}\right)$, where $\frac{p}{q} + \frac{\alpha}{\delta} > 1$.
   - $E_{(xy)_{1,2}}$ both exists, when $\frac{p}{q} + \delta < 1$ and $\left(1 - \delta - \frac{p}{q}\right)^2 > 4\delta\left(\frac{p}{q} + \frac{\alpha}{\delta} - 1\right)$.
   - If $\left(1 - \delta - \frac{p}{q}\right)^2 = 4\delta\left(\frac{p}{q} + \frac{\alpha}{\delta} - 1\right)$, then $\bar{E}(\bar{x}, \bar{y})$ exists, where $\bar{x} = \frac{1}{2}(1 - \delta - \frac{p}{q})$ and $\bar{y} = \frac{\gamma + \bar{x}}{q}$.

- If $\left(1-\delta-\frac{p}{q}\right)^2 < 4\delta\left(\frac{p}{q}+\frac{\alpha}{\delta}-1\right)$, no positive fixed point exists.

The Jacobian matrix for the discrete map (5) as arbitrary fixed point $(\widehat{x},\widehat{y})$ is given as

$$J(E)=\begin{pmatrix} 2-\left(2\widehat{x}+\frac{p\gamma\widehat{y}}{(\gamma+\widehat{x})^2}+\frac{\alpha\delta}{(\delta+\widehat{x})^2}\right) & -\frac{p\widehat{x}}{\gamma+\widehat{x}} \\ \frac{q\beta\widehat{y}^2}{(\gamma+\widehat{x})^2} & 1+\beta\left(1-\frac{2q\widehat{y}}{\gamma+\widehat{x}}\right) \end{pmatrix}.$$

The corresponding characteristic equation is written as

$$\lambda^2 - Tr\lambda + Det = 0 \tag{6}$$

where

$$Tr = 3+\beta-2\widehat{x}-\frac{p\gamma\widehat{y}}{(\gamma+\widehat{x})^2}-\frac{\alpha\delta}{(\delta+\widehat{x})^2}-\frac{2\beta q\widehat{y}}{\gamma+\widehat{x}}$$
$$Det = \left(2-2\widehat{x}-\frac{p\gamma\widehat{y}}{(\gamma+\widehat{x})^2}-\frac{\alpha\delta}{(\delta+\widehat{x})^2}\right)\left(1+\beta-\frac{2\beta q\widehat{y}}{\gamma+\widehat{x}}\right)+\frac{pq\beta\widehat{x}\widehat{y}^2}{(\gamma+\widehat{x})^3}$$

The dynamical behavior of the fixed points can be classified by the following lemma:

Lemma 1. *Consider a polynomial $\tau(\lambda)=\lambda^2-Tr\lambda+Det$, λ_1 and λ_2 be the eigenvalues. Suppose $\tau(1)>0$ then*

1. *$|\lambda_1|<1$ and $|\lambda_2|<1$ if and only if $\tau(-1)>0$ and $Det<1$;*
2. *$|\lambda_1|<1$ and $|\lambda_2|>1$ (or $|\lambda_1|>1$ and $|\lambda_2|<1$) if and only if $\tau(-1)<0$;*
3. *$|\lambda_1|>1$ and $|\lambda_2|>1$ if and only if $\tau(-1)>0$ and $Det>1$;*
4. *$\lambda_1=-1$ and $\lambda_2\neq 1$ if and only if $\tau(-1)=0$ and $Tr\neq 0,2$;*
5. *λ_1 and λ_2 are complex conjugate and $|\lambda_1|=|\lambda_2|$ if and only if $(Tr)^2-4Det<0$ and $Det=1$.*

3.1 Dynamical behavior around the trivial fixed point $E_0(0,0)$:

The Jacobian of (5) has eigenvalues $\lambda_1=2-\frac{\alpha}{\delta}$ and $\lambda_2=1+\beta$ at trivial fixed point E_0. The fixed point E_0 is a saddle when $\alpha>\delta$, a source when $\alpha<\delta$ and non-hyperbolic for both conditions $\alpha=\delta$ and $\alpha=3\delta$.

3.2 Dynamical behavior around the semitrivial fixed points:

(a) The eigenvalues of the Jacobian of the map (5) are $\lambda_1=2-2x_{1,2}-\frac{\alpha\delta}{(\delta+x_{1,2})^2}$ and $\lambda_2=1+\beta$ at semitrivial fixed point $E_{x_{1,2}}(x_{1,2},0)$. $E_{x_{1,2}}$ is a saddle point if $1<2x_{1,2}-\frac{\alpha\delta}{(\delta+x_{1,2})^2}<3$, a source if $0\leq 2x_{1,2}-\frac{\alpha\delta}{(\delta+x_{1,2})^2}<1$ and non-hyperbolic for both the conditions $2x_{1,2}-\frac{\alpha\delta}{(\delta+x_{1,2})^2}=1$ and $2x_{1,2}-\frac{\alpha\delta}{(\delta+x_{1,2})^2}=3$.

(b) The eigenvalues are $\lambda_1=2-\frac{p}{q}-\frac{\alpha}{\delta}$ and $\lambda_2=1-\beta$ at semitrivial fixed point $E_y(0,\frac{\gamma}{q})$.

3.3 Dynamical behavior at positive fixed point $E_{xy}(x^*, y^*)$:

The characteristic polynomial at $E_{xy}(x^*, y^*)$ is obtained as

$$\tau(\lambda) = \lambda^2 - (3 - \beta - A)\,\lambda + (2 - A + \beta(B-2))$$

where $A(x^*) = 2x^* + \frac{p\gamma}{q(\gamma+x^*)} + \frac{\alpha\delta}{(\delta+x^*)^2}$ and $B(x^*) = 2x^* + \frac{p}{q} + \frac{\alpha\delta}{(\delta+x^*)^2}$. The stability of the positive fixed point E_{xy} can be discussed by using the following results. The positive fixed point $E_{xy}(x^*, y^*)$ is said to be stable if:

$$\begin{aligned} &Tr(J(E_{xy})) - Det(J(E_{xy})) < 1 \\ &Tr(J(E_{xy})) + Det(J(E_{xy})) > -1 \\ &Det(J(E_{xy})) < 1. \end{aligned} \tag{7}$$

Theorem 1. *The dynamical behavior of the map (5) at positive fixed point $E_{xy}(x^*, y^*)$ is concluded as follows:*

1. *Sink when $\frac{2(A-3)}{B-3} < \beta < \frac{A-1}{B-2}$.*
2. *Source when $\beta > \max\left\{\frac{A-1}{B-2}, \frac{2(A-3)}{B-3}\right\}$ or $\beta < \frac{2(A-3)}{B-3}$.*
3. *Non-hyperbolic if one of the following condition holds:*
   (a) *$\beta = \frac{2(A-3)}{B-3}$, $\beta \neq \frac{A-2}{B-2}$ and $\beta \neq \frac{A}{B-2}$.*
   (b) *$\beta = \frac{A-1}{B-2}$ and $(1 + \beta + A)^2 < 4B\beta + 8$.*

4 Bifurcation of codimension 1

This subsection determines the conditions of occurrence of flip bifurcation and Neimark-Sacker bifurcation at positive fixed point $E_{xy}(x^*, y^*)$

Theorem 2. *(i) Flip bifurcation is occurred at $\beta = \frac{2(A-3)}{B-3}$ (ii) Neimark-Sacker bifurcation is occurred at $\beta = \frac{A-1}{B-2}$ around the positive fixed point $E_{xy}(x^*, y^*)$ in map (5).*

Proof.: It is clear, the Jacobian J has eigenvalues $|\lambda_1| \neq 1$ and $\lambda_2 = -1$ at the positive fixed point $E_{xy}(x^*, y^*)$ for $\beta = \frac{2(A-3)}{B-3}$. i.e. E_{xy} is non-hyperbolic.
Let $u = x - x^*$, $v = y - y^*$ and $\mu = \beta - \beta_1$, where $\beta_1 = \frac{2(A-3)}{B-3}$. The fixed point $E_{xy}(x^*, y^*)$ is shifted to the origin and expanding the right-hand side of map (5), it yields

$$\begin{pmatrix} u \\ v \end{pmatrix} \to \begin{cases} a_{11}u + a_{12}v + a_{13}uv + a_{14}u^2 + a_{15}u^2v + O(|u,v|^4) \\ b_{11}u + b_{12}v + b_{13}\mu + b_{14}v^2 + b_{15}\mu v + b_{16}u^2 + b_{17}\mu u \\ \qquad + b_{18}uv + b_{19}uv^2 + O(|u,v|^4) \end{cases}. \tag{8}$$

where $a_{11} = 2 - 2x^* - \frac{\alpha\delta}{(\delta+x^*)^2} - \frac{p\gamma y^*}{(\gamma+x^*)^2}$, $a_{12} = -\frac{px^*}{\gamma+x^*}$, $a_{13} = -\frac{p\gamma}{(\gamma+x^*)^2}$, $a_{14} = \left(\frac{\alpha\delta}{(\delta+x^*)^3} + \frac{p\gamma y^*}{(\gamma+x^*)^3} - 1\right)$, $a_{15} = \frac{p\gamma}{(\gamma+x^*)^3}$, $b_{11} = \frac{q\beta_1(y^*)^2}{(\gamma+x^*)^2}$, $b_{12} = 1 + \beta_1\left(1 - \frac{2qy^*}{\gamma+x^*}\right)$, $b_{13} = y^*\left(1 - \frac{qy^*}{\gamma+x^*}\right)$, $b_{14} = -\frac{q\beta_1}{\gamma+x^*}$, $b_{15} = \left(1 - \frac{2qy^*}{\gamma+x^*}\right)$, $b_{16} =$

$-\frac{q\beta_1(y^*)^2}{(\gamma+x^*)^3}$, $b_{17}=\frac{q(y^*)^2}{(\gamma+x^*)^2}$, $b_{18}=\frac{2q\beta_1 y^*}{(\gamma+x^*)^2}$ and $b_{19}=-\frac{q\beta_1(y^*)^2}{(\gamma+x^*)^3}$
Now linearizing the map (8) at $(0,0)$ and forming an invertible matrix,

$$T=\begin{pmatrix}\lambda_1-a_{11} & -a_{11}-1 & 0\\ a_{12} & a_{12} & 0\\ 0 & 0 & 1\end{pmatrix}.$$

By using the transformation $\begin{pmatrix}u\\ v\\ \mu\end{pmatrix}=T\begin{pmatrix}X\\ Y\\ w\end{pmatrix}$, the map (8) turns into

$$\begin{pmatrix}X\\ Y\\ w\end{pmatrix}\to\begin{pmatrix}\lambda_1 & 0 & 0\\ 0 & -1 & 0\\ 0 & 0 & 1\end{pmatrix}\begin{pmatrix}X\\ Y\\ w\end{pmatrix}+\begin{pmatrix}F_1(X,Y,w)\\ G_1(X,Y,w)\\ 0\end{pmatrix}$$

where

$$F_1(X,Y,w)=k_1X^2+k_2Y^2+k_3XY+k_4X^2Y+k_5XY^2+k_6X^3+O(|X,Y|^4)$$
$$G_1(X,Y,w)=e_1Y^2+e_2wY+k_3wX+e_4XY+e_5X^2+e_6X^3+e_7Y^3+O(|X,Y|^4).$$

Here $k_1=a_{12}a_{13}(\lambda_1-a_{11})+a_{14}(\lambda_1-a_{11})^2$, $k_2=a_{14}(1+a_{11})^2-a_{12}a_{13}(1+a_{11})$, $k_3=a_{12}a_{13}(\lambda_1-a_{11})-a_{12}a_{13}(1+a_{11})-2a_{14}(\lambda_1-a_{11})(1+a_{11})$, $k_4=a_{15}(\lambda_1-a_{11})^2-2a_{15}(\lambda_1-a_{11})(1+a_{11})$, $k_5=2a_{15}(1+a_{11})^2-2(\lambda_1-a_{11})(1+a_{11})$, $k_6=a_{15}(\lambda_1-a_{11})^2$, $e_1=b_{14}+b_{16}(1+a_{11})^2-b_{18}(1+a_{11})$, $e_2=b_{15}-b_{17}(1+a_{11})$, $e_3=b_{15}+b_{17}(\lambda_1-a_{11})$, $e_4=2b_{14}-2b_{16}(\lambda_1-a_{11})(1+a_{11})+b_{18}(\lambda_1-a_{11})-b_{18}(1+a_{11})$, $e_5=b_{14}+b_{16}(\lambda_1-a_{11})^2+b_{18}(\lambda_1-a_{11})$, $e_6=a_{12}^2(\lambda_1-a_{11})$ and $e_7=-a_{12}^2(1+a_{11})$
To discuss the stability of $(X,Y)=(0,0)$ near $w=0$, the center manifold is considered as

$$Z^c(0)=\{(X,Y,w)\in R^3|X=S(Y,w),S(0,0)=0,DS(0,0)=0\},$$

here X and w are sufficiently small. Let

$$S(Y,w)=S_1w^2+S_2wY+S_3Y^2+O(|Y,w|^3). \tag{9}$$

Then

$$\kappa(S(Y,w),w)=S(-Y+G_1(S(Y,w),Y,w))-\lambda_1S(Y,w)-F_1(S(Y,w),Y,w)=0. \tag{10}$$

Substituting (9) into (10) and comparing the coefficients of (10) we obtain $S_1=S_2=0$ and $S_3=\frac{k_2}{1-\lambda_1}$.
Then the map (8) restricted to the center manifold is given by

$$Y\sim\widetilde{G_1}(Y,w)=e_1Y^2-Y+e_2wY+e_3S_3wY^2+e_4S_3Y^3+e_5S_3^2Y^4+e_7Y^3+O|Y,w|^5$$

It can be seen that $\widetilde{G_1}(0,0)=0$, $\frac{\partial\widetilde{G_1}}{\partial Y}(0,0)=-1$, $\frac{\partial\widetilde{G_1}}{\partial w}(0,0)=0$, $\frac{\partial^2\widetilde{G_1}}{\partial Y^2}(0,0)=2e_1\neq 0$, $\frac{\partial^2\widetilde{G_1}}{\partial Yw}(0,0)=e_2\neq 0$ and $\frac{\partial^3\widetilde{F_1}}{\partial Y^3}(0,0)=6(e_4S_3+e_7)$.

$$\varrho_1 = \left(\frac{1}{2}\frac{\partial\widetilde{F_1}}{\partial w}\frac{\partial^2\widetilde{F_1}}{\partial X^2} + \frac{\partial^2\widetilde{F_1}}{\partial X w}\right)$$
$$\varrho_2 = \left(\left(\frac{1}{2}\frac{\partial^2\widetilde{F_1}}{\partial X^2}\right)^2 + \frac{1}{6}\frac{\partial^3\widetilde{F_1}}{\partial X^3}\right)$$

From above equation, $\varrho_1 = e_2 \neq 0$ and $\varrho_2 = e_4 S_3 + e_1^2 \neq 0$ (see more details [21,22]).
Therefore, the map (5) occurs flip bifurcation at fixed point E_{xy} for bifurcation parameter $\beta = \frac{2(A-3)}{B-2}$.
(ii) Now, we discuss Neimark-Sacker bifurcation at fixed point E_{xy} is non-hyperbolic at $\beta = \frac{A-1}{B-2}$ for $|\lambda_1| = 1$, $|\lambda_2| = 1$.
We transform the fixed point $E_{xy}(x^*, y^*)$ to the origin and expand the right-hand side of map (5) around the origin by using following translation $u = x - x^*$, $v = y - y^*$ and $\beta_1 = \frac{A-1}{B-2}$. The map (5) yields

$$\begin{pmatrix} u \\ v \end{pmatrix} \to \begin{cases} a_{11}u + a_{12}v + a_{13}uv + a_{14}u^2 + a_{15}u^2v + O(|u,v|^4) \\ b_{11}u + b_{12}v + b_{13}uv + b_{14}u^2 + b_{15}v^2 + b_{16}u^2v + b_{17}uv^2 + O(|u,v|^4) \end{cases} \tag{11}$$

where $a_{11} = 2 - 2x^* - \frac{\alpha\delta}{(\delta+x^*)^2} - \frac{p\gamma y^*}{(\gamma+x^*)^2}$, $a_{12} = -\frac{px^*}{\gamma+x^*}$, $a_{13} = -\frac{p\gamma}{(\gamma+x^*)^2}$, $a_{14} = \left(\frac{\alpha\delta}{(\delta+x^*)^3} + \frac{p\gamma y^*}{(\gamma+x^*)^3} - 1\right)$, $a_{15} = \frac{p\gamma}{(\gamma+x^*)^3}$, $b_{11} = \frac{q\beta(y^*)^2}{(\gamma+x^*)^2}$, $b_{12} = 1 + \beta\left(1 - \frac{2qy^*}{\gamma+x^*}\right)$, $b_{13} = \frac{2q\beta y^*}{(\gamma+x^*)^2}$, $b_{14} = -\frac{q\beta(y^*)^2}{(\gamma+x^*)^3}$, $b_{15} = -\frac{q\beta}{\gamma+x^*}$, $b_{16} = -\frac{2q\beta y^*}{(\gamma+x^*)^3}$, $b_{17} = \frac{q\beta}{(\gamma+x^*)^2}$.
Let us consider the following set of complex eigenvalues, obtained by linearizing the map (11) at $(0,0)$

$$\lambda_{1,2} = \frac{m(\beta) \pm \iota\sqrt{4n(\beta) - (m(\beta))^2}}{2}$$

with $|\lambda_{1,2}| = \sqrt{n(\beta)}$, followed by the transversality condition

$$\left(\frac{d|\lambda_{1,2}|}{d\beta}\right)_{\beta=\frac{A-1}{B-2}} = \frac{-1}{2\sqrt{n\left(\frac{A-1}{B-2}\right)}} \neq 0.$$

It is required to verify nondegeneracy condition ${\lambda^j}_{1,2} \neq 1, j = 1,2,3,4$ which is equivalent to $m(\beta) \neq 0, -1$ i.e. $A \neq \frac{4}{B-1}$ and $A \neq \frac{B+2}{B-1}$.
Now, assume an invertible matrix

$$T = \begin{bmatrix} a_{12} & 0 \\ M - a_{11} & N \end{bmatrix}$$

$M = \frac{m(\beta)}{2}$, $N = \sqrt{4n(\beta) - (m(\beta))^2}$.
The map (11) becomes

$$\begin{pmatrix} X \\ Y \end{pmatrix} \to \begin{pmatrix} M & -N \\ N & M \end{pmatrix}\begin{pmatrix} X \\ Y \end{pmatrix} + \begin{pmatrix} F_1(X,Y) \\ G_1(X,Y) \end{pmatrix} \tag{12}$$

$$F_1(X,Y) = k_{11}X^2 + K_{22}X^3 + k_{33}XY + k_{44}X^2Y + O(|X,Y|^4)$$
$$G_1(X,Y) = e_{11}X^2 + e_{22}Y^2 + e_{33}XY + e_{44}X^2Y + e_{55}X^3 + O(|X,Y|^4),$$

$k_{11} = a_{12}a_{13}(M-a_{11}) + a_{12}^2a_{14}$, $k_{22} = a_{12}^2a_{15}(M-a_{11})$, $k_{33} = -a_{12}a_{13}N$, $k_{44} = -a_{12}^2a_{15}N$, $e_{11} = a_{12}b_{13}(M-a_{11}) + a_{12}^2b_{14} + b_{15}(M-a_{11})^2 + a_{12}b_{17}(M-a_{11})^2$, $e_{22} = (b_{15} + a_{12}b_{17})N^2$, $e_{33} = -N(a_{12}b_{13} + 2b_{15}(M-a_{11}) + 2a_{12}b_{17}(M-a_{11}))$, $e_{44} = -a_{12}^2b_{16}N$ and $e_{55} = b_{16}a_{12}^2(M-a_{11})$.
It is easily noticed that (12) is exactly in form of center manifold, the non-degeneracy condition for the Neimark-Sacker bifurcation is given by

$$\hat{\beta} = -Re\left(\frac{(1-2\lambda)\bar{\lambda}^2}{1-\lambda}\Phi_{11}\Phi_{20}\right) - \frac{1}{2}|\Phi_{11}|^2 - |\Phi_{02}|^2 + Re(\bar{\lambda}\Phi_{21}) \tag{13}$$

where

$$\Phi_{20} = \frac{1}{4}\left[k_{11} + e_{33} + i(e_{11} - e_{22} - k_{33})\right]_{(0,0)}$$
$$\Phi_{11} = \frac{1}{2}\left[k_{11} + i(e_{11} + e_{22})\right]_{(0,0)}$$
$$\Phi_{02} = \frac{1}{4}\left[k_{11} - e_{33} + i(e_{11} - e_{22} + k_{33})\right]_{(0,0)}$$
$$\Phi_{21} = \frac{1}{8}\left[3k_{22} + e_{44} + i(3e_{55} - k_{44})\right]_{(0,0)}.$$

Thus, the aforementioned argument provides following theorem for the occurrence of Neimark-Sacker bifurcation [21,22]:

Theorem 3. *The map (5) undergoes Neimark-Sacker bifurcation if the both conditions $\beta \neq 3 - A$ and $\beta \neq 4 - A$ holds and $\hat{\beta} \neq 0$ at fixed point E_{xy}. Moreover, if $\hat{\beta} < 0$ ($\hat{\beta} > 0$) then a unique closed invariant curve bifurcates at $\beta = \frac{A-1}{B-2}$ which is supercritical (subcritical) and asymptotically stable (unstable).*

5 Numerical Simulation

In order to substantiate the obtained results and explore the complex dynamics in the map (5), the numerical simulation is performed for the following set of parameters [20]:

$$p = 0.40, \quad q = 1.0, \quad \alpha = 0.10, \quad \gamma = 0.10, \quad \delta = 0.05, \quad \beta = 0.25$$

For these set of parameters, the stability conditions of the fixed point $E_{xy}(x^*, y^*)$ are satisfied. Fig.1 shows the stable dynamics in the system (5). It confirms that both species coexist and converge to fixed point $E_{xy}(0.35, 0.45)$.
For these parameters, the results of first part of theorem 2 holds i.e. $\varrho_1 = -3.13426$, $\varrho_2 = 2741.9$, hence the system (5) undergoes flip bifurcation at E_{xy} and as $\varrho_2 > 0$ which shows period-2 point and its stability. Fig.2 gives bifurcation diagram for the parameter β at $\alpha = 0.095$ (without changing other

parameters). The system (5) exhibits flip bifurcation followed by chaos (period doubling route to chaos) at the parameter β. The system shows a stable window upto $\beta = 2.3$, followed by a cascade of period doubling. Further a dense chaotic region is occurred for $\beta \in (2.862, 3.012)$ along with intermittent quasi periodic windows at $(2.94, 2.952)$ which ends to a stable window beyond $\beta = 3.012$. The maximal Lyapunov exponent (MLE) for the same values is plotted in fig.3. The positive value of Lyapunov exponent confirms the presence of chaos in the system.

Further for substantiating the results of theorem 2(ii), we choose the new set of parameters

$$p = 0.9, \quad q = 2.0, \quad \alpha = 0.1695, \quad \gamma = 0.10, \quad \delta = 0.3$$

The value of nondegeneracy condition for Neimark-Sacker bifurcation is $\hat{\beta} = -0.13563 < 0$. According to theorem 3, the fixed point E_{xy} is stable when $\beta < \beta_1$, E^*_{xy} loses its stability and becomes unstable, a closed invariant curve appears when $\beta > \beta_1$. And $\hat{\beta} < 0$, supercritical NSB is occurred. The bifurcation diagram is plotted in (β, x) plane at $\beta_1 = 0.245$ in fig.4, a closed invariant curve appears.

6 Conclusion

In this paper, a discretized form of a modified Leslie-Gower prey-predator model with Michaelis-Menten type harvesting in prey, has been studied. Bifurcation theory and center manifold theory has been employed to exhibit various bifurcations of codimension 1 viz. Neimark-Sacker bifurcation, flip bifurcation. The approximate expression of bifurcation curves is also determined.The numerical simulation gives an extensive presentation about occurrence of different bifurcation and chaos.

References

1. J. B. Collings, The effects of the functional response on the bifurcation behavior of a mite predator–prey interaction model, J. Math. Biol., 36 (1997), 149–168.
2. J. Huang and D. Xiao, Analyses of bifurcations and stability in a predator-prey system with Holling type-IV functional response, Acta Math. Appl. Sinica Eng. Ser., 20 (2004), 167–178.
3. S. Ruan and D. Xiao, Global analysis in a predator-prey system with nonmonotonic functional response, SIAM J. Appl. Math., 61 (2001), 1445–1472.
4. L. Li and Z. J. Wang, Global stability of periodic solutions for a discrete predator–prey system with functional response, Nonlinear Dynam., 72, (2013) 507–516.
5. S. N. Elaydi, Discrete chaos: with applications in science and engineering, Chapman and Hall/CRC, (2007).
6. H. N. Agiza et al., Chaotic dynamics of a discrete prey–predator model with Holling type II, Nonlinear Anal. Real World Appl., 10(2009), 116–129.
7. W. Liu and D. Cai, Bifurcation, chaos analysis and control in a discrete-time predator–prey system, Adv. Difference Equ., Springer, 2019.

8. E. M. Elabbasy, A. A. Elsadany and Y. Zhang, Bifurcation analysis and chaos in a discrete reduced Lorenz system, Appl. Math. Comput., 228(2014), 184–194.
9. Q. Din, Complexity and chaos control in a discrete-time prey-predator model, Commun. Nonlinear Sci. Numer. Simul., 49(2017), 113–134.
10. A. Singh, A. A. Elsadany and A. Elsonbaty, Complex dynamics of a discrete fractional–order Leslie–Gower predator–prey model, Math. Methods Appl. Sci., 42(2019), 3992–4007.
11. A. Singh and P. Deolia, Dynamical analysis and chaos control in discrete-time prey-predator model, Commun. Nonlinear Sci. Numer. Simul., 90(2020), 105313.
12. J.M. Smith, Mathematical Ideas in Biology, Cambridge University Press, Cambridge, (1968).
13. S. H. Levine, Discrete time modeling of ecosystems with applications in environmental enrichment, Math. Biosci., 24(1975), 307–317.
14. X. Liu and D. Xiao, Bifurcations in a discrete time Lotka-Volterra predator-prey system, Discrete Contin. Dyn. Syst. Ser. B, 69 (2006), 559–572.
15. K. P. Hadeler and I. Gerstmann, The discrete Rosenzweig model, Math. Biosci., 98(1990), 49–72.
16. S. Li and W. Zhang, Bifurcations of a discrete prey-predator model with Holling type II functional response, Discrete Contin. Dyn. Syst. Ser B, 14 (2010), 159–176.
17. M. A. Aziz-Alaoui and M. Daher Okiye, Boundedness and global stability for a predator-prey model with modified Leslie-Gower and Holling-Type II schemes, Appl. Math. Lett., 16(2003), 1069–1075.
18. C. Ji, D. Jiang and N. Shi, Analysis of a predator-prey model with modified Leslie-Gower and Holling-type II schemes with stochastic perturbation, J. Math. Anal. Appl., 359(2009), 482–498.
19. C. Ji, D. Jiang and N. Shi, A note on a predator-prey model with modified Leslie-Gower and Holling-type II schemes with stochastic perturbation, J. Math. Anal. Appl., 377(2011), 435–440.
20. R. P. Gupta and P. Chandra, Bifurcation analysis of modified Leslie-Gower predator-prey model with Michaelis-Menten type prey harvesting, J. Math. Anal. Appl., 398 (2013), 278–295.
21. Y, Kuznetsov, Elements of Applied Bifurcation Theory, Springer-Verlag, New York, (1998).
22. J. Huang et al., Bifurcations in a discrete predator–prey model with nonmonotonic functional response, J. Math. Anal. Appl., 464(2018), 201–230.

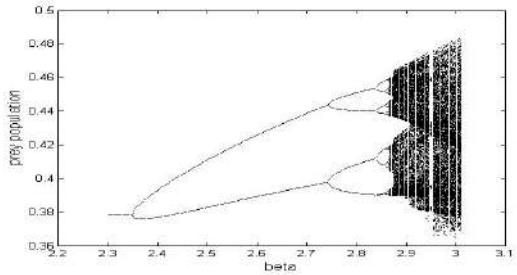

Fig. 1. Bifurcation diagram w. r. to β

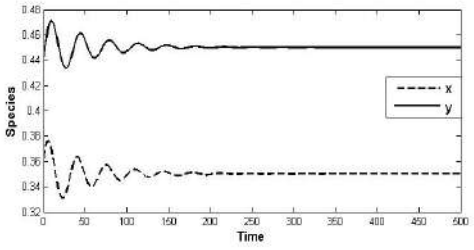

Fig. 2. Stable time series at $\beta = 0.25$

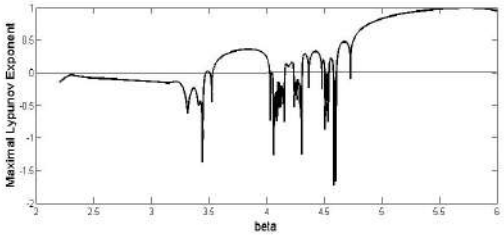

Fig. 3. Maximal Lyaupnov exponent w. r. to β

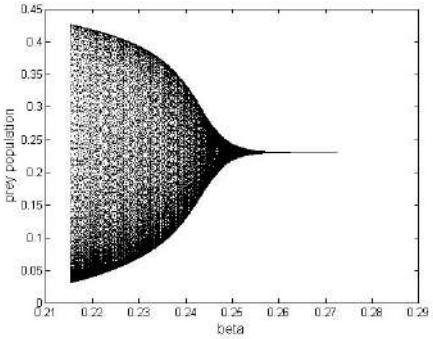

Fig. 4. NSB diagram w. r. to β

Connecting Bernoulli and Schrödinger Equations and its Impact on Quantum-Mechanic Wave Function and Entanglement Problems

Siavash H. Sohrab

Northwestern University, Robert R. McCormick School of Engineering and Applied Science, Department of Mechanical Engineering, 2145 Sheridan Road, Evanston, Illinois 60208-3111, U.S.A.
E-mail: s-sohrab@northwestern.edu

Abstract. An invariant model of Boltzmann statistical mechanics is applied to derive invariant Schrödinger equation of quantum mechanics from invariant Bernoulli equation of hydrodynamics. The results suggest new perspectives regarding quantum mechanics wave function and its collapse, stationary versus propagating wave functions, and wave-particle duality. The invariant hydrodynamic model also leads to the definition of generalized shock waves in "supersonic" flows at molecular-, electro-, and chromo-dynamic scales with (*Mach, Lorentz, and Michelson*) numbers exceeding unity. The invariant internal hydro-thermo-diffusive structure of such generalized "shock" waves are described.

1 Introduction

It is well known that our universe involves statistical fields at five major scales that are approximately separated by a factor of 10^{-17}, beginning at exceedingly small Planck scale of 10^{-35} m, electrodynamics 10^{-17}m, molecular-dynamics 10^{0} m, astrophysics 10^{17} m, and finally cosmology 10^{35} m, with each statistical field having a characteristic "atomic" particle graviton, electron, molecule, star, and galaxy. Schematic diagram in Fig. 1 shows hierarchies of such statistical fields from photonic to cosmic scales. Under the assumption of weak interactive forces known as ideal gas, Boltzmann statistical mechanics governs the generalized thermodynamics associated with such statistical fields of diverse scales. Studies on generalized Boltzmann statistical mechanics and turbulent phenomena that are common universal features shared by stochastic quantum fields [1-17] and classical hydrodynamic fields [18-30] resulted in recent introduction of a scale-invariant model of statistical mechanics and its applications to thermodynamics [31, 32], fluid mechanics [33,34], and quantum mechanics [35-37] at intermediate, large, and small scales.

In the present study, after a brief description of a scale-invariant model of statistical mechanics, the invariant forms of conservation equations are presented. Next, derivation of invariant Schrödinger equation from invariant Bernoulli equation for potential incompressible flow is discussed. The nature of quantum mechanics wave functions for both time-independent and time-dependent Schrödinger equations respectively associated with time-periodic stationary versus propagating states are identified. Also, the objective (real)

versus subjective (imaginary) aspects of wave function [3] in connection to particle localization and Born probabilistic interpretation are studied.

The invariant forms of conservation equations result in introduction of an invariant definition of Mach number leading to a hierarchy of generalized normal "shock" waves from photonic to cosmic scales. The internal hydro-thermo-diffusive structure of such shock waves is examined and some of its implications to dissipation in quantum gravity and black holes are discussed.

2 Scale–Invariant Model of Boltzmann Statistical Mechanics

The scale-invariant model of statistical mechanics for equilibrium galactic-, planetary-, hydro-system-, fluid-element-, eddy-, cluster-, molecular-, atomic-, subatomic-, kromo-, and tachyon-dynamics corresponding to the scale β = g, p, h, f, e, c, m, a, s, k, and t is schematically shown on the left hand side of Fig. 1.

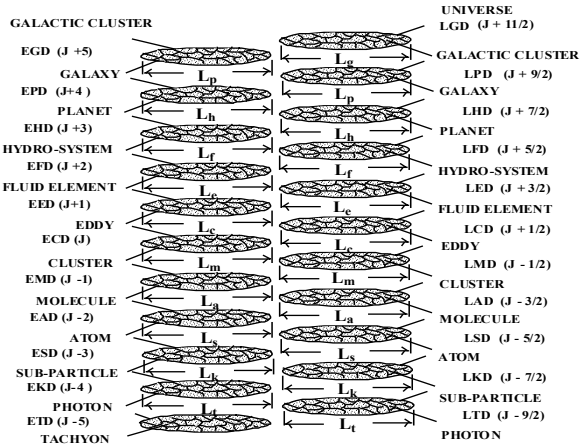

Fig. 1. A scale-invariant model of statistical mechanics. Equilibrium-β-Dynamics on the left-hand-side and non-equilibrium Laminar-β-Dynamics on the right-hand-side for scales β = g, p, h, f, e, c, m, a, s, k, and t as defined in [35]. Characteristic lengths of (system, element, "atom") are $(L_\beta, \lambda_\beta, \ell_\beta)$ and λ_β is the mean-free-path.

For each statistical field, one defines particles that form the background fluid and are viewed as point-mass or "*atom*" of the field. Next, the *elements* of the field are defined as finite-sized composite entities composed of an ensemble of "*atoms*". Finally, ensemble of a large number of "*elements*" is defined as the statistical "*system*" at that particular scale. The most-probable element of scale β is identified as the "atom" (system) of the next higher β+1 (lower β–1) scale.

Following the classical methods [19, 38-42], the invariant definitions of the density ρ_β, and the velocity of *atom* $\mathbf{u}_\beta$, *element* $\mathbf{v}_\beta$, and *system* $\mathbf{w}_\beta$ at the scale β are given as [36]

$$\rho_\beta = n_\beta m_\beta = m_\beta \int f_\beta du_\beta \quad , \quad \mathbf{u}_\beta = \mathbf{v}_{w\beta-1} \tag{1}$$

$$\mathbf{v}_\beta = \rho_\beta^{-1} m_\beta \int \mathbf{u}_\beta f_\beta du_\beta \quad , \quad \mathbf{w}_\beta = \mathbf{v}_{w\beta+1} \tag{2}$$

Similarly, the invariant definitions of the peculiar and diffusion velocities are introduced as

$$\mathbf{V}'_\beta = \mathbf{u}_\beta - \mathbf{v}_\beta \quad , \quad \mathbf{V}_\beta = \mathbf{v}_\beta - \mathbf{w}_\beta \quad , \quad \mathbf{V}_\beta = \mathbf{V}'_{\beta+1} \tag{3}$$

Following the classical methods [19, 38-40], the scale-invariant forms of mass, thermal energy, linear and angular momentum conservation equations at scale β are given as [33, 34]

$$\frac{\partial \rho_{i\beta}}{\partial t_\beta} + \nabla.(\rho_{i\beta}\mathbf{v}_\beta) = \Re_{i\beta} \tag{4}$$

$$\frac{\partial \varepsilon_{i\beta}}{\partial t_\beta} + \nabla.(\varepsilon_{i\beta}\mathbf{v}_\beta) = 0 \tag{5}$$

$$\frac{\partial \mathbf{p}_{i\beta}}{\partial t_\beta} + \nabla.(\mathbf{p}_{i\beta}\mathbf{v}_\beta) = -\nabla.\mathbf{P}_{ij\beta} \tag{6}$$

$$\frac{\partial \boldsymbol{\pi}_{i\beta}}{\partial t_\beta} + \nabla.(\boldsymbol{\pi}_{i\beta}\mathbf{v}_\beta) = \rho_{i\beta}\boldsymbol{\omega}_\beta.\nabla\mathbf{v}_\beta \tag{7}$$

involving the *volumetric density* of thermal energy $\varepsilon_{i\beta} = \rho_{i\beta}\tilde{h}_{i\beta}$, linear momentum $\mathbf{p}_{i\beta} = \rho_{i\beta}\mathbf{v}_{i\beta}$, and angular momentum $\boldsymbol{\pi}_{i\beta} = \rho_{i\beta}\boldsymbol{\omega}_{i\beta}$. Also, $\Re_{i\beta}$ is the chemical reaction rate and $\tilde{h}_\beta$ is the absolute enthalpy [32].

It is noted that the time coordinates in Eqs. (4-7) also have a scale subscript β. In a recent study [43], the nature of physical space and time was investigated and the concepts of *internal spacetime* versus *external space and time* were introduced. Assuming that a statistical field at scale β is in thermodynamic equilibrium with the physical space at scale (β −1) within which is resides, both fields will have a homogenous constant temperature $T_\beta = T_{\beta-1}$ defined in terms of Wien wavelength of particle thermal oscillations as [32]

$$m_\beta u_\beta^2 = m_{\beta-1} v_{w\beta-1}^2 = kT_{\beta-1} = k\lambda_{w\beta-1} \tag{8a}$$

Hence, constant internal measures of (extension $\lambda_{w\beta}$, duration $\tau_{w\beta}$) will be associated with every "point" of space at temperature $T_\beta = T_{\beta-1}$. For example,

at cosmic scale $\beta = g$ one employs internal (ruler, clock) of the lower scale of astrophysics $\beta = s$ to define *external space and time* coordinates defined as [43]

$$(x_\beta, y_\beta, z_\beta) = (N_{x\beta}, N_{y\beta}, N_{z\beta})\lambda_{wx\beta-1} \quad , \quad t_\beta = N_{t\beta}\tau_{w\beta-1} \tag{8b}$$

with the four numbers $(N_{x\beta}, N_{y\beta}, N_{z\beta}, N_{t\beta})$ being independent numbers.

3 Derivation of Invariant Schrödinger Equation from Invariant Bernoulli Equation

The connection between energy spectrum of photon gas given by *Planck* [44] distribution and both energy and dissipation spectrum of isotropic stationary turbulence has been recognized [35, 36]. In a recent study [35], the gap between problems of quantum mechanics and turbulence was investigated through connections between Cauchy, Euler, Bernoulli equations of hydrodynamics, Hamilton-Jacobi equation of classical mechanics, and Schrödinger equation of quantum mechanics. In a more recent investigation on foundation of classical thermodynamics [32] it was shown that stochastic definitions of Planck $h = h_k \equiv m_k \lambda_{rk} c$ and Boltzmann $k = k_k \equiv m_k \nu_{rk} c$ universal constants involve the speed of light identified as *root-mean-square speed of photons* $c = v_{rk}$ in Casimir [45] vacuum. The new insights into the statistical nature of both Planck and Boltzmann universal constants as well as the definition of absolute temperature [32] suggest a slightly modified derivation of Schrödinger equation [35, 46] discussed in the following.

For potential flow $\nabla \times \mathbf{v}_\beta = 0$ with velocity $\mathbf{v}_\beta = -\nabla \Phi_\beta$ [35], equation (6) leads to invariant Bernoulli equation

$$-\frac{\partial m\Phi_\beta}{\partial t'} + \frac{(\nabla m\Phi_\beta)^2}{2m} + \tilde{V}_\beta = 0 \tag{9}$$

where the atomic potential energy is $\tilde{V}_\beta = (p_\beta / \rho_\beta) m_\beta = p_\beta / n_\beta = p_\beta \hat{v}$. By Eq. (3), local velocity in an arbitrary direction is expressed in terms of the most probable or Wien velocity of the lower scale and peculiar velocity as perturbation

$$\mathbf{v}_{x\beta} = \mathbf{u}_{x\beta} - \varepsilon \mathbf{V}'_{x\beta} = \mathbf{v}_{wx\beta-1} - \varepsilon \mathbf{V}'_{x\beta} \quad , \quad \varepsilon << 1 \tag{10}$$

In absence of vorticity $\nabla \times \mathbf{v}_\beta = \nabla \times \mathbf{v}_{w\beta-1} = \nabla \times \mathbf{V}'_\beta = 0$ equation (10) gives

$$m_\beta \Phi_\beta = m_\beta \Phi_{w\beta\text{-}1} - \varepsilon m_\beta \Phi'_\beta \tag{11}$$

Comparison of Eq. (9) with Hamilton-Jacobi equation of classical mechanics [2] leads to the definition of invariant action [36]

$$S_\beta(x'_\beta, t'_\beta) = -m_\beta \Phi_\beta = -m_\beta \Phi_{w\beta\text{-}1} + \varepsilon m_\beta \Phi'_\beta = S_{w\beta\text{-}1} - \varepsilon S'_\beta \tag{12}$$

and quantum mechanics *wave function* Ψ_β defined as

$$\Psi_\beta(x'_\beta, t'_\beta) = -S'(x'_\beta, t'_\beta) / m_\beta = \Phi'_\beta \tag{13}$$

Substitution from equations (12)-(13) into Bernoulli Eq. (9) and separation of zeroth and first power of ε leads to [35]

$$\frac{\partial S_{w\beta}}{\partial t'_\beta} + \frac{(\nabla S_{w\beta})^2}{2m} + \tilde{V}_\beta = 0 \tag{14}$$

$$\frac{\partial \Psi_\beta}{\partial t'_\beta} + (v_{wx'})_{\beta\text{-}1} \nabla \Psi_\beta + \frac{\varepsilon}{2} (\nabla \Psi_\beta)^2 = 0 \tag{15}$$

To reveal the "*stationary states*" of the system one moves to coordinate system moving at the most-probable speed

$$z'_\beta = x'_\beta - (v_{wx'})_{\beta\text{-}1} t'_\beta \tag{16}$$

The solution of equation (14) results in conservation of energy due to internal and peculiar translational motions

$$\tilde{E}_{t\beta} = \tilde{T}_{t\beta} + \tilde{V}_\beta \tag{17}$$

where

$$\tilde{E}_{t\beta} \equiv m_\beta v^2_{wx\beta\text{-}1} \quad , \quad \tilde{T}_{t\beta} \equiv m_\beta v^2_{wx\beta\text{-}1} / 2 \quad , \quad \tilde{V}_\beta \equiv p\hat{v} = m_\beta V'^2_{x\beta} / 2 \tag{18}$$

The equality of translational kinetic and potential energies $\tilde{T}_{t\beta} = \tilde{V}_{t\beta}$ is in accordance with Boltzmann equipartition principle. In Eq. (18) the velocities refer to periodic motions in direction of a single translational coordinate say (x+, x-) and Eq. (17) corresponds to *atomic translational enthalpy* [32]

$$\hat{h}_{t\beta} = \hat{u}_{t\beta} + p_\beta \hat{v}_\beta = 2kT_\beta \tag{19}$$

where $\hat{u}_{t\beta} = mv^2_{wx} = mv^2_{wx+} / 2 + mv^2_{wx-} / 2 = mv^2_{wx+}$ is *atomic internal translational kinetic energy* [32].

As described in [32], the conventional assumption of particle undergoing translational motion along three degrees of freedom (x, y, z) is not appropriate since particle cannot *simultaneously* move in three independent coordinate directions. Also, according to Clausius [47], the kinetic energy due to random rotational and vibrational motions of particles cannot be properly neglected. Therefore, as discussed in [32], the conventionally assumed random translational kinetic energy in (y+, y-) and (z+, z-) directions are instead respectively attributed to particle rotational (θ+, θ-) and vibrational (r+, r-) kinetic energies [32]

$$\hat{u}_{ty\beta} \equiv m_\beta v_{wy\beta}^2 \qquad \Rightarrow \qquad \hat{u}_{r\beta} \equiv I_\beta \varpi_{\theta\beta}^2 = kT_\beta \tag{20a}$$

$$\hat{u}_{tz\beta} \equiv m_\beta v_{wz\beta}^2 \qquad \Rightarrow \qquad \hat{u}_{v\beta} \equiv k_\beta r_\beta^2 = kT_\beta \tag{20b}$$

According to equations (19-20), particles have four *simultaneously independent* degrees of freedom namely, translational, rotational, vibrational, and potential. Boltzmann principle of equipartition of energy requires that all four degrees of freedom have the same energy resulting in atomic internal energy and atomic enthalpy of ideal gas respectively defined as [32]

$$\tilde{E}_\beta = \hat{u}_\beta = \hat{u}_{t\beta} + \hat{u}_{r\beta} + \hat{u}_{v\beta} = 3kT_\beta \tag{21}$$

$$\tilde{H}_\beta = \hat{h}_\beta = \hat{u}_\beta + p_\beta \hat{v}_\beta = 4kT_\beta \tag{22}$$

Total internal energy, potential energy, and enthalpy are respectively $N_\beta \tilde{E}_\beta = N_\beta \hat{u}_\beta = U_\beta$, $N_\beta \tilde{V}_\beta = p_\beta V_\beta$, and $N_\beta \tilde{H}_\beta = N_\beta \hat{h}_\beta = H_\beta$ such that [32]

$$H_\beta = U_\beta + p_\beta V_\beta \tag{23}$$

In summary, by the above procedure Bernoulli equation in "three dimension" accounts for three types of *internal kinetic energies* $\tilde{E}_\beta$ as well as potential energy $\tilde{V}_\beta = p_\beta \hat{v}_\beta$ that is also a *kinetic energy* due to random *external peculiar motion* of particles. Another perspective concerning the results in Eqs. (19) and (20) is to view the particle as a small cylindrical object with period oscillations in axial (z+, z-), angular (θ+, θ-), and radial (r+, r-) directions in a cylindrical coordinate (z, θ, r) system.

Next, Bernoulli equation in the first order of ε is considered. In the limit $\varepsilon \to 0$, taking time derivative of Eq. (15) and substituting for $\partial \Psi_\beta / \partial t'_\beta$ in the resulting equation from Eq. (15) itself leads to the wave equation [35]

$$\frac{\partial^2 \Psi_\beta}{\partial t_\beta'^2} = \mathrm{v}_{\mathrm{w}\beta\text{-}1}^2 \nabla_{z'}^2 \Psi_\beta \tag{24}$$

Since wave function in Eq. (24) guides the motion of "particle" that is a singularity on the wave, one moves to the adjacent lower scale (β–1) and introduces *space and time coordinates* [35, 43]

$$\zeta = (z_\beta' - z_o') / \varepsilon \quad , \quad \tau = (t_\beta' - t_o') / \varepsilon \tag{25}$$

It is important to emphasize that the time and space coordinates (25) are based on internal *spacetime* governed by thermodynamic temperature $\mathrm{T}_{\beta-1}$ as discussed in [43]. Internal wavelength and frequency are not independent and wave number $k_\beta \equiv 2\pi / \lambda_\beta$ and angular frequency $\omega_\beta \equiv 2\pi \nu_\beta$ must follow the relations

$$k_{\mathrm{w}\beta} = 3k_{\mathrm{r}\beta} \quad , \quad \omega_{\mathrm{w}\beta} = \sqrt{3}\omega_{\mathrm{r}\beta} \tag{26}$$

in order to satisfy the relationship between root-mean–square and most-probable speeds $\mathrm{v}_{\mathrm{r}+\beta} = \sqrt{3}\mathrm{v}_{\mathrm{w}\beta}$ [43]. Therefore, one introduces the scaled space and time coordinates

$$\xi_\beta = 3\zeta_\beta \quad , \quad t_\beta = \sqrt{3}\tau_\beta \tag{27}$$

Substitution from Eq. (27) into Eq. (24) leads to the wave equation $\mathrm{v}_{\mathrm{r}+\beta} = \sqrt{3}\mathrm{v}_{\mathrm{w}\beta}$

$$\frac{\partial^2 \Psi_\beta}{\partial t_\beta^2} = \mathrm{c}_{\beta\text{-}1}^2 \nabla_\xi^2 \Psi_\beta \tag{28}$$

with root-mean-square speed or speed of "sound" defined as $\mathrm{c}_\beta^2 = \mathrm{v}_{\mathrm{r}^+\beta}^2 = 3\mathrm{v}_{\mathrm{w}\beta}^2$.

The separated product solution of Eq. (28) is the complex wave function

$$\Psi_\beta = \Phi_\beta'(\zeta, \tau) = \mathrm{e}^{i3k_\mathrm{r}\zeta}\ \mathrm{e}^{-i\sqrt{3}\omega_\mathrm{r}\tau}\ = \Phi_\beta'(\xi, t) = \mathrm{e}^{ik_\mathrm{r}\xi}\ \mathrm{e}^{-i\omega_\mathrm{r}t} \tag{29}$$

with frequency $\omega_{\mathrm{r}\beta-1}$ associated with *stationary state* thus the vanishing of time dependence. In other words, because at stationary state the mean velocity must

be zero, the frequency relation $\hbar^2\omega_r^2 = 2\hbar^2\omega_{r+}^2$ must hold in order to maintain the stationary internal kinetic energy given by the relation from Eq. (21).

The wave equation (28) and the solution in Eq. (29) after substitution from Eq. (23) for internal energy $\tilde{U}_\beta$ result in the *invariant time-independent Schrödinger equation* [35, 37, 48]

$$\frac{\hbar^2}{2m_\beta}\nabla_\xi^2\psi_\beta + (\tilde{H}_\beta - \tilde{V}_\beta)\psi_\beta = 0 \tag{30}$$

By equations (13, 27-30) ψ_β represent stationary state of spatial geometry of velocity potential $\Phi'_\beta(\xi)$ governing the peculiar motion of particles. Clearly, any interference with the stationary field by a measuring device will disturb the velocity potential and hence lead to "*collapse of the wave function*" ψ_β.

The time-independent Schrödinger equation is next employed to define a new time-dependent wave function

$$\Psi_\beta(\xi,t) = \Phi'_\beta(\xi,t) = \psi_\beta(\xi)e^{-2i\omega_r t'_\beta} = \psi_\beta(\xi)e^{-(4/3)i\omega_{r+}t_\beta} \tag{31}$$

involving a new time coordinate $t'_\beta = (2/3)^{1/2}\tau_\beta = (\sqrt{2}/3)t_\beta$. The multiplicative factor of two in frequency is because the period of traveling wave is half of that of stationary wave. The wave function in Eq. (31) with the factor of (4/3) multiplying the frequency $\omega_{r+\beta}$ results in total atomic thermal energy or atomic enthalpy $(4/3)\hbar\omega_{r+\beta} = (4/3)mv_{r+\beta}^2 = 4mv_{w\beta}^2 = 4kT_\beta = \tilde{H}_\beta$. In view of the definition of invariant Planck constant $h_\beta = m_\beta\lambda_{r\beta}v_{r\beta} = h$ [32], equation (31) gives energy and momentum *operators* [49]

$$i\hbar_\beta\frac{\partial\Psi_\beta}{\partial t_\beta} = \tilde{H}_\beta\Psi_\beta \tag{32a}$$

$$-i\hbar_\beta\frac{\partial\Psi_\beta}{\partial\xi_\beta} = \bar{p}_{r\beta}\Psi_\beta \tag{32b}$$

where $\bar{p}_{r\beta} = m_\beta v_{r\beta}$ is the root-mean-square momentum. Multiplying Eq. (30) by the new time-dependent part $e^{-(4/3)i\omega_{r+}t_\beta} = e^{-i\tilde{H}t_\beta/\hbar}$ from Eq. (31) and substitution from Eq. (32a) leads to the *invariant time-dependent Schrödinger equation* [35, 48]

$$i\hbar_\beta \frac{\partial \Psi_\beta}{\partial t_\beta} + \frac{\hbar_\beta^2}{2m_\beta}\nabla_\xi^2 \Psi_\beta - \tilde{V}_\beta \Psi_\beta = 0 \tag{33}$$

Therefore, the energy in Eq. (32a) corresponding to the classical Hamiltonian is the atomic enthalpy $\tilde{H}_\beta = (4/3)mc_\beta^2 = (4/3)(3mv_{w\beta}^2) = 4kT_\beta$ that is the sum of the atomic *internal energy* $\tilde{E}_\beta = mv_{r+\beta}^2 = mc_\beta^2 = 3mv_{w\beta}^2 = 3kT_\beta$ and *atomic potential energy* $\tilde{V}_\beta = mV_{x\beta}'^2 = p_\beta \hat{v}_\beta = \tilde{U}_\beta / 3 = kT_\beta$. Hence, enthalpy as the sum of kinetic or "*electromagnetic*" energy $\tilde{U}_\beta$ and potential or "*gravitational*" energy $\tilde{V}_\beta$ of equilibrium radiation in enclosures is in exact agreement with the pioneering prediction of Hasenöhrl [50, 51]

$$\tilde{H}_\beta = \tilde{E}_\beta + \tilde{V}_\beta = mc_\beta^2 + (1/3)mc_\beta^2 = (4/3)mc_\beta^2 \tag{34}$$

However, as opposed to $\tilde{E}_\beta = (p_x^2 + p_y^2 + p_z^2)/2m$ in classical model [49], the atomic internal energy is now defined as the kinetic energy associated with internal translational, rotational, and vibrational degrees of freedom [32] in accordance with Eq. (21).

Since the most probable element at scale β is the entire system of statistical field at lower scale β−1 (see Fig.1), once again one finds a velocity potential $\Phi'_{\beta-1}$ hence a new wave function $\Psi_{\beta-1} = \Phi'_{\beta-1}$. Therefore, in harmony with de Broglie [2, 3] picture of quantum mechanics, motion of "*particle*" or "*wave-packet*" is guided by an external wave function as shown in Fig. 2.

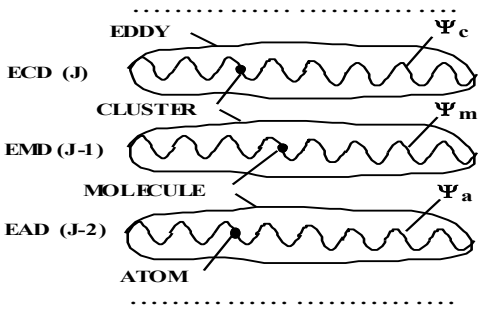

Fig. 2 Macroscopic wave functions Ψ_β or de Broglie guidance waves at (ECD), (EMD), and (EAD) scales that guide particles identified as wave-packets or de Broglie matter-waves [46].

As an example, let us consider stationary fluid corresponding to the field of equilibrium cluster-dynamics $\beta = c$ where the "atom" is a cluster $\mathbf{u}_c = \mathbf{v}_{wm}$ that by Eq. (2) is the most-probable element of the adjacent lower scale of equilibrium molecular-dynamics $\beta-1 = m$. The random motion of clusters accounts for the phenomena of Brownian motions as discussed in [35]. The molecules as sub-particles of $\beta = c$ field are confined within the most-probable molecular-cluster that is stabilized by an external force induced by *Poincaré stress* [35] and follow the wave equation (28) hence Schrödinger equation (30). It is important to emphasize that the wave equation (28) for quantum mechanics wave function Ψ_c by definition (13) is the velocity potential of the peculiar particle velocity in ECD field. Therefore, in harmony with de Broglie picture of quantum mechanics [2, 3], the "outer" scale $\beta = c$ wave function $\Psi_\beta = \Psi_c$ guides the motion of particle or molecule identified as wave-packet as shown in Fig. 2.

In order to connect the quantum mechanics wave function to *particle localization*, one moves to the stationary coordinates in Eq. (16) and obtains for the first perturbation of density $\rho'_\beta = \rho_{o\beta} + \varepsilon\rho_\beta$ from continuity equation (4) in the absence of chemical reactions

$$\frac{\partial \rho_\beta}{\partial \tau_\beta} + v_w . \nabla_\zeta \rho_\beta = 0 \tag{35}$$

Taking time derivative of Eq. (35) and substituting for $\partial\rho_\beta / \partial\tau_\beta$ in the resulting equation from equation (35) itself one obtains the wave equation propagating at $v_{w\beta-1}$ similar to Eq. (24) that after the introduction of scaled coordinates in Eq. (27) leads to the density wave equation [52]

$$\frac{\partial^2 \rho_\beta}{\partial t_\beta^2} = c_{\beta-1}^2 \nabla_\xi^2 \rho_\beta \tag{36}$$

Hence, under *stationary states*, density hence particle localization correlate with quantum mechanics wave function Ψ_β. Indeed, by equations (35) and (36) it can be shown that $\rho_\beta^{1/2}$ also satisfies a wave equation similar to Eq. (36) that when combined with Eq. (28) through cross-multiplication result in a new solution hence a modified quantum mechanics wave function $\mathbf{\Psi}_\beta = \rho_\beta^{1/2}\Psi_\beta$ such that $\mathbf{\Psi}_\beta \mathbf{\Psi}_\beta^* = \rho_\beta$ in harmony with the classical result [49]. Therefore, both objective and subjective aspect of quantum mechanics wave function discussed by de Broglie [3] are clarified. This is because density is the real hence

objective part of Ψ_β that accounts for particle localization. On the other hand, the complex i.e. imaginary part of Ψ_β is its *subjective* part that accounts for normalization hence success of Born [53] probabilistic interpretation of Ψ_β.

The results shown in Fig. 2 and the *objective* versus *subjective* aspects of Ψ_β discussed above also resolve the *wave-particle duality* problem in quantum mechanics. This is because particle that appears as a local singularity is actually a de Broglie *wave packet* at scale $\beta-1$ that is embedded within and is guided by an "external" complex hence virtual wave function Ψ_β associated with velocity potential of peculiar atomic motions in the background *space* composed of atoms of the same scale. The adjective "*external*" is because the velocity potential $\Psi_\beta = \Phi'_\beta$ refers to peculiar motion at outer scale β.

According to the new paradigm of physical foundation of quantum mechanics each equilibrium statistical field is composed of a spectrum of cluster or wave-packet sizes containing "atoms" with velocity, speed, and energy respectively following Gauss, Maxwell-Boltzmann, and Planck distribution functions. For example, the statistical field of equilibrium-electrodynamics ESD (Fig. 1) takes place within and is in thermodynamic equilibrium with the background physical space that is the field of EKD or Casimir vacuum. In view of Maxwell-Boltzmann distribution function, the spectrum of "atomic" clusters must remain *stochastically-stationary* by the principle of detailed balance. Transition of an electron from a small fast-oscillating "atom" (high energy-level-j) to a large slowly-oscillating "atom" (low energy-level-i) will results in emission of a "sub-particle" that is a photon γ_{ji} to carry away the excess energy given by Bohr [54] frequency formula $\Delta\varepsilon_{ji\beta} = h(\nu_{j\beta} - \nu_{i\beta})$ as schematically shown in Fig. 3a,

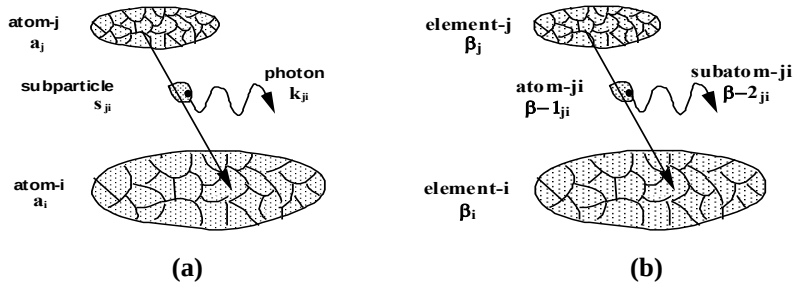

Fig. 3 (a) Transition of electron s_{ij} from atom-j to atom-i leading to emission of photon k_{ij} (b) Generalized transitions [36].

Therefore, *stochastically stationary* sizes of particle clusters (energy-levels) are identified as Bohr *stationary-states* of quantum mechanics [54] and must satisfy

the *stationarity criteria* imposed by Maxwell-Boltzmann distribution. A generalized scale-invariant concept of "atomic" transitions is shown in Fig. 3b. For example, at cosmic scales $\beta = g$ (Fig. 1), transition of an "atom" i.e. galaxy from a small rapidly-oscillating galactic cluster (high-energy-level j) to a large slowly-oscillating cluster (low-energy-level i) results in emission of a star s_{ij} that constitutes a "subatomic" particle of cosmic field [43]. Such quantum transitions between spectrums of particle clusters (Fig. 3) are in harmony with quantum transitions between different "cells" in recent *cellular automaton* model of quantum mechanics [55].

Finally, we examine the influence of the nonlinear term in Eq. (15) by taking the time derivative of equation (15) and substituting for $\partial\Psi_\beta / \partial\tau_\beta$ in the result from Eq. (15) itself, and introducing internal coordinates from Eq. (25) to obtain the non-linear equation

$$\frac{\partial^2\Psi}{\partial\tau^2} = v_{w\beta-1}^2\nabla_\zeta^2\Psi + 2v_{w\beta-1}\nabla_\zeta\Psi\nabla_\zeta^2\Psi + (\nabla_\zeta\Psi)^2\nabla_\zeta^2\Psi \tag{37}$$

Comparisons of numerical analysis of Eq. (37) for double-slit problem with results obtained from non-linear Schrödinger equations involving what de Broglie called *quantum potential* in de Broglie-Bohm [56] model of quantum mechanics will be most interesting.

4 Scale-Invariant Model of Normal Shock and its Hydro-Thermo-Diffusive Structure

The wave equations (28) and (36) correspond to "stochastically stationary" equilibrium state with coordinate system $z'_\beta = x'_\beta - v_{w\beta}t'_\beta$ involving the most probable speed v_{w_β}. Parallel to density wave in Eq. (36), one obtains a momentum wave equation from momentum conservation equation (6) that after introduction of coordinates in Eq. (27) results in

$$\frac{\partial^2\mathbf{v}_\beta}{\partial t_\beta^2} = c_{\beta-1}^2\nabla_\xi^2\mathbf{v}_\beta \tag{38}$$

The momentum waves in Eq. (38) propagate at the speed of "sound" or root-mean-square speed $c_{\beta-1} = v_{r^+\beta-1} = \sqrt{3}v_{w\beta-1}$ of molecules [32]. Similar procedures applied to conservation equations (4)-(5) lead to density, temperature (thermal), and pressure waves [52]

$$\frac{\partial^2 f_\beta}{\partial t_\beta^2} = c_{\beta-1}^2\nabla_\xi^2 f_\beta \quad , \quad f_\beta = \rho_\beta,\ T_\beta,\ p_\beta \tag{39}$$

The derivation of Eq. (39) involves the assumption of ideal gas $p_\beta = \rho_\beta R_\beta T_\beta$ with gas constant as ratio of universal gas constant and molecular weight $R_\beta = R^o / \tilde{w}_\beta$ and the absence of mass and heat diffusivities.

Since each statistical field in the hierarchy (Fig.1) has a root-mean-square speed $v_{r\beta}$ and usually a much faster "atomic" speed u_β, in view of (39) one may associate a "wave" and a "particle" speed with each statistical field [43,52]

$$v_{r^+\beta} = c_\beta \qquad \textbf{Wave speed} \tag{40a}$$

$$u_\beta = v_{w\beta-1} \qquad \textbf{Particle emission speed} \tag{40a}$$

For example, in statistical field of ECD at scale $\beta+1 = c$ the sound waves occur at the adjacent lower LMD scale $\beta = m$ and follow Eq. (39) and hence

$$v_{r^+m} = c_m \qquad \textbf{Acoustic speed} \tag{41a}$$

$$u_m = v_{wa} \qquad \textbf{Particle emission speed} \tag{41b}$$

where the speed of "*sound*" waves in standard atmospher is about $v_{r^+\beta} = v_{r^+m} = c_m \approx 340 \text{ m/s}$ [57]. The velocity of particle emission in Eq. (41b) on the other hand is the speed of single molecule $u_m = v_{wa} \approx 1200 \text{ m/s}$ that is the speed of typical detonation wave [58].

At the scale LKD (Fig. 1) physical space is identified as Casimir vacuum [45] and is considered to be a compressible fluid, Planck compressible ether [59] as discussed in [60]. Lorentz perceptions about the medium of space as Aristotle or Huygens ether [60] is further described in the following quotation by Verhulst [61] from Lorentz 1915 lecture at the Royal Academy of Sciences in Amsterdam:

> ***"Why can we not speak of the ether instead of vacuum? Space and time are not symmetric; a material point can at different times be at different spots, but not in different places at the same time"***

Therefore, it is reasonable to anticipate that density waves in Eq. (35) will be connected to waves of *space curvature* thus corresponding to the recently observed *gravitational waves* first discussed by Poincaré [62]. It is ironic that in their 1935 paper submitted to *Physical Review*, Einstein and Rosen denied the existence of gravitational waves but later changed their opinion due to discovery of the error by Robertson [63]. Although gravitational waves travel at the speed of light $v_{gw} = v_{r^+k} = c_k = c = 2.9978 \times 10^8$ m/s, *gravitational emission (gravitational radiation)* [52] propagates at exceedingly larger speed of tachyon waves estimated as $c_t = 7.7 \times 10^{13} c$ making the entire universe *causally connected* [52, 60]. This is in harmony with the perceptions of Laplace who, as was noted by Poincaré [64], believed that the speed of gravitational

signal is a million times faster than that of light. Such superluminal signals could resolve the *entanglement* problem by providing for *ontological* description of long-distance correlations between entangled particles such as photons [55].

The scale-invariant definition of the speed of "sound" waves described above leads to invariant dimensionless number v_β / c_β called (*Mach*, *Lorentz*, *Michelson*) numbers ($Ma = v / c_m$, $Lo = v / c_e$, $Mi = v / c_k$) associated with (supersonic, super-electronic, and superluminal) flows [43]. Thus, supersonic flow of gas ($Ma > 1$), super-electronic flow of plasma ($Lo > 1$), and superluminal flow of gravitons ($Mi > 1$) lead to the formation of (*Mach*, *Lorentz*, and *Poincaré-Minkowski*) cones as illustrated in Fig. 4 [43, 65].

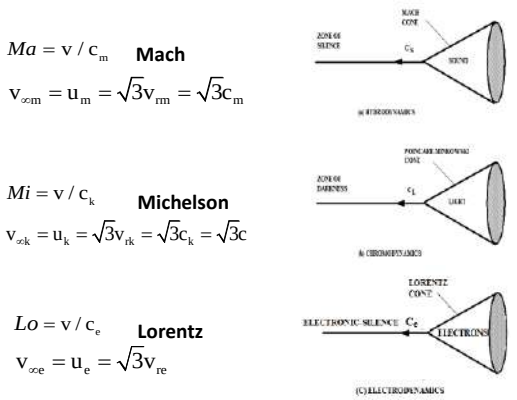

Fig. 4 "Supersonic" flows at (molecular-, chromo-, and electro-dynamics) scales leading to the formation of (*Mach*, *Poincaré–Minkowski*, *Lorentz*) cones [43].

As a result, statistical field of scale β will be separated from the statistical field at adjacent lower scale of β−1 by a surface of discontinuity called *shock wave* [65] as schematically shown in Fig. 5.

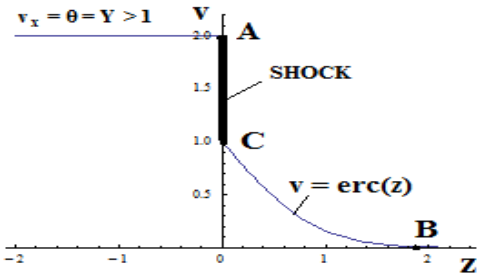

Fig. 5 Shock in polyatomic gas with thin and thick layers corresponding to type C shock structure of Taniguchi et al. [66].

In Fig. 5, a stationary body at B is being approached by supersonic flow from the left. Hence, the fluid with properties $(c_{\beta-1},\ \rho_{\beta-1},\ T_{\beta-1},\ p_{\beta-1})$ to the left of the shock is "supersonic" and that to the right of the shock with properties $(c_\beta,\ \rho_\beta,\ T_\beta,\ p_\beta)$ is subsonic. For example, gaseous supersonic flow at LAD scale $\beta = a$ with signal speed $\mathbf{v}_{r^+_a} = c_a > c_m$ arrives at point A of the shock and a subsonic flow $\mathbf{v} \le c_m$ at LMD scale $\beta = m$ leaves the shock wave at point C. Similarly, but at much higher speeds encountered in cosmology, a superluminal flow at LTD scale $\beta = t$ with wave speed $\mathbf{v}_{r^+_t} = c_t > c_k = c$ arrives at point A of the *event-horizon* or "shock" surrounding a black hole at point B and a luminal flow with wave speed $\mathbf{v}_{r^+_k} = c_k$ at LKD scale $\beta = k$ leaves the shock at point C. This invariant model of generalized shock waves is in harmony with Unruh [67] "*dumb-hole*" model of black hole.

The nature of jump-like transition across diverse types of generalized "shock waves" is interesting. In classical gas dynamics, the hydro-thermo-diffusive structure of normal shock will be governed by Eq. (39), with the reduced temperature Θ profile predicted as [65]

$$\Theta = -\mathrm{erf}(\xi) = \mathrm{erf}(0.2 - y) \tag{42}$$

in close agreement with the experimental data [68] shown in Fig. 6.

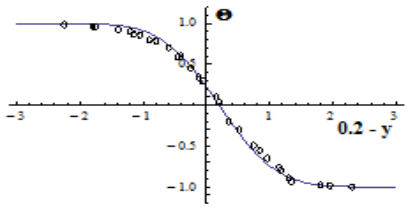

Fig. 6 Comparison between measured normalized wire temperature Θ versus position $(0.2 - y)$ in normal shock [68] and theory [65].

It is reasonable to anticipate that similar error-function type profiles (Fig. 6) would govern the dimensionless velocity, density, pressure, and temperature inside generalized "shock" waves in the hierarchy of statistical fields shown in Fig. 1. We next examine the nature of a superluminal shock wave at stochastic chromodynamics scale.

As discussed in Section 2, absolute thermodynamic temperature identified as Wien wavelength $T_\beta = \lambda_{w\beta}$ of thermal oscillations [32] also defines the internal measures of extension and duration $(\lambda_{w\beta}, \tau_{w\beta})$ called *spacetime* [43]. For example, crossing a shock wave from supersonic laminar-atomic-dynamic

(LAD) side with $T_a = \lambda_{wa}$ to the subsonic laminar-molecular-dynamic (LMD) side $T_m = \lambda_{wm}$ corresponds to transition from one Euclidean space with larger λ_{wa} (high temperature) to another Euclidean space with smaller λ_{wm} (low temperature). However, the description of shock internal structure necessarily involves varying temperatures (Fig. 5) hence *variable-measure* or *non-Euclidean* geometry.

Following Poincaré [69] description of hyperbolic space, one expresses temperature as $T_\beta = \left(R^2 - r^2\right)^{1/2}$ with square root added to account for the dimension of absolute temperature (meter) as Wien wavelength of thermal oscillations [32]. If one postulates that space "curvature" be inversely related to absolute temperature $\kappa_\beta \propto 1/T_\beta$ it will lead to $(\kappa \to 0\,, \kappa \to \infty)$ at $T_\beta = (\infty,\ 0)$ resulting in formation of (white hole, black hole) at (center, circumference) of *Poincaré disk* [43, 69]. Also, as discussed in Section 2, thermodynamic temperature defines internal spacetime leading to Poincaré [62] and Minkowski [70] 4-dimesional spacetime $(x_\beta, y_\beta, z_\beta, t_\beta)$. However, 6 additional *compactified* dimensions could be associated with 3-rotational and 3-vibrational *internal degrees of freedom* in Eq. (20). Therefore, the total number of dimensions required for the description of each statistical field (Fig. 1) including the physical space or Casimir [45] vacuum will be 4 + 6 = 10 in harmony with models of superstring theories [71].

By the equation of state $p_\beta = \rho_\beta R_\beta T_\beta$ at constant pressure, density is also inversely related to absolute temperature. Because pressure can be viewed as *volumetric energy density* of the field [32], negative values of pressure, often assumed in inflationary models of cosmology, are expected to be nonphysical. In view of finite value of Casimir [45] zero-point energy, it is reasonable to anticipate a finite positive pressure of Casimir vacuum in accordance with modified van der Waals equation of state [72]

$$p_{rg} = p_{ra} - p_{rv} = \frac{1}{Z_c}\left[\frac{T_r}{\tilde{v}_r - 1/3} - \frac{9}{8\tilde{v}_r^2} + Z_c - \frac{3}{8}\right] \tag{43}$$

Since critical compressibility factor of all substances are smaller than that of van der Waals fluid $Z_{c,vdw} = 3/8$, in the limit $\tilde{v}_r \to \infty$ equation (43) leads to positive reduced vacuum pressure [72]

$$p_{rv} = (3/8)/Z_c - 1 \geq 0 \tag{44}$$

A schematic diagram of physical space as states of a compressible fluid from infinite rarefaction (*white hole* WH) to infinite compression (*black hole* BH)

corresponding to pressure range $0 = p_{WH} < p_{am} < p_v < p_m < p_{BH} = \infty$ is shown in Fig. 7.

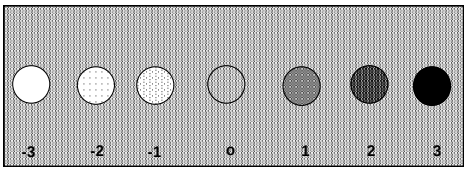

Fig. 7 Different degrees of rarefaction and compression of Casimir vacuum identified as a compressible fluid. **(-3)** White hole $\rho_{WH} = 0$ **(-2, -1)** Anti-matter $\rho_{AM} < \rho_v$ **(0)** Casimir vacuum $\rho = \rho_v$ **(1, 2)** Matter $\rho_{MA} > \rho_v$ **(3)** Black hole $\rho_{BH} = \infty$ [43, 60].

Therefore, if one introduces the concept of space "scalar curvature" as deviation of space density from the density of Casimir [45] vacuum $\kappa \equiv \rho - \rho_v$, one finds that $(\kappa > 0\ ,\ \kappa = 0\ ,\ \kappa < 0)$ could be respectively associated with (Riemannian, Euclidian, Lobachevskian) space. The hydrodynamic model of chromodynamics shock waves in compressible space (Fig. 7) is in harmony with the perceptions of 't Hooft [73] concerning quantum gravity as a dissipative deterministic dynamic system. The application of the model to derive Schrödinger Eq. (33) at photonic scale of Casimir vacuum $\beta = k$ suggests that density waves in Eq. (39) correspond to *gravitational waves* that propagate at the speed of light [32, 43, 52, 60].

5 Concluding Remarks

A scale-invariant model of Boltzmann statistical mechanics was applied to derive invariant Schrödinger equation from invariant Bernoulli equation by way of Hamilton-Jacobi equation of classical mechanics. The nature of time-dependent and time-independent Schrödinger equations and the corresponding quantum mechanics wave functions in connection to *stationary states* of the system were described.

The invariant hydrodynamic model resulted in generalized shock waves and introduction of a scale-invariant definition of Mach number v_β / c_β. Hence, "supersonic" flows at molecular-, electro-, and chromo-dynamics scales result in formation of (…, *Mach*, *Lorentz*, *Poincaré–Minkowski*, …) cones separating "super-sonic" from "sub-sonic" sides. The internal hydro-thermo-diffusive structure of generalized shock waves were discussed. Finally, a model of space curvature as deviation of density from Casimir vacuum density $\kappa = \rho_\beta - \rho_v$ was introduced leading to $(\kappa > 0,\ \kappa = 0,\ \kappa < 0)$ corresponding to (*Riemannian, Euclidean, Lobachevskian*) space. The results are in harmony with quantum gravity considered as dissipative deterministic dynamic system [73].

Acknowledgments: This research was in part supported by NASA grant No. NAG3-1863.

References

1. L. de Broglie, Interference and Corpuscular Light, Nature 118, 441-442, 1926; Sur la Possibilité de Relier les Phénomènes d'Interférence et de Diffraction à la Théorie des Quanta de Lumière, C. R. Acad. Sci. Paris, 183, 447-448, 1927; La Structure Atomique de la Matière et du Rayonnement et la Mécanique Ondulatoire, 184, 273-274, 1927; Sur le Rôle des Ondes Continues en Mécanique Ondulatoire, 185, 380-382, 1927.
2. L. de Broglie, *Non-Linear Wave Mechanics: A Causal Interpretation*, Elsevier, New York, 1960.
3. L. de Broglie, The Reinterpretation of Wave Mechanics, Found. Phys. 1, 5, 5-15, 1970.
4. E. Madelung, Quantentheorie in Hydrodynamischer Form, Z. Physik. 40, 332-326, 1926.
5. E. Schrödinger, Über die Umkehrung der Naturgesetze, Sitzber Preuss Akad Wiss Phys-Math Kl, 193, 144-153, 1931.
6. R. Fürth, Über Einige Beziehungen zwischen klassischer Staristik und Quantenmechanik, Z. Phys. 81, 143-162, 1933.
7. D. Bohm, A Suggested Interpretation of the Quantum Theory in Terms of "Hidden Variables" I, Phys. Rev. 85, 2, 166-179, 1952.
8. T. Takabayasi, On the Foundation of Quantum Mechanics Associated with Classical Pictures, Prog. Theor. Phys. 8, 2, 143-182, 1952.
9. D. Bohm, and J. P. Vigier, Model of the Causal Interpretation of Quantum Theory in Terms of a Fluid with Irregular Fluctuations, Phys. Rev. 96, 1, 208-217, 1954.
10. E. Nelson, Derivation of the Schrödinger Equation from Newtonian Mechanics, Phys. Rev. 150, 4, 1079-1085, 1966.
11. E. Nelson, *Quantum Fluctuations*, Princeton University Press, Princeton, New Jersey, 1985.
12. L. de la Peña, New Foundation of Stochastic Theory of Quantum Mechanics, J. Math. Phys. 10, 9, 1620-1630, 1969.
13. L. de la Peña, and A. M. Cetto, Does Quantum Mechanics Accept a Stochastic Support? Found. Phys. 12, 10, 1017-1037, 1982.
14. A. O. Barut, Schrödinger's Interpretation of ψ as a Continuous Charge Distribution, Ann. der Phys. 7, 4-5, 31-36, 1988.
15. A. O. Barut, and A. J. Bracken, Zitterbewegung and the Internal Geometry of the Electron, Phys. Rev. D 23, 10, 2454-2463, 1981.
16. J. P. Vigier, De Broglie Waves on Dirac Aether: A Testable Experimental Assumption, Lett. Nuvo Cim. 29, 14, 467-475, 1980; C. Cufaro Petroni, and J. P. Vigier, Dirac's Aether in Relativistic Quantum Mechanics, Found. Phys. 13, 2, 253-286, 1983; J. P. Vigier, Derivation of Inertia Forces from the Einstein-de Broglie-Bohm (E.d.B.B) Causal Stochastic Interpretation of Quantum Mechanics, Found. Phys. 25, 10, 1461-1494, 1995.
17. F. T. Arecchi, and R. G. Harrison, *Instabilities and Chaos in Quantum Optics*, Springer-Verlag, Berlin, 1987.
18. O. Reynolds, On the Dynamical Theory of Incompressible Viscous Fluid and the Determination of the Criterion, Phil. Trans. Roy. Soc. A 186, 1, 123-164, 1895.

19. D. Enskog, Kinetische Theorie der Vorgange in Massig Verdunnten Gasen, Almqvist and Wiksells Boktryckeri-A.B., Uppsala, 1917. English translation: G. S. Brush, *Kinetic Theory*, 125-225, Pergamon press, New York, 1965.
20. G. I. Taylor, Statistical Theory of Turbulence-Parts I-IV, Proc. Roy. Soc. A 151, 873, 421-478, 1935.
21. T. Kármán, and L. Howarth, On the Statistical Theory of Isotropic Turbulence, Proc. Roy. Soc. A 164(917), 192-215, 1938.
22. H. P. Robertson, The Invariant Theory of Isotropic Turbulence, Proc. Camb. Phil. Soc. 36, 209-223, 1940.
23. A. N. Kolmogoroff, Local Structure on Turbulence in Incompressible Fluid, C. R. Acad. Sci. U. R. S. S. 30, 301-305, 1941; A Refinement of Previous Hypothesis Concerning the Local Structure of Turbulence in a Viscous Incompressible Fluid at High Reynolds Number, J. Fluid Mech. 13, 82-85, 1962.
24. A. M. Obukhov, On the Distribution of Energy in the Spectrum of Turbulent Flow, C. R. Acad. Sci. U. R. S. S. 32, 19-22, 1941; Some Specific Features of Atmospheric Turbulence, J. Fluid Mech. 13, 77-81, 1962.
25. S. Chandrasekhar, Stochastic Problems in Physics and Astronomy, Rev. Mod. Phys. 15, 1, 1-89, 1943.
26. S. Chandrasekhar, *Stochastic, Statistical, and Hydrodynamic Problems in Physics and Astronomy*, Selected Papers, vol.3, University of Chicago Press, Chicago, 199-206, 1989.
27. W. Heisenberg, On the Theory of Statistical and Isotropic Turbulence, *Proc. Roy. Soc.* A 195, 402-406, 1948; Zur Statistischen Theorie der Turbulenz, Z. Phys. 124, 7-12, 628-657, 1948.
28. G. K. Batchelor, *The Theory of Homogeneous Turbulence*, Cambridge University Press, Cambridge, 1953.
29. L. D. Landau, and E. M. Lifshitz, *Fluid Dynamics*, Pergamon Press, New York, 1959.
30. H. Tennekes, and J. L. Lumley, *A First Course in Turbulence*, MIT Press, 1972.
31. S. H. Sohrab, Some Implications of a Scale Invariant Model of Statistical Mechanics to Classical and Relativistic Thermodynamics, Int. J. Thermo. 17, 4, 233-248, 2014.
32. S. H. Sohrab, On a Scale-Invariant Model of Statistical Mechanics and the Laws of Thermodynamics J. Energy Resources and Technol. 138, 3, 1-12, 2016.
33. S. H. Sohrab, Invariant Forms of Conservation Equations and Some Examples of Their Exact Solutions, J. Energy Resources Technol. 136, 1-9, 2014.
34. S. H. Sohrab, Solutions of modified equation of motion for laminar flow across (within) rigid (liquid) and sphere and cylinder and resolution of Stokes paradox, *AIP Conference Proceedings* 1896, 130004 (2017).
35. S. H. Sohrab, Quantum Theory of Fields from Planck to Cosmic Scales, WSEAS Trans. Math. 9, 734-756, 2010.
36. S. H. Sohrab, On a Scale Invariant Model of Statistical Mechanics, Kinetic Theory of Ideal Gas, and Riemann Hypothesis, Int. J. Mod. Communication Tech. & Research. 3, 6, 7-37, 2015.
37. S. H. Sohrab, Scale Invariant Model of Statistical Mechanics and Quantum Nature of Space, Time, and Dimension, *Chaotic Modeling and Simulation (CMSIM)* **3**, 231-245, 2016.
38. R. S. de Groot, and P. Mazur, *Nonequilibrium Thermodynamics*, North-Holland, 1962.
39. H. Schlichting, Boundary-Layer Theory, McGraw Hill, New York, 1968.
40. F. A. Williams, *Combustion Theory*, 2nd Ed., Addison Wesley, New York, 1985.

41. J. O. Hirschfelder, C. F. Curtiss, and R. B. Bird, *Molecular Theory of Gases and Liquids*, Wiley, New York, 1954.
42. S. Chapman, and T. G. Cowling, *The Mathematical Theory of Non-Uniform Gases*, Cambridge University Press, Cambridge, 1953.
43. S. H. Sohrab, An Invariant Model of Boltzmann Statistical Mechanics and Some of its Implications to Thermodynamics and Quantum Nature of Space and Time, *WSEAS Tran, Appl. Theo. Mech*. 13, 199-212, 2018.
44. M. Planck, On the Law of the Energy Distribution in the Normal Spectrum, Ann. der Phys. 4, 553-558, 1901.
45. H. B. G. Casimir, On the Attraction between Two Perfectly Conducting Plates, Proc. K. Ned. Akad. Wet. 51, 793-795, 1948.
46. S. H. Sohrab, Universality and Statistical Nature of Turbulence, Quantum Mechanics, and Chaos, *9th CHAOS Conference Proceedings*, 23-26 May 2016, Senate House, University of London, UK.
47. R. Clausius, Über die Art der Bewegung, welche wir Wärme nennen. *Annalen der Phyzik*, 176 (3), 353-380; 1957. *Philosophical Magazine* 14,108-127, 1957.
48. E. Schrödinger, Quantization as a Problem of Proper values, Part I, Ann. der Phys. 79, 4, 1926.
49. W. Schommers, Evolution of Quantum Mechanics, in *Quantum Theory and Pictures of Reality*, W. Schommers (ed.), Springer, Berlin, 1-48, 1989.
50. F. Hasenöhrl, Zur Theorie der Strahlung in bewegten Körpern. *Ann. der Phys*. 16, 589-592, 1905.
51. S. H. Sohrab, Invariant laws of thermodynamics and validity of Hasenöhrl mass-energy equivalence formula m = (4/3) E/c^2 at photonic, electrodynamic, and cosmic scales, *Bull. Amer. Phys. Soc.* 62, 1, 124, 2017.
52. S. H. Sohrab, Implications of a Scale Invariant Model of Statistical Mechanics to Nonstandard Analysis and the Wave Equation, *WSEAS Trans. Math.* **3**(5) 93, 2008.
53. M. Born, Zur Quantenmechanik der Stoßvorgänge, *Z. Physik* 37, 863, 1926.
54. B. L. van der Waerden, Towards Quantum Mechanics, in: *Sources of Quantum Mechanics*, B. L. van der Waerden (Ed.), Dover, New York, 1-59, 1967.
55. G**.** 't Hooft, *The Cellular Automaton Interpretation of Quantum Mechanics*, Springer, 2016.
56. J. T. Cushing, *Quantum Mechanics*, the University of Chicago Press, Chicago, 1994.
57. K. A. Krout and S. H. Sohrab, On the Speed of Sound, *Int. J. Thermodynamics*, 19 (1) 29-34, 2016.
58. B. Lewis, A chain reaction theory of the rate of explosion in detonating gas mixtures, *J. Amer. Chem. Soc.* **52** (8), 3120, 1930.
59. H. A. Lorentz, *Selected Works of L.H. Lorentz*, vol.5, Nersessian, N. J., and Cohen, H. F., (Eds), p.7, Palm Publications, Nieuwerkerk, 1987.
60. S. H. Sohrab, Invariant Model of Statistical Mechanics, Quantum Mechanics, and Physical Nature of Space and Time, *8th CHAOS Conference Proceedings, 26-29 May 2015, Henri Poincaré Institute*, Paris, France.
61. F. Verhulst, *Henri Poincaré, Impatient Genius*, p. 63, Springer, 2012.
62. H. Poincaré, Sur la Dynamique de l'Electron, C. R. Acad. Sci. Paris 140, 1905, 1504-1508; *Rend. Circ. Mat. Palermo* 21, 9-175, 1906.
63. D. Kenneflick, Einstein Versus the Physical Review, Physics Today, September, 43-48, 2005.
64. H. Poincaré, The Present and the Future of Mathematical Physics, Address delivered before the Section of Applied Mathematics of the *International Congress of Arts and Science*, St. Louis, September 24, 1904; *Bull. Amer. Math. Soc.* 37(1) 25-38, 2000.

65. S. H. Sohrab, On a Scale Invariant Model of Statistical Mechanics and Derivation of Invariant Forms of Conservation Equations," *WSEAS Trans. Heat and Mass Trans.* **9**(15), pp. 169-194, 2014.
66. S. Taniguchi, T. Arima, T. Ruggeri, and M. Sugiyama, Thermodynamic theory of the shock wave structure in a rarified polytrophic gas: Beyond the Bethe-Teller theory, *Phys. Rev. E.* 89, 013025, 2014.
67. W. Unruh, Sonic analogue of black holes and the effects of high frequencies on black hole evaporation, *Phy. Rev. D.* 51, 2827, 1995.
68. F. S. Sherman, A low-density wind tunnel study of shock wave structure and relaxation phenomena in gases, *NACA Tech. Notes* 3298, 1955.
69. H. Poincaré, *Science and Hypothesis*, Dover, New York, 65, 1952.
70. H. Minkowski, Space and Time, in *Theory of Relativity*, p. 75, Dover, New York, 1952.
71. G. 't Hooft, *In Search of the Ultimate Building Blocks*, p. 161, Cambridge University press, 1998.
72. S. H. Sohrab, Modified van der Waals Equation of State, *WSEAS Transactions on Biology and Biomedicine* 1 **(**4), 422-424, 2004.
73. G. 't Hooft, Quantum Gravity as a Dissipative Deterministic System, *Class. Quant. Grav.* 16, 3263-3279, 1999.

THE PHYSICS OF EVOLUTION AND BREAKING SYMMETRY

V.M. Somsikov[1]

[1]Al-Farabi Kazakh National University, Almaty, 050040, Kazakhstan.
(E-mail: vmsoms@rambler.ru)

Abstract. Paper is devoted to explaining the nature of symmetry breaking of dynamical classical and quantum systems in the framework of evolutionary physics. A brief explanation of the deterministic mechanism of irreversibility is presented. The nature of the non-potential forces, which leads to symmetry breaking, is analyzed. The concept of evolutionary nonlinearity and the deterministic symmetry breaking based on the motion equation for the structural particle and modified Schrödinger equation is discussed. The nature of the potential, which follows from evolutionary nonlinearity and leads to violation of symmetry in classical and quantum systems, is considered.
Keywords: symmetry, irreversibility, evolution, principle of least action, entropy, quantum systems, mechanics, dynamics.

1. Introduction

The world is a collection of open nonequilibrium dynamic systems. Therefore, this world is characterized by the evolutionary processes of the emergence of new structures of matter, phase transitions, the appearance and disappearance of objects of the Universe, catastrophic phenomena on Earth, the climate change, and so on. To understand these processes, it is necessary to have a theoretical foundation to answer questions such as how, why and in what direction nature is developing. For this, first of all, it is necessary to understand the essence of the physical nature of evolution [1-6]. However, there is a big obstacle to this understanding [6]. It is a fact that the basic laws of physics, its formalisms are reversible. Therefore, modern physics describes the stationary world rather well, but does not always adequately describe the irreversible processes of evolution. This is also the reason for the lack of unity in various fields of physics, for example, mechanics, thermodynamics, statistical physics, quantum mechanics.

The search for an explanation of irreversibility first led to its probabilistic mechanism. It is based on the property of exponential instability of phase trajectories of Hamiltonian systems and the hypothesis of the existence of random external fluctuations [5]. The probabilistic mechanism of irreversibility significantly helped in the development the kinetical and statistical methods of irreversible processes, in understanding the nature of chaos, in explaining spontaneous symmetry breaking in quantum systems [8].

The need to describe irreversible processes occurring in different forms of matter with symmetry breaking forces us to develop empirical methods for their description. Today these methods are based primarily on the Hamilton formalism. Although these methods are extremely complex and diverse, their essence reduces to perturbation theory by adding the corresponding empirical terms to the Hamiltonian [8, 10]. In addition, In addition, empirical equations of physical kinetics and statistical physics are actively used today to describe nonequilibrium evolutionary systems.

10th *CHAOS Conference Proceedings, 30 May - 2 June 2017, Barcelona, Spain*

Although good agreement with experiments was obtained based on these methods, they do not reveal the nature of symmetry breaking and the mechanism of irreversibility. Moreover, these methods encounter problems in determining the scope of their use, in explaining the correctness of applying the Hamilton reversible formalism to solve irreversible problems in explaining cause-effect relationships in the corresponding processes [8, 13]. It does not answer key questions about the evolution of the picture of the world. For example, the following questions remain open: how does order emerge from chaos, how does nature choose the path "from simple to complex," how symmetry breaking leads to evolution, where evolution is directed. This is due, in particular, to the fact that probabilistic laws and principles are incompatible with the fundamental laws of physics. Indeed, the solution of problems concerning with the construction of an evolutionary picture of the world cannot but rely on the ideas of determinism, the cognoscibility of the world, its uniqueness, and also the closeness of the laws of physics. However, these ideas exclude probability in their starting positions. Therefore, the search for the mechanism of irreversibility within the framework of the determined laws of physics did not stop even after the discovery of the probabilistic mechanism of irreversibility [5, 6].

Only taking into account the role of the body structure in its dynamics, the deterministic mechanism of irreversibility (DMI) was discovered [11]. DMI has opened up the possibility of building a "physics of evolution". The task of the «physics of evolution" is to describe the key processes of evolution: the emergence, development and destruction of systems, the definition of the principles for constructing an evolutionary picture of the world "from simple to complex" based on the fundamental laws of the physicist.

A method for constructing the physics of evolution was found as follows. First of all, the model of a structured particle (SP) replaced the unstructured material point model in classical mechanics, where the SP is an equilibrium system of potentially interacting material points. Then, according to the principle of dualism of symmetry, the energy of the system was presented as the sum of the energy of motion and internal energy. After that, from this form of energy, the equation of motion of the system was obtained. This equation is irreversible. Irreversibility is determined by the nonlinear terms of this equation, which are proportional to the gradients of external forces. These terms provide the linking of the elements of the symmetry groups of micro and macro variables, which determine the change in the internal energy and the system's motion energy respectively. Thanks to these conditions, the motion energy is converted into internal energy when the total energy is conserved. Thus, due to the interaction of dynamic symmetry groups arising in the presence of gradients of external forces, irreversibility appears. In turn, DMI has opened the possibility of building a "physics of evolution".

In this paper, based on the deterministic mechanism of irreversibility in classical mechanics, an alternative explanation of the nature of symmetry breaking for quantum mechanics is proposed. For this, the properties of the equation of motion for a system of material points are first explained. Then the DMI mechanism and the concept of evolutionary nonlinearity is analyzed. It is shown how the free energy function follows from the evolutionary nonlinearity and how symmetry breaking in classical and quantum systems follows from this function. Then, the universal nature of symmetry breaking for nonequilibrium dynamical systems of classical and quantum mechanics is discussed.

2. System's motion equation

The key idea that led to the emergence of DMI was the idea of the need to take into account the influence of body structure on its dynamics. This idea arose as a result of studying the interaction of the simplest systems of elastically colliding disks [11, 12]. As

a result of studying disks systems, the question arose of how to take into account the role of the body structure in its dynamics. As it turned out, this should be done based on the principle of dualism of symmetry. According to this principle, the motion of the structured bodies is determined not only by the symmetry of space, as in the case of an unstructured material point, but also by the internal symmetry of the body. The second question was how to take into account that these types of symmetry determine the motion of the system. As it turns out, this question is solved by representing the total energy of the system as the sum of the motion energy and internal energy. The body's motion equation was found from this form of energy when its model was represented in the form of systems of potentially interacting material points [11, 12]. The generality of this representation of the body model follows from the fact that, as a rule, all bodies with a good degree of approximation can be represented by a set of potentially interacting material points. As a result, the system's motion equation was obtained in the framework of the laws of classical mechanics without using Hamilton's reversible formalism, since this formalism is not applicable to the description of dissipative systems [14, 15].

Thus, the equation of motion of the system was obtained based on fundamental laws and principles. These laws and principles include the laws of conservation of energy, momentum, the Galileo principle, and the principle of dualism of symmetry. Using the principle of dualism of symmetry solved two problems. Firstly, this principle took into account the role of system symmetry in its dynamics. Secondly, its use made it possible to understand that symmetry breaking within the framework of formalisms of classical mechanics is impossible. This approach to the derivation of the system's motion equation completely has justified himself.

The system's motion equation and the DMI mechanism resulting from it were explained in sufficient detail in previous works [11, 12]. Therefore, the key stages of its construction were emphasized below, and then its main properties are described.

In accordance with the principle of dualism of symmetry, there are exists two groups of variables that determine the total energy of the system [12]. Variables that define internal energy are micro variables. The variables that determine the energy of motion SP are macro variables. These micro and macro variables belonging to two different symmetry groups are independent [15]. As it turned out, the total energy in these variables breaks down into the internal energy of the system and its energy of motion.

In accordance with the law of conservation of energy, the sum of the energy of the system's motion and internal energy is invariant along its trajectory, but each of these types of energy is not an invariant of the system's motion. A violation of the symmetry of time is associated with a violation of the invariance of the system's motion energy.

The system's motion equation is obtained by differentiating the energy with respect to time, and then by summing the scalar values of the changes in the energies of each material point. This equation has the form [15, 17]:

$$M_N \dot{V}_N = -F_N^0 - \mu V_N, \tag{1}$$

where $F_N^0 = -\sum_{i=1}^{N} F_i^0$; F_i^0 - is external force acting on the i-th material point; $\mu = \dot{E}_N^{\text{int}} / (V_N^{max})^2$; F_{ij} - is the strength of interaction i and j material points; $F_{ij}^0 = F_i^0 - F_j^0$; $\dot{E}_N^{\text{int}} = \sum_{i=1}^{N-1} \sum_{j=i+1}^{N} \tilde{v}_{ij} (m\tilde{v}_{ij} + F_{ij}^0 + NF_{ij})$; $V_N^{max} + \dot{E}_N^{\text{int}} / F_N^0 = 0$.

The first term on the right side of the equation. (1) determines the potential external forces that act on the center of mass. These forces change the system's velocity.

The second term is nonlinear and bisymmetric, since it depends on micro and macro variables simultaneously. This term determines non-potential forces that change of the

system's internal energy. The work of these forces is non-equal to zero only when the field of external forces is non-homogeneous. This term is called evolutionary nonlinearity [18]. It is responsible for the origin of the DMI. In the general case, this term links two symmetry groups of micro- and macro variables and determines the mutual transformation of the system's motion energy and internal energy.

The eq. (1) is true for systems consisting from any number of material points. In the approximation of a solid body, the eq. (1) becomes the reversible Newton's motion equation. The eq. (1) is true for systems consisting from any number of material points. In the approximation of a solid body, the eq. (1) becomes the reversible Newton motion equation.

The canonical Lagrange and Hamilton equations do not take into account evolutionary nonlinearity and therefore these equations are reversible and cannot be used to analyze the dissipative dynamics of a body [14, 23]. This is due to the use of golonomic restrictions in obtaining them. However, extended Hamiltonian, which was constructed based on eq. (1), can be used to analyze the SP's dissipative dynamics. The phase trajectory can be determined in the dual phase space [12, 21].

In the general case, from eq. (1) we will have that *the body is at rest or motion at a constant velocity if the nonlinear forces are equal to external forces*.

In according with the principle Galilee, in evenly moving system it is impossible to determine the fact of its motion, because dynamic equations do not depend from the choice of an inertial coordinate system. In according with eq. (1) a similar situation arises at the system's motion in the homogeneous field of forces, when we have: $F_{ij}^{0} = 0$. For clarification this statement, let us take as example a star system with planets moving with uniform acceleration in an external gravitational field of forces. If someone moves in the gravitational field of one of the planets, then by the nature of these motions it is impossible to establish inside the system that system as a whole moves with acceleration. This conclusion is consistent with the D'Alembert equation and Einstein's ideas [14].

Analysis of system dynamics using eq. (1) performed in micro and macro variables. As a result, the role of the body structure in its dynamics was taken into account. Therefore, we will say that eq. (1) gives a "***complete description***" of the dynamics of bodies in an inhomogeneous force field.

Of course, solving eq. (1) for a system with a large number of elements is a difficult task. However, studying the properties of this equation makes it possible to determine the general properties of the behavior of dissipative systems and establish how statistical and thermodynamic laws follow from the basic laws of classical mechanics [11, 15].

3. Irreversibility of the nonequilibrium systems

Below we consider the processes of equilibrating nonequilibrium systems using the eq. (1). In the approximation of local thermodynamic equilibrium with a sufficient degree of generality, the nonequilibrium system can be specified by a set of SP's moving in relative to each other [13, 16]. In this case, SP is already playing the role of system elements. The motion of each SP in an inhomogeneous field of forces, created by all SP is determined by eq. (1) [14]. In this case, the proof of equilibration is reduced to the proof that the energy of the relative motions of the SP is irreversibly converted into their internal energy. Thus, in order to prove irreversibility, it is necessary to show that such transformations take place. To do this, we estimate the energy flows for SP [13, 18].

Obviously, for the nonequilibrium system consisting from a set of SP, the mechanism of the formation of direct and reverse energy flows is associated with the mutual transformation of the energies of the relative motions of the SP and their internal energies. Hence, the proof of the irreversibility of the dynamics of the nonequilibrium

system is reduced to the proof that the influx of internal energy of the SP is greater than the outflow.

Let us ΔE^{tr} is the energy of the relative motion of the SP, which is transformed into its internal energy. According to eq. (1), ΔE^{tr} is determined by a bilinear term whose value is equal to the second order of smallness. Therefore we can write: $\Delta E^{tr} \sim \chi^2$, where χ is any small parameter. If it so, then $\Delta E^{tr} / E^{\text{int}} << 1$ and the equilibrium violation of the SP can be neglected. Let us notice that the value ΔE^{tr} has a second order of smallness also in according with the estimations of an increment of entropy [19].

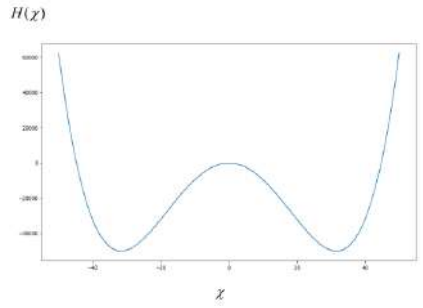

Fig. 1. The graph of the formula 2.

Thus, as it follows from eq. (1), the SP dynamics in a weak inhomogeneous field of external forces is irreversible. Indeed, in such a field of force the changes of SP's internal energy is a second order smallness, and the violation of the SP equilibrium can be neglected. However, according Galileo principle, the system's motion energy cannot increase due to of internal energy of the system, which is in equilibrium. Therefore, we have the decreases of the SP's motion energy along its trajectory. In this case, irreversibility takes place. The internal motions of the material points that determine the internal energy are also irreversible due to the dependence of internal energy from the time.

If the SP's interaction forces or their gradients are the great enough, the equilibrium of the SP can be disturbed. Then each SP, like a nonequilibrium system, can be represented as a set of equilibrium subsystems moving relative to each other. In this case, for increment of the SP's internal energy one can write: $\Delta E^{tr} = \Delta E^{tr}_{ins} + \Delta E^{h}$, where ΔE^{tr}_{ins} is the increment of the energy of the relative motions and ΔE^{h} is the increment of the subsystem's internal energies. That is, $\Delta E^{tr}_{ins} < \Delta E^{tr}$.

The energy of the equilibrium subsystems cannot be transformed into their motion energy. Therefore, we will consider that only energy of relative motions of subsystems can be transformed back into the motion energy of the SP. Let us denote this reverse flow of the SP's internal energy, as ΔE^{tr}_{ret}. According to eq. (1), the value ΔE^{tr}_{ret} is determined by the bilinear function of the subsystems variables, which determined its motion energies and the internal energies. These are terms of the second order of smallness of their micro and macro variables. But because: $\Delta E^{tr} \sim \chi^2$, we will have that $\Delta E^{tr}_{ret} \sim \chi^4$. Thus, the reverse flow of the internal energy of the SP, ΔE^{tr}_{ret}, into of its motion energy during their strong interactions cannot to be more, than the fourth order of smallness. In this case, a potential, which corresponds to the change of the SP motion energy, can be defined by the next equation:

$$H = \alpha\chi^2 - \beta\chi^4 \tag{2}$$

Here the α, β constants can be determined using of the eq. (1).

Fig. 1 shows a graph of eq. (2). For values: $|\chi| \prec \chi_0$, where $\pm\chi_0$ are the roots of eq. (2), the irreversibility or violation of symmetry of time takes place. For stationarity of the non-equilibrium system it is necessary to fulfill the equality: $H = 0$.

If to take any complex system with a large number of hierarchical levels, then for its stationarity this equality should hold for each hierarchical level [17]. The study of these conditions goes beyond the laws of classical mechanics, because for this study it is necessary to take into account Planck radiation and different quantum effects [13].

To prove and understand the nature of system's equilibration, we studied the change in the internal energy of the system during its motion in a stationary external inhomogeneous field of forces depending on the number of particles in the system. This was done numerically based on the eq. (1) [21, 22].

It turned out that for some initial conditions and for sufficiently small systems, the internal energy could not only increase, but also decrease. The calculations showed that for an oscillator with N=2 which moved in an inhomogeneous field of external forces, depending on the initial phase of its oscillations, the internal energy can be converted into energy of motion [17]. With an increase in the number of particles in the system, the part of internal energy, which can be converted into the energy of movement of the system decreases, and when N> 100, internal energy can only increase.

When $N>10^3$ there is no increase in the increase in internal energy [22]. Thus, $N\sim10^3$ determines the range of applicability of the thermodynamic description for the system. This is in consistent with [23] where stated, that the irreversibility is qualitative: the more particles in the system, the more irreversibly it behaves.

The calculations showed that the magnitude of fluctuations of the internal energy of the system due to a changes in the initial conditions for given energy values and for a given number of elements in the system obeys the law: $\delta E^{tr} \sim 1/\sqrt{N}$ [22]. This corresponds to the statistical law of fluctuations of quadratic functions [19]. Because the above statistical laws for dynamical systems are derived basing on the deterministic eq. (1), it can be argued that they follow from the deterministic laws of physics. A similar conclusion was made in [24]. It follows that the fundamental laws of physics determine the scope of statistical laws. And if it so, then probabilistic laws can be considered as possible simplifications for analysis of the complex systems. This view coincides with the well-known position of Leibniz and Einstein [25].

Thus, in accordance with eq. (1) from a mathematical point of view, the DMI mechanism can be explained by the fact that there is a connection for vectors from different symmetry groups. For SP, these are the groups of symmetry SP and space symmetry. This linking is determined by bilinear terms since these terms depend on variables belonging to different symmetry groups. These bilinear terms determine the conversion of the body's motion energy into its internal energy and lead to a violation of the conservation law of the motion energy, when the sum of the internal energy and the motion energy is preserved. Bilinear terms arise when the body moves in an external inhomogeneous field of forces. The forces between SPs play the role of these forces in nonequilibrium systems. Thus, the energy of the relative motion SP is transformed into the internal energy of the chaotic motion of the elements SP. This is the essence of the second law of thermodynamics. The eq. (2) characterizes the efficiency of converting the energy of movement of the system into internal energy.

The existence of dissipation is a necessary condition for the formation of attractors [26]. However, dissipation is possibly only for structured bodies due to the transformation of the motion energy into their internal energy. Hence the conclusion about the infinite divisibility of matter [12, 27]. This means that according to the laws of classical mechanics, matter should be an infinite hierarchy of systems. That is, any

selected part of the matter is a system.

Let us accept the condition of the matter's infinite divisibility, demand the unity of the picture of the world and the evolutionary origin of matter. In this case, the basic element of matter should be an open nonequilibrium dynamic system [15]. If this is so, then the following explanation of the Heisenberg uncertainty principle can be proposed [28, 29]. In according with the eq. (1), the trajectory of an element depends on its structure. This means that its trajectory, determined based on the canonical formalism of classical mechanics, has uncertainty. This uncertainty is determined by the value: $\Delta E_N^{tr} \Delta t > 0$. In any interaction of particles, or in any measurement process, this uncertainty will occur. The attractiveness of this explanation is that it reinforces the position of the principle of know ability of the world [30].

Below we consider how to explain the spontaneous symmetry breaking for quantum systems.

4. DMI and spontaneous symmetry breaking

The modern theory of quantum systems is based on the canonical Hamiltonian formalism. The scope of this formalism is limited to holonomic systems that are invariant with respect to the direction of time. Therefore, within the framework of the Hamiltonian formalism, only non-dissipative reversible systems can be studied [5, 23, 31]. Indeed, how it is follows from the eq. (1), the dissipation is due to the nonlinear conversion of its motion energy into internal energy. However, the use of the condition of the holonomicity of connections in deriving the Lagrange and Hamilton equations precludes the possibility of describing such a transformation. Therefore, the search for an explanation of the mechanisms of the spontaneous symmetry breaking for phase transitions led to a phenomenological model that describes the thermodynamics and kinetics of superfluidity [9].

The explanation of the mechanism of spontaneous symmetry breaking was based on the so-called order parameter. Using this parameter, the empirical type of the free energy function in the phase transition region was determined. Thus, the restriction of the canonical Hamiltonian formalism related to its reversibility is circumvented empirically, for example, taking into account the additional terms of the expansion of the potential function in the Hamiltonian. The final solution to the problem is based on the idea of the existence of an external infinitely small influence on the system [8, 9, 35]. Therefore, in this case we also have a probabilistic explanation of spontaneous symmetry breaking. Let us briefly recall the essence of this explanation of the nature of symmetry breaking in the theory of phase transitions.

Landau and Ginsburg offered the mathematical description of spontaneous violation of symmetry in 1937 [9]. They explained this effect to infinitesimal fluctuations in the values of operating parameters near an unstable line of phase transitions. They called these parameters scalar order parameters. They themselves determined symmetry breaking due to the expansion of free energy, representing it in the phase transition region as follows [8, 9]:

$$F(\varphi) = F_0 + V(a_2\varphi^2 / 2 + a_4\varphi^4 / 4 - h\varphi), \quad (3)$$

where $F(\varphi)$ is the thermodynamic potential (Gibbs energy); φ is the scalar order parameter; a_2, a_4, h are the empirical coefficients.

The eq. (3) is similar as eq. (2). This expression is sometimes called the "Mexican hat", based on its graphic form (see Fig. 1). To explain the spontaneous symmetry breaking in superfluidity and superconductivity, Ginzburg and Landau used the effective electron

wave function. It performed the role of a two-component order parameter: $\psi(r) = |\psi(r)| \exp[i\phi(r)]$ [8]. In accordance with this, properties of the superconductor were specified by the wave function, which depends on the magnetic field, $B(r)$. It was determined by the functional of the free energy [8]:

$$F(\psi) = F_{n0} + \int dr\{|B|^2/(8\pi) + a|\psi^2| + b|\psi^4| + \sum_{\alpha} 1/(2m)|(-i\hbar\nabla_{\alpha} - (q/c)A_{\alpha})\psi(r)^2|\} \quad (4)$$

Here F_{n0} is the free energy in the normal state, $B(r) = rot(A)$, q, m is the effective charge and mass of superconducting electrons.

Bogolyubov proposed an explanation of the physical nature of the two-component wave function, as well as the theory of superconductivity and superfluidity. He showed the unity of the phenomena of superfluidity and superconductivity, which was subsequently confirmed experimentally [8]. As it turned out later, a similar scalar potential as formula (2) is acceptable not only for spontaneous symmetry breaking during phase transitions. A similar type of expansion of thermodynamic potentials or scalar functions is also used to describe the violation of superfluidity, superconductivity, particle formation processes, the appearance of mass, etc. [3, 8, 31, 33].

Let us consider how a deterministic explanation of symmetry breaking in quantum systems can be introduced. The dynamics of quantum systems is determined by the canonical Schrödinger equation. This equation, like Newton's equation of motion, is reversible. To describe the irreversible dynamics of quantum systems, the Schrödinger equation was modified [29]:

$$\{i\hbar\frac{\partial}{\partial t} + \frac{\hbar^2}{2M}\nabla_R^2 - U(\tilde{r}_1, \tilde{r}_2, ...\tilde{r}_N, R, t) + \sum_{i=1}^{N}[\frac{\hbar^2}{2m}\nabla_{\tilde{r}_i}^2 - W_{\text{int}}(\tilde{r}_i)]\}\psi(\tilde{r}_1, \tilde{r}_2, ...\tilde{r}_N, R, t) = 0 \quad (5)$$

Here R - coordinates of the center of mass of system; $\tilde{r}_i$ - these are coordinates i - particles concerning the center of mass of system; $i = 1, 2, 3...N$; N –is a number of particles; M -is a system's mass; m –is a mass of i - th particle; U, W_{int} external and internal potential energy consequently; wave function ψ represents work of wave functions for each particle and for all system when the external field is homogeneous.

The eq. (5) was obtained in the same way as in classical mechanics, using the principle of dualism of symmetry. In connection with this principle, the energy of a quantum system should be represented by the sum of the motion energy and internal energy. For this, the Hamiltonian in eq. (5), in accordance with the *complete description* method, was written in micro and macro variables, as the sum of the Hamiltonians for the internal dynamics of the elements of the system and for the dynamics of the system as a whole. In this case, irreversibility in quantum systems will be explained by evolutionary nonlinearity.

It is important that in the *complete description* of the extended Schrödinger equation there is no singular bifurcation point for eq. (2), since this point is a region of the space of micro variables. In this point, the motions of the body's elements affect on the system's motion. From this, it is clear that with a macroscopic description of the system's motion in the bifurcation point, which was used in the general Schrödinger equation, we lose the determinism of the description [11, 17]. Thus, spontaneous symmetry breaking can be explained due to the linking of micro- and macro variables through the terms of evolutionary nonlinearity and due to instability of the system's motion at the bifurcation

point, where the motions of the body's elements determine the system's motion. This allows us to conclude that, despite the difference in the processes of symmetry breaking in classical and quantum mechanics, its nature is universal, and the mechanism of spontaneous symmetry breaking in quantum mechanics can be explained in the same way as in classical mechanics. This conclusion is based on the condition of infinite divisibility of matter [30, 31]. Therefore, symmetry-breaking processes can be studied using the *complete description*. This description can be implemented based on the motion eq. (1) for classical systems or based on the eq. (5) for quantum systems [29].

In accordance with eq. (1), micro and macro variables are linked due to the inhomogeneous field of external forces. This will be determined by the terms of evolutionary nonlinearity, should depend simultaneously on micro and macro variables. These terms leads to a violation of symmetry of time, since the motion energy of the system due to these terms is converted into internal energy of the elements.

The conclusion that the nature of irreversibility in quantum mechanics should be similar to the nature of irreversibility in classical mechanics is confirmed by the similarity of the form of potential (2) for classical mechanics and the potential in (3), used to explain spontaneous symmetry breaking in quantum mechanics.

Thus, the differences between explanation of the symmetry breaking in quantum systems and DMI for systems of classical mechanics are as follows. To explain the spontaneous symmetry breaking in quantum systems for superconductivity, superfluidity, etc., the method of second quantization of systems was used. It was assumed that the state of the system is determined by the available statistical states of its elements. Therefore, due to the empirical shape of the transition matrix, used to explain spontaneous symmetry breaking, it was necessary to use the hypothesis of the existence of external arbitrarily small oscillations.

To explain the symmetry breaking in classical mechanics the method of *complete description* was used. In this explanation of symmetry breaking, the deterministic motions of system elements play the role of random external influence. Due to the instability in the bifurcation point, the micro processes leads to macro processes.

The advantage of a *complete description* of quantum systems is that it basically takes into account the role of the internal dynamics of quantum systems in their dynamics and can help to understand and find analytically the creation and destruction operators of the corresponding particles, for example, in the case of supersymmetres [35].

5.Conclusions

The canonical Hamiltonian formalism is built based on Newton's reversible mechanics, when the conditions of holonomic restrictions and the potentiality of all collective forces acting on the systems are met. Such an empirical solution to the irreversibility problem does not follow from closed equations of dynamics and is equivalent to a probabilistic explanation of symmetry breaking processes. However, in the framework of mechanics of structured bodies, a deterministic way of describing these processes becomes possible.

The motion equation of a structured body is obtained by representing the body as a system of potentially interacting material points. In according with the principle of dualism of symmetry, the dynamics of this system is determined not only by the symmetry of space, but also by symmetry of the system. Therefore, to determine its dynamics, the system's energy should be presented in the form of sums of the system's motion energy and its internal energy. Such representation is realized in the spaces of two independent groups of micro and macro variable. Micro variables determine the system's internal energy, and macro variables determine the system's motion energy in space. The violation of symmetry for the system is caused by the conversion of the system's motion

energy into its internal energy, when the system moves in an inhomogeneous field of forces. Such a transformation is defined by bilinear terms of evolutionary nonlinearity, which connects the dynamics of the elements of the system with its dynamics, as a whole. In according with the extended Schrödinger equation, violation of symmetry in quantum systems will also be determined by bilinear terms of evolutionary nonlinearity.

It turned out that evolutionary nonlinearity for systems of classical mechanics is determined by the potential, which coincides with the potential that determines the spontaneous symmetry breaking in quantum systems. This allows us to conclude that the symmetry breaking mechanism is universal for classical and quantum systems. If so then the nature of symmetry breaking in quantum and classical systems can be studied as a result of a *complete description* of the dynamics of systems using micro- and macro-descriptions of dynamics based on the principle of dualism of symmetry.

In mathematical language, this means that for deterministic irreversibility or, in other words, for breaking deterministic symmetry, at least two symmetry subgroups are needed. These two subgroups of symmetry form a complete symmetry group, which determines the dynamics of the body. In this case, the invariant of motion is the total energy, which is equal to the sum of the energies corresponding to these two subgroups of symmetry. When a body moves in an inhomogeneous field of forces between these subgroups of symmetry, an interaction occurs, that is, the engagement of the elements of the symmetry from different subgroups. As a result, the motion energy is converted into internal energy. This means a violation of symmetry or irreversibility.

References

1. E. Wigner, Symmetry and conservation laws, UFN, **84 (**4) (1964);
Events, laws of nature and principles of invariance, UFN, **85 (**4) (1965);
Violation of symmetry in physics, UFN, **89(**3) (1966)
2. G. Ya. Lyubarsky, Group theory and its applications in physics, (Nauka, Moscow, 1958)
3. F. Wilchek, The origin of mass. Modern Physics Letters A, **21 (**9) (2006)
4. N. Bor, The problem of causality in atomic physics, UFN, **147(**2) (1985)
5. G.M. Zaslavsky, Stochasticity of dynamical systems, (Nauka, Moscow, 1984)
6. I. Prigogine, From the existing to the arising, (Nauka, Moscow, 1980)
7. H. G. Callaway, Fundamental Physics, Partial Models and Time's Arrow. Proc. of the 2015 Conference on Model-based Reasoning, Springer, (2016)
8. D.V. Shirkov, 60 years of broken symmetries in physics (From Bogolyubov's theory of superfluidity to the Standard Model), UFN, **179(**6) (2009)
9. L.D. Landau, To the theory of phase transitions. I. JETP, **7**, (1937); Landau L.D. To the theory of phase transitions. II JETP, **7**, (1937)
10. J. Mabillard, P. Gaspard, Microscopic approach to the macrodynamics of matter with broken symmetries. arXiv:2005.14012v1 [cond-mat.stat-mech] 28 May 2020.
11. V. Somsikov, Deterministic mechanism of irreversibility. JAP, **14 (**3) (2018)
12. V.M. Somsikov, To the basics of physics evolution, (Almaty, Nauka, 2016)
13. Y. B. Rumer, M. S. Rivkin, Thermodynamics. Stat. phys. and Kinetics, (Nauka, Moscow, 1977)
14. G. Goldstein, Classical mechanics, (Nauka, Moscow, 1975)
15. V.M. Somsikov, Transition from the mechanics of material points to the mechanics of structured particles, Modern Physics Letter B, **4** (2016)
16. L.D. Landau, E.M. Lifshits, Physical kinetics, (Nauka, Moscow, 1979)
17. V.M. Somsikov, Deterministic irreversibility and the matter structure. JAP, **16** (2019)
18. V.M. Somsikov, Non-Linearity of Dynamics of the Non-Equilibrium Systems, World Journal of Mechanics, **2 (**7) (2017)

19. L.D. Landau, E.M. Lifshits, Statistical Physics, (Nauka, Moscow, 1976)
20. C. Lanczos, Variational principles of mechanics. (Mir, Moscow, 1962)
21. V.M. Somsikov, Deterministic Irreversibility Mechanism and Basic Element of Matter. In *Proc.12th Chaotic Modeling and Simulation*. *Inter*. *Conf*.,Springer, (2020)
22. V.M. Somsikov, A. B. Andreev, On criteria of transition to a thermodynamic description of system dynamics, Russian Physics Journal, **58** (11) (2016)
23. O. Penrose, Reversibility and irreversibility. ("PDE and Materials", report no.44/2006 of the Mathematisches Forschungsintitut Oberwolfach (ed. J.M. Ball, R.D. James and S.Muller)), 2006.
24. F. Baldovin, L.G. Moyano, C. Tsallis, Boltzmann-Gibbs thermal equilibrium distribution descends from Newton laws: A computational evidence. arXiv:cond-mat/0402635 v1 25Feb 2004.
25. L. Peliti, R. Rechtman, Einstein's Approach to Statistical Mechanics: The 1902–04 Papers. J. Stat. Phys. **167** (2017)
26. Yu.A. Loskutov, Charm of chaos, UFN, **150(**12) (2010)
27. V.M. Somsikov, The method of the description of dynamics nonequilibrium systems within the frames of classical mechanics. arX: physics / 0703242 v1 29 September 2007.
28. S. Boughn, Wherefore Quantum Mechanics? arXiv:1910.08069[physics.hist-ph].
29. V.M. Somsikov, Limitation of classical mechanics and ways it's expansion. PoS (Baldin ISHEPP XXII-047). XXII Inter. Baldin Seminar on High Energy Physics Problems. 15-20 JINR, Dubna, (2014)
30. V. Famourzadeh, M. Sefidkhosh, Straddling between determinism and randomness: Chaos theory vis-à-vis Leibniz. arXiv:1909.13635v1 [physics.hist-ph] 30 Aug 2019.
31. J. Bernstein, A question of mass, Am. J. Phys., **79 (**1) (2011)
32. N.E. Mart´ınez-P´erez, C. Ram´ırez, Symmetry breaking in non conservative systems. arXiv: 1602.05255v1 [physics.class-ph] 17 Feb 2016.
33. P.W. Higgs, How was it possible to circumvent the Goldstone theorem. UFN. **85**(10) (2015)
34. V.G. Zelevinsky, Lectures on quantum mechanics, (Nsk., Sib. Univer. Publ. house, 2002)
35. L. E. Gendenstein, I. V. Krive, Supersimmetriya in quantum mechanics. UFN. **146**(4) (1985)

PROBLEMS OF CREATING AN EVOLUTIONARY PICTURE OF THE WORLD

V.M. Somsikov[1, 2], S.N. Azarenka[3]

[1]Institute of Ionosphere, Almaty, 050020,
[2]Al-Farabi Kazakh National University, Almaty, 050040, Kazakhstan.
(E-mail: vmsoms@rambler.ru)
[3]Almaty Academy of the Ministry of Internal Affairs of the Republic of Kazakhstan.
(E-mail: sveta.azarenko@gmail.com)

Abstract. The paper is devoted to study, how the physics of evolution allows developing an evolutionary picture of the world. Here we briefly examine the basic concepts of the world's picture and how these concepts can find development based on the physics of evolution. For this purpose, the next questions will be analysed: how physics of evolution leads to the conclusion about the infinite divisibility of matter; how nature solves the problem of the static state of matter, when motion is a way of existence of matter; how symmetry and its violation determine the evolution of matter; what are the principles of building "from simple to complex", etc. As a result, we show how taking into account the structure of matter in its dynamics leads to the possibility of describing evolutionary processes in nature. This means the possibility of constructing a deterministic evolutionary picture of the world within the framework of the laws of physics.

Keywords: Irreversibility, entropy, chaos, phase space, physics of evolution.

Introduction

Creating a picture of the world is the main task of science. However, many problems arise on the way to its creation. The most important of them is the problem of knowability of nature. This problem is most clearly manifested in the clash of ideas of reductionism and holism.

Proponents of reductionism believe that all phenomena in nature are knowable in principle, and there is a finite set of fundamental laws, the knowledge of which allows you to create a picture of the world, moving from "simple to complex" [1,2]. Proponents of holism, on the contrary, believe that the properties of the "whole" do not follow from the properties of its elements. In addition, there was even an opinion that the "golden age" of science was over, and its further development is possible only on the path of expanding knowledge without intensification. As evidence, they use examples such as a misunderstanding of the relationship between the laws of inert matter and living matter. In their opinion, these relations cannot be established within the framework of the laws of physics. All this causes heated debate between supporters of reductionism and holism [3,4,5].

The problem of the cognizability of nature is directly related to the problem of the principle of causality in physics. Here the development of a picture of the world is faced with a problem related to the fact that the causality principle is still not even among the fundamental principles of physics. This occurs mainly because the fundamental laws of physics are reversible, and natural processes are usually irreversible [6]. Consequently, not only the physical picture of the world does not correspond to the principles of causality and its unity, but also physics itself represents a multitude of separate areas of knowledge that are weakly interconnected. These are, for example, classical mechanics, thermodynamics, and quantum mechanics. As a result, physics explains how the world

works, but does not answer questions about how the world develops, in what direction the processes of its evolution are going, and what determines these directions [6,7,8].

The problem of irreversibility has arisen since the creation of Newtonian mechanics. In the process of solving this problem, Boltzmann et al., Scientists discovered its probabilistic mechanism, according to which evolutionary processes are random [9, 10]. If this is so, then it is not clear how to build a physical picture of the world based on the laws of physics, how to understand the emergence of organized structures of matter from chaos. It also means that on the way to the development of knowledge, insurmountable epistemological problems arise [11,12,13]. Therefore, the search for a solution to the problem of irreversibility within the framework of the laws of physics was continued.

Finally, a **deterministic irreversibility mechanism (DMI)** has been proposed. DMI has opened up the possibility of building physics of evolution. The task of "physics of evolution" is to study the processes of evolution of matter and to develop methods for constructing its evolutionary models within the framework of the fundamental laws of physics [14].

In a previous paper, we examined the question of how DMI strengthens the positions of determinism in physics and the cognoscibility of a picture of the world [11]. The purpose of this paper is to show how the physics of evolution opens up opportunities for constructing a deterministic evolutionary picture of the world, how it affects the development of philosophical concepts that underlie the modern picture of the world.

Basic concepts of a picture of the world and physics of evolution

Here we briefly examine the fundamental concepts of the picture of the world that are related to the physics of evolution, and how these concepts can find their development on the basis of physics of evolution.

The key concepts on which the picture of the world is based arose in antiquity. One of the first fundamental concepts was related to the question of what everything consists of. Many ancient philosophers, as a result of observations of nature, came to the conclusion that matter consists of elementary particles or indivisible bricks. The father of this idea can be considered Democritus [13, 15]. He claimed that matter is composed of atoms. Subsequently, modern ideas appeared for discretizing the structure of matter, its fractality and self-similarity [16]. Today we are witnessing the discovery of an increasing number of components of matter, and so far this limit has not been discovered. In this regard, **we will show here how the physics of evolution leads to the conclusion about the infinite divisibility of matter**.

On the one hand, the Universe, the Milky Way, stars, as we see, are static. However, on the other hand, according to Heraclitus, we have, that "everything flows, everything changes" [15]. That is, the world is evolving. In connection with it there was an opinion that **motion is a way of existence of matter**. It was strengthened in the works of Galilee, Newton, and Leibniz. They found the fundamental laws of motion. They introduced modern concepts of energy, acceleration, angular momentum, etc., characterizing matter in its dynamics [17]. Here **we show how nature solves the problem of the static nature of matter, when motion is a way of existence of matter.**

The rate of change in the position of matter in space is determined by the concept of time. Therefore, it is impossible to describe matter without using space-time concepts. The relationship between the concepts of matter, dynamics, space and time is established using the concept of symmetry. The concept of symmetry appeared in connection with Plato [18]. According to Plato, symmetry is the cornerstone of the picture of the world.

Thanks to the dynamics, matter takes such diverse forms that are determined by the interaction of the elements of matter in accordance with the symmetry of space and time. **The problem of conformity of form and content, provided that both form and content are in constant evolution, stands in the way of the further development of the picture of the world.**

However, the violation of symmetry is also characteristic of nature, as well as its conservation. Apparently, the second law of thermodynamics is the first law in the history of physics, which is associated with the violation of symmetry. In recent decades, it has been discovered that in quantum physics spontaneous symmetry breaking also occurs. Until recently, these symmetry violations, one way or another, were explained in a probabilistic manner. But this contradicts the principle of causality. Moreover, in quantum mechanics there is the Heisenberg uncertainty principle, which actually means the existence of a limit to the cogniscability of a picture of the world [19]. These problems lead to questions: **how symmetry, its violation, determine the evolution of matter, what is the nature of symmetry breaking.**

We find the first fundamental laws of logical thinking, fundamental concepts about the world around us, such as matter, force, motion, space and time, at Aristotle [15]. He believed that the world is one, and the laws of its development are universal. But how to connect the unity of the world and the universality of the laws of its development with the existence of many weakly coordinated sections of physics? Here we discuss**, how this problem is related to the physics of evolution by the example of the relationship of the laws of classical mechanics, thermodynamics and quantum mechanics.**

A millennium after Aristotle, the laws of classical mechanics were discovered. These laws determine the motion of material objects. They also define concepts such as acceleration and energy[15]. According to Galileo, Descartes, Newton, not the velocity of the body is proportional to the force, as Aristotle claimed, but to its acceleration [17, 20]. However, experience shows that the acceleration of the body becomes equal to zero when the force acting on it, becomes equal to the force of friction. This corresponds to the irreversible mechanics of Aristotle. Newton, on the contrary, sought to eliminate friction in order to reveal the essence of the law of motion, regardless of the various properties of bodies and the environment. Thanks to a model of a body in the form of an unstructured particle, he discovered that acceleration, not speed, is proportional to force. A natural question arises, **how to combine the mechanics of Aristotle and Newton?**

An important problem in the development of knowledge concerns the principles of constructing a scientific picture of the world and the limitations of cognizability of the world. Two points of view can be distinguished here. From the point of view of those who adhere to the positions of cognizability of the picture of the world, there must be principles that allow movement in the direction of construction of knowledge from "simple to complex". In this case, the whole picture of the world should be based on fundamental laws that give rise to the whole variety of known empirical laws. Reductionists support this view [1, 2]. In particular, Weinberg believes that the "theory of everything" should be based on laws that make it possible to understand the whole picture of the world. Holists hold the opposite point of view [3, 4]. They argue that the whole contains "new", not arising from the laws of its elements. They say: "The whole is not the sum of its parts" [20]. This raises important questions**: is it possible to build a holistic picture of the world within the framework of the laws of physics, are there physical principles for building a picture of the world "from simple to complex".**

That is, we approach the problem of the existence of principles for constructing systems based on their elements in the framework of the fundamental laws of physics.

Below we will try to show how the problems that were shown in this chapter are related to the physics of evolution.

DMI and physics of evolution

It is hardly possible to understand how the physics of evolution expands the possibilities of developing a picture of the world, if we do not briefly explain the nature of DMI. It is most convenient to begin an explanation of the nature of DMI based on the concepts of symmetry. Indeed, without breaking the symmetry of time that leads to DMI, evolution itself is impossible [18, 21].

1. Principle of dualism of symmetry. As already noted, symmetry is a key concept for a picture of the world [18]. Indeed, the principle of least action, which determines the harmony of the world, follows from the types of symmetries of bodies. This is because the different types of symmetry of time and space correspond to the invariants of dynamics, in particular energy, momentum. These invariants determine the properties and laws of the dynamics of bodies. For example, the dynamics of a structureless **material point (MP)** as the simplest model of a body that Newton used to reveal the essence of the laws of dynamics is determined only by the symmetries of space and time. MP energy is determined in accordance with their symmetries. The motion equation of MP follows from its energy [14].

Boltzmann showed that the body model, within the framework of the laws of classical mechanics, is well approximated by a system of potentially interacting MPs. And knowing the energy of the MP system, in principle, you can find the system's motion equation.

Usually, the system's motion equation is determined using the canonical formalisms of classical mechanics. Canonical formalisms were built on the assumption that all collective forces are potential, since the forces between elements of the system are potential. This assumption is confirmed by the fact that the total forces of moving systems are potential. But it turned out that the dynamics of systems determined by the canonical formalisms of classical mechanics is reversible, as is the motion of a single MP [22]. Any search for a solution to the problem of irreversibility within the framework of canonical formalisms led to a probabilistic mechanism of irreversibility. However, this mechanism is excluded the existence of causal relationships. Therefore, the search for a deterministic solution of the problem of irreversibility was continued.

A study of the simplest systems of elastically colliding disks led to the conclusion that irreversibility is possible only for systems interacting with each other and that the fundamental laws of physics did not prohibit irreversibility. This led to the assumption that the reversibility of Hamiltonian systems, which follows from the formalisms of classical mechanics, is associated with the restrictions used in their construction. This assumption was confirmed. It became clear why all attempts to find DMN in the framework of formalisms of classical mechanics were unsuccessful [21, 23].

Thus, the first key idea providing a breakthrough in solving the problem of irreversibility was the idea of the need to take into account the role of the body structure in its dynamics. The essence of this idea is easy to understand by the example of body motion on a surface with friction. Aristotle was guided by this example. Boltzmann also tried to find the mechanism of irreversibility. He relied on the statistical methods he developed. However, these methods are incompatible with the deterministic laws of classical mechanics.

Systems, unlike MP, also have symmetry. Then the equation of motion of the system should also depend on their symmetry. This means the need to take into account the symmetry of bodies in their dynamics. The fact that **the dynamics of bodies is determined by the symmetries of the body and the symmetries of the surrounding space was the second idea necessary to solve the problem of irreversibility. It was**

called the principle of dualism of symmetry (PDS). The essence of PDS is that the state of the body, the nature of its interaction with external objects, its dynamics and evolution are determined by both the symmetries of the external world and the symmetries of the body. Based on the PDS and the dual representation of energy, as a sum of internal energy and of the motion energy, the body's motion equation was obtained. This equation is irreversible, and DMI follows from this equation. Thus, it turns out that the property of the irreversibility of their system arose from the reversible properties of the dynamics of elements in a deterministic way. The question arises: **how can the irreversibility of the MP's system motion arise when the motion of each MP is reversible?**

It was shown that irreversibility is connected with the fact that the motion energy, which determines the trajectory of the system in space, is transformed into the internal energy [21]. The system's motion energy we will call the energy of "order". We will call the internal energy of an equilibrium body the energy of "chaos". That is, the system's motion energy turns into "chaos" energy in an inhomogeneous space, but the energy of "chaos" cannot be converted into energy of the "order". This is a process of breaking the symmetry of time, since the invariance of the body's motion energy is violated. **But why this process is irreversible? The answer on this question is hidden in the nature of the forces, which transform the system's motion energy into internal energy.**

The dissipative nature of the forces that transform the energy of motion into internal energy follow from the MP's system motion equation. For each MP, forces are determined through the efficiency of the transformation of potential energy into its kinetic energy. The fact that these forces are potential ensures the reversibility of this energy conversion. For a structured body, forces are determined through the efficiency of the transformation of external energy. In this case, the external energy is transformed into both the motion energy and internal energy. Consequently, in the case of a structural body, forces are divided into two classes: forces that determine the change in the energy of motion of the body, and forces that determine the change in internal energy. The forces performing the work on moving the system are equal to the sum of the external forces acting on the elements of the system. They are potential. This corresponds to classical mechanics [22].

The forces that change the internal energy of a system are made up of two parts. One part is the potential forces of interaction of the elements of the system. Another part of the forces performing work on changing internal energy is proportional to the gradients of external forces. **Non-potential friction forces arise as a gradient of potential external forces!** This is the mechanism of the emergence of non-potential friction forces from potential forces [23]. The difference in the collective forces that determine the system's motion and the change in internal energy is related to the difference between internal energy and the motion energy. Internal energy also exists if the system is at rest, due to the continuous motions of the elements relative to its center of mass. The system's motion energy exists only when it moves in space. This energy does not depend on the internal motion of the system's elements. The internal energy of an equilibrium system is the energy of "pure chaos". The word "pure" means that when a system is divided into subsystems, these subsystems are in equilibrium and do not have the energy of relative motions.

Without taking into account the role of body structures in their dynamics, irreversibility cannot be explained. But without dissipation, attractors and structures do not arise [16]**. And if the world evolved "from simple to complex", then this means that the primary element of matter had to have a structure**. The assumption of the need to take into account the structural nature of bodies already at the first stages of describing open systems also follows from statistical considerations [24].

The development of nonlinear dynamics has shown that the appearance of various forms of matter or attractors is possible only in the presence of dissipation. The dissipation occurs only in the interaction of systems. Therefore, to describe the evolutionary processes, it is necessary to take into account the openness of bodies [12, 16]. If we also take into account the infinity of divisibility of matter and accept its evolutionary origin, we conclude that the structureless elements of matter cannot arise and exist. This inevitably leads to the conclusion that **the main element of matter should be an open nonequilibrium dynamic system (ONDS)**, **and the matter itself is a hierarchy of ONDS** [23].

The dynamics of the ONDS is described using the extended formalism of classical mechanics, which takes into account the role of the structure of systems in their dynamics. Such a formalism is obtained in the same way as canonical formalisms from the D'Alembert equation, but instead of the Newton's motion equation, the MP motion equation is used [14, 32].

The most important concept that derives directly from PDS is D-entropy. D-entropy determines how internal energy changes due to change of the motion energy. Unlike the thermodynamic concept of entropy, D-entropy is applicable for both large and small systems. D-entropy can be used to analyze the processes of occurrence, evolution, destruction of new systems. D-entropy reveals the epistemological significance of existing types of entropy, since it directly connects the dynamics and states of the system, implements the relationship of "order" and "chaos".

For a deeper understanding of the role of the body's structure in the mechanism of violation of time symmetry, the oscillator motion in an inhomogeneous force field has been numerically studied [25]. As a result, a previously unknown effect of passage of an oscillator through a potential barrier was discovered. The effect occurs when its motion energy is less than the energy of the barrier, but when the sum of internal energy and the motion energy is greater than the energy of the barrier. It turned out that such a passage of an oscillator through a potential barrier is determined by its phase. The nature of this effect cannot be established without taking into account the PDS [14, 26].

2. Physics of evolution in the world picture. Below we discuss the contribution that the "physics of evolution" can make to the evolutionary picture of the world.

The simplest ONDS can be represented by a set of equilibrium subsystems, which we called SP, and SP, in turn, can be represented by a set of potentially interacting MPs. Thus, ONDS is the third step in bringing the body model closer to reality. SP mechanics arise from MP mechanics, and mechanics of ONDS arise from SP mechanics. **This means that there are principles for constructing a model of matter "from simple to complex."** Here are some of these principles [23].

1. The principle of the relationship of the laws of systems and their elements. ONDS mechanics are built based on fundamental laws that apply to their elements. These are the laws of conservation of energy, momentum. The energy of structureless particles has only the motion energy. However, the ONDS energy consists from the motion energy and internal energy. Changes in these energies occur so that their sum is conserved. The nature of the change in the internal energy of the ONDS obeys the second law of thermodynamics. That is, **from the fundamental laws of element dynamics follows the empirical law of the dynamics of ONDS**.

The presence of a nonlinear interrelation between the laws of adjacent hierarchical levels for MP, SP, ONDS, determined by the "evolutionary nonlinearity" of the SP motion equation [23], suggests that such a relationship should exist for all hierarchical levels of matter. It means opportunity of constructing the entire hierarchical picture of matter for all its hierarchical levels, if the laws of behavior of one of the hierarchical

levels of matter are known. Thus, the reductionism is valid for any hierarchical level of matter.

2. *The parameters of the upper hierarchical levels of ONDS are determined based on the parameters of the lower levels.* The parameters of the upper hierarchical level are constructed based on the parameters of the lower hierarchical level. For example, parameters characterizing the dynamics of MP systems are based on parameters that determine the dynamics of MP. MP parameters are coordinates, velocity, mass. For ONDS, there are also these parameters, but for ONDS, the mass is the sum of the MP masses. The ONDS coordinates are determined by its center of mass. The coordinates and speeds of the ONDS center of mass are determined through the coordinates and velocities of the MPs included in them.

New concepts also appear for ONDS. For example, dissipative forces are determined by gradients of external potential forces. They lead to the concept of D-entropy, which characterizes the change in the internal energy of the ONDS. D-entropy leads to the concept of entropy in thermodynamics. The concepts of the thermodynamics and statistical physics are appeared from here: temperature, pressure, density, distribution function. The emergence of new concepts for ONDS leads to a modification of the methods and techniques for their description. For example, instead of the phase space, it is more convenient to use the SD-space for ONDS analysis. This modification of the phase space is dictated by PDS.

3. *The evolution of ONDS is the result of double symmetry breaking.* At each hierarchical level of ONDS, evolution is determined by breaking the symmetries of this level and the symmetry of the lower hierarchical level. That is, the violation of symmetry is always associated with the interaction of the adjacent hierarchical level of matter.

The process of symmetry breaking in quantum systems is characterized by bifurcation [16, 23]. The essence of bifurcation is that a change in the topology of the system occurs at special points in the phase space. Probabilistic laws were used to solve bifurcation problems. However, according to the mechanics of the SP, an analytical method for solving them follows from the condition of infinite divisibility of matter [23]. Indeed, if we take into account the infinite divisibility of matter, then the bifurcation point will become a region of micro variables. **The description of the system at the micro level eliminates the peculiarity of the macro-description of the dynamics of the body at the bifurcation point!** The possibility of a deterministic micro-description of the dynamics of a system at the bifurcation point means that the use of probabilistic models can be considered as coarsening of models of bodies and theories. This coarsening allows us to describe processes in the absence of knowledge about the initial data's. The physical laws themselves determine the region of permissible coarsening. This mechanism of symmetry breaking at the bifurcation point indicates its universality, both for classical and for quantum mechanics, since it is always associated with the interaction of the upper level with the lower level [23].

3. The conditions of the ONDS existence. Although "motion is the way of existence of matter", in practice we often deal with stationary objects. Let us assume that **the ONDS is stationary if the characteristic time of its existence is much longer than the characteristic times of internal processes that ensure this existence**. From the point of view of physics, stationarity means that at all physical points of the ONDS, the values of its parameters do not change during the characteristic times of internal processes.

The way in which stationary ONDS exists is the balance of incoming and outgoing flows of matter, energy, entropy at all hierarchical levels [21, 28]. Bernard's convection cell is one of the simplest stationary objects. It exists due to the flow of matter, which transfers energy from the heated region to the cold region. This flow is created by the temperature difference at the boundaries of the gas or liquid [7]. The larger the

temperature gradient, the smaller the structure of convective cells. With a sufficient value of the gradient, turbulence appears.

The stationarity of the complex ONDS requires stationarity at all its hierarchical levels. If for the existence of a Bernard's cell it is sufficient to maintain a temperature gradient, then for the existence of more complex ONDS, for example, a living cell, a balance of flows of various types of matter and energy is necessary. In this case, the flow of matter entering the ONDS is a similar of combination of ONDS lower hierarchical levels. Therefore, all levels of ONDS can exist only through interactions between themselves and with the outside world. It follows from PDS that these interactions are determined by the symmetries of both body and space.

In fact, the stationarity of the ONDS cannot be absolutely. During a time long enough, its structure will change. This **time, which determines the ONDS lifetime, can be called evolutionary.** For complex systems, the lifetime will be determined by the existence of various channels of energy conversion between different hierarchical levels of ONDS. The connection between the steps of this hierarchical ladder of the ONDS is determined by *evolutionary nonlinearity*, which also responsible for symmetry breaking.

Then, the greater the gradient of external forces, the deeper the hierarchy of systems is violated [21]. This corresponds to the established by Einstein and other laws, according to which, the deeper the energy levels of an atom, the more short-wave photon it can be excited.

The existence and evolution of two adjacent hierarchical levels of matter, MP and SP, can be described in the framework of the laws of classical mechanics. However, the processes connecting the more distant hierarchical levels of matter are much more complicated. Since the number of hierarchical levels of matter is infinite, a complete description of evolution is a task of enormous complexity. Nevertheless, **the existence of deterministic interrelations of laws for the two adjacent hierarchical levels allows us to state that such relationships exists for all hierarchical levels of matter.**

One of important example for used of the physics of evolution is the problem of the Universe. Indeed, the physics of evolution can be directly used to solve some problems of astrophysics, since it allows one to calculate the energy fluxes in the Universe during the motion of galaxies, stars, planets, in inhomogeneous fields of gravity forces, particles flows. Today, astrophysics is based on the Newtonian motion equation and on the Einstein equation, which is a relativistic analogue of the Newton motion equation. In many ways, the contradictions between the results of observations and these equations compel us to introduce hypotheses about hidden matter, about dark energy, etc. This may be because Newton's motion equation does not take into account the role of matter structures in their dynamics. This disadvantage can be eliminated by using the equations of physics of evolution. [26]. For example, taking into account changes in the internal energy of a star when this star moves in inhomogeneous gravitational fields will give corrections to the energy balance of stars [23, 27]. According to the physics of evolution, for the existence of a nonequilibrium Universe, it must expand. This will provide it with the negentropy necessary to maintain nonequilibrium processes, for organize new structures and compensate for the growth of D-entropy in the Universe.

Thus, the physics of evolution includes the mechanics of systems, the extended formalisms of classical mechanics, the principles of the relationship of the hierarchical steps of the ONDS, obtained from the analysis of the properties of the SP's motion equations [14, 23].

Physics of evolution and philosophical principles

The essence of the physics of evolution has been explained in previous sections. In this section we will consider the philosophical problems associated with the physics of evolution.

1. Unity and the struggle of opposites. A search for DMI led to PDS. From PDS we came to the dualism of energy, according to which the invariant of the body's motion is the sum of the body's motion energy and the internal energy. Thus, each of these energies can change, but its sum is invariant. The concept of "symmetry of ideal chaos" is associated with the internal energy of an equilibrium system. This symmetry corresponds to the absence of relative motion for all subsystems, the combination of which can represent this system. It follows that the equilibrium of the system means that the sum of the moments of the subsystems relative to the center of mass of this system is always zero. Thus, we have "chaos", which we associate with the internal energy of the equilibrium system. In addition, we have an "order", which we associate with the body's motion energy as a whole.

That is, the nature of DMI is due to the transition of the body's motion energy into the internal energy of the chaotic motion of their elements. Hence, the evolution of matter, the formation of its structures are due to the struggle of two opposites - "chaos" and "order". Chaos plays the role of a "black hole", providing the absorption of the body's motion energy. This is the destructive role of chaos. However, on the other hand, the existence of "chaos" is necessary for the emergence of a new order. That is, **the process of evolution occurs according to the law of unity and struggle of opposites "chaos" and "order".**

The measure of the transformation of "order" energy into energy of "chaos" is characterized by D-entropy. That is, D-entropy plays the role of a measure of increasing "chaos" [29]. The violation of the symmetry of time is also associated with the transformation of the motion energy into internal energy. This allows us proposing a measure of "evolutionary time", defined as the rate of change of D-entropy. There is no perfect "chaos" or "order" in nature and entropy does not reach an absolute maximum. This means that the body's motion energy and internal energy cannot be equal to zero [30]. That is, matter cannot be in a state of absolute motion or absolute chaos! "Chaos" and "order" can only coexist.

The "birth" of new systems is inextricably linked with the destruction of previous systems and occurs in accordance with the laws of conservation of energy and matter of both systems and the world around them. This is reflected in the principle of dualism of symmetries, according to which the evolution of the world proceeds in the unity and struggle of "chaos" and "order".

2. The unity of the world's picture and the universality of the fundamental laws of physics. The unity of nature follows from the condition of openness. This is extremely important for building a physical picture of the world. The Universe cannot be divided into independent parts that is always done for its mathematical description. This is a huge flaw in mathematical models. Dirac suggested that it can be eliminated if one knows the principles of interaction of system elements and evolution [31]. This assumption is confirmed by the existence of principles for constructing a hierarchical structure of matter "from simple to complex", as well as the fact that matter is an ONDS hierarchy. Thus, these principles are consistent with evolutionism, with the idea of unity, interconnection and interdependence of all structures of the Universe.

If the world develops in accordance with deterministic physical laws, then in nature there is nothing that does not arise from a simpler one [12]. Thus, the physics of evolution confirms the integrity and uniqueness of the picture of the world, as well as the universality of the laws of physics for the Universe.

Let us to give a historic fact. Aristotle, not knowing the concepts of energy and acceleration, found of the body's motion equation, based on observations. According to his equation, the velocity of bodies is proportional to the force. This result is fundamentally contrary to Newtonian mechanics. However, as follows from the mechanics of SP, the Aristotle motion equation is true in the limiting case, when the body's velocity reaches its maximum value due to friction. The SP motion equation contains these two, at first glance, mutually exclusive limit cases. As follows from this equation, when the role of the structure of the body in its dynamics is small, then Newtonian mechanics is valid. However, when the work of external forces goes only for increase in internal energy due to the friction, the Aristotle equation is valid [14]. It follows that the lack of unity in the existing physical picture of the world may be due to the use of restrictions in the creation of a particular theory. If these restrictions are removed, then the contradictions may disappear, and the lost unity will be restored.

Thus, the physics of evolution reinforce the principles of the unity of the world's picture and the universality of the fundamental laws of physics [14].

3. Intensive way of constructing new knowledge. The main method for the development of physics is the study of new phenomena, objects, the identification of new laws and their explanation in the framework of existing fundamental theories. But in the process of the development of science, the limitations that were used in their construction began to appear. This can be seen in the example of elementary particle physics and cosmology. For example, here theories are faced with the problems of spontaneous symmetry breaking in understanding the Heisenberg uncertainty principle. In astrophysics there is a problem of dark matter. A similar difficulty existed to explain the problem of irreversibility in the framework of theories of classical mechanics [30]. This difficulty was overcome by the expansion of formalisms of classical mechanics as a result of taking into account the role of the structure of bodies in their dynamics. Thanks to such accounting, DMI was found, which opened the way to the physics of evolution. It follows that there is a possibility of the development of physics by identifying and eliminating the limitations on which its theories were based. This demonstrated **that physical theories can go the intensive way if existing theories are improved using more realistic models.**

Newton found new laws of classical mechanics, thanks to the simplest model of the body in the form of MP, which excludes from consideration the structure of bodies. However, as it turned out, to describe the processes of evolution in nature, it is necessary to take into account the structure. This has led to the possibility of constructing evolutionary physics based on the fundamental laws of physics. In turn, the physics of evolution has opened up the possibility of studying nature during its evolution.

The construction of the physics of evolution has revealed the need to develop new approach to the construction of a mathematical apparatus that allows us to describe the universal processes of symmetry breaking in physics. The essence new approach lies in the description of the interaction of symmetry groups arising from the motion of the ONDS in inhomogeneous external force fields. The interaction of symmetry groups leads to a violation of the symmetry of time and then to DMI. These violations are associated with "evolutionary nonlinearities" that describe the transformation of energies between independent spaces of variables from different symmetry groups [21, 23].

4. Nonlinear reductionism, the principle of causality and holism. Reductionism plays an important role in the development of science. Today this principle collides with the great difficulties. These difficulties, as a rule, indicate that the further development of knowledge about nature along the path of "*primitive reductionism*" and the extension of theory based on its existing foundation, is no longer a sufficiently effective way of understanding the world, as it was in the initial stages of the development of science.

Let us call by the "primitive reductionism" or linear reductionism such reductionism for which the sum of information about the elements gives complete information about the entire system. This reductionism does not take into account a qualitative leap in information due to the transition of quantity into quality. However, the processes of evolution in nature are impossible without these leaps. Therefore, in "*primitive reductionism*" it is impossible to search for laws and principles that establish a nonlinear relationship between the properties and laws that characterize the upper hierarchical level of matter, with the properties and laws of the elements of the lower level.

DMI, which establishes the causality principle in the physics of evolution, is non-linear. This suggests a nonlinear relationship of qualitatively new laws of system behavior based on the laws of the dynamics of their elements. Therefore, this also speaks of the nonlinearity of reductionism and the principle of causality.

In connection with the physics of evolution, **it is necessary to use as we call "*nonlinear reductionism*" to study the evolutionary process.** "*Nonlinear reductionism*" may be one of the promising ways to develop a picture of the world. This path is justified by the existence of general principles for the synthesis of knowledge about the laws of ONDS behavior, based on knowledge of physical laws that determine the dynamic and evolutionary characteristics of their elements. Using these principles, you can build a picture of the world, climbing the hierarchical ladder of matter.

A pre-existing explanation of irreversibility is based on probabilistic principles. However, it is one thing to use the concept of randomness for a statistical description of systems, and another when it is a principle that determines the evolution of the world. If the concept of randomness belonged to the fundamental principles of nature, this would mean the absence of determinism [31]. And this, in turn, would mean the absence of "nonlinear reductionism", according to which there is the possibility of knowledge developments from "simple to complex" due to the universality and self-consistency of the physics laws.

The absence of "*nonlinear reductionism*" will mean the triumph of holism, an alternative to the principle of reductionism, which has deep roots in ancient Eastern philosophy. A brief definition of holism: "the whole is greater than the sum of its parts" [20]. For example, according to holism, life has properties that do not follow from the properties of inanimate matter. These are the properties of reproduction, homeostasis, regeneration, etc. However, if the properties of the whole are not related to the properties of its parts, this means the unknowability of nature. Consequently, the question of the validity of reductionism is a question of the cognoscibility of the world and the possibility of constructing its closed, self-consistent picture. Thus, the physics of evolution has expanded the position of the principle of cognitive ability of nature due to the "*nonlinear reductionism*", since it demonstrates the possibility of constructing a hierarchical structure of matter based on the fundamental laws of physics.

Reductionism is impossible without the principle of causality. DMI, which underlies the physics of evolution, establishes the principle of causality in evolution. Indeed, DMI made it possible to connect evolution with the fundamental laws of physics, taking into account the influence of the structure of bodies on their dynamics.

According to principles of the physics of evolution, there is a causal relationship between the laws of different hierarchical steps of matter because the laws of the dynamics of elements determine qualitatively new laws of evolution of their systems. For example, the second law of thermodynamics, reflecting the irreversibility of processes in the system, follows from the reversible laws of the dynamics of the elements of system. This led to the possibility of a deterministic description of evolutionary processes [16, 29].

Without taking into account evolution, determined by the processes of organization, development and destruction of natural systems, the evolution picture of the world not only cannot be complete, it cannot be constructed in principle. The fact that the physics of evolution satisfies the causality principle opens the way to building an evolutionary picture of the world.

Thus, in the frame of the "nonlinear reductionism" it became possible to unite different fields of science in accordance with the principles of the unity of the picture of the world and the universality of the laws of nature.

5. Transition of quantity into quality. DMI was found due to the possibility of establishing the physical properties of systems based on knowledge of the properties of their elements. For example, if we build ONDS from the MP set, then it will have the irreversibility property, while the MP motion is reversible. Therefore very existence of DMI in the framework of the laws of physics indicates the deterministic way transition of quantity to quality.

DMI follows from the ONDS motion equation. According to this equation, DMI is associated with the conversion of motion energy into internal energy [14]. This transition is characterized by D-entropy. An analysis of D-entropy for systems with different number of elements moving in an inhomogeneous space showed that key statistical laws, for example, the law of fluctuations of quadratic functions [21], follow from the fundamental laws of physics.

Using methods of numerical calculations of the dynamics of systems in an inhomogeneous force field, it was found that for the number of elements in the system $N > 100$, the D-entropy can only be positive. This number characterizes the transition of the system to a new quality, in which the laws of statistics are applied. When $N > 1000$, the behavior of D-entropy ceases to depend on an increase in the number of elements. This number determines the area of validity of thermodynamics. That is, the fundamental laws of physics determine the scope of the empirical laws [11]. For example, take the Boltzmann equation [28]. Its importance for physics is difficult to overestimate. But this is an empirical equation, and therefore it has a number of limitations and even contradictions. For example, this equation contradicts the Poincare reversibility theorem, although formally, like the Poincare theorem, it is constructed based on the Hamiltonian formalism. These shortcomings are eliminated if the Boltzmann equation is directly derived from the extended Liouville equation [32]. Even when solving the problem of *N*-bodies, it is impossible to do without taking into account the fact that the energy of ONDS always consists of internal energy and the motion energy of its structures.

6. The unity of the micro and the macro world. The basic laws of physics, regardless of their field of application, must be closed, self-agreements and satisfy the causality principle if the world has evolved from simple to complex. This is true for objects of classical mechanics. However, in quantum mechanics, these conditions are violated due to the Heisenberg uncertainty principle. According to this principle, it is impossible to simultaneously determine the position and momentum of microparticles [19, 33]. This violates the causality principle in the micro world and therefore, excludes the possibility of constructing an evolutionary picture of the world. However, based on the conditions of the infinite divisibility of matter and the fulfillment of PDS, a deterministic explanation of the uncertainty principle can be proposed. If matter is divisible infinitely, it should be a combination of ONDS and possess internal energy. In this case, the principles of the formation macrosystems from microsystems are valid.

Using the canonical Schrödinger equation to describe their dynamics will lead to the uncertainty of their trajectory. Indeed, the canonical Schrödinger equation is obtained from the Hamilton formalism of classical mechanics, which does not take into account the role of the structure of the system in its dynamics.

This uncertainty is similar to the trajectory uncertainty that will arise when describing the dynamics of a system using the Newton equation since this equation does not take into account the influence of the body structure on its dynamics. Thus, the uncertainty in the description of dynamics based on the canonical Schrödinger equation can also be explained by the fact that it does not take into account the influence of the structure of quantum particles on their dynamics. As in classical mechanics, this uncertainty will be determined by changes in internal energy.

It is known that in quantum mechanics the internal energy of a system cannot be equal to zero. Therefore, as in classical mechanics, this will give uncertainty in the calculations of the volume of the phase space of interacting quantum systems, which is comparable with the value of the Planck constant. To eliminate this uncertainty, one needs to use the extended Schrödinger equation. This equation takes into account the role of changes in internal energy in the dynamics of quantum particles during their interaction [34]. Therefore, the Heisenberg uncertainty principle can be associated with existing methods for describing quantum systems that do not take into account the role of their structures in dynamics, but not because it is dictated by the nature of the microworld. This conclusion is confirmed by the above calculation results of the passage of a classical oscillator through a potential barrier. Only taking into account the role of internal energy in the dynamics of the system, we take into account this effect [25]. If this dependence is not taken into account, we will come to the problem of Aristotelian dichotomy between potentiality and relevance, which Heisenberg has deeply studied and which is still controversial [19, 35].

If so, the problem of substantiating the possibility of constructing physics of evolution, associated with the principle of uncertainty in quantum mechanics, is removed. This testifies in favor of the unity of the laws of physics and in favor of the existence of a "theory of everything".

Conclusion

The physics of evolution is based on the mechanics of structural particles. The mechanics of structural particles arose as a result of taking into account the influence of the structure of bodies on their dynamics. This mechanics is based on the motion equation of structural particles arising from the laws of classical mechanics and the principle of dualism of symmetry. From the motion equation of structural particles, it became possible to establish how non-potential dissipative forces arise from potential external forces. This allowed us to create the physics of evolution. The task of evolutionary physics is to describe the evolutionary processes of the appearance, development, and disappearance of physical systems in the framework of the fundamental laws of physics.

According to the physics of evolution, matter is infinitely divisible and represents an infinite hierarchy of open nonequilibrium dynamical systems. There are principles that allow you to climb the hierarchical levels of the structure of matter, getting the laws of the dynamics of the upper levels of matter according to the laws of the dynamics of the lower level. As a result, you can go “from simple to complex”, relying on the fundamental laws of physics, without involving any probabilistic laws. This allows you to build a hierarchical picture of matter, if the laws of behavior of only one of the hierarchical levels of matter are known.

Obviously, the number of principles that determine the relationship of hierarchical levels will increase with the development of knowledge. New principles will dictate new laws, such as the laws of evolution of living beings: the laws of self-reproduction, homeostasis, the adaptation of the body and its elements to external conditions. For

example, if we stand on the position of Marx, according to which consciousness is a property of matter, which reflects itself, and not a separate, independent entity, then in principle we can develop the physics of consciousness. Thus, in the process of developing knowledge, new laws of behavior of higher hierarchical levels of matter will become known. However, since new laws are built on the basis of the well-known, none of these new laws should contradict the well-known ones, which corresponds to the principle of "common foundations".

The physics of evolution reveals the essence of the law of unity and struggle of opposites, as is seen in the example of dualism "chaos" and "order". Chaos and order coexist only together. The mediator of these opposites is D-entropy, which determines the relationship of "chaos" and "order".

The physics of evolution strengthens the positions of those philosophical concepts that confirm the possibility of constructing an evolutionary picture of the world based on the fundamental laws of physics. In particular, this applies to reductionism.

The very possibility of constructing evolutionary physics testifies in favor of the existence of the causality principle within the framework of the basic laws of physics. As Einstein said: "God does not play dice." Indeed, according to the physics of evolution, the future arises from the present in a deterministic way. In general, the physics of evolution opens up the possibility of building a picture of the world within the framework of universal evolutionism, climbing the hierarchical ladder of matter from "simple to complex."

In accordance with the physics of evolution, the possibility of constructing an evolutionary picture of the world does not mean at all that someday in a very distant future, humanity will create the final picture of the world. The fact is that the number of hierarchical levels of matter is infinite, and the complexity of the process of cognition rapidly increases with the growth of the hierarchical level. Indeed, it is easy to see the history of the explanation of the second law of thermodynamics, which began about 200 years ago. However, this is only the second step in the hierarchy of matter from MP to SP! However, any natural phenomenon will eventually become known. That is, although the processes of studying nature are endless, but the limitations of existing knowledge are associated with the limitations of theories and models used, and not with the existence of the boundaries of knowledge.

Thus, taking into account the structural nature of matter and its role in dynamics has led to the possibility of describing irreversibility, the establishment of infinite divisibility of matter, the universality of the mechanism of symmetry breaking, and, ultimately, the possibility of describing evolutionary processes within the framework of the basic laws of physics. All this means the possibility of constructing a deterministic evolutionary picture of the world within the framework of the laws of physics.

REFERENCES

1. G. W't. Hooft. Free will in the theory of everything arXiv:1709.02874v1[quant-ph]8
2. S.Weinberg. Dreams of a Final Theory, Vintage, New York, 1992.
3. R. B. Laughlin. and David Pines.The Theory of Everything. PNAS January 4, 2000 97 (1) 28-31; https://doi.org/10.1073/pnas.97.1.28.
4. J. Horgan. The End of Science: Facing the Limits of Knowledge in the Twilight of the Scientific Age. xii + 322 pp., bibl., index. Reading, Mass." Addison-Wesley, 1996.
5. K. Mahendra. Verma Microscopic laws vs. macroscopic laws: Perspectives from kinetic theory and hydrodynamics. arXiv:1904.12044v1 [physics.flu-dyn]
6. H. G. Callaway. Fundamental Physics, Partial Models and Time's Arrow. Dec.2016 https://www.researchgate.net/publication/296327588.

7. I. Prigogine. From Being to Becoming, Nauka, Moscow, 1980.
8. V. L. Ginzburg. Special session ed. Collegium of the journal, dedicated to the 90th anniversary of the Ginzburg V.L. UFN, 177, 4, 345, 2007.
9. G. Nicolis, I. Prigogine. Exploring complexity, Mir, Moscow, 1990
10. G. M. Zaslavsky. Stochasticity of dynamical systems, Nauka, Moscow, 1984.
11. V. M. Somsikov, S. N. Azarenko. Determinism in Physics and Cognoscibility of a Picture of the World. Open Journal of Philosophy, 9, {265, 2019.
12. V.V. Aristov. Ernest Mah and Ludwig Boltzmann. A drama of ideas, a drama of people. Metaphysics, № 3 (21), {100, 2016.
13. V. Anry. Modern scientific worldview. UFN, 1, {3, 1929.
14. V. M. Somsikov. To the basics of the physics of evolution, Almaty, 2016.
15. V. F. Asmus. Ancient philosophy, Moscow, 1976.
16. A. Yu. Loskutov, A.S. Mikhailov. Introduction to Synergetics, Sci., Moscow, 1990.
17. N. S. Kryilov. Papers on substantiation of statistical physics: L. Publishing House of USSR AS, 1950.
18. E. Wigner. Symmetry and preservation laws, UFN, T LXXX111, 4, {729, 1964.
19. W. Heisenberg. Planck's opening and the basic philosophical problems of the nuclear theory, UFN, LXVI, 2, 163{175, 1958.
20. P. W. Anderson. More Is Different. Science, New Series, 177, 393{396, 1972.
21. V.M. Somsikov. Deterministic Irreversibility Mechanism and Basic Element of Matter. (2020).12th CMSIC CHAOS. Springer, Cham. 245{256.
22. C. Lanczos. The variational principles of mechanics, Peace, Moscow, 1962.
23. V. Somsikov. Deterministic irreversibility and the matter structure. JAP, 1{26, 2019.
24. Yu. L. Klimontovich. Statistical theory of open systems, Janus, Moscow, 1995.
25. V. M. Somsikov, A.B. Andreev, A.I. Mokhnatkin, V.I. Kapytin. Dual phase space of a nonequilibrium system. PEOS, 20, {1, 2018.
26. V. M. Somsikov. Transition from the mechanics of material points to the mechanics of structured particles, Modern Physics Letter B, 4, 1{11, 2016.
27. V. M. Somsikov. Irreversibility and physics of evolution. Chaotic Modeling and Simulation (CMSIM) 1, 2018.
28. Yu. B. Rumer, M. Sh. Rivkin. Thermodynamics, Stat. physics and Kinematics, Nauka, Moscow, 1977.
29. L. D. Landau, E.M. Lifshitz. Statistical physics, Nauka, Moscow, 1976.
30. J. Greenstein, A. Zaionz. Quantum challenge. Modern research of the foundations of quantum mechanics. Dolgoprudny, Intellect Press, 2012.
31. P.F.V. Dirac. The relation between metaphysics and physics. Proceedings of the Royal Society. Edinburg A V. 59 {122, 1938-1939.
32. V.M. Somsikov. The equilibration of a hard–disks sys.IJBC,14, 11,4027{4033, 2004.
33. R. F. Werner, T. Farrelly. Uncertainty from Heisenberg to Today. 2019.
34. V. M. Somsikov. Extension of the Schrodinger equation, EPJ Web of Conferences Baldin, ISHEPP XXIII, Dubna, 1{7, 2017.
35. A. N. Shirazi. Heisenberg's Equality of Inequivalents Problem. arXiv:2003.06517v1 [physics.hist-ph] 14 Mar 2020.

The ac driven Frenkel-Kontorova model: from Shapiro steps to chaos

Jasmina Tekić[1], Andre Botha[2], Petar Mali[3], and Yuri M. Shukrinov[4]

[1] "Vinča" Institute of Nuclear Sciences, Laboratory for Theoretical and Condensed Matter Physics - 020, University of Belgrade, PO Box 522, 11001 Belgrade, Serbia
(E-mail: jasminat@vin.bg.ac.rs)
[2] Department of Physics, University of South Africa,Science Campus, Private Bag X6, Florida Park 1710, South Africa
(E-mail: bothaae@unisa.ac.za)
[3] Department of Physics, Faculty of Science, University of Novi Sad, Trg Dositeja Obradovića 4, 21000 Novi Sad, Serbia
(E-mail: petar.mali@df.uns.ac.rs)
[4] BLTP, JINR, Dubna, Moscow Region, 141980, Russia
Dubna State University, Dubna, 141980, Russia
(E-mail: shukrinv@theor.jinr.ru)

Abstract. The appearance of devil's staircase and chaos have been studied in the dc+ac driven Frenkel-Kontorova model. In the overdamped limit, the devil's staircase structure arising from the complete mode-locking of an entirely nonchaotic system was observed. Even though no chaos was found, a hierarchical ordering of the Shapiro steps was made possible through the use of a previously introduced continued fraction formula. When the inertial term is included, unlike in the overdamped case, the increase of mass led to the appearance of the whole series of subharmonic steps in the staircase of the average velocity as a function of average driving force in any commensurate structure. At certain values of parameters, the subharmonic steps became separated by chaotic windows while the whole structure retained scaling similar to the original staircase.
Keywords: Frenkel-Kontorova Model, Shapiro steps, Devil's Staircase, Chaos.

1 Introduction

One of the most interesting properties of nonlinear dynamical systems with competing time scales is their ability to exhibit frequency locking phenomena. One such phenomenon, that occurs in nonlinear systems under some external radiation or force are Shapiro steps, which appear as a result of dynamical mode-locking of frequencies. Due to significance for various technological applications, for years, they have been the subject of intensive theoretical and experimental studies in charge-density wave systems [1–4], vortex matter [5–7], irradiated Josephson junctions [8–10], and, more recently, even in superconducting nanowires [11,12]. In the search for an optimum way to control the dynamical mode-locking, one should keep in mind that there is one usually unwanted but often present phenomenon in nonlinear dynamical systems, which is highly sensitive to the initial condition, and which can affect the stability of locked states, this phenomenon is the chaos. Therefore, studies of chaotic be-

havior are necessary in order to get a complete microscopic picture of frequency locking in nonlinear systems.

One of the models capable of capturing the essence of frequency locking, and the appearance of Shapiro steps is the Frenkel - Kontorova (FK) model under external periodic forces [13–15]. The standard FK model represents a chain of harmonically interacting identical particles subjected to the sinusoidal substrate potential [13,14]. When the external dc and ac forces are applied locking occurs between the frequency of the particles motion over the periodic potential and the frequency of external ac force [14]. On the macroscopic scale, this effect is characterized by the appearance of a staircase of Shapiro steps in the curve for average velocity as a function of the average external driving force $\bar{v}(\bar{F})$. The steps are called harmonic if the locking appears at integer multiples of the ac frequency or subharmonic at noninteger rational multiples.

It is well known that dissipative dynamical systems with competing frequencies can be described by the circle map. Depending on the coupling strength, the circle map can develop a cubic inflection point leading to the appearance of a devil's staircase and the transition to chaos [16,17]. When the coupling is below some critical value, the staircase is incomplete, i.e., there are quasiperiodic intervals between the frequency locked plateaus (steps) of periodic behavior. As coupling increases, the frequency locked regions start to broaden, and at some critical value, they fill up all the space. Though the quasiperiodic intervals have zero measure, and the devil's staircase is said to be complete, they have nonzero fractal dimension (scaling index) which is *universal*, i.e. the same $D = 0.87$ for all the systems (at least for those described by the circle map with a cubic inflection point), and thus often considered as a constant of nature [16]. The mechanism leading eventually to chaos is the interaction between different resonances caused by the nonlinear coupling and overlapping of resonant regions when coupling exceeds certain critical value. However, the universality of this scenario as well as the universality of the fractal dimension have been questioned in the past years, and numerous studies in the wide range of biological, chemical, and physical systems have been devoted to models showing the occurrence of the entire nonchaotic regions with complete phase locking [18–21]. Nonchaotic transition from quasiperiodicity to complete locking [18] and *deviation from the universality* with fractal dimension varying from 0.64 to 0.98 have been observed [20,22].

In this paper we will explore the appearance of devil's staircase and chaos in the dc+ac driven Frenkel-Kontorova model. The discrete FK model is not integrable, and in general, its dynamics can be chaotic [13] since due to its nonintegrability, atomic motion is always accompanied by energy exchange between different modes leading to intrinsic chaotisation of its dynamics [13]. We will analyze both over- and underdamped models and examine how the system dynamics changes with the changing of parameters and transferring from one limit to another.

The paper is organized as follows. The model is introduced in Sec. II, and simulation results are presented in Sec. III and IV. The devil's staircase structure is revealed in Sec. III, while the chaos was examined in Sec. IV. Finally, Sec. V concludes the paper.

2 Model

We consider the dynamics of the standard *damped* FK model, which consists of a series of coupled harmonic oscillators u_l of mass m, subjected to the periodic substrate potential $V(u)$:

$$V(u) = \frac{K}{(2\pi)^2}[1 - \cos(2\pi u)], \tag{1}$$

where K is the pinning strength. This potential belongs to the family of nonlinear periodic deformable potentials, introduced by Remoissent and Peyrard [23] as a way to model many specific physical situations without employing perturbation methods. By changing the shape parameter r, the potential can be tuned in a very fine way, from the simple sinusoidal one for $r = 0$ to a deformable one for $0 < |r| < 1$.

The system is driven by dc and ac forces,

$$F(t) = F_{dc} + F_{ac}\cos(2\pi\nu_0 t), \tag{2}$$

where F_{ac} and ν_0 are amplitude and frequency of the ac force respectively.

If the system is *overdamped*, its dynamics is described by the following system of equations of motion:

$$\dot{u}_l = u_{l+1} + u_{l-1} - 2u_l - V'(u_l) + F(t). \tag{3}$$

where $l = -N/2, ..., N/2$.

In the *underdamped* case we will consider the following set of equations:

$$\begin{aligned} \dot{u}_l &= v_l \\ m\dot{v}_l &= u_{l+1} + u_{l-1} - 2u_l - \frac{K}{2\pi}\sin(2\pi u_l) - v_l + F(t), \end{aligned} \tag{4}$$

where $l = 1, ..., N$ labels the particles, and the term, which comes from the substrate potential is given for the case $r = 0$. The damping is fixed by two parameters m and K, and for some constant force F, the system is overdamped for [24,25]:

$$0 < m \leq \frac{1}{4(2+K)}. \tag{5}$$

When the system is driven by a periodic force, two frequency scales appear in the system: the frequency ν_0 of the external periodic (ac) force and the characteristic frequency of the particle motion over the periodic substrate potential driven by the average force $\bar{F} = F_{dc}$. The competition between these two frequency scales can result in the appearance of dynamical mode-locking. The solution of the system (4) is called resonant if the time average mean velocity $\bar{v}$ satisfies the relation:

$$\bar{v} := \left\langle \frac{1}{N}\sum_{i=1}^{N} v_i \right\rangle_t = \frac{i\omega + j}{s}\nu_0, \tag{6}$$

where i, j, s are integers and ω is the winding number [15], which is fixed to rational or irrational values, characterizing commensurate or incommensurate structures, respectively.

The above systems of equations (3) and (4) have been integrated for the commensurate structures $\omega = \frac{1}{2}$. using the fourth-order Runge-Kutta method with the periodic boundary conditions for the system of $N = 8$ particles. The force has been increased from zero with the very fine discretization $10^{-4} - 10^{-6}$. Unlike in the overdamped case, the behavior of the underdamped system depends on its previous history therefore, the initial condition at the each step of driving force was obtained from the last step in the integration, at its previous value.

3 Devil's staircase in a nonchaotic system

We will consider first the overdamped FK model described by Eq. (3). It is well known that the standard overdamped FK model with sinusoidal substrate potential for commensurate structures with integer values of ω reduces to single particle model where no subharmonic locking exists, while for rational, noninteger ω subharmonic steps do appear, however, their size is so small that they are hardly visible on the $\bar{v}(\bar{F})$ characteristics [13]. By introducing some form of deformable potential such as the one in Eq. 1 the whole series of halinteger and higher order subharmonic steps start to emerge [14].

In Fig. 1, the average velocity as a function of the average driving force is presented for two values of the ac amplitude. The number and size of Shapiro

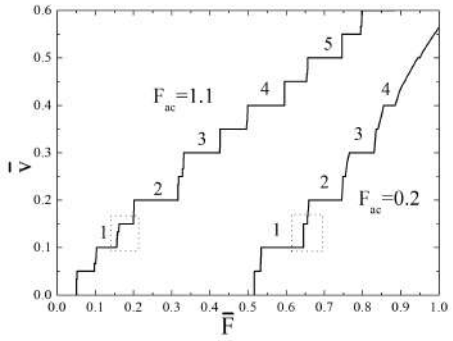

Fig. 1. The average velocity $\bar{v}$ as a function of the average driving force $\bar{F}$ for $K = 4$, $\nu_0 = 0.2$, $\omega = \frac{1}{2}$ $r = 0.5$, and different values of the ac amplitude $F_{ac} = 0.2$ and 1.1. The numbers mark harmonic steps.

steps, which appear on the response function are determined by the amplitude of the ac force and the extent of deformation of the potential. In Fig. 1, beside harmonic, only halfinteger steps are clearly visible, however, the high resolution analysis reveals a devil's stair case, i.e., an infinite series of higher order subharmonic steps in between them. In Fig. 2, the high resolution views

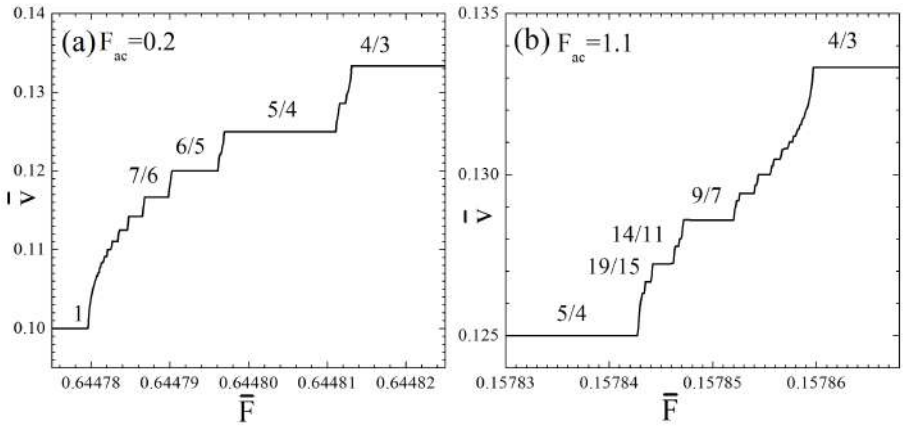

Fig. 2. The high-resolution views of the selected areas in Fig. 1 for $F_{ac} = 0.2$ in (a) and 1.1 in (b). The rest of parameters are the same as in Fig. 1

of the selected areas in Fig. 1 are presented. In the devil's staircase structure, the steps appear following the continued fraction formula [9,10], which in the case of the ac driven FK model can be written as:

$$\bar{v} = \left(i \pm \frac{1}{m \pm \frac{1}{n \pm \frac{1}{p \pm \ldots}}} \right) \omega\nu_0, \tag{7}$$

where $i, m, n, p, ...$ are positive integers. Harmonic steps are presented by the first-level terms, which involve only i, while the other terms involving other integers describe subharmonic or fractional steps. Terms involving i and m are called second-level terms, those with i, m, and n third-level terms, etc. In Fig. 2 (a) and (b) the sequences of the third and fourth level become visible. Our calculations of fractal dimensions shows that it varies with deformation of the potential and the ac amplitude, for small deformation it changes around 0.87, while for higer deformation it decreases depending on the ac amplitude.

Appearance of devil's staircase in the overdamped FK model might lead to the conclusion that if it exhibits complete locking, it must also, therefore, exhibit the chaos. In our search for chaos we applied the largest Lyapunov exponent (LE) computational technique and extend our examination to a very high resolution and wider range of parameters, the ac amplitudes in particular. Regardless of system parameters, no chaos was ever observed. The overdamped Frenkel-Kontorova model remained entirely non chaotic.

The absence of chaos in the ac driven overdamped FK model can be attributed to the dissipative character of the system and the Middleton no-passing rule [26,27]. According to this rule which applies on one-dimensional, strictly overdamped systems, the order of particles must be preserved in dynamics or, in other words, the particles cannot jump over each other while they move. In such case, there could be no overlapping of resonances which is the main cause of the chaotic behavior in frequency locking systems [10,17,16].

4 The appearance of chaos

When the inertial term is present (Eq. 4) and the FK model is underdamped its behavior changes completely. One of well known inertial effects is the appearance of subharmonic mode-locking even in the commensurate structures with integer values of ω [14]. However, the increase of mass in the ac+dc driven FK model may have much more dramatic effects than just simply inducing subharmonic streps. In Fig. 3, the response function $\bar{v}(\bar{F})$ and the corresponding Lyapunov exponents (LE) λ_i are presented for two different values of mass. In

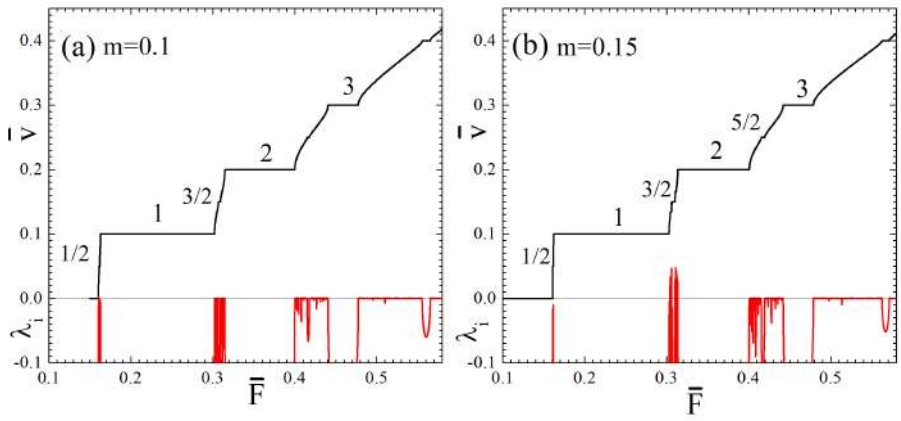

Fig. 3. The average velocity $\bar{v}$ as a function of the average driving force $\bar{F}$ and the corresponding Lyapunov exponents λ_i for $K = 4$, $r = 0$, $F_{ac} = 0.2, \nu_0 = 0.2, \omega = \frac{1}{2}$, and $m = 0.1$ and 0.15 in (a) and (b), respectively. On this scale of y axis only the largest Lyapunov exponent is visible. Numbers mark the harmonic steps.

order to also examine the effect of the mass on the appearance of subharmonic steps, we consider here the standard FK model with sinusoidal substrate potential ($r = 0$). As we can see in Fig. 3 (a) since $m \neq 0$, subharmonic steps start to appear. As the mass increases in Fig. 3 (b) chaotic behavior starts to appear indicated by the positive values of the LE.

Further, we will focus on the chaotic regions between the large harmonic steps, and examine in detail the onset on chaos on subharmonic steps. In Fig. 4, the staircase structure of the average velocity as a function of the average driving force $\bar{v}(\bar{F})$ and the corresponding LE for $m = 0.2$ are presented. Chaotic behavior appears only in the region of subharmonic steps as we can see in Fig. 4 (a). As the force increases the response of the system approaches to the that of the dc driven one. If we further examine the chaotic region, the high resolution view in Fig. 4 (b) reveals the staircase of subharmonic steps separated by chaotic windows. Devil's staircase containing Shapiro steps separated by self-similar chaotic regions has been observed both in the single and in the one dimensional stack of Josephson junctions [28,29]. It was shown that in the current-voltage characteristics of the junctions the staircase with

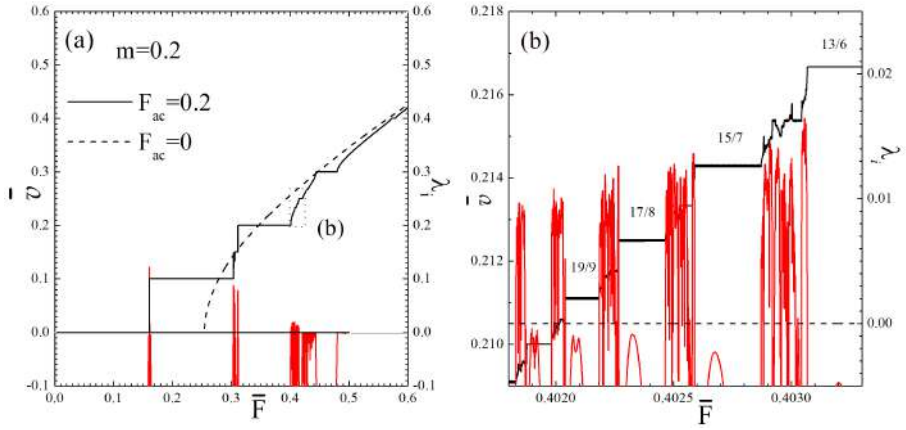

Fig. 4. (a) The average velocity $\bar{v}$ as a function of the average driving force $\bar{F}$ and the corresponding Lyapunov exponents λ_i for $K = 4$,r=0, $F_{ac} = 0.2, \nu_0 = 0.2, \omega = \frac{1}{2}$, and $m = 0.2$. Dashed line corresponds to the dc driven system $F_{ac} = 0$. (b) The high-resolution views of the selected areas in (a).

chaotic intervals preserves the scaling of the original staircase with the fractal dimension close to 0.87. In our case, for the fractal dimension D in the region between the second and third harmonic step, we obtained D=0.8759 with an uncertainty of ±0.0166.

5 Conclusion

In this work the appearance of devil's staircase and chaotic dynamics have been studied in the dc+ac driven Frenkel-Kontorova model. In the overdamped limit, though entirely non chaotic, the system exhibits the devil's staircase arising from the complete mode-locking, where the Shapiro steps appear following continued fraction formula. In the underdamped limit, on the other hand, the increase of mass leads to the appearance of the whole series of subharmonic steps in the staircase of the average velocity as a function of average driving force in any commensurate structure. At certain values of parameters, the subharmonic steps become separated by chaotic windows while the whole structure retained scaling similar to the original staircase.

This work could be important for all nonlinear physical systems with competing frequencies from physical to chemical and byological, which exhibit devil's staircase and potentially could go under the transition to chaos. Shapiro steps have been studied for years in Josephson junction systems, which posses a great potential for technological applications from device building to voltage standards and detection of Majorana fermions [30], and situations in which the parameters should be set to produce desired dynamical effects without evoking chaos are a common engineering problem [31]. In voltage standards or other applications, both quasiperiodic and chaotic behavior must be avoided; however, surprisingly, the optimum operating region is actually near the onset of

chaos. Therefore, further comparative studies of the resonance phenomena in the Frenkel-Kontorova model and other physical systems, particularly experiments, would be very interesting.

References

1. A. Zettl and G. Grüner, Phys. Rev. B, **29**, 755 (1984).
2. G. Grüner and A. Zettl, Phys. Rep. **119**, No. 3 (1985).
3. G. Grüner, Rev. Mod. Phys. **60**, 1129 (1988).
4. R. E. Thorne, J. S. Hubacek, W. G. Lyons, J. W. Lyding, and J. R. Tucker, Phys. Rev. B, **37**, 10055 (1988).
5. N. Kokubo, R. Besseling, V. M. Vinokur, and P. H. Kes, Phys. Rev. Lett., **88**, 247004 (2002).
6. C. Reichhardt and C. J. Olson Reichhardt, Phys. Rev. B **92**, 224432 (2015).
7. A. B. Kolton, D. Domínguez, and N. Grønbech-Jensen, Phys. Rev. Lett. **86**, 4112 (2001).
8. S. P. Benz, M. S. Rzchowski, M. Tinkham, and C. J. Lobb, Phys. Rev. Lett., **64**, 693 (1990).
9. Yu. M. Shukrinov, S. Yu. Medvedeva, A. E. Botha, M. R. Kolahchi, and A. Irie, Phys. Rev. B **88**, 214515 (2013).
10. Yu. M. Shukrinov, A. E. Botha, S. Yu. Medvedeva, M. R. Kolahchi and A. Irie, Chaos **24**, 033115 (2014).
11. R. C. Dinsmore III, M. H. Bae, and A. Bezryadin, Appl. Phys. Lett. **93**, 192505 (2008).
12. M. H. Bae, R. C. Dinsmore III, T. Aref, M. Brenner, and A. Bezryadin, Nano Lett. **9**, 1889 (2009).
13. O. Braun and Yu. S. Kivshar, *The Frenkel-Kontorova Model* (Springer, Berlin, 2003).
14. J. Tekić and P. Mali, *The ac driven Frenkel - Kontorova model*, (University of Novi Sad, Novi Sad, 2015).
15. L. M. Floría and J. J. Mazo, Adv. Phys. **45**, 505 (1996).
16. P. Bak, Phys. Today **39**, 38 (1986).
17. M. H. Jensen, P. Bak, and T. Bohr, Phys. Rev. Lett. **50**, 1637 (1983).
18. P. Alstrøm, B. Christiansen and M. T. Levinsen, Phys. Rev. Lett. **61**, 1679 (1988).
19. P. Alstrøm, B. and M. T. Levinsen, Phys. Rev. B **40**, 4609 (1989).
20. J. Maselko and H. L. Swinney, J. Chem. Phys. **85**, 6430 (1986).
21. A. Cumming and P. S. Linsay, Phys. Rev. Lett. **59**, 1633 (1987).
22. S. E. Brown, G. Mozurkewich and G. Grüner, Phys. rev. Lett. **52**, 2277 (1984).
23. M. Remoissenet and M. Peyrard, Phys. Rev. B **29** , 3153 (1984).
24. C. Baesens, Lecture Notes in Physics **671**, 241 (2005), (Springer, Berlin, Heidelberg).
25. C. Baesens, R. S. MacCay, Nonlinearity, **17**, 567 (2004).
26. A. A. Middleton, Phys. Rev. Lett. **68**, 670 (1992).
27. A. A. Middleton, and D. S. Fisher, Phys. Rev. B **47**, 3530 (1993).
28. Yu. M. Shukrinov, A. E. Botha, S. Yu. Medvedeva, M. R. Kolahchi and A. Irie, Chaos **24**, 033115 (2014).
29. A. E. Botha, Yu. M. Shukrinov, S. Yu. Medvedeva and M. R. Kolahchi, J. Supercond. Nov. Magn. **28**, 349 (2015).
30. L. F. Rokhinson, X. Liu, and J. K. Furdyna, Nat. Phys. **8**, 795 (2012).
31. R. I. Kauz, Rep. Prog. Phys. **59**, 935 (1996).

Switching Frequency Bifurcations in an LED Boost Driver

Elias D. Tsirbas[1], **Frangiskos V. Topalis**[1], **Evangelos N. Skoubris**[2]

[1]National Technical University of Athens, Zografou, Athens, Greece
E-mail: etsirbas@central.ntua.gr, fvt@central.ntua.gr
[2]University of West Attica, Egaleo, Athens, Greece
E-mail: eskoubris@uniwa.gr

Abstract. Under specific conditions LED driver circuits can be as susceptible to chaotic bifurcations, as conventional boost converters have proven to be. A significant relationship between the switching frequency of the boost converter's transistor and the circuit's nonlinear behaviour is shown. In order to examine such transistor switching frequency effects, an open-loop configuration is employed, since a feedback control system would obscure these particular nonlinearities. A theoretical method has been devised to predict the unstable frequency regions based on certain dependence equations. There are particular nonlinear parameters which influence the circuit's behaviour, such as the reverse-recovery time of the boost diode, as well as the collective effect of the inductance and the diode's junction capacitance. The dependence equations prove a correlation between these inherent nonlinearities and the switching frequency of the boost transistor. Period doublings and transitions to chaos occur for several regions of the examined switching frequency range. The theoretical method used for the numerical analysis is based on the periodicity of certain voltage waveform peaks, probed at key points on the converter. The LED boost driver displays a wealth of nonlinear phenomena and detrimental effects on its brightness levels throughout the nonlinear frequency regions.

Keywords: LED boost converter, chaotic oscillations, nonlinear dynamics, bifurcations, lighting circuits.

1 Introduction

Plenty of practical applications that employ power conversion circuits would benefit from an alternative circuit model, one that takes into account the nonlinear nature of the converter's characteristics. Conventional modelling techniques utilized so far, can omit various nonlinear effects and as a result the circuit designer might miss certain operating behaviours that may significantly degrade a power converter's performance. Such unpredictable phenomena might arise in current-mode DC-DC boost converters [1] or in Power Factor Correction (PFC) power supplies in the form of slow-scale instabilities, which can degrade the power factor significantly [2]. As a consequence, the linearization approach that is still commonly used in the industry can provide inaccurate solutions to designers, since nonlinear instabilities that can affect a power converter's response, cannot be easily detected without a certain type of analysis. Such an analysis can offer an in-depth view into the behaviour of these nonlinear circuits that may embrace specific properties such as subharmonics [3] as well as several chaotic phenomena within numerous power converter configurations [4].

A diode circuit in the form of a resonator made an early introduction to electronics chaos [5]. The inductor and the diode of this simple circuit have proven to be highly nonlinear circuit elements as shown in [6] and [7] amongst others. When the nonlinear capacitance of the diode's equivalent circuit is combined with a nonlinear resistor at high frequencies chaos emerges [8].

Diode resonator circuits have also been initially used for the study of the *period-doubling* phenomenon that can lead a system towards chaos. At the course of this phenomenon, a signal waveform's period is doubled successively as a control parameter of the circuit is varied, until the time-series finally become chaotic and the signal's period becomes undetectable. The circuit diverges from its designated operation, as in the example of rectifiers that employ slow-response diodes [9]. Since LED driver circuits are essentially modified DC-DC power converters [10], it is important to explore the conditions that could cause chaos in such a system. In most published papers though, chaos appears mainly due to controller instabilities of the feedback loop in such power converters [11] or as a result of slope disturbances [12]. The possibility of chaos is examined without the feedback loop, in order to prove that chaos can be possible only due to the inherent nonlinear properties of the boost diode and inductor combined.

2 Diode physical characteristics

A Light Emitting Diode (LED) forms a special type of diode. A specific forward voltage is required in order to switch on an LED, which will then enable the nominal operating current through it. LEDs are nonlinear devices, in the sense that they do not possess a linear relationship between the voltage applied, and the current drawn. Once the forward voltage is reached, the current through the LED will rise exponentially, and visible radiation is emitted.

The equation shown below from the authors' published work [13], shows that the instantaneous current of the diode is linked with an exponential relationship to its reverse current,

$$i(v) = i_0(e^{\frac{q_e v}{kT}} - 1) \qquad (1)$$

which is the i_o term shown above. LEDs will switch on only when they are forward-biased with a positive voltage polarity to its anode and a negative voltage to its cathode. If this voltage polarity is reversed, current should not normally flow, as the diode behaves as an insulator under reverse polarity.

Under normal current flow, a spontaneous recombination of electrons and holes takes place in the PN junction of the diode's semiconductor material, and it is through their interaction that light is generated. Under specific circumstances however, a small reverse current might flow. Such an event occurs when the temperature is varied and when minority charge carriers move inside the junction.

The power electronic circuits which drive LED devices can either operate under AC or DC voltage, although it is more common to operate LEDs under direct current.

In the case of the LED boost driver circuit, a DC-DC boost converter is utilised. A DC input voltage supplies the converter, while energy is stored in both the inductor and its output capacitor. A MOSFET transistor switch controls this energy transfer by switching on & off rapidly and the LED is supplied with this combined capacitor and inductor voltage. The combined output voltage is higher than the input voltage and it should be near the LED's nominal forward voltage.

For the purposes of the experiments of this paper, the MOSFET duty cycle was set at D=0.5 (50% pulse on-50% pulse off) which should double the input supply voltage. For the LED boost driver, this results in an LED output voltage of 1.7x2= 3.3 V. This is the calculated LED forward voltage in order to switch on the particular power LED module. The average LED current is also estimated in the range between 350-450 mA. Two main DC-DC boost converter topologies form the basis of the experiments. One open-loop boost converter with a resistive load, and one LED boost driver. The circuit in Fig. 1 shows the experimental configuration of the LED boost driver. Table 1 shows the experiment settings for the resistive boost converter.

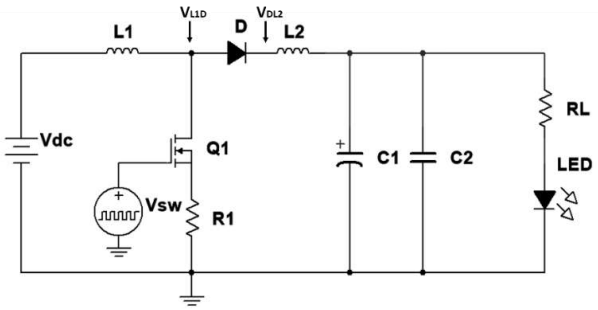

Fig. 1. LED boost driver experimental circuit schematic

Table. 1. Resistive boost driver circuit configuration

Resistors	R_L = 24 kΩ (Load) R_1 = 1.2 Ω (Q1-MOSFET source)
Inductors	L_1 = 4.48 mH, L_2 = 470 μH
Boost diodes	D_2 = type BYG20J (C_j = 25 pF, τ_{RR} = 75 ns) D_5 = type 1N4007 (C_j = 10 pF, τ_{RR} = 5 μs)
Output capacitor	C = 10 μF (C_1//C_2)
DC Voltage source amplitude	V_{dc} = 14 V
Frequency of pulsed voltage source	f_{sw} = 1 kHz to 1 MHz

3 Theoretical Analysis

There are certain nonlinear characteristics which influence the diode's operation. One of them is the reverse-recovery time, the time that the diode needs to recover the positions of its electrons and holes, when a reverse current goes through it.

The resonant frequency which relates the diode's reverse-recovery time is shown below.

$$f_{\tau_{RR}} = \frac{1}{\tau_{RR}} \qquad (2)$$

A second nonlinear parameter is the diode parasitic junction capacitance. When a reverse current flows through the diode, certain electrical charge is held at the junction, due to this capacitance. When the input voltage changes polarity again, that is from negative to positive, the inductor tries to maintain this reverse current.

The resonant frequency which relates the parasitic capacitance and the total inductance of the circuit is shown below.

$$f_{LD} = \frac{1}{2\pi\sqrt{LC_j}} \qquad (3)$$

As a result, two inherent resonant frequencies emerge from these nonlinear characteristics, $f_{\tau_{RR}}$ and f_{LD}. A specific method with dependence equations has been used in order to derive the unstable switching frequency regions of this circuit. These dependence equations have been successfully utilized in resonator circuits in the past [14]. This theoretical method is supported by both simulation and laboratory experiments, whereby a circuit model has been designed for each experiment type. In other published works of Hamill [15] or Dobson [16], a different model type predicts the behaviour of generic boost converters. However, the model of this paper aims to define the physical principles behind the formation of chaos in such boost converter circuits. When these resonant frequencies are synchronised with the switching frequency of the transistor, chaos occurs at multiples of these resonant frequencies. The dependence equations shown here, were used to support this theoretical analysis.

$$f_{sw} \approx f_{LD} \qquad (4)$$
$$f_{sw} \approx f_{\tau_{RR}} \qquad (5)$$

In order to examine the reverse recovery effects on the diode's operation, a resonator circuit was initially simulated, built and examined. This original diode resonator includes an AC source, an inductor, a diode and a resistor load [5]. When the AC voltage changes direction, chaotic oscillations are formed at specific frequencies, right at the load's voltage due to the aforementioned reverse current effects.

The next experiment involves a pulsed input as the excitation source of the diode resonator. A similar nonlinear response to the original diode circuit was observed, which proves that chaotic and resonant oscillations under an alternating or pulsed signal input are indeed feasible. At a later stage, the resistive boost converter was used to test the theoretical model. Finally, the LED boost driver was utilised in order to verify these findings in a lighting application circuit.

For the theoretical analysis, specific voltages on the LED driver were selected, and their waveforms have been examined. This theoretical analysis follows an iteration sample procedure which examines the periodicity of the waveform peaks. The voltage waveforms have been sampled at the same switching frequency of the transistor, and if the peaks repeat at the same amplitude and shape periodically, then the system is in a stable and linear state. If the peaks show period doubling, the waveform peaks appear twice, before the waveforms' period starts again. If the peaks do not show a regular periodic pattern, chaos has been reached in the system. The suggested iteration procedure is described below. The reader may select the two voltage variables of the system, that is the MOSFET drain voltage V_{L1D} and the diode voltage V_{DL2}. The suggested peak analysis method involves an iteration algorithm for the two voltages as shown below

$$V_{L1D,(n+1)T} = f(V_{L1D,nT}) \qquad (6)$$
$$V_{DL2,(n+1)T} = f(V_{DL2,nT}) \qquad (7)$$

where T is the switching period and n is the iteration number (n =1, 2, … k), which is an independent variable. Typical switching frequencies for most boost converters range from tens to hundreds of kHz, but modern LED drivers have reached 2-3 MHz. In order to observe such chaotic phenomena in the laboratory, Poincaré sections, Fourier transform spectra and phase space XY plots have been calculated and displayed as follows (Fig.2-3).

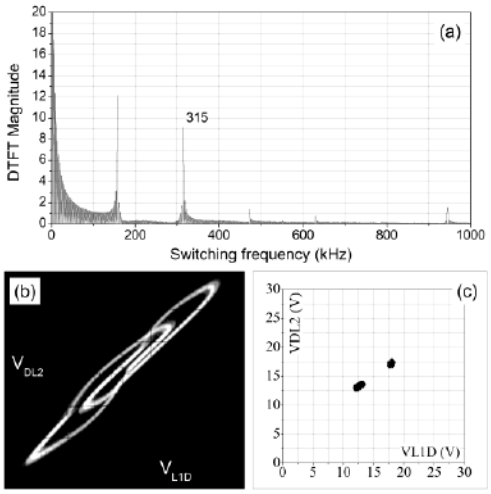

Fig. 2. (period-2, f_{sw}=315 kHz): (a) VDL2 voltage Fourier spectra, (b) XY plot, (c) Poincaré plot

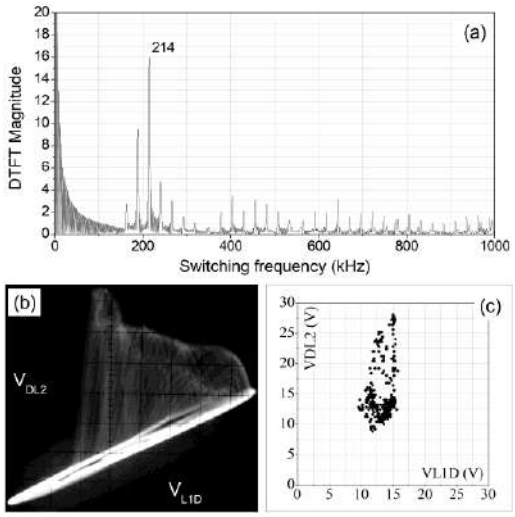

Fig. 3. (chaos, f_{sw}=214 kHz): (a) VDL2 voltage Fourier spectra (b) XY plot, (c) Poincaré plot

For the initial experiments with the resistive boost converter, a bifurcation diagram has been generated for the entire examined frequency range. Period-doublings have been witnessed at 315 kHz and chaos at 214 kHz. Both of these frequencies were multiples of the resonant frequency that the theoretical model predicts for this particular diode type. These results are plotted in phase space plots, frequency spectra and Poincare sections.

For the transistor switching frequency range from 15 kHz up to 350 kHz the experimental voltage waveform data was analysed, and the bifurcation diagram of Fig. 4 was generated. Linear regions are indicated with single solid lines, and the sparse regions indicate strong nonlinear regions with wide voltage differences. It should be stressed that in some cases (e.g. near 25 kHz), the inspected diode voltage reached almost 80 V, with only 14 V of input voltage.

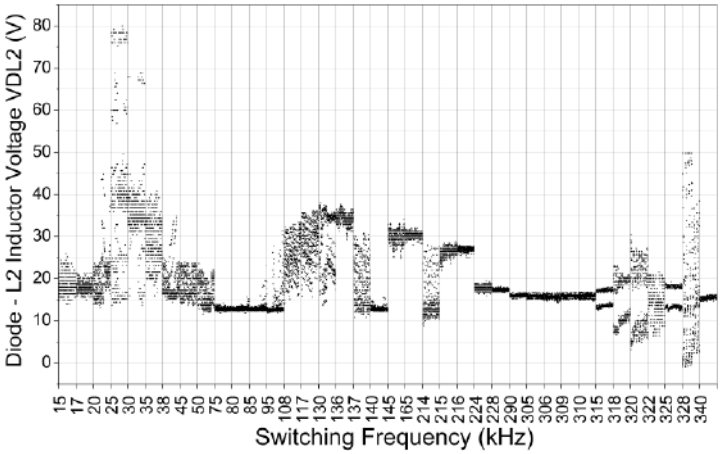

Fig. 4. Bifurcation diagram of V_{DL2} voltage-as a function of the switching frequency

4 Illuminance Experiments

Following the experiments with the resistive boost converter, the same switching frequency variation procedure was performed, in order to investigate the LED boost driver behaviour. For the LED boost driver the following circuit configuration has been used.

Table. 2. LED boost driver circuit configuration

Resistors	R_L = 10 Ω (2W) (Load) R_1 = 1.2 Ω (Q1-MOSFET source)
Inductors	L_1 = 4.48 mH, L_2 = 470 μH
Boost diodes	D_2 = type BYG20J (C_j = 25 pF, τ_{RR} = 75 ns) D_5 = type 1N4007 (C_j = 10 pF, τ_{RR} = 5 μs)
Output capacitor	C = 10 μF (C_1//C_2)
DC Voltage source amplitude	V_{dc} = 1.7 V
Frequency of pulsed voltage source	f_{sw} = 1 kHz to 1 MHz

Boost diode-1N4007 (slow-response): Throughout the different switching frequencies, periodic behaviour at 50 kHz was recorded, along with relatively high brightness levels (230 lx) (Fig. 5-6). At much lower switching frequencies the LED illuminance peaks at 460 lx. With the same diode type, a strange attractor appears at 80 and 200 kHz (Fig. 7-8), in a similar fashion to the resistive boost converter. The illuminance levels drop considerably at these frequencies, due to the high nonlinearity of the system.

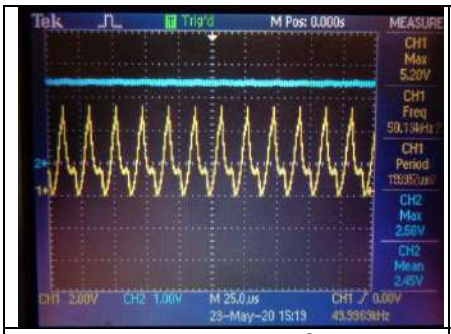

Fig. 5. LED Driver period-1 response, 50 kHz, Time-domain waveform

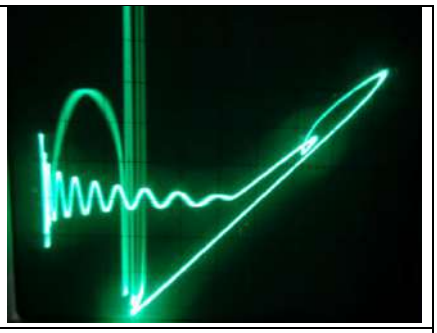

Fig. 6. LED Driver period-1 response, 50 kHz, Phase plot

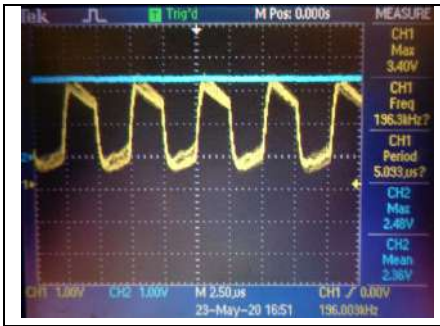

Fig. 7. LED Driver chaotic response, 200 kHz, Time-domain waveform

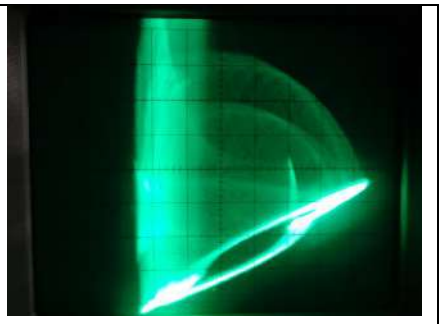

Fig. 8. LED Driver chaotic response, 200 kHz

The illuminance data has been processed in order to plot them against the switching frequency. The illuminance graph for the slow-response 1N4007 diode is shown in Fig. 9.

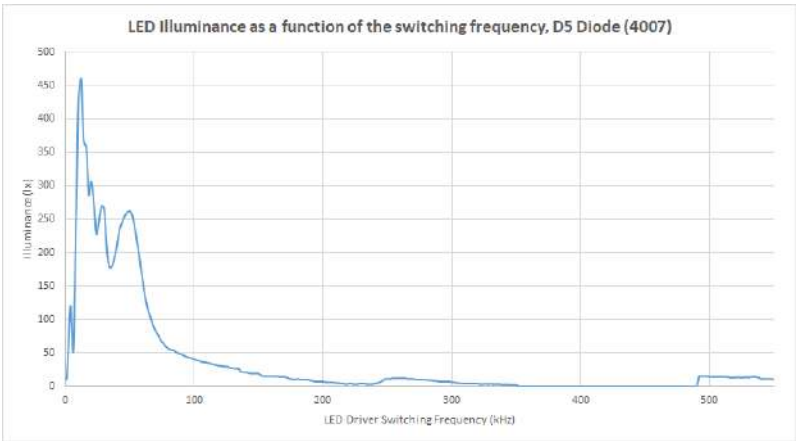

Fig. 9. Illuminance as a function of the MOSFET switching frequency (slow-response diode)

High illuminance is recorded in periodic or relatively stable period-4 or period-5 attractors. In the frequencies that the system reached chaos, extremely small illuminance levels have been recorded.

Boost diode-BYG20J (fast-response): With the ultra-fast diode, larger areas of linear behaviour have been observed, as this diode's reverse recovery time is considerably faster than the 1N4007 diode. A very high illuminance was recorded in the periodic regions reaching a maximum of 1353 lx, whilst the illuminance falls to just 17 lx in the chaotic attractor regions (Fig. 10). The theoretical method predicts these nonlinear resonant frequencies where chaos dominates the system.

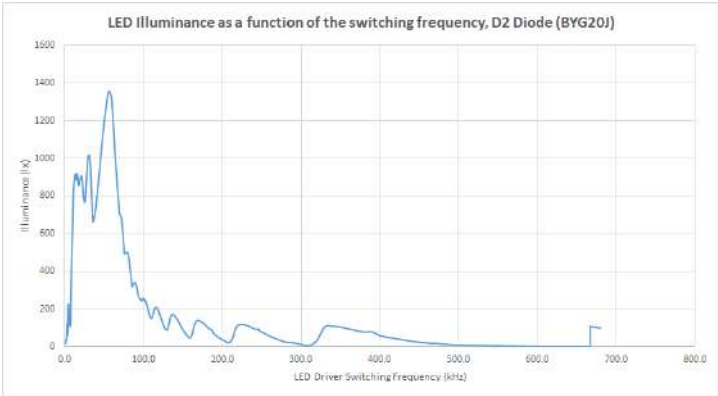

Fig. 10. Illuminance as a function of the MOSFET switching frequency (fast-response diode)

The ultra-fast diode exhibits more illuminance peaks at higher frequencies, where the slow diode was going through a very unstable region. Still, chaos is observed at certain frequencies at the lower peaks of the graph, e.g. at 80, 130 or 200 kHz.

5 High Sensitivity to Initial Conditions

There is a particular type of phenomenon which occurs often in such nonlinear systems. Even with the BYG20J ultra-fast diode, a sensitive dependence on the initial conditions of the system has been recorded. With only a 100 Hz of difference between the switching frequencies of 666.6 kHz and 666.7 kHz, the LED driver circuit moves suddenly from an unstable region of almost zero illuminance, to a stable region of considerable illuminance (Fig. 11).

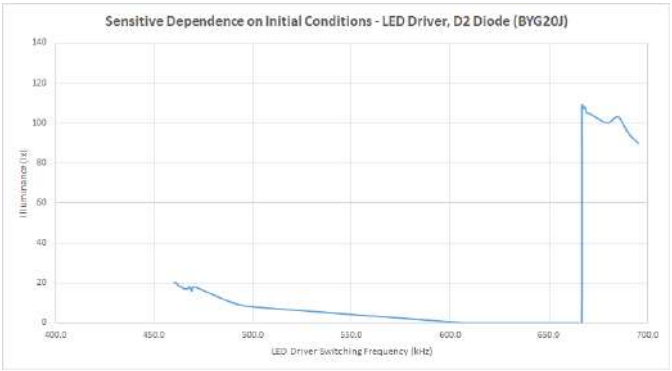

Fig. 11. Illuminance as a function of the MOSFET switching frequency

Conclusions

Two nonlinear resonant frequencies of an LED driver circuit have been detected, which influence harmfully its performance. This behaviour manifests itself only in the power section of the boost driver, and unlike previous literature, chaos occurs without a feedback loop. The synchronisation of these resonant frequencies with the transistor switching frequency, steers the LED converter towards chaos. The negative effects include a significant degradation in illuminance performance, especially at the chaotic regions. The suggested nonlinear analysis includes a bifurcation peak-to-peak method, in order to guide the interested researcher to avoid such unstable regions. A number of research suggestions for further steps of this work can be considered. In this context, the resonant response of even faster diodes can be investigated. The interested reader can also explore the low-frequency chaos that has been found in such fast diodes. Finally, some abrupt transitions to chaos that have been recorded at specific frequencies, could be investigated as forms of interior crisis within this nonlinear system.

References

1. D. Giaouris, S. Banerjee, O. Imrayed, K. Mandal, B. Zahawi, and V. Pickert, Complex Interaction Between Tori and Onset of Three-Frequency Quasi-Periodicity in a Current Mode Controlled Boost Converter, IEEE Trans. Circuits Sys. I, Reg.Papers, 59, 1, 207{214, 2012.
2. D. Dai, S. Li, X. Ma, and C.K. Tse, Slow-Scale Instability of Single-Stage Power-Factor-Correction Power Supplies, IEEE Trans. Circuits Sys. I, Reg.Papers, 54, 8, 1724{1735, 2007.
3. K. Mandal, A. Abusorrah, M. M. Al-Hindawi, Y. Al-Turki, D. Giaouris and S. Banerjee, Dynamical Analysis of Single-Inductor Dual Output DC-DC Converters, IEEE International Symposium on Circuits Sys. (ISCAS), 2013, 2755{2758.

4. S.Banerjee and G. Verghese, Nonlinear Phenomena in Power Electronics, John Wiley & Sons Ltd, 2001.
5. T. Caroll and L. Pecora, Nonlinear Dynamics in Circuits, World Scientific Publishing, 1995.
6. L. O. Chua and R. N. Madan, Sights and Sounds of Chaos, IEEE Circuits Devices Mag., 4, 1, 3{13, 1988.
7. J. - M. Collantes, and A. Suárez, Period-Doubling Analysis and Chaos Detection Using Commercial Harmonic Balance Simulators, IEEE Trans. Microw. Theory Tech., 48, 4, 574{581, 2000.
8. T. Matsumoto, Chaos in Electronic Circuits, IEEE Proc., 75, 8, 1033{1057, 1987.
9. L.V. Karadzinov and D. C. Hamill, Influence of Diode Reverse Recovery on the Operation and Design of High-Frequency Rectifiers, IEEE Applied Power Electronics Conf. Proc., APEC, Thirteenth Annual, vol.1, 1998, pp. 447-453.
10. ON Semiconductors Application Note, NCP5007 Compact Backlight LED Boost Driver, Rev. 5, 1{21, 2014.
11. B. Basak and S. Parui, Exploration Of Bifurcation And Chaos In Buck Converter Supplied From A Rectifier, IEEE Transactions on Power Electronics, 25, 6, 1556{1564, 2010.
12. H. Wu, V. Pickert, D. Giaouris, and B. Ji, Nonlinear Analysis And Control Of Interleaved Boost Converter Using Real-Time Cycle To Cycle Variable Slope Compensation, IEEE Trans. Power Electron., 32, 9, 7256{7270, 2017.
13. E. Gluskin, E. Tsirbas, I. Kateri and F.V. Topalis, Use of logarithmic sensitivity in power system analysis: the example of lighting circuits (hot filament, LED and fluorescent lamp circuits), IET Science, Measurement and Technology, 7, 6, 297{305, 2013.
14. R.M. de Moraes and S.M. Anlage, Unified model and reverse-recovery nonlinearities of the driven diode resonator, Phys.Rev.E.026 201, 68, 1{10, 2003.
15. D.C. Hamill and H. B. J. Deane, Instability, Subharmonics, and Chaos in Power Electronic Systems, IEEE Trans. Power Electron., 5, 3, 260{268, 1990.
16. I. Dobson, Stability of ideal thyristor and diode switching circuits, IEEE Trans. Circuits Sys. I, Reg.Papers, 42, 9, 517{529, 1995.

Halo Dynamics: From Rainbows to Black Holes

Alberto Tufaile[1], Adriana Pedrosa Biscaia Tufaile[2]

[1] Soft Matter Lab, Escola de Artes, Ciências e Humanidades, 03828-000, University of São Paulo, São Paulo, Brazil
(E-mail: tufaile@usp.br)
[2] Soft Matter Lab, Escola de Artes, Ciências e Humanidades, 03828-000, University of São Paulo, São Paulo, Brazil
(E-mail:atufaile@usp.br)

Abstract. Here we applied some of concepts of dynamical systems in an experiment involving a laser beam injected in a glass cylinder, recording the light patterns from the scattering of light from a finite cylinder. We have studied some aspects of the representation of dynamical systems in this experiment, along with the observation of the existence of a sequence of numbers which characterizes this dynamics, known as Farey sequence, due to its connection with trajectories following star polygons. We also report the observation of arcs with folds in these light patterns. We studied the case when the cylinder change its shape into the case of a foot of a wine glass, and compared some solutions of the cylindrical lens with epicycloid dynamics and halo formation, for the case of patterns formation based in the observation of relativistic effects.
Keywords: Relativity, Farey Sequence, Billiards.

1 Introduction

The word halo brings to mind a picture of an optical phenomenon by light interaction with ice crystals suspended in the atmosphere, such as the circular halo, which is a representative of a family of luminous patterns whose main effect is a large ring of light around a point. Here, we consider a halo any distribution of a light pattern around a point. The essence of these phenomena is somehow related to any property that is capable of bending light from the source as the light travels towards the observer. The presence of a halo can therefore reveal the extent of the optical properties of the medium where light spreads. For example, luminous arcs are present in rainbows (Fig. 1(a)), 22 degrees halo around the Sun (Fig. 1(b)) or in relativistic effects such as Einstein rings (Fig. 1(c)), with the presence of partial or complete circumferences. From these examples, we see that there are different types of systems that can present formation of luminous halos, based on quite different physical environments. In the previous examples, the halos are related to the presence of ice crystals or drops in space, deflecting light, in other cases the very constitution of the structure of the space-time creates the effect of the curvature of light path, due to the presence of massive objects such as quasars, galaxies or black holes.

Due to the visual appeal of these phenomena in the mankind, this subject has been observed and studied intensely by centuries with a significative impact on history of science. The study of rainbows, glories and halos helped the

development of optics and mathematics [1], and many authors have described the aspects of the theory of rainbows and its applications [2], the elementary physical features of halos [3], and advanced aspects such as considering a rainbow as diffraction catastrophe [4]. The existence of multiple rainbows was done using glass rods with normally incident light and for diagonal incidence [5, 6]. Interesting patterns obtained with cylindrical symmetry in optical systems is also related with some studies of dynamical systems and solitons [7].

Fig. 1. Some halos and luminous arcs found in nature. In (a) rainbow observed at Newark, California, USA, in (b) the 22 degrees halo around the sun formed by the interaction of the sun light and ice crystals suspended in the atmosphere, and in (c) the gravitational mirage known as Einstein ring obtained with a simulation of a gravitational lens.

Stimulated by the observation of some patterns obtained in our experiments, we have explored the use of the concepts present in dynamical systems and topology to give a new perspective in the comprehension of halo formation. For this reason, it is appropriate to discuss the light beams like particles travelling in an open billiard, exploring these motions from the point of view of dynamical

systems, and this is the aim of this paper. The description of light rays in open billiards creating light patterns forming circles was explored in our previous works [9-13], as well as the role of the hyperbolic geometry in some light pattern formation [15]. In this paper we explore the formation of some of these halos and arcs from the point of view of dynamical systems based on some concepts of optics using two lenses, a cylindrical one and another with the shape of a pseudosphere. We start studying the scattering of rays in a cylinder and present a direct analysis of the observed pattern based on the conceptual structure of the dynamical systems. After that, we propose a topological transformation of the cylinder to a pseudosphere and analyze some properties of gravitational lenses.

2 The cylinder as an open billiard

Our first experiment consists of a laser beam hiting a glas rod, as it is shown in Figs. 2(a)-(b). The theory of rainbows here is the following. For the case of circular section of Fig. 2(c), light reaching the cylinder with angle $\alpha_i = 0$, creates rainbows for specific angles, due to the formation of caustics. Usually, caustics can be defined as the envelope of rays that describes the flow of energy, and this energy flow increases significantly on caustics compared to the adjacent space, forming more intense light patterns. Lenses with circular sections exhibit the formation of caustics similar to those observed in the case of the rainbow, and the main ray of the caustics is called Cartesian ray, which can be obtained considering the total deviation of a ray for the general case of *k*-internal reflections giving by [16]:

$$\theta_{TRT} = 180^o k + 2\theta_i - 2\gamma(k+1), \tag{1}$$

and the incident angle θ_i corresponding to the minimum deviation after *k* internal reflection is the Cartesian ray angle θ_{Cr}:

$$\theta_{cr} = \min(\theta_{TRT}) = \arccos\sqrt{\frac{n^2-1}{k(k+2)}}. \tag{2}$$

For the case of values of α_i different for zero of Fig. 2(d) and $\theta_i = 0$, the laser beam hitting the cylinder at distance *dsc* of the screen will give an image at height h_k from the axis of the cylinder for the *k*th point is giving by:

$$h_k = \{[dsc + d(1-k)(tg\alpha_r)[tg(90^o - \alpha_i)]\}, \tag{3}$$

in which when *k* is even the projection of this point is at upper part of the screen, and when *k* is odd the point is at the down part of the screen, considering the vertical axis perpendicular to the cylinder axis.

However, the light rays are not always scattered about a cone whose axis is in the cylinder axis [17], because the laser hits the cylinder obliquely, as it is shown in the diagrams of Fig. 2(e)-(f). For example, one ray that hits the axis of the cylinder is associated with one cone, while another ray grazing the cylinder surface is associated with another rays' cone with intermediary impact

parameters generate intermediary cone of Fig. 2(f). Basically, this effect of the laser hitting the cylinder obliquely causes an optical flattening of the circular cross section of the cylinder, creating similar effects of a cylinder with an elliptical section, and coupling the radial and longitudinal modes.

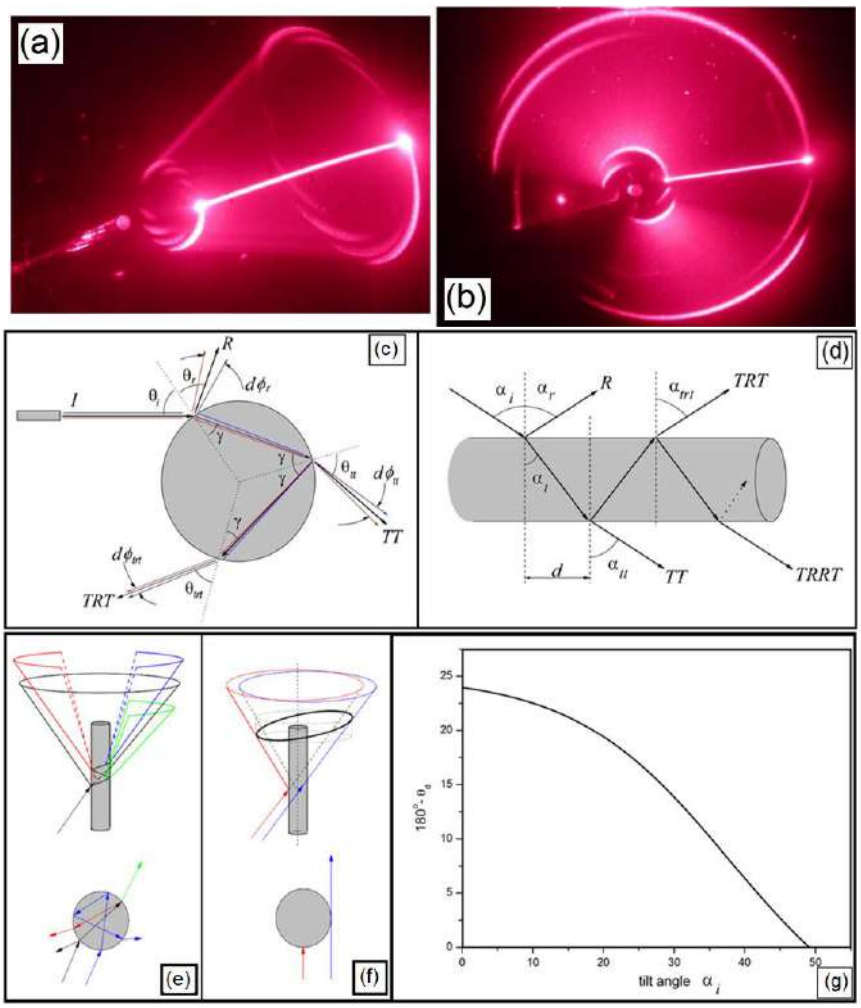

Figure 2 – Two views of a laser hitting a cinder in a tilting angle, with the emerging light traveling in space. In (a) we can see the glass cylinder at the left side and the scattered light forming a cone on the right side. In (b), we have a frontal perspective of this experiment. Diagrams of light rays in a cylinder: (c) normal incidence and (d) oblique incidence. Diagrams of conical projections in (e) and (f), and the angle of Cartesian ray in function of the tilt angle α_i for a glass cylinder with refraction index $n = 1.50$ in (g).

3 Dynamical system optics

Consider a light ray of a laser beam traveling inside a glass plate undergoing a sequence of internal reflections on the upper (1) and down sides (2) of this plate, like a light ray trapped in a kaleidoscope formed by two parallel mirrors. This sequence of reflections can be represented in the sequence of events with the reflections "1" evolving in space at the top of this plot and reflections "2" at the bottom part of this plate. Considering the sequence of spatial events, we can associated a temporal evolution for the trajectory of the light ray for each reflection, so that the first reflection in time is closer to the laser source, while the most distant ones occurred later. The pattern associated with this dynamics in a cylinder is shown by the caustics of Fig. 3(a), and the external pattern of Fig. 3(d) for an angle of incidence $\theta_i = 0$. Changing this angle, we obtain the patterns of Figs. 3(e)-(f), associated with the caustics of Fig. 3(b)-(c).

The simplest dynamical system related to the ray tracing described previously is the one-dimensional circle map [14]:

$$f(\theta) = \theta + \Omega - {}^{K}\!/_{2\pi} \sin(2\pi\theta) \quad \text{(mod 1)}, \tag{4}$$

which describes a motion on a three-dimensional torus, characterized by two frequencies ω_1 and ω_2 given by $\Omega = \omega_2/\omega_1$. If the non-linear term K vanishes in eq. (4), the ratio of the two frequencies $\omega_2/\omega_1 = p/q$ is a rational number, and the trajectory is closed after q internal reflections and the motion is periodic. Irrational numbers Ω lead to quasi-periodic internal reflections which creates spiral patterns. The case when the ratio of the two frequencies gives a rational number is related to a structure in the space of control parameters known as Arnold tongues.

In Fig. 3(g) we can see how these patterns are associated with the dynamics of a particle bouncing in a billiard for a period-2 (1,2) and for a particle for the case of a period-3 (1, 3), with its respective patterns. From the dynamics obtained from equation (4), there is the existence of a closed orbit with the shape of a pentagram of Fig. 3(h), which is defined as the Farey mediant between the period-2 and period-3, because this period-5 orbit is part of a family of star polygons, linked to a special array of rational numbers in the unit interval, which is defined by the Farey mediant [14], given the three consecutive fractions p_1/q_1, p_2/q_2, p_3/q_3:

$$\begin{aligned} & q_1 p_2 - q_2 p_1 = 1, \\ & \frac{p_2}{q_2} = \frac{p_1}{q_1} \oplus \frac{p3}{q3} \equiv \frac{p_1 + p_3}{q_1 + q_3}, \end{aligned} \tag{5}$$

which is a special addition of fractions. This idea is valid for the flattened case of the ellipsis of Fig. 4(a)-(b). In Fig. 4(c) we present the Farey diagram associated with the circle map, along with some orbits obtained in our experiment.

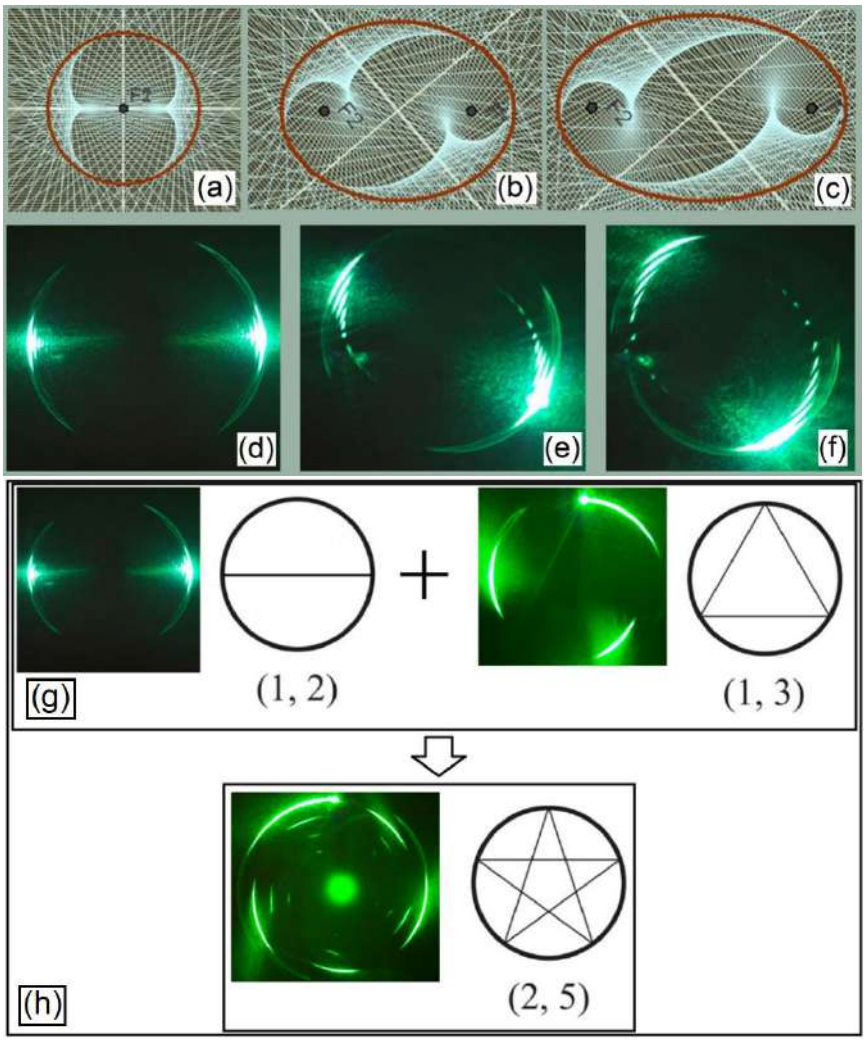

Figure 3 – Observing the flattening of the section of the cylindrical lens due to the coupling between the azimuthal and longitudinal modes. A similar behavior of flattening can be seen in the caustics from a circle in (a) to an ellipse in (b), to another ellipse in (c). In our experiment, the equivalent of a circle is shown in (d) ($\theta = 0^o$, $\alpha = 30^o$), with the elliptical sections in (e) ($\theta = 7^o$, $\alpha = 30^o$) and (f) ($\theta = 12^o$, $\alpha = 30^o$). The dynamics of Farey mediant in (g) and luminous pattern formation from a cylinder due the combination of different modes in (h).

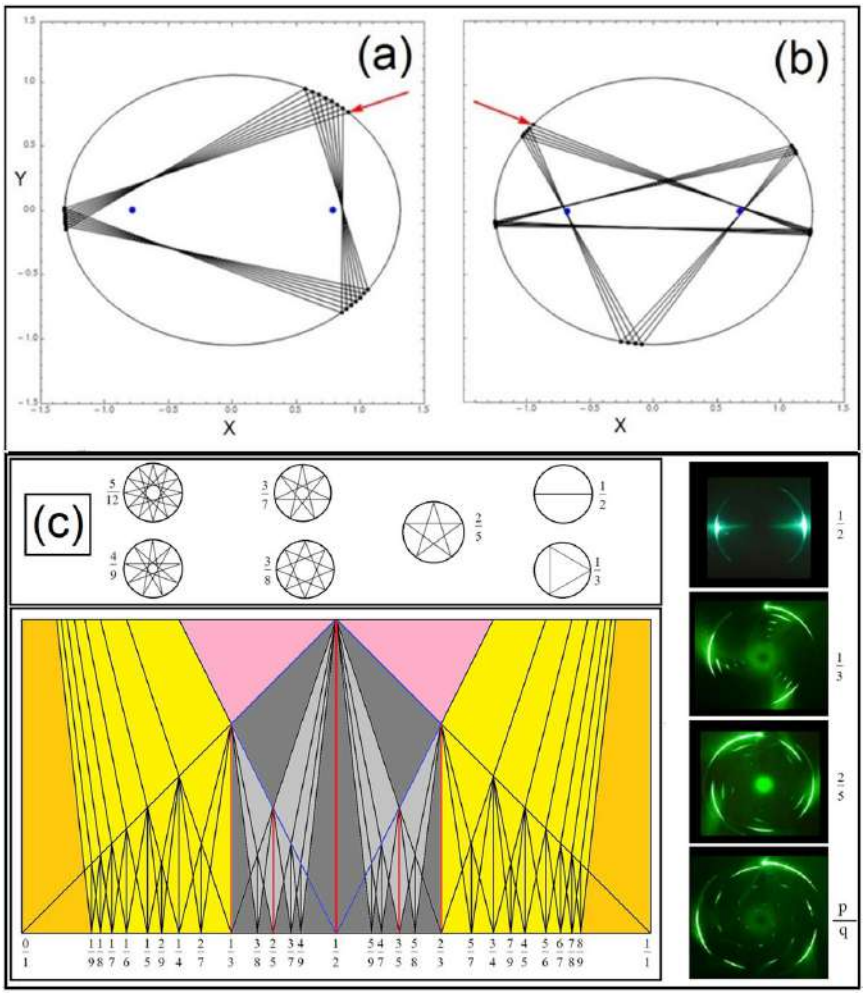

Figure 4 – Elliptical billiards and Farey diagram for star polygons trajectores. The dynamics of a circunferece is similar in an elliptical billiard, as is shown in (a) the quasiperiodic orbit close to a period-3, and in (b) the quasiperiodic behavior close to a period-5, for a ray injected at the point indicated by the red arrow. In (c) star polygons and the diagram of the Farey sequence for $\Omega = p/q$ from 0 to 1, along with some light patterns obtained from our experiment.

4 Caustics-like patterns

In our experiment, we have observed the formation of arcs with fold. Considering that the laser beam maintains its shape inside the glass cylinder, for some of the rays that escape from its surface, in addition to the divergence

projected in the screen there is a fold property, forming these arcs with two branches represented in the plot of Fig. 5(a). Looking for a possible explanation for these arcs with folds in the literature of optics, we have found an analogy with the mechanism of caustics formation and folded wavefront of Fig. 5(b) caused by the involutes of Fig. 5(c)-(d) for each branch of the caustics.

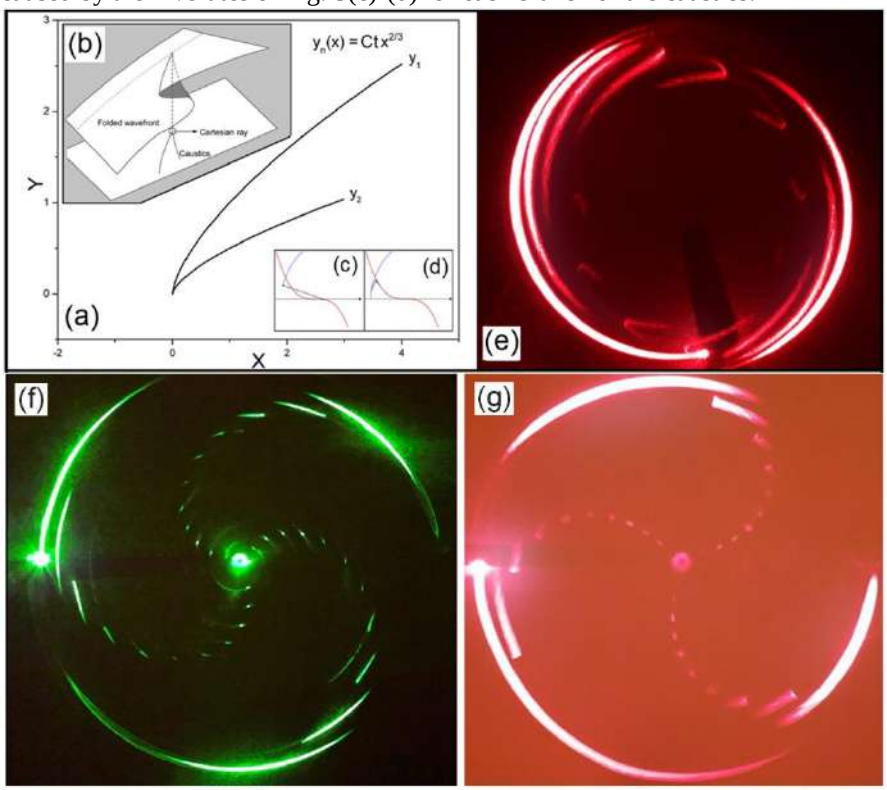

Figure 5 – Light arcs and folding light due to caustic formation. In(a) the plot of the caustic obtained from the folded wavefront (b) due to the glass cylinder. Each side of this caustic (y1 and y2) is associated with the involutes shown in (c) and (d). The image of the multiple caustics is projected in a screen (e) ($\theta = 27^o$, $\alpha = 33^o$). The pattern obtained with green laser ($\theta = 18^o$, $\alpha = 13^o$) rotates counterclockwise in (f), while the pattern with red laser in (g) rotates clockwise ($\theta = -18^o$, $\alpha = 13^o$). The longest arc of light is always the first reflected ray R of the diagram of Fig. 2(a).

Considering the incident light as a plane wave there is a folding of this wave in the cylinder and formation of a caustic [2] as it is shown in Fig. 5. This caustic is the involute of the plane wave represented in Fig. 5(c)-(d). The projection of these involutes in the screen forms different patterns for different values of θ_i and α_i, and for some projections is possible to observe two arcs of Fig. 5(a). According to catastrophe theory each side of this caustic forms an arc parametrically modeled by a constant *Ct* in the following function:

$$y_n = Ct(x^{2/3}). \quad (6)$$

Returning to our experiment and using the same representation for the arcs with folds discussed above, we can see some arcs with folds in the pattern of Fig. 5(e), analogous to the case of the Fig. 5(a).

The existence of non-closed orbits is related to quasi-periodic dynamics of the laser inside the billiard, such as the spirals shown in Fig. 5(f)-(g). The rotation orientation of these spirals shows which side of the Farey diagram are the orbits in relation to the center of the diagram for the value of Ω = ½. The green pattern of Fig. 5(f) rotates in clockwise direction for positive values of θ_i, while using a red laser in Fig. 5(g), with a negative value of θ_i, these arclets rotate in counterclockwise direction. The patterns of Figs. 5(f)-(g) have up to 30 rays each one. The longest arc of light is always the first reflected ray *R* of the diagram of Fig. 2(a), while the brightest point is the laser hitting the screen directly.

5 From cylinder to gravitational lens

The next step in this work of halo dynamics is to remark the association of this pattern formation with images like epicycloids, observed in another optical system related with gravitational lensing, in which there is the formation of the Einstein's ring, which here we compare with halos.

First, we can transform a cylinder to a foot of a wine glass with the transformation of Fig. 6(a). The realization of this optical lens is shown in Fig. 6(b). Using the terms of hyperbolic geometry, this foot of a wine glass shape is related to the surface of a tractrix curve and the pseudosphere, in our case a half pseudosphere. Second, placing this lens of three horizontal parallel lines, we have obtained the pattern of Fig. 6(c), which are related with the Möbius transformations [15].

The transformations associated with this type of geometry is analogous to the path traced by a point *P* on the edge of a circle of radius *b* rolling on the outside of a circle of radius *a* of the period-2 of Fig. 3, and it is related with the caustic of epicycloids of Fig. 3(a), which are given by the parametric equations [18]:

$$x = (a+b)\cos\varphi - b\cos\left[\tfrac{(a+b)\varphi}{b}\right], \quad (7a)$$

$$y = (a+b)\sin\varphi - b\sin\left[\tfrac{(a+b)\varphi}{b}\right], \quad (7b)$$

in which *a*, *b* are the parameters of the epicycloids. In this way, the dynamics of the caustics of period-2 of the cylindrical lens is still present in the foot of a wine glass lens, considering the profiles of caustics in a cylinder Fig. 3(a) and the Möbius transformation of Fig. 6(c)

Now, we explain why this lens can be associated with a black hole. To obtain this lens, we start with the Einstein's gravity field equations [19]:

$$R_{\mu\upsilon} - \tfrac{1}{2}Rg_{\mu\upsilon} + \Lambda g_{\mu\upsilon} = \frac{8\pi G}{c^4}T_{\mu\upsilon}. \quad (8)$$

The two first terms are related with the space time-curvature, the third term is the stress from empty space-time itself, and the last term is the stress from an object in space-time.

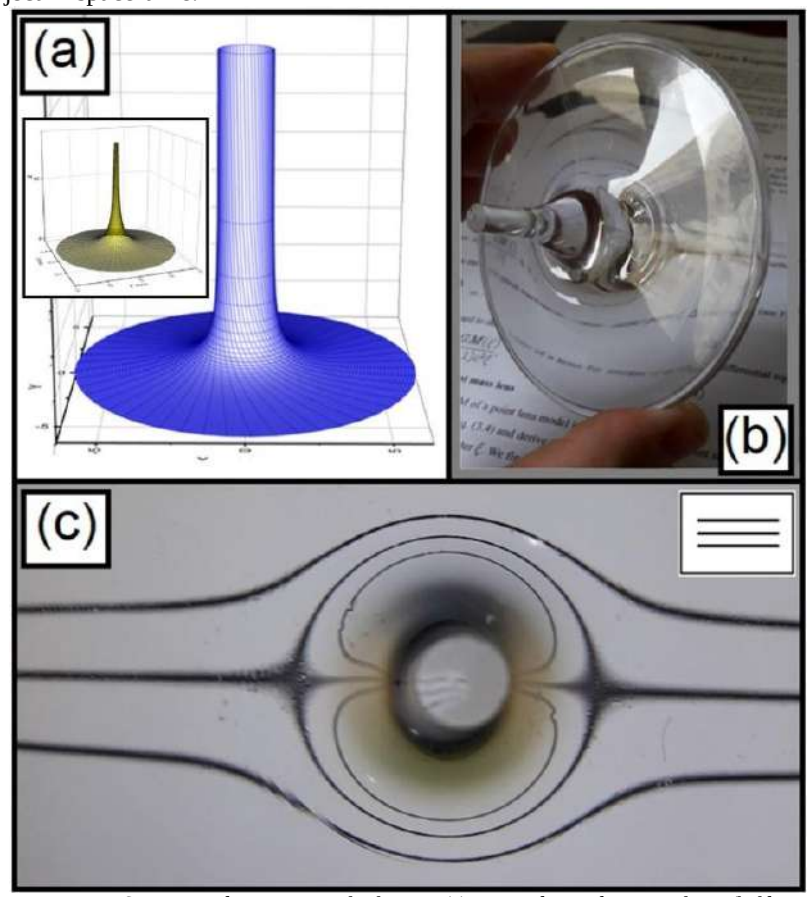

Figure 6 – Transforming a cylinder in (a) in a foot of wine glass (half pseudosphere) shown with yellow surface in the inset. The realization of this lens is shown in (b). In (c) we can see the image obtained with the lens with the shape of a pseudosphere of three parallel lines, shown in the inset at the top of this image.

One possible solution of these equations is the pseudosphere lens, because they can be broken into simpler equations, which are more appropriate to understand the gravitational lensing, considering the case of the lens with the shape of a foot of a wine glass for a point mass model, and the angle which light is deflected by this poit mass is [19, 20]:

$$\hat{\alpha} = \frac{4GM}{c^2 b}, \tag{9}$$

where G is the universal gravitational constant, M is the mass and b is the impact parameter. This point mass could be the black hole.

The images obtained for the solution in Eq. (9) are comparable to the period-2 observed of Fig. 7(a) with the cylindrical lens and are related with the parametric equations of the epicycloid of Eqs. (7a)-(7b) due to Möbius transformations of space-time of Fig. 7(b). The diagrams of Fig. 7(c)-(d) describes how the Eq. (9) is related with the image perceived by the observer in the point O, from a star source of the light at the distance of some gigaparsecs $D_S$from this observer, when a massive object L with the size of some megaparsecs is at distance D_L placed betweem them. When the star source S, the massive object L and the observer O are perfectly aligned, there is the possibilty of the formation of the ring (halo) of Fig. 9(e), known as Einstein's ring. Like the case of the cylinder acting as a lens, the control parameter here is the alignement of the system S-L-O, with the system triggered in the period-2 due to the lens configuration. This halo pattern is present in a system which is analogous to the case of gravitational lens observed in Fig. 1(c), and we observed that it is similar to the dynamics involving Farey diagram of Fig. 4, for the case of frequency ½.

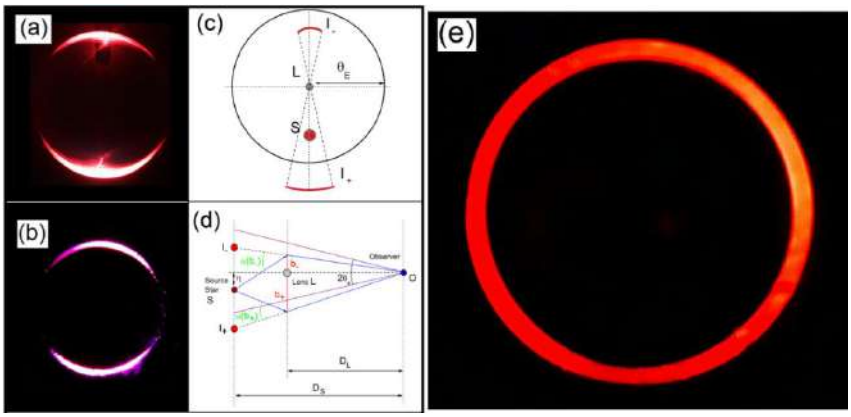

Figure 7 – The period-2 compared with the gravitational lens model. In (a) the period-2 obtained with the cylinfrical lens. The luminous arcs obtained with the foot glass. In (c) diagram of the image formation of the gravitational lens. The lateral view of the same diagram in (d). Simulation of the Einstein's ring (e) obtained from our experiment is another example of halo dynamics.

One important thing to note for the case of the gravitational lensing is that the formation of both arcs occurs simultaniously, suggesting that the dynamics of halo formation here is related to a supercritical pitchfork bifurcation [14], as it is shown from the images obtained from a point source of Fig. 8 for different values of the control parameter b. Multiple images can be present in gravitational lensing [19-21], involving a more complex analysis of the halo

dynamics, due the presence of multiple lens planes, resmbling the previous case of the cylinder with oblique incidence.

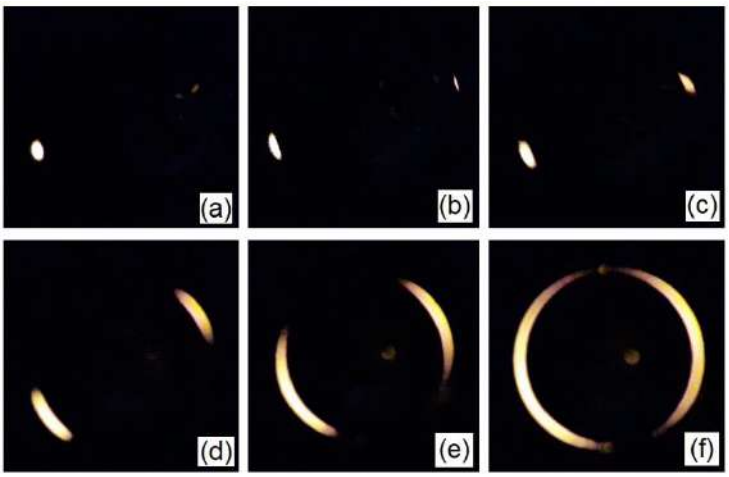

Figure 8 – Evolution of arcs using the foot of wine glass lens for a period-2, like a supercritical pitchfork bifurcation in a surface of a cylinder for the parameter *b* from 1.1 in (a), 1.0 in (b), 0.8 in (c), 0.6 in (d), 0.4 in (e), and 0.2 in (f).

Conclusions

We have explored the halo formation based in the concepts of rainbow ray formation and caustics in parallel with the studies of dynamical systems, such as particles bouncing in an open biliard. We have observed the existence of pattern formation following the dynamics observed in the Farey Diagram, using an approach based in the experiment of a laser beam hitting obliquelly a glass cylinder. After that, we investigated the pattern formation when this cyclinder suffers deformations until it has the shape of a foot of a wine glass lens, used to study patterns in systems affected by relativistic effects. In our explorations, we have found patterns for this system as two light spots, which converges to a halo when the light source, the lens and the observer are aligned.

Acknowledgments

The authors would like to thank to Lan Ma for picture of the rainbow and Tony Klein for picture of the solar halo in Fig. 1.This work was partially supported by Conselho Nacional de Desenvolvimento Científico e Tecnológico (CNPq), Instituto Nacional de Ciência e Tecnologia de Fluidos Complexos (INCT-FCx), and by Fundação de Amparo à Pesquisa do Estado de São Paulo (FAPESP), FAPESP/CNPq#573560/2008-0.

References

1. J. A. Adams, “The mathematical physics of rainbows and glories,” Phys. Reports **356**, 229-365, 2002.

2. M. H. Nussenzweig, “The theory of rainbow”, Sci. Am.,**April**, 116-127, 1977.
3. R. Greenler, *Rainbows, Halos and Glories* (Cambridge University Press), 1980.
4. M. V. Berry and C. Upstill, *Catastrophe optics: Morphologies of caustics and their diffraction patterns*, in: E. Wolf (ed.), *Progress in Optics*, Vol. XVIII, (North-Holland), Chap. 4, 1980.
5. C. L. Adler, J. A. Lock, B. R. Stone, “Rainbow Scattering by a cylinder with a nearly elliptical cross section,”Appl. Opt. **37**, 1540-1550,1988.
6. P. L. Marston, “Descartes Glare Points in Scattering by icicles,”Appl. Opt. **37**, 1551-1556,1998.
7. E. Garza, S. Lopes-Aguayo, J. C. Gutierrez-Veja, “Soliton Dynamics in finite non local media with cylindrical symmetry,” Phys. Rev. A **99**, 033804, 2019.
8. R. Nemiroff and J. Bonnell,“A Horseshoe Einstein Ring from Hubble,”ESA/Hubble&NASA, https://apod.nasa.gov/apod/ap111221.html
9. A. Tufaile, A. P. B. Tufaile, “Rainbows, Billiards and Chaos,” in Proceedings of 11th Chaotic Modeling and Simulation International Conference. CHAOS 2018, C. Skiadas, I. Lubashevsky (eds) (Springer Proceedings in Complexity), pp. 289-301, 2019.
10. A. P. B. Tufaile, J. D. da Silva, A. Tufaile, "Optical elements based in dynamical systems," in *Frontiers in Optics + Laser Science APS/DLS*, OSA Technical Digest (Optical Society of America), paper JW4A.38, 2019.
11. A. Tufaile, A. P. B. Tufaile, “The dynamics of diffracted rays in foams,”Phys. Lett. A **379**, 3059-3068, 2015.
12. A. Tufaile, A. P. B. Tufaile, “Parhelic-like circle from light scattering in Plateau borders,” Phys.Lett. A **379**, 529-534, 2015.
13. R. J. Fitzgerald,“Soap Halos,” Phys. Today **72**(7) 68, 2019.
14. J. Argyris, G. Faust, M. Haase, *An Exploration of Chaos, An Introduction for Natural Scientists and Engineers*(North-Holland), 1994.
15. A. Tufaile, A. P. B. Tufaile,“Hyperbolic prisms and foams in Hele-Shaw cells,” Phys. Lett. A **375**, 3693-3698, 2011.
16. J. D. Walker, “Multiple rainbows from single drops of water and other liquids,” Am. J. Phys.**44**, 421-433, 1976.
17. L. Mees, K. F. Ren, G. Gréhan, G. Gouesbet, “Scattering of a Gaussian beam by an infinite cylinder with arbitrary location and arbitrary orientation: numerical results,” Appl. Opt. **38**, 1867-1876,1999.
18. E. Weistein, “Epicycloid”, http://mathworld.wolfram.com/Epicycloid.html
19. J. Wambsganss, *Gravitational Microlensing*, in: G. Meylan, P. Jetzer, P. North (eds.)*Gravitational Lensing: Strong, Weak and Micro*, (Springer-Verlag), 2006.
20. M. Dominik, “The physics and mathematics of gravitational lensing,”http://www.artemis-uk.org/Microlensing_physmath.html
21. A. O. Petters, M. C. Werner, “Mathematics of Gravitational Lensing:
22. Multiple imaging and magnification,”Gen. Relativ. Gravit. **42**, 211-246, 2009.

Investigating dynamical systems using Optic-Fluidics

Alberto Tufaile[1], Michael Snyder[2], Timm A. Vanderelli[3],
Adriana Pedrosa Biscaia Tufaile[4]

[1] Soft Matter Lab, Escola de Artes, Ciências e Humanidades, Universidade de São Paulo, Brazil.
(E-mail: tufaile@usp.br)
[2] Technical Space Science Center, 235, Martindale Drive, Morehead State University, Morehead, KY 40531, USA;
(E-mail: snyder1michael@hotmail.com)
[3] Ferrocell USA, 739 Route 259, Ligonier, PA 15658, USA
(E-mail: tvan@ferrocell.us)
[4] Soft Matter Lab, Escola de Artes, Ciências e Humanidades, Universidade de São Paulo, Brazil.
(E-mail: atufaile@usp.br)

Abstract. We are presenting experimental results and simulations of dynamical systems using magneto-optics. These light patterns are obtained by the observation of a thin film of ferrofluid in the presence of a magnetic in the presence of a magnetic field.
Keywords: Magnetism, Isoclines, Chiral.

1 Introduction

In our previous work, we have considered the analogy between the general properties of vector fields of the phase space of dynamical systems with the properties of potential of magnetic charges using magneto-optics [1], as it is shown in Fig. 1.

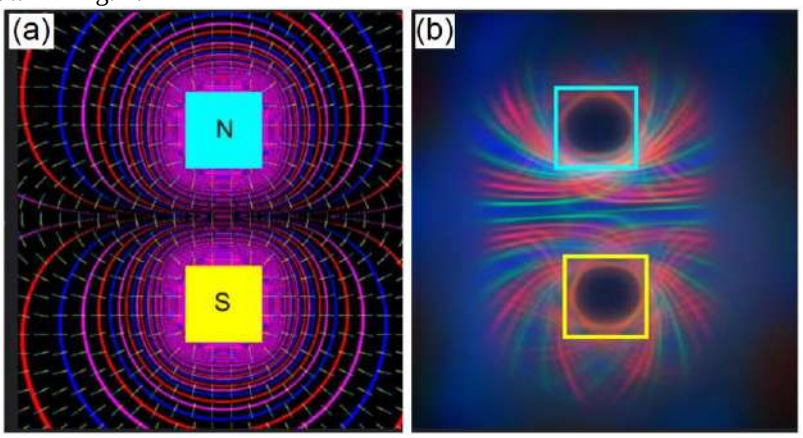

Fig. 1 – (a) Two magnetic charges with the field lines represented by the arrows and isopotentials represented by the colored lines and its magneto-optical counterpart in (b).

We have proposed this representation because the representation of both fields is comparable, the existence of two different types of "charges" enable us to obtain elliptic points and saddles. Basically, the colored lines observed from our magneto-optical system are obtained from the light diffraction of light sources in micro-needles aligned with magnetic field. In Fig. 1 and Fig. 2, we can see that the isopotentials are perpendicular to the lines of the magnetic field.

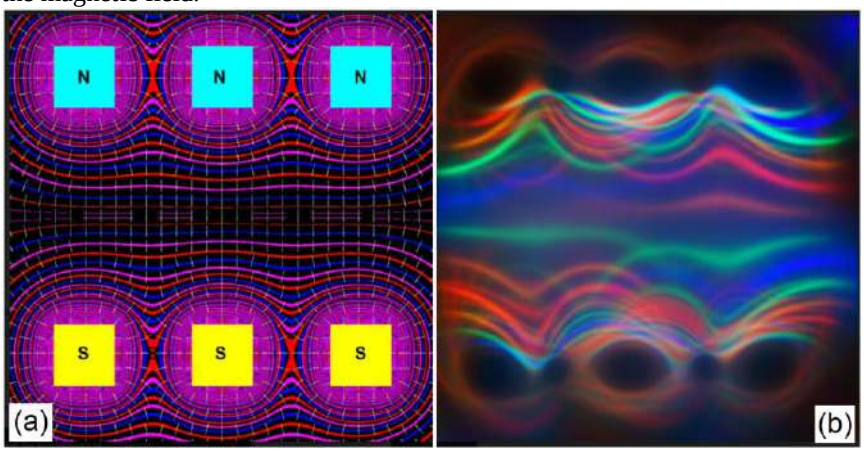

Fig. 2 - (a) Three magnetic charges with the field lines represented by the arrows and isopotentials represented by the colored lines and its magneto-optical counterpart in (b).

It is important to note that the representation of magnetic charges is a valid way to represent the magnetic field and this is not incompatible with the idea of the Lorentz force, as the same way that a phase space represents states of motion, not the motion itself.

However, there is an apparent contradiction in this analogy, because the representation of isopotentials and the colored lines of our magneto–optical is not perfect. A close observation of the light patterns of the experiment shows the existence of crossing lines, which could imply in indeterminacy in a dynamical system, violating the classical representation of dynamical systems. The light patterns mimic the isopotentials, because the light patterns are a combination of the magnetic field and the position of the light source. For different positions of the light source, we have different diffracted lines, which eventually will cross each other. In this way, metaphorically speaking, these luminous patterns linked to the isopotentials are equivalent to the representation of the nature by the impressionist painters, with emphasis in depiction of light in its changing qualities with unusual visual angles.

Consider now the Hénon conservative map given by:

$$x' = x\cos\alpha + (y - x^2)\sin\alpha,$$
$$y' = x\sin\alpha + (y - x^2)\cos\alpha. \qquad (1)$$

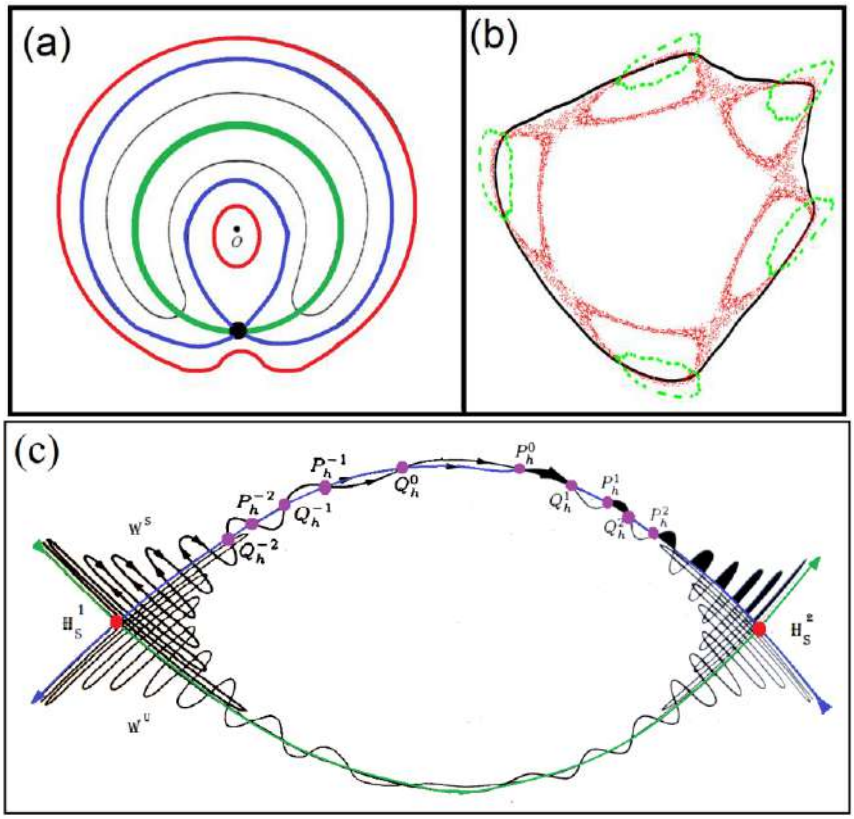

Fig. 3 – In (a) diagram of separatrix chaos. In (b) the diagram of a Henon-Heyles map with chaotic oscillations. In (c) the concept of chaos in conservative systems close of hyperbolic points.

For the case of Hamiltonian systems, we can observe the existence of chaos for perturbations close to the separatrix of the system, as it is shown in Fig. 3(a), which shows the conditions of the nonlinear resonance on the phase space, in which the green line is the unperturbed trajectory. The blue line is the new separatrix of the phase oscillations. The classical plot of chaotic behavior can be obtained for the Hénon conservative map of the Fig. 3(b) from eq. (1), with chaotic behavior given by red region ($\alpha = \pi/2$-0.228), quasiperiodic behavior in green color ($\alpha = \pi/2$-0.200), and another chaotic region in black ($\alpha = \pi/2$-0.250).

The idea o f chaos in this case can be understood if we follow the stable (W^s) and unstable manifolds (W^u) of Fig. 3(c), until their intersection points in

red, called homoclinic points H_S^1 and H_S^2. Applying the perturbation repeatedly to P_h^0, we have the sequence of image points P_h^k converging towards hyperbolic point for *k* tending to infinite, and consequently W^u and W^s can only intersect after an infinite sequence, and the same is valid for the reversing points Q_h^k. The result is an extraordinary complex view of intersecting invariant manifolds. One example of this behavior is shown in Fig. 4 using the eq. (1), for the case of α equals to (π/2-0.228). (see ref. 2).

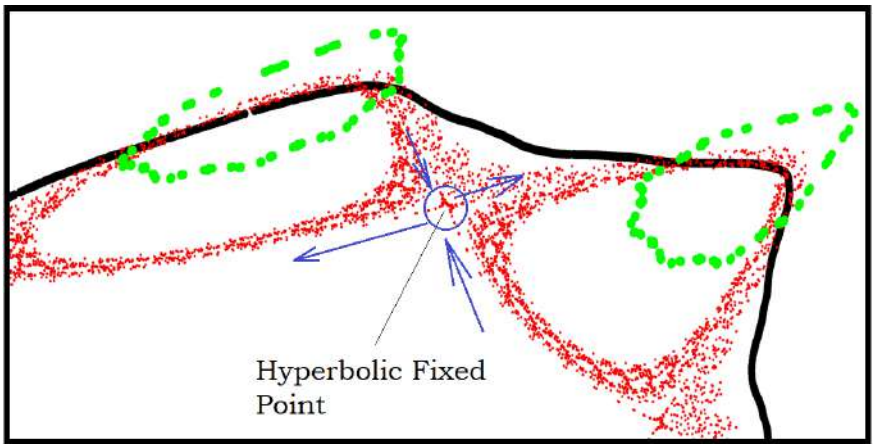

Fig. 4 – Chaos close of a hyperbolic point in the Hénon map.

For the case of the magneto-optics in our experiment, we observed that the light patterns are oriented by the vectorial product of Fig. 5 [1, 3, 4, 6, 7].

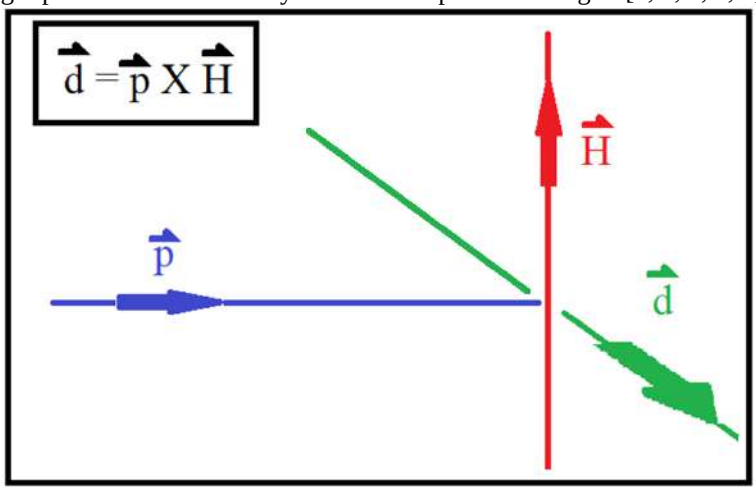

Fig. 5 - The vector **d** is the direction of the tangent line of the diffracted lines, which is perpendicular to the direction of propagation of the light ray **p** and the orientation of the magnetic field **H**.

This approach is well known in celestial mechanics, demonstration of chaotic pendulum, or in electromagnetism, where physicists look for the dynamics of particles in magnetic fields. We are investigating in this paper the equivalent case of chaotic scenario in magnetostatics interacting with light from our experiment involving magneto-optics. We were inspired by the direct observation of luminous patterns and properties of magnetic fields.

2 Experimental Apparatus and Modeling Isopotentials

In Fig. 6 we present the experimental apparatus of this system. The luminous patterns observed in the thin film of ferrofluid is a direct effect of the magnetic field with the iron particles, which take a shape that scatters light in a certain shape for the viewer. In this way we have to use an array of magnets of Fig. 7, above the magnets we have a mirror. The device known as Ferrolens of Fig. 8, the Hele-Shaw cell containing the ferrofluid, is placed above this assembly. We use different light arrays above this setup, which represent the ferro-mirror experiment. The ferrofluid is a stable colloidal dispersion using light mineral oil. The nanoparticles are spheres of the order of 10nm in diameter. The magneto-optic effect results in the change of some optical parameters of the ferrofluid, forming images. For more details see Refs. 1, 3, 5 and 6.

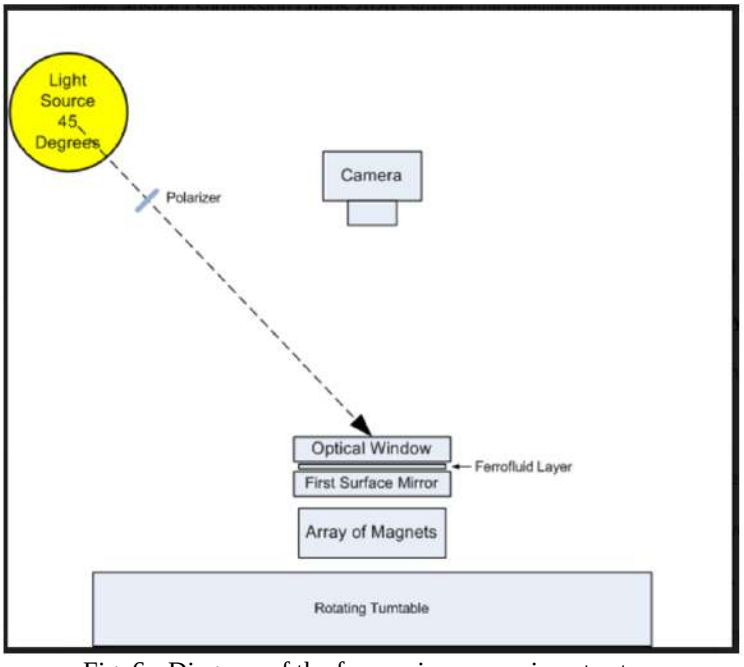

Fig. 6 - Diagram of the ferro-mirror experiment setup.

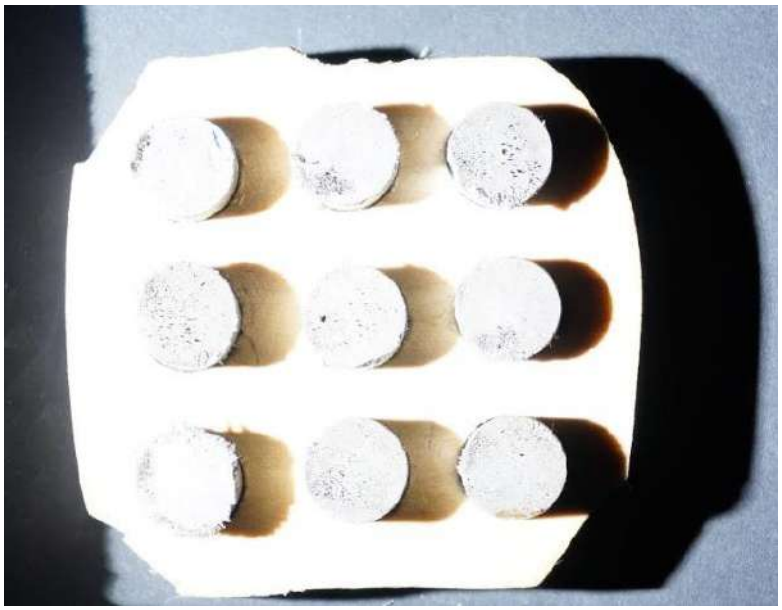

Fig. 7 - Magnets fixed in a base.

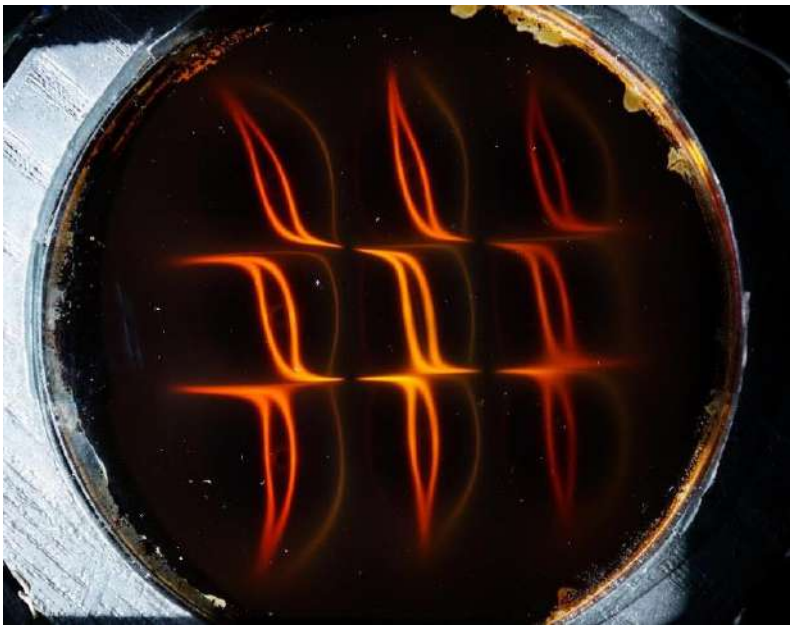

Fig. 8 – Pattern obtaine with the Ferrolens.

The software Pic2Mag [5] simulates some aspects of magnetic field arrangement of a magnet array, such as vector field and isopotentials, like the case of two magnets of Fig. 9(a), wich can be compared to a phase space like the one in Fig. 9(b), which represents the phase space of a pendulum.

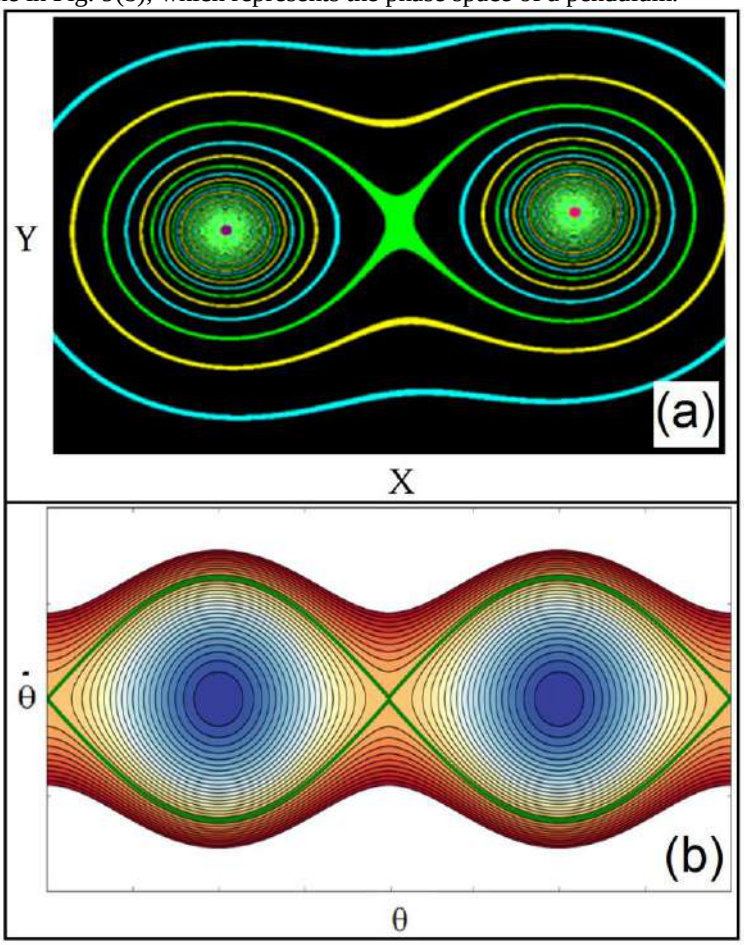

Fig. 9 – Comparison between isopotentials of magnetic field and the phase space of a pendulum. The green curves represents the separatrix.

3 The patterns of eyes and Chirality

One interesting phenomenon observed is a magneto-chiral pattern of Fig. 10, which there is three magnets to create this pattern, in a three-pole configuration formed by south-north-south poles. The pattern resembles three eyes arranged in a column-like alignment. Fig. 10(c) is the top view of the light pattern, Figs. 10 (a)-(b) is from the same system observed from the right side,

and Figs. 10(d)-(e) are perspective obtained from the left. We can see that the pattern suffers distortions. However, these patterns cannot be overlapped with other in order to be reproduced. One image is a reflection of the other, in such way that there is a chiral effect. We can consider that the assembly of nanoparticles is somehow affecting these light patterns, because nanoscale particles could self-assemble into helical-like structures due to the interplay of magnetic dipoles and van der Walls interactions [3, 4, 7]. The consequence of this anisotropy is the emergence of optical chiral structures.

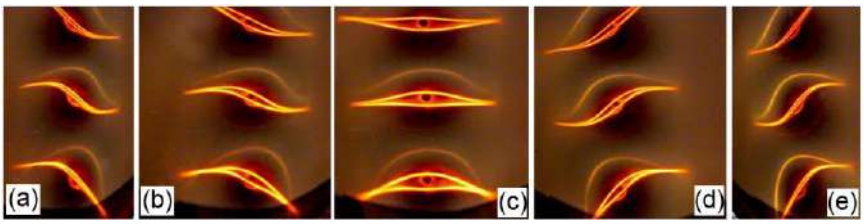

Fig. 10 - Magneto chiral effect.

4 Hyperbolic points

For the case of Hamiltonian systems, the existence of saddle point is the important key to observe the existence of chaos. The stable and unstable manifolds are called separatrices, and when a weak perturbation is added, the separatrix are destroyed and replaced by a separatrix chaotic layer. The same way as the separatrix is obtained numerically by integration of the equations with a set of initial conditions in the vicinity of the separatrix, we can explore in our system what is happening around the saddle points in our experiment. Let's consider the case of Fig. 11 with a configuration of isopotentials equivalent of a torus. Observing the detail of the central area of this image in Fig. 12(a) with the experiment in Fig. 12(b), we can see what is happening with the four saddle points around the center of the light pattern observed with experiment. The colored lines converge to the saddle point and vanish. In contrast, the center point of the image, which represents the center point of a dynamical system, the colored lines swirls around it, and the central region is dark.

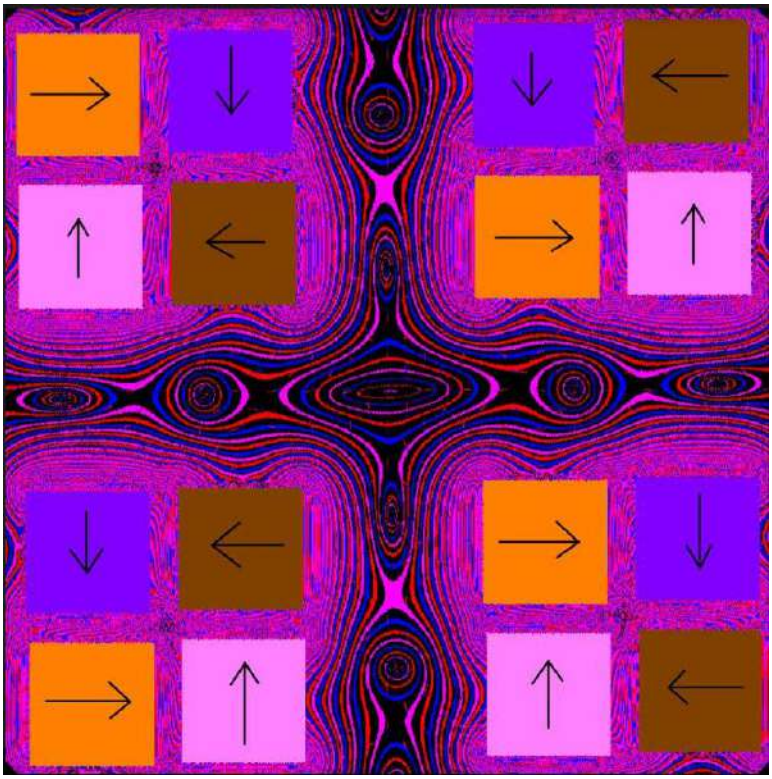

Fig. 11 - Simulation of isopotentials in a a torus.

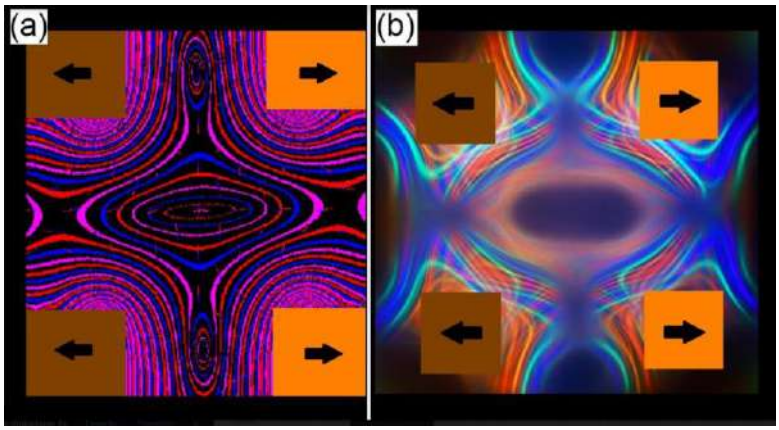

Fig. 12 - Exploring Center and saddle points: simulation and experiment

Fig. 13 was obtained by placing the pattern obtained experimentally on the simulation. With this picture, we can observe that the saddle points of the simulation is slightly different from the experiment, for example the green cross at the right side, at the top of Fig. 14, in which the experiment is the red circle A, and simulation is the green circle B.

Fig. 13 –Another array of magnets superposed on the simulation of the magnetic field and isopotentials.

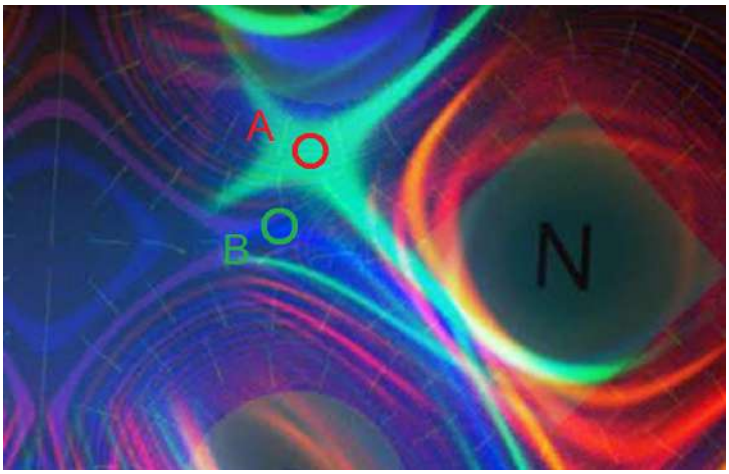

Fig. 14 Observing a hyperbolic magnetic point from the previous figure: the experiment is the red circle A, and simulation is the green circle B.

Conclusions

We have explored some aspects of the analogy between dynamical systems and the magneto-optical system formed by a thin film of ferrofluid. Magnetic static fields have some general properties of Hamiltonian systems, and using different magnetic fields configurations, we look for hyperbolic points and observed how the experiment behaves around these regions. The light patterns are related to the vectorial product between the ray light **p** and the orientation of the magnetic field **H**, given locally the tangent vector **d**. During theses explorations of this magneto-optical system, we have found some evidences of chiral effects and we suggested that this effect is related to anysitropic properties of magnetic nanoparticles.

We have observed that the presence of the thin film of ferrofluid affects the magnetic field, and the formation of patterns can show the differences between the values of the patterns observed experimentally and the computed values.

References

1) *Observing jumping laser dogs*, A. Tufaile, T. A. Vanderelli, A. P. B. Tufaile, J. Appl. Math. Phys. 4, 1977-1988, 2016

2) *An Exploration of Chaos*, J. Argyris, G. Faust, M. Haase, Elsevier, p. 108, Amsterdam, 1994.

3) *Light polarization using ferrofluids and magnetic fields*, A. Tufaile, T. A. Vanderelli, A. P. B. Tufaile, J. Adv. Condens. Matter Phys. 2583717, 2017.

4) *Observing dynamical systems using magneto-controlled diffraction*, A. Tufaile, T. A. Vanderelli, M. Snyder, A. P. B. Tufaile, Condens. Matter 4(2), 35, 2019.

5) Program for simulation of magnetic field: www.pic2mag.com

6) *Non-linear stability observation using magneto-controled diffraction with optic-fluidics*, A. Tufaile, M. Snyder, T. A. Vanderelli, A. P. B. Tufaile, in 11th Chaotic Modeling and Simulation International Conference, C. H. Skiadas and I. Lubashevsky (eds), p. 275, Springer Proceedings in Complexity, 2019.

7) Controlling light diffraction with nanostructures, M. Snyder, A. Tufaile, A. P. B. Tufaile, T. A. Vanderelli, TechConnect Briefs 2019, p. 369-372, June 17, 2019.

Hysteresis Loops, Dynamical Systems and Magneto-Optics

Adriana Pedrosa Biscaia Tufaile, and Alberto Tufaile

Soft Matter Lab, Escola de Artes, Ciências e Humanidades, Universidade de São Paulo, São Paulo, Brazil.
(E-mail: atufaile@usp.br)

Abstract. The interest in hysteresis and magnetism is shared by scientists with an impressive variety of backgrounds, such as mechanics, thermodynamics, electromagnetism, catastrophe theory, mathematics and dynamical systems, because hysteresis loop is a concept at the core of non-linear systems in which the dependence of the evolution of the states of these systems are related with their history. In this work we present a connection between dynamical systems and hysteresis loops and after that, we present some interesting hysteresis loops obtained using the Transverse Magneto-Optical Kerr effect (TMOKE), of thin films of sperimagnetic amorphous alloys with rare-earth and transition metal. The samples present first and second order transitions. The first order transition occurs at the compensation temperature when the total magnetic moment or magnetization is minimal. The second one occurs at the transition magnetic field when the behavior of the derivative of the signal changes, and it can be spin-reorientation or spin-inversion.

Keywords: Bistable system, Hysteresis loop, Sperimagnetism.

1 Introduction

Magnetism is a property of matter, and we can observe their magnetization **M** under several specific conditions of measurement or geometry when some materials are subjected to an external magnetic field **H**, as it is shown in Fig. 1 [1].

These curves give us some interesting ideas of the properties of the materials, helping to categorize them paramagnetic, diamagnetic, ferromagnetic, and so on. The blue curve representing the ferromagnetism presents the interesting feature known as hysteresis curve, in which the response of the system depends on its history. Ferromagnetism here represents several kinds of materials with ferro and antiferromagnetic materials that have exchange interactions that align the atomic magnetic moment without external applied field. The sperimagnetism is included.

Systems with hysteresis are in general nonlinear systems, and they are common in nature, and the word is used in different contexts to express some kind of state of a system that is dependent of its history, with some kind of lag between the input or control parameter and the output or state variable, enabling to make memory devices, such as magnetic tapes or hard-disks [1].

The magnetic field H is the input or control variable and the magnetization or total magnetic moment M is the output or state variable. H and M are conjugate work variables meaning that their product is work. G is the Gibbs free energy of the system and the thermodynamic potential controlling

spontaneous transformations. G_L is the Landau free energy, after L. D. Landau phenomenological theory of phase transitions. G is different of G_L, but after symmetry arguments and proper approximations, we can consider that Gibbs is equal Landau free energy, and search the local minima using the derivatives of G_L. The lowercases represents some convenient dimensionless form [1].

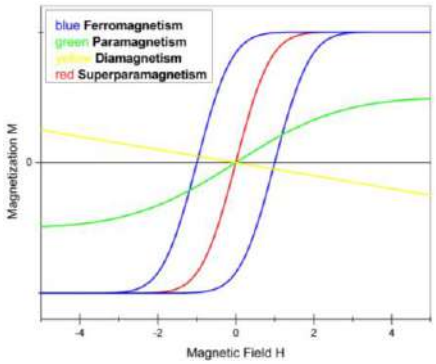

Figure 1. Magnetic curves for different magnetic materials.

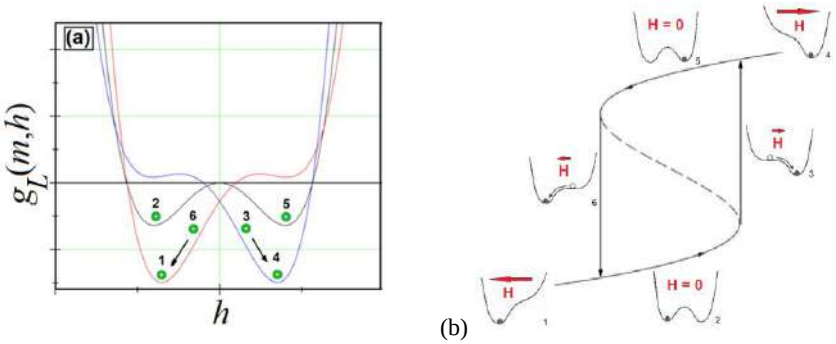

Figure 2. The system is in the state *m* of the green dots for the temporal evolution (1, 2, 3, 4, 5 and 6) of the potential $g_L(m,h)$ controlled by the input *h* in (a). The three different functions of g_L are represented by red, black, and blue curves. In (b), we have the hysteresis loop associated with this bistable system [1].

First, we will concentrate on bistable systems [2] and rate independent hysteresis, as it is shown in Fig. 2.

The potential represented with the black plot in Fig. 2(a) is the free energy of the bistable system for $h = 0$ for the expression [1]:

$$g_L(m, h) = m^4 - 2am^2 - hm. \quad (1)$$

where *a* is a positive parameter.

The hysteresis loop of this bistable system is shown in Fig. 2(b) changing the control parameter *h*. This system always moves towards a

minimum value, when h is increased from the saturated state 1, to state 2, jumps abruptly in state 3 by a Barkhausen jump, reaching another saturated state 4. Reversing the control parameter, the system evolves from state 4 to state 5, a different minimum of the bistable potential. After that, there is another Barkhausen jump in state 6 the initial saturated state 1. This behavior exemplifies how the system can have different values of one variable depending on the direction of change of the control parameter.

2 Dynamical Systems

We can observe that the hysteresis is related to a supercritical pitchfork bifurcation, with this example. Related with dynamical systems by look the derivatives, considering the state variable x, representing the magnetization, that will change in time.

Stable points have first derivative equal to zero, and a positive second derivative. Unstable points have first derivative equal to zero, but a negative second derivative. The first derivative is

$$f(h,x) = dg_L/dx = 4x^3 - 4ax - h. \quad (2)$$

Changing the magnetic field will change the first derivative $f(h,x)$ and one can construct a hysteresis loop. In Fig. 3(a), the system evolves from only one stable fixed point to a saddle-node bifurcation, with two new stable fixed points, as it is shown in Fig. 3(b). Then, in Fig. 3(c), the hysteresis is seen when the system goes back and forth, and just one stable fixed point is visited each time, before the Barkhausen jump. The intermediate region between the two stable fixed points is unstable, in contrast to the case when the parameter $h < 0$. The pitchfork bifurcation of each branch of the hysteresis cycle is shown in Fig. 3(d).

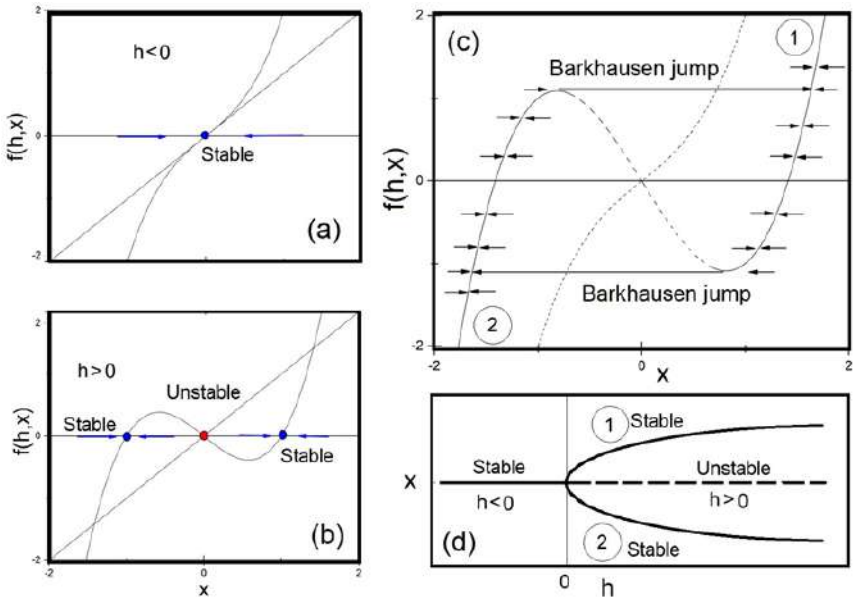

Figure 3. Relation between hysteresis loop and a supercritical pitchfork bifurcation. In (a), the system evolves to only one stable fixed point for a control parameter $h < 0$. A saddle-node bifurcation is shown in (b) as we change the control parameter h. The complete hysteresis cycle depends on the history of the initial conditions. The pitchfork bifurcation of each branch of the hysteresis cycle is shown in Fig. 3(d).

3 Sperimagnetism

The samples are thin films made of amorphous alloys contain rare-earth and transition metal. They have transition metal cobalt Co and a rare-earth metal as gadolinium Gd or holmium Ho. The films were deposited by magnetron sputtering in glass and silicon Si substrates cooled to free the atoms and make amorphous alloys. We took the loops of the films in glass substrates; the Si ones were used the measure the thickness of the layers. In Fig. 4, we represent the profile of the films.

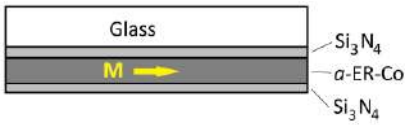

Figure 4. The structure of the samples shown in cross section. The Si_3N_4 are antireflexive and protective layers. The axis of easy magnetization (arrow) is on the plane of the film.

The composition and thickness of the samples are shown in the Table 1. They were measured by analyzing Rutherford Backscattering Spectrometry (RBS) spectra obtained with normal beam incidence of $4He^+$ de 2.4MeV. We used the films with silicon substrates for this analysis.

Composition of the metallic layer	Layer thickness (nm)		
	Metallic layer	1st Si_3N_4	2nd Si_3N_4
$Ho_{33}Co_{67}$	108	32	31
$Ho_{36}Co_{64}$	116	32	31
$Gd_{20}Co_{80}$	153	55	55

Table 1. Composition and thickness of the samples.

It is important to note that, in amorphous materials, atoms are frozen in random positions and orientations, unlike a crystalline structure, where the positions and orientations of atoms, or ions, are periodically ordered. So, in amorphous alloys, the direction of anisotropy for each ion is random. The interaction responsible for the ordering of spins in the material, and therefore, for the existence of spontaneous magnetization, was recognized by Heisenberg, in 1926, and called exchange interaction. The type of exchange interaction that occurs between two atoms depends on the electronic structure of the interacting atoms.

The antiferromagnetic exchange interaction between gadolinium or holmium and cobalt make the magnetization of these two sublattices points to opposites sides. This gives rise to a compensation temperature $\mathbf{T_{comp}}$, in which the total magnetization of the alloy is minimal.

The sperimagnetism [3] occurs because of two aspects, local or ion anisotropy and interaction between the alloy components. The intensity of exchange interaction between cobalt and cobalt is one order of magnitude greater than the exchange interaction between cobalt and rare-earth, which in turn is one order of magnitude greater than the interaction between rare-earth ions. So, the cobalt sublattice is well aligned, but the alignment of the rare-earth sublattice it is weaker in the struggle against temperature.

The rare-earth elements have the electronic structure of the most energetic layers represented by: $4f^N\ 5s^2\ 5p^6\ 5d^1\ 6s^2$, where N = 0 to 14, corresponding to the elements from La to Lu. For Ho, N = 10, because its atomic number is 66, for Gd N = 7 (no orbital angular momentum, L = 0). The rare-earth magnetism comes from the unpaired electrons of layer 4f, and in an alloy they are usually in the form of a 3+ ion, that is, the electrons of layers 5d and 6s are conduction electrons. Layer 4f is said to be deep, as it has an average radius of approximately 0.3 Å, while the ionic radius is around 1.8 Å. Thus, the superposition of layer 4f of neighboring ions is negligible, and therefore, there is no direct exchange interaction between these ions. Its alignment is due to a low intensity indirect exchange interaction. Gadolinium ion is spherical, much more symmetric than holmium, so the local ion anisotropy is stronger in holmium. The exchange interaction between ions of transition metal as Co happens with electrons of the 3d that have large volume of superposition, therefor a large exchange integral [3].

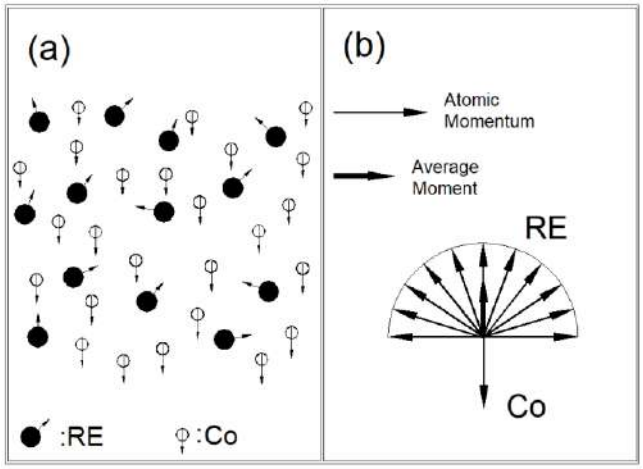

Figure 5. T = 0. In (a), we have a spatial representation of the amorphous RE-TM alloy (rare-earth/transition metal), where we see that the positions and orientations of the ions are random, and for RE the local anisotropy is dominant, so the orientations of its spins are random. However, for TM the dominant interaction is the exchange interaction, which promotes the perfect alignment of the spins of these ions. In (b), we have a schematic representation of the directions of the spins, where we see that the average magnetic moment of RE is in the opposite direction to that of Co, since there is an anti-ferromagnetic coupling [3].

The sperimagnetism that appears in amorphous rare-earth (RE) alloys and transition metal (TM) is a special arrangement of spins, in which the directions of the spins corresponding to the rare-earth ions are randomly distributed inside a cone or a semi-sphere, while the spins of the transition metal are all aligned with the axis of the rare-earth spin cone. This type of arrangement is represented in Fig. 5(a), the dark circles represent the rare-earth ions, and the light circles, the TM ions. In Fig. 5(b), we have a schematic representation of the arrangement, showing the random distribution of the RE spins and the TM alignment. This representation corresponds to the fundamental state, that is, temperature equal to zero Kelvin.

During the hysteresis loops, this type of alloy suffers a second order phase transition, when the applied magnetic field can turn the direction of the magnetization of the sublattices, the transition magnetic field $\mathbf{H_t}$. And it can change with the temperature.

The phenomenon called spin-reorientation is the change in direction of the average magnetic moments of each sublattice, in relation to the direction of the applied field [4]. When the applied field is weak, we have sperimagnetic arrangements before and after the compensation temperature, this phase transition is first order. But if the applied magnetic field is larger than the critical field, H_{cri}, for temperatures close to $\mathbf{T_{comp}}$, then the magnetic moments of the two sublattices start to have a projection in the direction of the applied field. With the hysteresis loops, we identify the $\mathbf{H_t}$. This phase transition is second order. In Fig. 6, before the spin reorientation, we have small shaded regions that

correspond to the phases where the transition metal also has a random distribution of the spin directions. The dashed lines above H_{cri} represent the behavior of coercivity. The dashed lines below H_{cri} correspond to the loss of stability of the collinear phases. Zvezdin [4] used films with the axis of easy magnetization perpendicular to the plane of the film, our samples have it in the plane of the film.

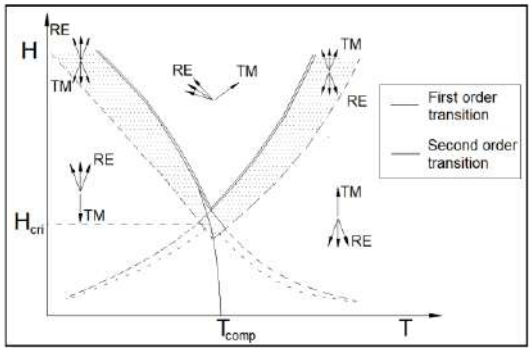

Figure 6. Phase diagram for amorphous films of RE-TM, applied magnetic field H versus temperature T. The axis of easy magnetization is normal to the film plane. In our case, the axis of easy magnetization is in the plane of the film [4].

4 Thermal Behavior of the Hysteresis Plots

The magnetic signal was measure by vibrating sample magnetometer (VSM) at room temperature or SQUID: Superconducting Quantum Interference Device, at 5 K < T < 300 K. A magnetic hysteresis loop is shown in Fig. 7, where we can see the transition magnetic field.

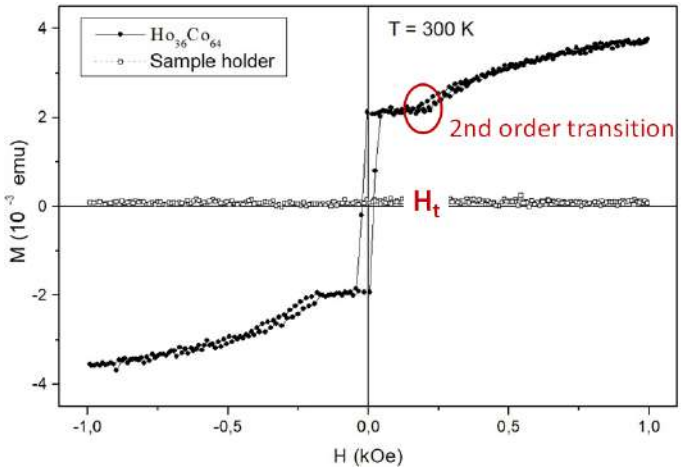

Figure 7. Magnetic hysteresis loop (VSM), where we can see the transition magnetic field, H_t. It is a second order phase transition.

The magneto-optical signal is the Transverse Magneto-Optical Kerr Effect (TMOKE) measured using laser diode. $\lambda = 670$ nm, at $7\ K < T < 300\ K$, angle of incidence: 45° [5] [6]. The Magneto-Optical Kerr Effects are shown in Fig. 8.

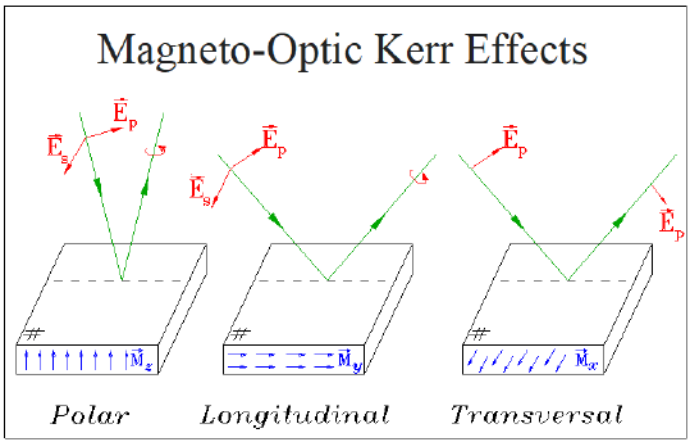

Figure 8. The three configurations of the Magneto-Optical Kerr Effects.

Representing the light by its electric field components with respect to the plane of incidence, the material surface is represented by the R matrix:

$$\begin{pmatrix} E_p \\ E_s \end{pmatrix}^{r} = \mathbf{R} \begin{pmatrix} E_p \\ E_s \end{pmatrix}^{i} \quad \text{where} \quad \mathbf{R} = \begin{pmatrix} r_{pp} & r_{ps} \\ r_{sp} & r_{ss} \end{pmatrix} \tag{3}$$

The reflectivity of the component in the plane of incidence (p) is

$$R_p = \left| r_{pp} \right|^2 = r_{pp} . r_{pp}^* \tag{4}$$

The TMOKE signal is the relative variation in reflectivity in p component. For visible light, TMOKE is sensitive to the component of the magnetization of the transition metal sublattice parallel to the applied magnetic field:

$$\frac{\Delta R}{R} \propto M_x^{Co} \tag{5}$$

The two types of phase transition happen due to the competition between the magnetization of the sublattices. This behavior creates variety of hysteresis loops, more complex than the bistable system of Fig. 2.

In the Fig. 8, there are hysteresis loops for six different temperatures that we obtained with magneto-optical effect for another composition of

amorphous holmium-cobalt alloy. As you can see, the loops are more complicated that a bistable system. But it is possible to find out what is happening. Before the compensation temperature, the magneto-optical loop is inverted, because this signal is sensitive to cobalt, which has less magnetization than holmium. The compensation temperature is around 218 K and the main thermal behavior is in the signal of saturation. The magneto-optical saturation signal increases with increasing temperature. We did not notice thermal variation of the transition magnetic field [5].

Here inverted hysteresis loops have different meaning of those ones observed by Ghising, Samantaray, and Hossain [7].

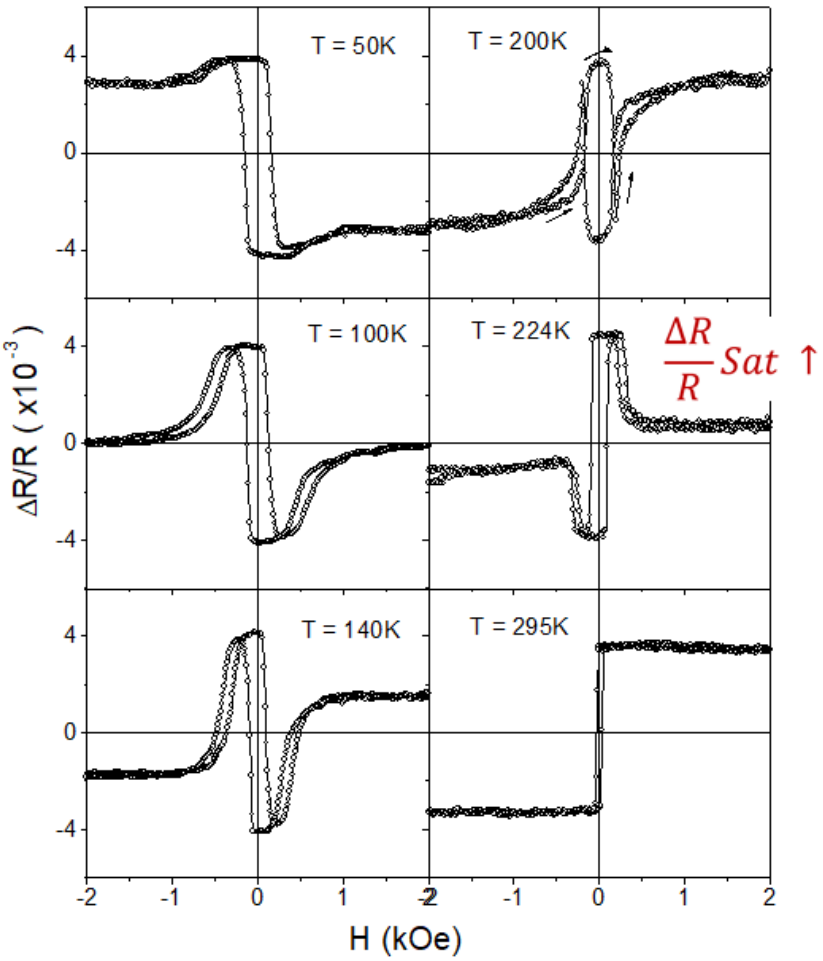

Figure 9. Magneto-optical hysteresis loops for a thin sperimagnetic film of *a*-$Ho_{33}Co_{67}$. The T_{comp} ~ 218 K, and H_t is approximately constant.

We have a superposition of the magnetic and magneto-optical loops taken of the sample *a*-$Ho_{33}Co_{67}$ in Fig. 10.

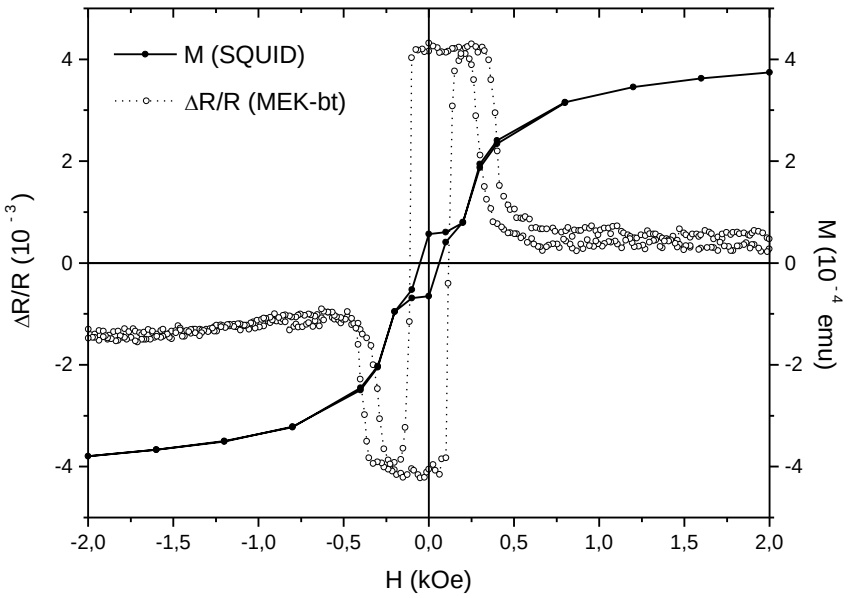

Figure 10. Magnetic and magneto-optical hysteresis loops for the sample of *a*-$Ho_{33}Co_{67}$, at 224 K. We can see that the effect of the second order phase transition occurs in the same value of the applied field.

The comparison of magnetic and the magneto-optical loops for a film of *a*-$Gd_{20}Co_{80}$ is in Fig. 11. The compensation temperature is around 92 K, and we can see that the transition field increased with temperature. The magneto-optical saturation signal is constant, but further analyzes show that the transition magnetic field increases exponentially with temperature.

In Fig. 12, there is the schematic explanation for the phenomena we observed in the hysteresis loops.

For gadolinium-cobalt alloy, the magneto-optical signal has the same intensity before and after the transition field, indicating that cobalt sublattice has the same component of magnetization in the direction of the field, but in the opposite sense. Therefore, we conclude that the second order transition is not a spin-reorientation. We call it a spin-inversion because there is no non-collinear sublattice situation.

As gadolinium ion is spherical, so the local anisotropy is less than in the case of holmium, which has strong local anisotropy because it has a large orbital angular moment. So, it is easier for the ionic magnetic moment (spin) of Gd to turn in the direction of the magnetic field than spin of Ho.

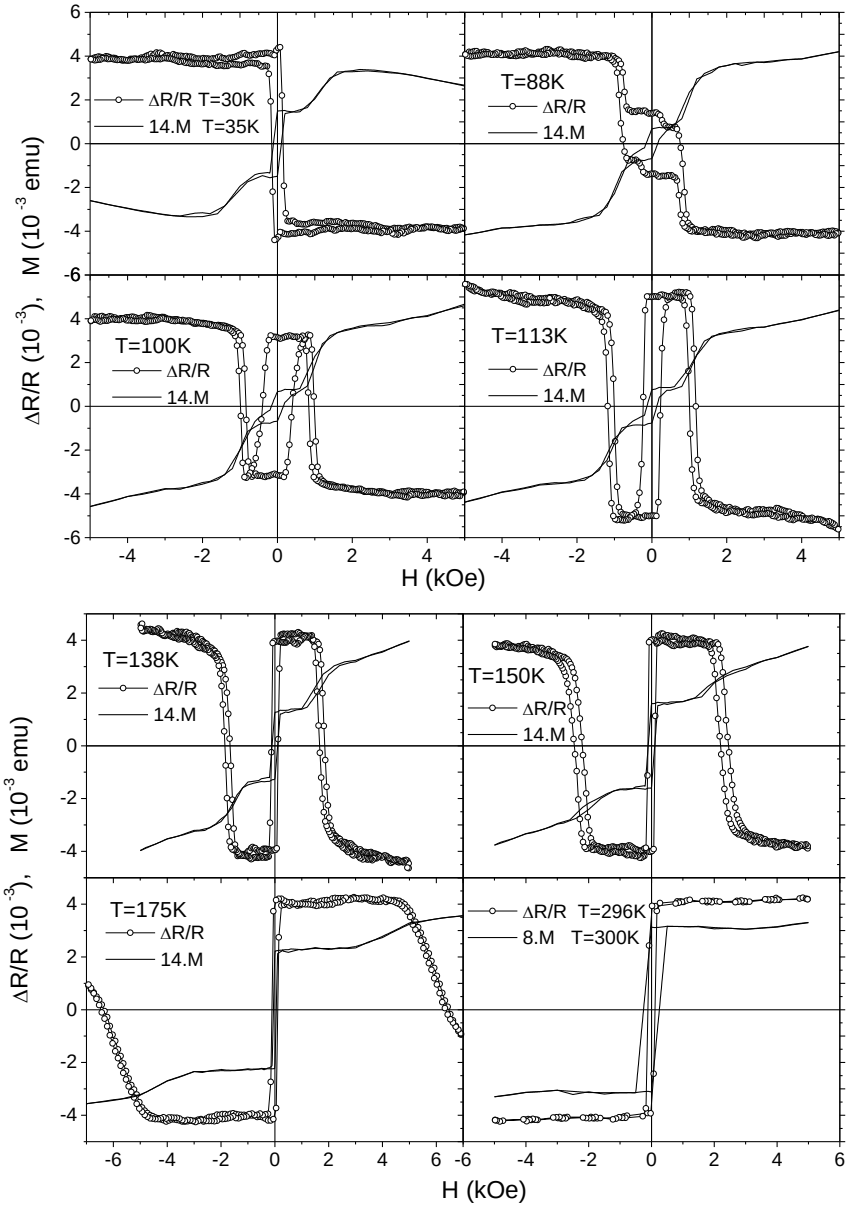

Figure 11. Superposition of magnetic and magneto-optical hysteresis loops for the sample of *a*-$Gd_{20}Co_{80}$. The compensation temperature is around 92 K, the transition field increased with temperature [5].

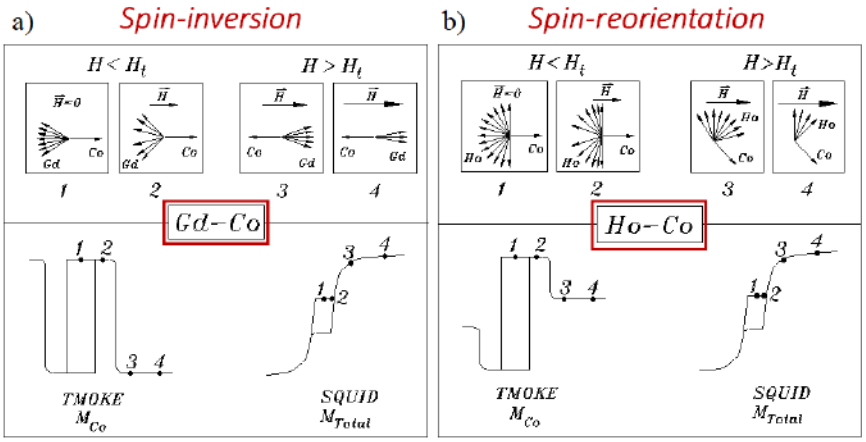

Figure 12. The analysis of magnetic and magneto-optical hysteresis loops for the sample of *a*-$Gd_{20}Co_{80}$ indicates that it has a spin-inversion, and the sample of *a*-$Ho_{33}Co_{67}$ has spin-reorientation.

Conclusions

We started showing the connections between hysteresis loops and dynamical systems. We have presented the complexity of hysteresis loops present in some sperimagnetic thin films of Gd-Co and Ho-Co, by looking magnetic and magneto-optical signal. Both samples presented a first order phase transition and a second order phase transition. The difference in local anisotropy between Gd and Ho ions led to different types of second-order phase transition. Ho-Co film has a spin-reorientation phase transition (collinear phase to non collinear phase). Gd-Co film has a spin-inversion phase transition (collinear phase to opposite collinear phase). Despite the complexity, we know the characteristics of the transitions, these types of hysteresis loops deserve a more complex bistable system model.

Acknowledgments

Thanks to A. D. dos Santos (LMM) and M. H. Tabacniks (LAMFI), Instituto de Física, Universidade São Paulo. This work was supported by FAPESP (Proc. 96/04507-5).

References

1. G. Bertotti. Hysteresis in Magnetism, for physicists, material scientists, and engineers, Academic Press, San Diego, 1998.
2. E. Colli, V. S. M. Piassi, A. Tufaile, J. C. Sartorelli. Bistability in bubble formation, Phys. Rev. E 70, 066215, 2004.
3. R. Arrese-Boggiano, J. Chappert, J. M. D. Coey, A. Liénard, J. P. Rebouillat. Mössbauer spectra of the amorphous alloys DyM_3 (M = Fe, Co, Ni), J. Physique **37**, C6-771, 1976.

4. A. K. Zvezdin. Field induced phase transitions in ferrimagnets. In K. H. J. Buschow (ed.) Handbook of Magnetic Materials, v. 9, Elsevier, London, 1995.
5. A. P. B. Tufaile. Efeito Magnetoóptico espectral e Sperimagnetism de filmes amorfos de terra rara-Co, PhD Thesis, Universidade de São Paulo, 2001. https://www.teses.usp.br/teses/disponiveis/43/43134/tde-05072012-171055/pt-br.php
6. P. Ghising, B. Samantaray, Z. Hossain. Spin inhomogeneities at the interface and inverted hysteresis loop in La0.7Sr0.3Mno3/SrTiO3, Phys. Rev. B 101, 024408, 2020.
7. A. P. B. Tufaile and A. D. Santos. Low temperature magnetic characterization of sperimagnetic films by TMOKE, Mater. Sci. Forum **302-303**, 120, 1999.

Innovative Trends in Modern International Terrorism

Alexandr Valyaev

Nuclear Safety Institute of the Russian Academy of Sciences, Moscow, Russia
(E-mail: anvalyaev@mail.ru)

Abstract. Today the main great treats for existence of all humanity are intensity increasing and including wide scale natural and manmade catastrophes and international terrorism (IT). According to forecasts, this negative trend will increase over time in the 21st century. And very dangerous COVID -19 was added to them. Here we present the results of our IT researches on the results of participation in international thematic events, such as the international scientific events of NATO and the ISTC. This is my own report of my work as the member of the International Scientific Committee of Chaotic Modeling and Simulation International Conference (CHAOS) and chief of its Special Session: "Modeling risk assessment for nuclear, environment and manmade sources". The special attention is paid to the organization and conduct of such events aimed at increasing their effectiveness and implementation. Information is provided on new methods of combating IT and preventing its possible acts.
Keywords: Treat, Terrorism, Environment, NPP, Monitoring, System, Water objects

Today the main great treats for existence of all humanity are wide scale natural and manmade catastrophes, international terrorism (IT), in the last year COVID -19 was added.
Here some thematic IT remarks are presented and discussed. At first I should like shortly present the results of my participation with own oral communications in the following events 2002-2011 in the 12-th NATO thematic scientific events, held by NANO Scientific Committee: Advanced Study Institutes (ASI), Advanced Research Workshop (ARW), Advanced Training Course (ATC) [1-12] and meeting of International Science Technical Centre (ISTC) in France, Italy, Russia, Lithuania, Armenia, Georgia, Ukraine and Kazakhstan. Some of them were devoted to the development and application of the special high technologies against terrorism.

NATO scientific events are completely different from ordinary scientific conferences and symposia with a large number of participants. The latter today they have already acquired the nature of scientific tourism, in which anyone who can often participate, having paid the registration fee in advance and having the desire to visit the country, where this event is held, can often participate.
The time and place of any NATO event is usually tied to a specific significant international political event.
At all NATO events training of progressive advanced scientific youth. Of the world is carried out by participants, the scientists, who have universally recognized their own scientific thematic achievements.
Scientists report their latest results, give lectures and conduct practical exercises with young people, usually graduate students and post docs in highly equipped training centers, such as NATO Center in Erice, Sicilia, Italy [9].

Here the right principle is strictly observed and takes place: if you yourself do not study in science, then you have no right to teach others the sciences. The maximum number of participants of NATO scientific events is usually from the host countries and a wide circle of their students is involved here. Everyone receives certificates of participants, which are very significant for their scientific career.

As for the closed NATO Workshop [3] it was carried out during 300 years St.-Petersburg Celebration, when 45 Presidents from different countries were honor guests of City. In addition we had to analyzed the attempts and facts of different hidings and sheltering of explosives in luggage and at human bodies, their electronic note books, clothes and shoes of terrorists, who were and disguised as officially invited guests of St. Petersburg.
The particular attention was paid to the detectors and techniques for detecting explosives in the baggage, clothes and shoes of passengers. Then there were first attempts to hide explosives in shoes. That is why among the participants [3] were many participants from the previous [2]. A special technique was used to trap explosives vapors and traces. For example, using special vacuum cleaners, especially sensitive detection of traces and vapors of explosives was carried out. The numerous latest tools - radiation-nuclear control devices were presented and partially demonstrated in actions for the participants at the specially organized exhibition.
The results of own thematic experience on this very actual and urgent IT problems, including my work as the scientific director and manager of ISTC Russian Project No 3269 "Study of the Radionuclide and Chemical Contamination Level and Character and Creation of Radiation and Hydrochemical Monitoring System for the Volga and of Ural River Basins" on the Joint International Program: "Investigation of Contamination of the Russia, Kazakhstan, Georgia, Azerbaijan and Armenia Rivers belonging to the Caspian Sea Basin for transboundary monitoring system" The Caspian Sea Basin is the place for intensive hydrocarbon world mining and production of oil and gas. Our Project is supported by collaborators from 11 West countries:

- Sandia National Laboratories / Geosciences and Environment Center – USA;
- Technical University of Denmark / Kemisk Institut – Denmark;
- Forschungszentrum Julich / Department of Safety and Radiation Protection – Germany;
- Alfred Wegener Institute for Polar and Marine Research – Germany;
- Universita degli Studi di Milano / Dipartamento di Fisica Italy;
- Universitat Sälzburg / Institute of Physics and Biophysics Austria;

- EMonument Belgium;
- Carleton University Canada;
- CNRS / Université de Reims / Laboratoire de Geographie Zonale pour le Developpement France;
- Institute of Dynamic Change USA;
- Université de Bordeaux 1 / Centre de Développement des Géosciences Appliquées France;
- Supporters Norwegian Radiation Protection Authority / Statens Stralevern.

Since 2009 I was the main scientific consultant in another ISTC Project # KR-1678 "Assessment and decreasing risks and damages, caused by Tien –Shan mountain lakes outbursts". This Project was also devoted urgent economic and ecological Central Asia (CA) problems, such as monitoring of Kyrgyzstan (KR) numerous uranium tailings storages and the environmental situation in the areas of gold mining sites, especially to prevent disasters and cataclysms associated with the outbursts of such lakes.

But its funding of this Project was interrupted for the reasons due to the sharp unsatisfactory political situation inside the KR. In particular, due to KR Tudypan revolutions - mass protests against its government in 2005 and 2009.

In our adopted ISTC Projects some transmission of infections and pathogens in the Caspian Sea and in water basin of Naryn, KR largest river, its inflows, artificial reservoirs, high mountains lakes and other have been presented. That creates the real reasons for the violation of the sustainable development of the vast industrial and densely populated Russian (RF) and CA regions with global widespread irreversible negative consequences for the whole Eurasian continent.

The US Department of Energy (DOE USA) was ISTC Russian Project No 3269 Project initiator and appointed Project collaborator, who was the thematic scientist and management from US Sandia National Laboratories. Also DOE USA was the sponsor of our International Program in monitoring of the Caspian Sea basins of all large rivers at the territories of Caucus (Georgia, Armenia, Azerbaijan) and Central Asia (Kazakhstan, Kyrgyzstan, Tajikistan, Uzbekistan). The Eurasian special international ISTC Navrus Program was successfully implemented at CA territory on the CA basins of Syr Darya and Amur Darya, CA main rivers for more than 10 years [15, 17, 18] Their main results were presented by professor and Navrus scientific leader, professor Vladimir Solodukhin from Kazakhstan Nuclear Physics Institute in Almata city.

The serious obstacles to the thematic projects and programs implementation was the introduction of Crimean sanctions, prohibiting the financing of the ISTC Projects and Programs at the whole RF territory, that significantly complicated and weakened the fight against IT.

Now the US and RF scientific-technological collaboration has narrowed down. The US President Trump allowed it only in Space and the Arctic, that is also constantly narrowing. That is why the functioning of all international funds and programs, such as ISTC, G. Soros, CRDF, TACIS and others. But their important main unsolved tasks and problems still remained. As the result, the international situation escalated, that was negatively reflected in intensification with IT struggle.

The constant decline of real living standards in underdeveloped Muslim countries has created the premise of creating new IT centers there.

It was in the Muslim faith that such trends as the Caliphate and Radical Islamism arose and developed. Another trend of "Guardians of the Islamic Revolution" actually rules in Ideology, Politics, and the Development of Military Power in Iran (Available from: https://deepblue.lib.umich.edu/bitstream/handle/2027.42/64683/afshon_1.pdf). These trends lie in Iran ideological IT basis.

The difference in faiths, for example, the Muslim and Christian Orthodox, creates major absolutely unscientific contradictions between the scientists of these countries. For example, Azerbaijan and Armenia, which is clearly manifested at international scientific conferences. For example, at the Conferences of the Institute of Nuclear Physics in Almaty Kazakhstan. In addition, fighting has been ongoing in the border areas of these countries since 1987 - Nagorno-Karabakh (Available from: https://en.wikipedia.org/wiki/Nagorno-Karabakh).

These factors create very negative demographic processes such as intensive population migration from IT-dominated territories from African and Middle East countries to EU. Today the situation has significantly worsened, as part of migrants are carriers of very dangerous **COVID-19**.

It is noticed the dangerous distinct tendency for terrorist groups to unite with state structures, that took place early and now. For example Alkaida and Islamic State join each others (October 10, 2014 Washington Times). And today this often happens in Ukraine.

Radical Islamism claims that the more his supporter in the attack takes other lives with him, the happier he will be in Paradise. And his duty is to commit any global large-scale terrorist attack with mass casualty emergencies and victims. That is why special NATO ATC was held in 2011 [12] In addition, this is the significant reason to exclude the possession of nuclear weapons of Muslim countries, such as Iran.

Such centers were disguised there under the guise of sponsorship of educational and religious ones with the active participation of the World Muslim countries such as Saudi Arabia, Pakistan, Somalia, Afghanistan and some others. In fact, they trained new IT members, that were discovered by intelligence agencies. For example, the Federal RF Security Service (FSB) detected them in the so-called "independent" CA countries, formed as the result of USSR collapse. The activities of these centers were actively supported in existing and frozen IT centers of Caucasus, such as Chechnya, where new IT centers were created, as well as in some RF regions such as Tatarstan, Bashkortarstan, including Volga and Moscow regions. Their own highly paid thematic scientists work in such centers to train new

terrorists and develop innovative technical means for carrying out terrorist attacks. Note that destroying is always much easier than creating and construction useful human objects. The good example of this is the USSR destruction. Therefore, scientists of IT centers are really ahead of the normal honest thematic world scientists.

Some details of the closed ARW. Advanced Techniques against Terrorism: «Bulk detection of explosives» (Radium Institute of V. Khlopin of Russian Atom Minister. St. Petersburg, Russia, June 16-21, 2003) [16] are following. During my long (45 min) communication in English "Using of Acoustic Techniques for Detection of Explosives in Gas, Liquid and Solid Mediums" and the wide 15 minute discussing I was speaking that the terrible IT countenance we have to contrast high advanced scientific techniques. This communication has been completely published [16].

Nerses H. Krikorian professor, Armenian-American chemist and intelligence officer at Los Alamos National Laboratory is the real living atomic legend and previously worked with Robert Oppenheimer and Enrico Fermi, the creators of the world first atomic bomb, reported about his work as the leader of diagnostics of all-penetrating neutrino particles by special detectors, which US located in different parts of the territory of neighboring Israel with Iran. Also he is the CIA Lead Analyst. Neutrino particles are intensively generated in different closed regions of Iran, such as Bushehr NPP, during the production of weapons-grade plutonium and enriched uranium, and in their spectra are different from neutrinos generated by the Sun and reaching our Earth. Trump, US President declares that he fully trusts the information of his special services, including the CIA, which was the reason for USA to withdraw from the International Agreement on Iran 2015. US policy was in the sharp confrontation with the policies of all other states of this Agreement. However, Trump ignored this fact, as the United States was the only country that had reliable information about Iran on this issue. Nerses H. Krikorian (born in 1921). He is still working intensively. In addition to his scientific work, he is also an expert-analyst of the CIA. Born in Turkey, due to the Armenian Genocide, the family fled to Greece, then to Canada and finally to the USA. 64 years ago (until 2007), he began working at the Los Alamos National Laboratory (New Mexico state). Nearby is another Sandia National Laboratory. These laboratories are small underground cities (30–40 thousand employees) with their own airfields and fighter aircraft. I was there in 1996 under the program of J. Soros. Now these laboratories are leading world centers and are closest to solving the problem of controlled thermonuclear fusion. But in recent years, these studies have been suspended due to the need to combat global terrorism and global widespread catastrophes. Nerses worked there under the leadership of the fathers of the world's first atomic bomb, Robert Oppenheimer and Enrico Fermi, created in 1945 (RF bobm was appeared in 1949).

In 1939, R. Oppenheimer illegally came to the USSR to Beria, the future curator of all Soviet atomic projects, with the proposal of joint development of the US Manhattan atomic bomb project. But it's the pity, then they did not agree.

The roots and reasons for the emergence and prosperity of illegal IT groups lie in the unstable political, economic and demographic situations in the individual separated regions, where there are military operations, local wars and there are large sources of minerals. Syria and Libya are the good demonstrative examples.

The great disadvantage of the fight against IT is that the intensification of the struggle against terrorism begins in the affected countries after the next terrorist attack. While it is much more preferable to constantly combat it and implement measures to prevent possible terrorist attacks. The measures to improve the culture of the population and its behavior in terrorist attacks are clearly insufficient in all directions.

As it was for NATO ARW St. Peterbsurg [3] the particular attention was paid to the detectors and techniques for detecting explosives in the baggage, clothers and shoes of passengers. Also under consideration [3] were the criminal events, when terrorists from Chechnya shot and killed by another methods RF oligarchs, living in their villas in France, Spain and Italy, significantly enriched during the war between Russia and Chechnya as early as the beginning of the 21st century.

The subject of NATO scientific schools (NATO ASI) usually refers to the fundamental problems of science, where there are already many developments. And on current, acute and global world problems, operational NATO Advanced Research Workshops (NATO ARW) Workshop) and NATO Advanced Training Courses (NATO ATC) are held. For example, to combat terrorism and disasters, etc. I have already been to such schools and meetings 12 times. I am sure on own experience that many persons mistakenly think that NATO is only the hostile militaristic bloc. This is not true. Thousands of world scientists successfully working under the programs of the NATO Scientific Committee, and grants are provided for particularly relevant research. True, they are given to NATO member countries and its partners. Russia is not here. But grants are given to potential partners. For example, Georgia, Armenia, Ukraine, Moldova, where NATO often holds its events. Scientists from these countries benefit from the support and financial assistance of the OSCE - the Organization for Security and Co-operation in Europe (OSCE). Again, the Russia does not apply to them. Russia is also not at all in the List of countries of the world that can be assisted in conducting research by the United Nations Development Program (UNDP). In 2013, I myself suffered a lot from this fact.

The shot contents of some communications of NATO ARW [3] were following. The Victor Luchinin leader of thematic researches and professor from the St. Petersburg Electrotechnical University presented his device for remote monitoring of passengers person's pulse. This device was developed and commissioned by the US Department of Homeland and Defense Security. It was supposed, and so it turned out, in fact, that the pulse at potential terrorists during their pre-flight inspection is speeded due to their internal psychological stress.

P. Mostak, M. Stancl professors from Research Institute of Industrial Chemistry Czech Republic informed about their long standing experience in preparation and use of service dogs in various regions of our planet with fundamentally different climatic conditions (Sweden, South Africa, Japan and others) for the detection of explosives. The work of such dogs is very sensitive to climate and regions.

Michel Krausa, Fraunhofer Institut for Cytmischer Yechnologie of Phinztal Germany, the head of the specialized laboratory in the Institute of Chemical Technology in Carslow, Germany, which is the head of the EU, reported on studies on modeling the nose of a service dog when searching for and detecting explosives. For these purposes, the dog's nose was divided into a thousand separate parts and the functioning of each part were analyzed.

For example an ordinary mosquito male may detect a female mosquito at 12 km distance. And pigs are even more sensitive than dogs, but it's a pity they are not learning and training.

The US scientists reported about beer's using for explosive detect. A bee begins to perform a special dance in the air in the presence of odors. But it is impossible to put hives, for example, at metro stations or when boarding an airplane airports.

RF scientists from the electronic company reported about their special device for detecting electronic devices intended for initiating an explosion. For example, when using their device, in Chechnya successfully discovered the place of explosive deposit on the railroad tracks and 2 terrorist suicide bombers going to the Kremlin with explosive belts of death were remotely blown up.

The RF Transport Safety Administration introduces the sensitive technology for checking and detecting of explosives tracks on passenger's documents.

In recent years, IT has made significant strides in explosive using. For example, terrorists suture explosives into human organs, where it is extremely difficult to detect, since the composition of its explosive compositions of C, N, O, H elements are closed to the human cells composition. And airport landing control services may not detect the presence of explosives in terrorists. For these purposes the special explosive was developed. Then such terrorist in an airplane can sit at the porthole and initiates an explosion of explosives by swallow drinks with the certain composition. Then depressurization of the cabin during the flight can cause a plane crash.

Today the wide complex of special measures to protect against terrorist attacks implemented on the Crimean Russian-constructed parallel bridges, spanning the Strait of Kerch between the Taman Peninsula of Krasnodar Krai and the Kerch Peninsula.

In the US Los Alamos National Laboratory invented the E-Bomb, the electromagnetic bomb, which, when exploded, creates powerful electromagnetic radiation that can damage all computers and other electronic equipment with a long range. This E-Bomb was successfully used in Iraq war in 2003. This is not a bulky missile system, the transfer of which from the USA to Ukraine will be noticeable. In addition, it is not necessary to transfer the bomb itself. It is enough to transfer the technology of its creation. And then it can be easily created on the territory of Ukraine itself, where there are already qualified scientific organizations that have successfully used intensive pulsed sources of charged particles for more than 20 years, ion and electron accelerators, Here they play the role of microwave guns. They also are capable of hitting targets located deep underground (Available from: http://www.newsru.com/world/24nov2005/voor.html).

I'm sure. there is also the US electric shock weapon (another E-bomb)with several kilometers range on the base of High Powered Microwave (HPM). And then these two types of "The E-Bomb" paralyze the work of all special services for the Crimean Bridge protection (Available from: https://obzor.westsib.ru/article/38229).

The NATO scientific events, related to IT and transport safety, were attended by directors of security services of major world airlines such as Lufthansa, Air France, Delta, Transaero Airlines, Ryanair, Swiss, Aeroflot and representatives of related services, for example, the Aviation Security Certification Center of the RF Ministry of Transport. Here, these officials stated that they have instructions from their respective governments to primarily purchase devices manufactured in their countries. Free market laws do not work here. By the way, they take place in numerous US economic sanctions. The growth of the Chinese economy is not due at all to the fact that they are developing new advanced technologies. They steal them from high developed countries. Now the Chinese population is 10 times more than in the RF and 5 times more than US ones. Today orders banning of cooperation China, for example using of China electronics in important industrial homeland areas, such as the defense, aviation and cosmic one.

In recent decades, very dangerous and pervasive cyber terrorism has appeared. Its implementation is characterized by low financial costs and efforts. Enough to have the Internet and computers. Although there are special methods of dealing with it, they are not considered here.

The US National Homeland Security Service acts correctly and decisively in cases of possible terrorist attack.

At the beginning of the 21st century, the group of Arab terrorists with atomic bomb drawings were caught in one US southern state.

It was not possible to identify the criminal group ties. Then the circle was drawn with the center in the place of capture with the 100 km radius and the entire Arab population was deported without the right to USA re-enter.

Today there is the actual problem of leakage and theft of nuclear materials to create a low-activity dirty atomic bomb, as well as the trafficking of these materials from the places of their production and burial - storage of radioactive waste. Although a Dirty Bomb is not able to cause great destruction, but it can cause a huge negative psychological impact in the population if used.

Otherwise, terrorism is called an irregular war. Where absolutely non-standard techniques and actions are implemented. But with a definite ultimate goal. Sometimes it may seem like chaos. But this chaos is strictly controlled. Therefore, exactly the same methods must be implemented in the fight against it.

My thematic proposals are the following:

1. To invite more widely the scientists from such countries in all similar situations. NATO may use its possibilities here. For example, Turkey is NATO member. As for Iran this country is greatly closed in plan of

international communications, including scientific ones. But I met Iran scientists in Moscow at International Conferences on Space technologies in 2003 and 2005 years. The Iran participation in NATO scientific events will promote to the successful decision of the important Problems of Nuclear Military Materials and Technologies non transferring may be partially resolved by these ways. It will be "the heavy drop" from NATO on decreasing of political frictions with Iran and strengthening of peace.

2. Last years and today too Humanity has faced with such constantly intensive growing global threats, such as natural and manmade catastrophes and disasters and of cause IT at first time. There are not special and effective methods for struggle against them. In 21 century number of disasters will be constantly increase. The weakly guarded borders of Chechnya, Afghanistan and other zones of not only "frozen" conflicts, but also operated ones, can further stimulate insurgencies, especially characteristic as the modern waves of an increasing struggle against racism in the USA.

3. Possible terrorist attacks, including with using of explosives, at European and Asian continents can result to global pollution (and may be infections) of river's basins in the Caspian, Black, Kara Seas, Arctic Ocean and consequently, the World Ocean.

4. These problems are under consideration at another special organizations, where high qualified scientists are constantly working. That is why it will be useful to invite some its representatives in the theatrical NATO ARW participation. For example, in above mentioned NATO events the organizers and participants were IAEA, ISTC, the USA Homeland Security Department and DOE, the Commission on Nuclear Regulation, the Center of Non Profile Investigations, the Center of Nuclear Safety, Ministers of Custom and Boundary Protection, European Scientific Academy.

5. The IT organizations have its own scientists, that work in security and mystery at problems of effective realization of different terrorism attacks with huge disasters and mass victims. To destroy is more easily than to construct. This fact worse greatly the successful decision of problems on struggle against disasters and terrorisms.

6. As for problem of thematic education for culture-enhancing population, my proposal is the following. In some Moscow Universities there are the Departments on preparation of specialists on studying of disasters and catastrophes. The mission of NATO Scientific Committee is not only organization of NATO ARW, but also two weeks NATO ASI, where scientists, having their own scientific results, realize lectures and practice lessons for effective modern education of young scientists from the whole world. Today is the time for such education through NATO ASI. I may propose its possible theme: "Some Threats for World Civilization and its prediction/prevention/elimination" for provision of stable development" And not only for NATO ASI, but also for NATO ARW. Another title may be the following: "Modern methods and technologies in prediction/prevention natural and manmade disasters and in struggle against terrorism".

7. The important social aspect. In the countries of Former USSR the population consider NATO only as the aggressive military Block of non-friendship west states. NATO scientific events, its grants and support of the main actual investigations help to create right opinion and vary such negative relations. In addition today there are some common programs NATO with Former USSR countries, for example in struggle against IT.

8. There should be the single administration system of state, which handicrafts the whole country and its key industries, regardless of the interest of private companies. For example, if the state of Japan did not follow the entreaties of the national "Tepko" energy company, then the Fukushima disasters could have been avoided. In the absence of such a rigid management system, IT has more opportunities to achieve its goals. For example, through bribery and corruption.

In 2016 the bribed Egypt Terrorist planted a bomb on the A321 airliner flying from Sharm el-Sheikh to St. Petersburg. And it exploded with 224 passengers at 10 thousand meters altitude. Since then, air traffic between the RF and Egypt has been discontinued.

9. Russia is not NATO member and not its panther. In addition Russia is often considered as "sensitive country" as the zone of political and terrorist conflicts. But I consider it is not the reason for refuse from Russian scientists in participation in the thematic scientific events. Our Nuclear Safety Institute of Russian Academy of Sciences (IBRAE RAS) has own experience in these scientific directions (http://www.ibrae.ac.ru). Some of them are the following:

- Comparable analysis on the ecological risks, related to the impact of the radioactive and chemically hazardous substances on the environment and population.
- Emergency response in radiation accidents. Scientific and technical support in decision making on protection of population and territories.
- Analysis of risks, related to the management, transportation and processing of the spent nuclear fuel and radioactive waste. Analysis of risks and counter-measures against radiological terrorism.
- The thematic workshops on the mentioned problems with the participation of the 8-th Big Main Countries are often held in our Institute.

We have own Program, devoted to "Assessments of Risks and Possible Ecological and Economic Damages from Large-Scale Natural and Man-Induced Catastrophes in Ecology-Hazard Regions of Central Asia and the Caucasus», connected with the development of new methods on prevention of threats and struggle against possible acts of ecological terrorism. Some Program aspects have been reflected in of NATO ARW Proceedings.

The widening of the income gap of the entire population of the world is also characteristic, for example due to globalization, which is another reason for the increase in IT.

Some our thematic results are presented in our articles of this these Proceedings of this Conference Chaos 2020 and will be presented in future.

In conclusion our latest results on nanotechnologies and nanomedicine [15-18] are shortly presented in my oral Chaos 2020 communications. Nano is the wonderful unique world with its own laws. It is not simple huge reduction of all objects. I guess that this world reflect the plans of the Universal Creator on our Earth creation. And undoubtedly its recearch will help the successful fight against Covid - 19.

Acknowledgments

For fruitful cooperation and useful information, I am grateful to professors Vladimir Solodukhin from the Institute of Nuclear Physics, Almaty, Kazakhstan and Sergey Petrov from the Pedagogical University of Moscow.

References

List of science events [1-12] in which Alexander Valyaev participated

1. Unresolved Issues Remaining in the Decommissioning of Nuclear Powered Vessels and in the Environmental Remediation of Their Supporting Infrastructure, April 22-24, 2002, Moscow, Russia. As the participant.
2. Vapor and Trace Detection of Explosives for Anti-Terrorism Purposes, March 19-20, 2003, Moscow, Russia. As the participant.
3. Bulk Detection of Explosives: Advance Techniques Against Terrorism, June 16-21, 2003, St. Petersburg, Russia, Radiological Risks in Central Asia, June 20-22, 2006, Almaty, Kazakhstan, Prevention, Detection and Response to Nuclear and Radiological Threat, May 2-7, 2007, Yerevan, Armenia.
4. Natural Disasters and Water Security: Risk Assessment, Emergency Response and Environmental Management, October 18-22, 2007, Yerevan, Armenia.
5. Stimulus for human and social dynamics in the prevention of catastrophes, October 5-8, 2010, Yerevan, Armenia.
6. Correlation between Human Factors and the Prevention of Catastrophes, September 12-15, 2011, in Dnipropetrovsk, Ukraina.
7. Chemical Physics of Thin Film Deposition Processes for Micro-and Nano-Technologies, September 3-14, 2001, Kaunas, Lithuania.
8. Microstructure, Thermodynamics and Plasticity, September 2-13, 2002, Frejus, France.
9. Radiation effects in solids, July 17-29, 2004, Erice, Sicilia, Italy.
10. Integrated Emergency Management for Mass Casualty Emergencies, October 26-29, 2011, Florence, Italy.
11. ISTC Workshop "DISTANT TRANSFER of RADIONUCLIDES in MOUNTAINOUS REGIONS", November 6-10, 2006, Tbilisi, Georgia.
12. NATO ARW and ISTC Meeting "Radiological Risks in Central Asia", 20-22 June, 2006, Almaty, Kazakhstan.
13. V.P. Solodukhin. Radionuclides and toxic elements in transboundary rivers of Kazakhstan - results of a 10-year monitoring. International Scientific Forum NUCLEAR SCIENCE END TECHNOLOGIES. ABSTRACTS, September 12-15, 2017, Almaty, Republic of Kazakhstan, P. 12.
14. A.N. Valyaev and V.A. Yanushkevich. Using of Acoustic Techniques for Detection of Explosives in Gas, Liquid and Solid Mediums. NATO Science Series II "Detection of Bulk Explosives: Advanced Techniques against Terrorism" (Mathematics, Physics and Chemistry, 2004, vol. 138, pp. 175–183). Kluwer Academic Publishers, Netherlands. Proc. of NATO Advanced Research Workshop, June 16-21, 2003, St. Petersburg, Russia.
15. V.L Poznyak, G.M. Kabirova, L.A. Ryazanova, S.G. Lennik, A.S. Liventsova, A.N. Bychenko, D.A. Zheltov. Radionuclide and toxic chemical elements in the transboundary «Kyrgyzstan - Kazakhstan» rivers. J Radioanal. Nucl. Chem, 2016, vol. 309, pp. 115-124.
16. .V. Solodukhin, I. Silachev, V. Poznyak, I. Gorlachev. Development the complex of nuclear-physical methods of analysis for geological and technological tasks in Kazakhstan. J Radioanal. Nucl. Chem, 2016, vol. 309, pp. 125-134.
17. S. Petrov, A. Valyaev, A. Valiaev, G. Aleksanyan. Ways to Accelerate Nanotechnologies Implementation in The Health Care System. J Nanom Nanos Tech (JNNT): 2018, Vol. 108, Issue 01, pp. 1-6. Available from: https://www.arvinmedonline.org/assets/article-pdf/ways-to-accelerate-nanotechnologies-implementation-in-the-health-care-system.pdf.
18. S. Petrov, A. Valyaev, A. Valiaev, G. Aleksanyan. Ways to Accelerate Nanotechnologies Implementation in The Health Care System, HSOA. J Nucl Med Radiol Radiat Ther, ISSN: 2572-7419, 2019, vol. 5, pp. 011. DOI: 10.24966/NMRR-7419/100011. Available from: http://heraldopenaccess.us/fulltext/Nuclear-Medicine-Radiology-&-Radiation-Therapy/Ways-to-Accelerate-Nanotechnologies-Implementation-in-the-Health-Care-System.php.
19. S. Petrov, A. Valyaev, A. Valiaev. Application of special nanomaterials for substituting bone tissue defects. International Journal of Biosensors & Bioelectronics (IJBB) 2019, Vol. 5, Issue 6, pp. 185-186. Available from: https://medcraveonline.com/IJBSBE/IJBSBE-05-00175.pdf.

20. S. Petrov, A. Valyaev. Nanotechnologies in the health care system. International Journal of Biosensors & Bioelectronics Mini Review, 2020, Vol. 6, Issue 1, pp.14-18. Available from: https://medcraveonline.com/IJBSBE/IJBSBE-06-00181.pdf.

Inversive generators of second order

Sergey Varbanets[1] and Yakov Vorobyov[2]

[1] Department of Computer Algebra and Discrete Mathematics, Odessa I.I. Mechnikov National University, Dvoryanskaya street 2, Odessa, Ukraine (E-mail: varb@sana.od.ua)

[2] Department of Mathematics, Informatics and Information Activities, Izmail State University of Humanities, Repina street 12, Odessa, Ukraine (E-mail: yashavo@mail.ru)

Abstract. Inversive congruential method for generating the uniform pseudorandom numbers is a particulary attractive alternative to linear congruential generators, which show many undesirable regularities. In present paper, we investigate the equidistribution of sequences produced by inversive congruential generator of second order by using the discrepancy bounds of such sequences of pseudorandom numbers (PRN's). Also there are obtained the estimates of special exponential sums of these sequences.
Keywords: inversive generator, exponential sum, discrepancy.

1 Introduction

The sequences of random numbers have the various applications in the numerical analysis and cryptography. But in practice instead the sequences of random numbers we use the pseudorandom sequences, i.e. the sequences which pass appropriate statistical test on randomness. An assortment of statistical tests depends on the type solved problem.

Our main point here is to elucidate the motivation for construction the sequences of PRN's with some specific properties that foster their applications in Quasi-Monte Carlo methods and cryptography. For the numerical analysis there are tests for the uniform distribution in certain region. Such tests go with success the sequences of linear congruential pseudorandom numbers (abbr., LCPRN's) (see, [4]). For cryptographic applications it is essential that except "equidistribution" it performs yet a requirement of "unpredictability". But to this requirement the sequence of PRN's produced by linear congruential generator does not satisfy.

D. Knuth[3] and Marsaglia[5] proved that LCPRN's are predictable. This motivated the creation of the nonlinear congruential pseudorandom sequences having the unpredictable property.

The inversive congruential generator initiated by I. Eichenauer and I. Lehn [2] in 1986 make sure the "equidistribution" and "unpredictability" of the sequence of PRN's produced by the congruential recursion

$$y_{n+1} \equiv a y_n^{-1} + b \pmod{p},$$

where $a, b \in \mathbb{Z}$, p be a prime number, y^{-1} denotes a multiplicative inverse of y modulo p, y_0 be initial value.

In present paper, we study the sequence of PRN's $\{y_n\}$ defined by the congruential recursion

$$y_{n+1} = a y_{n-1}^{-1} y_n^{-1} + b \pmod{p^m}. \tag{1}$$

This generator of $\{y_n\}$ we call the inversive congruential generator of second order. We distinguish two type of respective sequences

(I) type: $\nu_p(a) = 1$, $\nu_p(b) = \nu \geq 1$;

(II) type: $\nu_p(a) = \alpha$, $\nu_p(b) = 1$.

In case of inversive generator of first order (which was studied by Eichenauer, Lehn, Niederreiter and others) the sequence $\{y_n\}$ of type (II) steadies starting from a certain index n, and therefore it will not be the uniformly distributed sequence.

The sequences produced by the congruential generator of k^{th} order

$$y_{n+1} \equiv f(y_n, y_{n-1}, \ldots, y_{n-k+1}) \pmod{M}$$

have the least period length $\tau \leq M^k$.

The function $f(y_n, y_{n-1}, \ldots, y_{n-k+1})$ ought to choose so as a period $\{y_n\}$ was as large as possible.

Some results about the period and distribution of inversive congruential sequences of first order can be found in the survey paper [1].

The inversive generators of first order generate the sequences of PRN's which pass the test on "equidistribution" and "unpredictability" but they do not satisfy to requirement of "security". Indeed, if we know more than one sequential values $y_n, y_{n+1}, \ldots, y_{n+k}$, we easy can obtain the parameters a and b of the inversive generator of first order. However, the "security" of sequence of PRN's can be remained if the parameter of shift c change to $c + n + p^\mu F(n)$, where $\mu > \nu$ and $F(n)$ is some random polynomial from $\mathbb{Z}[n]$ (see, [9]).

In this paper we continue investigation of the inversive generator of second order of two types.

Our purpose in this work is to show the passing of test on equidistribution and statistical independence for the sequence $\{x_n\}$, $x_n = \frac{y_n}{p^m}$, and hence, the main point is to show the possibility for such sequences to be used in the problem of real processes modeling and in the cryptography.

In the sequel we will use the following notations.

Variables of summation automatically range over all integers satisfying the indicated condition. The letter p denotes a prime number, $p \geq 3$. For $m \in \mathbb{N}$ the notation $\mathbb{Z}_{p^m}$ (respectively, $\mathbb{Z}^*_{p^m}$) denotes the complete (respectively, reduced) system of residues modulo p^m. For $z \in \mathbb{Z}$, $(z, p) = 1$ let z^{-1} be the multiplicative inverse of z modulo p^m; instead of $\frac{a}{b} \pmod{p^m}$ we will write $a \cdot b^{-1}$. We write $\nu_p(A) = \alpha$ if $p^\alpha | A$, $p^{\alpha+1} \nmid A$ for $A \in \mathbb{Z}$. For integer t, the abbreviation $e_q(t) = e^{\frac{2\pi i t}{q}}$ is used.

Let $f(x)$ be a periodic function with a period τ. For any $N \in \mathbb{N}$, $1 \leq N \leq \tau$, we denote

$$S_N(f) := \sum_{x=1}^{N} e^{2\pi i f(x)}$$

2 Auxiliary results

Let $a, b \in \mathbb{Z}$, $p \geq 3$ be a prime, and let $m > 1$ be a positive integer. Let us consider the transformation Ψ defined on $\mathbb{Z}_{p^m}^*$ by

$$\Psi(y_n, y_{n-1}, \ldots, y_{n-s+1}) = a y_n^{-1} \cdots y_{n-s+1}^{-1} + b, \quad (y_0, p) = (y_1, p) = 1,\ 0 \leq y_n < p^m. \tag{2}$$

We put $x_n = \frac{y_n}{p^m}$, $n = 0, 1, \ldots$. And then the transformation Ψ we call the inversive congruential generator of second order of the sequence of pseudo-random numbers (abbr., PRN's).

In order that the sequence $\{y_n\}$ exists for any $n \in \mathbb{Z}$ it is sufficient that $(a, p) = 1$, $b \equiv 0 \pmod p$ or $a \equiv 0 \pmod p$, $(b, p) = 1$. These conditions generate various of sequences of PRN's. Henceforth, we call that sequences as inversive congruential sequences of type I or II.

For example, the inversive congruential sequence $\{y_n\}$ of first order with $a \equiv 0 \pmod p$, $(b, p) = 1$ has a period $\tau = 1$, but in the case $(a, p) = 1$, $\nu_p(b) = \nu \geq 1$, the relevant sequence of PRN's can be a period with $\tau = 2p^{m-\nu}$.

In our paper we study the inversive congruential generator of second order, i.e. $s = 2$. We will illustrate that the least period length of sequence $\{y_n\}$ can be equal to $3p^{m-\mu}$ or $p^{m-\nu}$.

We need the following lemmas.

Lemma 1. *Let $f(x)$ be a periodic function. For any $N \in \mathbb{N}$, $1 \leq N \leq \tau$ the following estimate*

$$|S_N(f)| \leq \left(\max_{1 \leq n \leq \tau} \left| \sum_{x=1}^{\tau} e^{2\pi i \left(f(x) + \frac{nx}{\tau} \right)} \right| \right) \log 2\tau$$

holds.

This statement can be derived by inequalities for complete exponential sums on a usual way.

Lemma 2. *Let h_1, h_2, k, ℓ be positive integers and let $\nu_p(h_1 + h_2) = \alpha$, $\nu_p(h_1 k + h_2 \ell) = \beta$, $\delta = \min(\alpha, \beta)$. Then for every $j = 2, 3, \ldots$ we have*

$$\nu_p(h_1 k^{j-1} + h_2 \ell^{j-1}) \geq \delta.$$

Moreover, for every polynomial $G(u) = A_1 u + A_2 u^2 + p^t G_1(u) \in \mathbb{Z}[u]$ we have

$$h_1 G(k) + h_2 G(\ell) = A_1(h_1 k + h_2 \ell) + A_2(h_1 k^2 + h_2 \ell^2) + p^{t+s} G_2(k, \ell),$$

where $s \geq \min(\nu_p(h_1 + h_2), \nu_p(h_1 k + h_2 \ell))$, $h_1, h_2, k, \ell \in \mathbb{Z}$, $G_2(u, v) \in \mathbb{Z}[u, v]$.

Proof. By the equality

$$h_1 k^j + h_2 \ell^j = (h_1 k^{j-1} + h_2 \ell^{j-1})(k + \ell) - k\ell(h_1 k^{j-2} + h_2 \ell^{j-2}),$$

applying the method of mathematical induction, we obtain at once $\nu_p(h_1 k^j + h_2 \ell^j) \geq \delta$, $j = 2, 3, \ldots$ □

Lemma 3. *Let $p > 2$ be a prime number, $m \geq 2$ be a positive integer, $m_0 = \left[\frac{m}{2}\right]$, $f(x)$, $g(x)$, $h(x)$ be polynomials over $\mathbb{Z}$*

$$f(x) = A_1 x + A_2 x^2 + \cdots, \quad g(x) = B_1 x + B_2 x^2 + \cdots,$$

$$h(x) = C_\ell x + C_{\ell+1} x^{\ell+1} + \cdots,\ \ell \geq 1,$$

$$\nu_p(A_j) = \lambda_j, \quad \nu_p(B_j) = \mu_j, \quad \nu_p(C_j) = \nu_j,$$

and, moreover,

$$k = \lambda_2 < \lambda_3 \le \cdots, \quad 0 = \mu_1 < \mu_2 < \mu_3 \le \cdots,$$
$$\nu_p(C_\ell) = 0,\ \nu_p(C_j) > 0,\ j \ge \ell + 1.$$

Then the following bounds occur

$$\left|\sum\nolimits_1\right| := \left|\sum_{x \in \mathbb{Z}_{p^m}} e_m(f(x))\right| \le \begin{cases} 2p^{\frac{m+k}{2}} & if\ \nu_p(A_1) \ge k, \\ 0 & if\ \nu_p(A_1) < k; \end{cases}$$

$$\left|\sum\nolimits_2\right| := \left|\sum_{x \in \mathbb{Z}^*_{p^m}} e_m(f(x) + g(x^{-1}))\right| \le I(p^{m-m_0})p^{\frac{m}{2}}$$

$$\left|\sum\nolimits_3\right| := \left|\sum_{x \in \mathbb{Z}^*_{p^m}} e_m(h(x))\right| \le \begin{cases} 1\ if\ \ell = 1, \\ 0\ if\ \ell > 1, \end{cases}$$

where $I(p^{m-m_0})$ is a number of solutions of the congruence

$$y \cdot f'(y) \equiv g'(y^{-1}) \cdot y^{-1} \pmod{p^{m-m_0}},\ y \in \mathbb{Z}^*_{p^{m-m_0}}.$$

Proposition 1. *Let the sequence $\{y_n\}$ be produced by the recursion (2) with $(a,p) = (y_0,p) = (y_1,p) = 1$, $\nu_p(b) = \nu_0 > 0$, $\nu_p(c) = \mu_0 > 2\nu_0$. There exist the polynomials $F_0(x), F_1(x), F_2(x) \in \mathbb{Z}[x]$ with the coefficient depending on y_0, y_1, such that*

$$y_{3k} = A_0 + A_1 k + A_2 k^2 + p^\mu G_0(k, y_0, y_0^{-1}, y_1, y_1^{-1}), \tag{3}$$
$$y_{3k+1} = B_0 + B_1 k + B_2 k^2 + p^\mu G_1(k, y_0, y_0^{-1}, y_1, y_1^{-1}), \tag{4}$$
$$y_{3k+2} = C_0 + C_1 k + C_2 k^2 + C_3 k^3 + C_4 k^4 + p^\mu G_2(k, y_0, y_0^{-1}, y_1, y_1^{-1}), \tag{5}$$

where

$$A_1 \equiv b + a^{-1}b^2 y_0 y_1 - \frac{1}{2}a^{-1}b^2 y_0^2 - a^{-1}b y_0^2 y_1 - 2b^2 y_0^3 y_1^2 - \frac{1}{2}a^{-1}b^2 y_0 y_1,$$
$$A_2 \equiv -a^{-1}b^2 y_0 y_1 - \frac{1}{2}a^{-1}b^2 y_0^2 + b^2 y_0^3 y_1^2 + \frac{1}{2}a^{-1}b^2 y_0 y_1,$$
$$B_1 \equiv b\left(\frac{1}{2}b\left(y_0^{-1} - a^{-1}y_1^2\right) + 1 - y_0^{-1}y_1\right),$$
$$B_2 \equiv b^2\frac{1}{2}\left(-y_0^{-1} + a^{-1}b^2 y_1^2\right),$$
$$C_1 \equiv b\left((-a y_0^{-2} y_1^{-1} + 1) - \frac{1}{2}b y_1^{-1}\left(a y_0^{-2} y_1^{-1} - 1\right)\right),$$
$$C_2 \equiv b^2\frac{1}{2}y_0^{-1}\left(-1 + a^{-1}y_0 y_1^2\right),$$
$$\mu = \min\left(\nu_0 + \mu_0, 3\nu_0\right).$$

(see, [7])

Corollary 1. *Let $\nu_p(y_0 - a y_1^{-2}) = \alpha \le \nu_0$ and let τ be a period length of the sequence $\{y_n\}$ generated by recursion (2) of type (I) with initial values y_0, y_1. Then we have*

$$\tau = 3p^{m-\nu_0-\alpha},$$

and $\tau \le 3p^{m-\nu_0}$ on all occasions.

Corollary 2. *For $k = 3, 4, \ldots$, we have modulo p^μ, $\mu = \min(2\nu_0, \mu_0)$*

$$y_{3k} = \left(1 + b^2\left(a^{-1}y_1 + \frac{1}{2}a^{-1}ky_1 - a^{-1}k^2y_1 + \frac{1}{2}a^{-1}k^2y_1\right)\right)y_0 +$$
$$+ \left(a^{-1}by_1 - \frac{1}{2}a^{-1}kb^2 - \frac{1}{2}a^{-1}b^2k^2\right)y_0^2 + \left(-2ky_1^2b^2 + k^2b^2y_1^2\right)y_0^3,$$
$$y_{3k+1} = \left(1 - kby_0^{-1}\right)y_1 + \left(-a^{-1}b^2 - a^{-1}bk + a^{-1}k^2b^2\right)y_1^2,$$
$$y_{3k+2} = ay_0^{-1}y_1^{-1} + \left(\frac{1}{2}kb^2y_0^{-1} + \frac{1}{2}ab^2ky_0^{-2} + \frac{1}{2}b^2k^2\right)y_1^{-1} -$$
$$- \frac{1}{2}k^2b^2y_0^{-1} + a^{-1}b^2k^2y_0y_1^2.$$

Proposition 1' *Let $\{y_n\}$ be a sequence of PRN's generated by the recursion (2) of type (II), and let $\nu_p(a) = \alpha > 1$, $\nu_p(b) = 0$. Then for $n = 9, \ldots$ the following representation*

$$y_{n+1} = \frac{A_0^{(n+1)} + A_1^{(n+1)}y_0 + A_2^{(n+1)}y_0y_1}{B_0^{(n+1)} + B_1^{(n+1)}y_0 + B_2^{(n+1)}y_0y_1} \tag{6}$$

holds,
where

$$A_0^{(n)} = (n-4)a^2b^{n-5} + ab^{(n-2)}, \qquad B_0^{(n)} = (n-5)a^2b^{n-6} + ab^{n-3},$$
$$A_1^{(n)} = (n-5)a^2b^{n-6} + ab^{(n-3)}, \qquad B_1^{(n)} = (n-6)a^2b^{n-2} + ab^{n-4},$$
$$A_2^{(n)} = \frac{(n-5)(n-4)}{2}a^2b^{n-3} + \qquad B_2^{(n)} = \frac{(n-7)(n-6)}{2}a^2b^{n-8} +$$
$$+ (n-3)ab^{(n-4)} + b^{(n-1)}, \qquad + (n-4)ab^{n-5} + b^{n-2},$$

Proof. The straightforward computations on congruent recursion (2) allow to obtain the representations for y_7 and y_8 modulo $p^{3\alpha}$:

$$y_7 = \frac{3a^2b^2 + ab^5 + (2a^2b + ab^4)y_0 + (a^2 + 4ab^3 + b^6)y_0y_1}{2a^2b + ab^2 + (a^2 + ab^3)y_0 + (3ab^2 + b^5)y_0y_1},$$
$$y_8 = \frac{4a^2b^3 + ab^6 + (3a^2b^2 + ab^5)y_0 + (3a^2b + 5ab^4 + b^7)y_0y_1}{3a^2b^2 + ab^5 + (2a^2b + ab^4)y_0 + (a + 4ab^3 + b^6)y_0y_1}$$

And now by a mathematical induction we at once have the assertion of Proposition 1'. □

Corollary 1' *The elements of sequence $\{y_n\}$ generated by (1) with $\nu_p(a) = \alpha > 1$, $\nu_p(b) = 0$ can be represented as the following polynomials on n modulo $p^{3\alpha}$*

$$y_{n+1} = A_0(y_0, y_1) + nA_1(y_0, y_1) + n^2A_2(y_0, y_1), \tag{7}$$

where

$$A_0 = by_0y_1 + a(b^{-4}y_0 - 3b^{-2}y_0y_1) + a^2A_0'(y_0, y_1, y_0^{-1}, y_1^{-1}),$$
$$A_1 = -ab^{-2}y_0y_1 + a^2A_1'(y_0, y_1, y_0^{-1}, y_1^{-1}),$$
$$A_2 = -a^2b^{-1}(b^4 - y_0y_1) + a^3A_2'(y_0, y_1, y_0^{-1}, y_1^{-1}),$$
$$A_i'(y_0, y_1, y_0^{-1}, y_1^{-1}) \in \mathbb{Z}[y_0, y_1, y_0^{-1}, y_1^{-1}],\ y_0y_0^{-1} \equiv y_1y_1^{-1} \equiv 1 \pmod{p^m}.$$

Proof. Indeed, (6) shows that all summands in denominator of representation y_{n+1}, except y_0, y_1, are congruent to zero modulo p^α. Thus, using a congruence

$\frac{1}{c+p^\alpha d} = c^{-1}(1 - p^\alpha c^{-1}d + p^{2\alpha}(c^{-1}d)^2) \bmod p^{2\alpha}$ with $(c,p) = 1$, we obtain (4) at once. □

Corollary 2' *For every sequence of PRN's produced by (2) with $\nu_p(a) = \alpha \geq 1$, $\nu_p(b) = 0$, the least period length is equal to $p^{m-\alpha}$.*

Actually, we have modulo p^m

$$y_{n+\ell} - y_n = -2ab^{-2}y - 0y - 1(1 + aF_0(n\ell)),\ F_0(n,\ell) \in \mathbb{Z}[n,\ell].$$

So, $y_{n+\ell} \equiv y_n \pmod{p^m}$ if only $n \geq 8$ and $\ell \equiv 0 \pmod{p^{m-\alpha}}$.

The following lemmas need to study the exponential sum of special type on the sequences of PRN's.

Lemma 4. *Let $p > 2$ be a prime number, $b_0, b_1 \in \mathbb{Z}$, $(b_0, p) = (b_1, p) = 1$. We have for $k < m$*

$$S_1 := \sum_{x \in \mathbb{Z}_{p^m}} e_{p^m}\left(\frac{a_0 + a_1 p^k x}{b_0 + b_1 p^k x}\right) = \begin{cases} 0 & if\ a_0 b_1 \not\equiv a_1 b_0 \pmod{p^{m-k}} \\ p^m & if\ a_0 b_1 \equiv a_1 b_0 \pmod{p^{m-k}}. \end{cases} \tag{8}$$

Proof. In view of $\frac{1}{b_0 + b_1 p^k} \equiv b_0^{-1}(1 - b_0^{-1}b_1 p^k x + (b_0^{-1}b_1)^2 p^{2k}x^2 + \cdots) \pmod{p^m}$ we get by Lemma (3)

$$S_1 = \sum_{x \in \mathbb{Z}_{p^m}} e_{p^m}(b_0^{-1}(a_0 + a_1 p^k x)(1 - b_0^{-1}b_1 p^k x + (b_0^{-1}b_1)^2 p^{2k}x^2 - \cdots)) =$$

$$= \sum_{x \in \mathbb{Z}_{p^m}} (b_0^{-1} + (a_1 - a_0 b_0^{-1}b_1)p^k x + b_0^{-1}(a_0 b_0^{-2}b_1^2 - a_1 b_1 b_0^{-1})p^{2k}x^2 + \cdots) =$$

$$= \begin{cases} 0 & if\ a_0 b_1 \not\equiv a_1 b_0 \pmod{p^{m-k}}, \\ p^m & if\ a_0 b_1 \equiv a_1 b_0 \pmod{p^{m-k}}. \end{cases}$$

□

Lemma 5. *Let $a_i, b_i \in \mathbb{Z}$, $(a_i, p) = (b_i, p) = 1$, $i = 0, 1$; $p > 2$ be a prime number, and m, k be positive integers, $m \geq 3k$. Then*

$$S_2 := \sum_{x \in \mathbb{Z}_{p^m}} e_{p^m}\left(\frac{a_0 + p^k a_1 x + p^{2k} a_2 x^2}{b_0 + p^k b_1 x + p^{2k} b_2 x^2}\right) \ll p^{\frac{m}{2}+k} \tag{9}$$

with the absolute constant in the symbol "$\ll$".

Proof. First we assume $m = 2m_0$, $m_0 \in \mathbb{N}$. Let $x = y(1 + p^{m_0}z)$. We obtain

$$\sum_{x \in \mathbb{Z}_{p^m}} e_{p^m}\left(\frac{a_0 + p^k a_1 x + p^{2k} a_2 x^2}{b_0 + p^k b_1 x + p^{2k} b_2 x^2}\right) =$$

$$= \sum_{y \in \mathbb{Z}_{p^{m_0}}} \sum_{z \in \mathbb{Z}_{p^{m_0}}} e_{p^m}\left(\frac{A_0 + p^{k+m_0}(a_1 y + p^k a_2 y^2)z}{B_0 + p^{k+m_0}(b_1 y + p^k b_2 y^2)z}\right),$$

where

$$A_0 = a_0 + p^k y + p^{2k} a_2 y^2,$$
$$B_0 = b_0 + p^k y + p^{2k} b_2 y^2.$$

It follows

$$S_2 = \sum_{y\in\mathbb{Z}_{p^{m_0}}} e_{p^m}(A_0B_0^{-1}) \sum_{z\in\mathbb{Z}_{p^{m_0}}} e_{p^m}(-A_0B_0^{-1}(b_1y+p^kb_2y^2)zp^{k+m_1}) =$$

$$= p^m \sum_{y\in\mathbb{Z}_{p^{m_0}}} e_{p^m}(A_0B_0^{-1}) \sum_{z\in\mathbb{Z}_{p^{m_1}}} e_{p^{m_1-k}}(-A_0B_0^{-1}(b_1y+p^kb_2y^2)z) =$$

$$= p^{m_1} \sum_{\substack{y\in\mathbb{Z}_1 \\ y\equiv 0 \pmod{p^{m_0-k}}}} e_{p^m}(A_0B_0^{-1}) =$$

$$= p^{m_0} \sum_{y_0\in\mathbb{Z}_{p^k}} e_{p^m}((1-p^{m_0}b_0^{-1}b_1y_0)(a_0+p^{m_0}a_1)) =$$

$$= p^{m_1} e^{2\pi i\frac{a_0}{p^m}} \sum_{y_0 \pmod{p^k}} e_{p^m}(a_0b_0^{-1}b_1y_0) \ll p^{m_0+k}.$$

For $m = 2m_0 + 1$ we infer by a similar way

$$S_2 \ll p^{\frac{m}{2}} + k$$

□

3 Evaluation of exponential sums over the sequences of PRN's

Let $\{y_n\}$ be the sequence of PRN's produced by the inversive generator of second order of the first or second type. In the propositions 1 and 1' it was received a description of elements y_n as polynomials at n that essentially make easier the construction of estimates for exponential sums. We will consider the following exponential sums over the sequence $\{y_n\}$ of PRN's generated by the recursion (1) of type (I) or (II) with the least period τ.

$$\sigma_{k\ell}(h_1,h_2) := \sum_{y_0,y_1\in\mathbb{Z}_{p^m}^*} e_{p^m}(h_1y_k+h_2y_\ell),\ h_1,h_2\in\mathbb{Z};$$

$$S_N(h,y_0) := \sum_{n=0}^{N-1} e_{p^m}(hy_n),\ h\in\mathbb{N},\ 0<N\le\tau;$$

$$K(h_1,h_2;p^m) := \sum_{n=1}^{\tau} e_{p^m}(h_1y_n+h_2y_n^{-1}),\ (h_1,h_2\in\mathbb{Z});$$

$$G(h,p^m) := \sum_{n=1}^{\tau} e_{p^m}(hy_n^2),\ (h\in\mathbb{Z}).$$

These sums are called σ-sum, S-sum, Kloosterman sum and Gauss sum, respectively.

Theorem 1. *Let the sequence $\{\omega_k\}$ has the maximal period τ, $\tau = 2p^{n-\beta}$. Then the following bound*

$$|S_\tau(h,\omega)| := \left|\sum_{k=0}^{\tau-1} e_{p^n}(h\omega_k)\right| \le \begin{cases} 0 & if\ \ \beta+\delta<n, \\ \\ \tau & if\ \ \beta+\delta\ge n, \end{cases}$$

holds.

(see, [7], Th. 3)

Theorem 1' *Let $h_1, h_2 \in \mathbb{Z}$, $\nu_p(h_1+h_2) = p^s$, $0 \le s \le m$. Then for the sequence $\{y_n\}$ of type (II) we have*

$$\sigma_{k,\ell}(h_1,h_2) = \begin{cases} 0 & if \quad k \not\equiv \ell \pmod{p^m} \\ & and \quad \nu_p(h_1+h_2) < m-1; \\ p^{2(m-2)}(p-1)^2 & if \quad k \not\equiv \ell \pmod{p^m} \\ & and \quad \nu_p(h_1+h_2) = m-1; \\ p^{2(m-1)}(p-1)^2 & if \quad k \overset{\equiv}{\not\equiv} \ell \pmod{p^m} \\ & and \quad \nu_p(h_1+h_2) = m. \end{cases} \tag{10}$$

Proof. By Corollary 1' we can write

$$h_1 y_k + h_2 y_\ell = b(h-1+h_2) y_0 y_1 + (h_1+h_2) p^\alpha F(y_0, y_0^{-1}, y_1, y_1^{-1}), \tag{11}$$

where $F(y_0, y_0^{-1}, y_1, y_1^{-1})$ is a polynomial with the integer coefficients. Now we obtain

$$\sigma_{k,\ell}(h_1,h_2) = \sum_{y_0,y_1 \in \mathbb{Z}^*_{p^m}} e_{p^m}((h_1+h_2)b\ell_1\ell_2 + p^k(h_1+h_2)F(y_0,y_0^{-1},y_1,y_1^{-1})) =$$

$$= \sum_{y_0 \in \mathbb{Z}^*_{p^m}} \sum_{y_1 \in \mathbb{Z}^*_{p^m}} e_{p^m}((h_1+h_2)by_0y_1 + p^k(h_1+h_2)F_1(y_1,y_1^{-1})) =$$

$$= \sum_{y_1 \in \mathbb{Z}^*_{p^m}} \begin{cases} 0 & if\ \nu_p(h_1+h_2) < m-1, \\ p^{2(m-2)}(p-1)^2 & if\ \nu_p(h_1+h_2) = m-1, \\ p^{2m(m-1)}(p-1)^2 & if\ \nu_p(h_1+h_2) = m. \end{cases}$$

Here we took into account that for $(a,p)=1$

$$\sum_{x \in \mathbb{Z}^*_{p^m}} e^{2\pi i \frac{ax}{p^m}} = \begin{cases} -1 \ if\ m=1, \\ 0 \ \ if\ m \ge 1. \end{cases}$$

□

In Theorem 1' the initial values y_0, y_1 run the set $\mathbb{Z}^*_{p^m}$ independently of each other. Now we shall assume that $y_0 = y_1$.

Theorem 1" *Under conditions of Theorem 1' and the proposal $y_0 = y_1$ we have*

$$|\sigma_{k,\ell}(h_1,h_2)| = \begin{cases} p^{\frac{m+s}{2}} & if\ s < m, \\ p^{m-1}(p-1) & if\ s = m. \end{cases} \tag{12}$$

Proof. By (11) and $y_0 \equiv y_1 \pmod{p^m}$ we obtain modulo p^m

$$h_1 y_k + h_2 y_\ell = b(h_1+h_2)y_0^2 + p^\alpha (h_1+h_2)F_1(y_0, y_0^{-1}).$$

Thus Lemma 3 gives

$$|\sigma_{k,\ell}(h_1,h_2)| = \left| \sum_{y_0 \in \mathbb{Z}^*_{p^m}} e_{p^m}((h_1+h_2)by_0^2 + p^\alpha(h_1+h_2)F_1(y_0,y_0^{-1})) \right| =$$

$$= \begin{cases} p^{\frac{m+2}{2}} & if\ s < m, \\ p^m(p-1) & if\ s = m. \end{cases}$$

□

Now we will construct the estimates for G- and K-sums.

Theorem 2. *Let the sequence of PRN's is generated by recursion (1) with $\nu_p(a) = 0$, $1 \le \nu_p(b) = \nu \le \frac{m}{3}$. Then for G-sum the following estimate*

$$G(h, p^m) \ll p^{\frac{m+s}{2}}, \;\; s = \nu_p(h, p^m)$$

holds.

Proof. By Proposition 1 we easy obtain

$$y_{3k}^2 = \frac{(y_0 + A_0' p^\alpha) + 2k(by_0 + A_1' p^{2\alpha}) + k^2(b^2(1 + a^{-1}y_0y_1) + A_2' p^{3\alpha})}{(1 + B_0' p^\alpha) + k(by_0y_1 + B_1' p^{2\alpha}) + k^2(b^2a^{-2}y_0^2y_1^2 + B_2' p^{3\alpha})},$$

$$y_{3k+1}^2 = \frac{(y_0^2y_1^2 + A_0' p^\alpha) + 2k(by_0^2y_1 + A_1' p^{2\alpha}) + k^2(b^2y_0^2y_1^2 + A_2' p^{3\alpha})}{(y_0^2 + B_0' p^\alpha) + 2k(by_0 + B_1' p^{2\alpha}) + k^2(b^2(1 + a_0^{-1}y_0y_1) + B_2' p^{3\alpha})},$$

$$y_{3k+2}^2 = \frac{(1 + A_0' p^\alpha) + 2k(by_0y_1 + A_1' p^{2\alpha}) + k^2(b^2(ay_0 + y_0^2y_1^2) + A_2' p^{3\alpha})}{(y_0^2y_1^2 + B_0' p^\alpha) + 2k(by_0y_1 + B_1' p^{2\alpha}) + k^2(b^2y_0^2 + B_2' p^{3\alpha})},$$

where A_j', B_j' are some polynomials from $\mathbb{Z}[y_0, y_1, k]$.
Next, we have

$$\begin{aligned} G(h, p^m) &= \sum_{n=1}^{3p^{m-\nu}} e_{p^m}(hy_n^2) = \\ &= \sum_{k=1}^{p^{m-\nu}} e_{p^m}(hy_{3k}^2) + \sum_{k=1}^{p^{m-\nu}} e_{p^m}(hy_{3k+1}^2) + \sum_{k=1}^{p^{m-\nu}} e_{p^m}(hy_{3k+2}^2) \ll \\ &\ll p^{s-\nu} \sum_{j=0}^{s} \left| \sum_{k=1}^{p^{m-s}} e_{p^{m-s}}(hy_{3k+j}) \right| \ll p^{s-\nu} p^{\frac{m-s}{2}+\nu} = p^{\frac{m+s}{2}}. \end{aligned}$$

□

It is similarly investigating the inversive congruential sequence of PRN's of second order type (II).

Theorem 2' *The G-sum for the inversive congruential sequence of type (II) with $\nu_p(a) = \alpha$ estimates by*

$$G(h, p^m) \ll p^{\frac{m+s}{2}}, \;\; s = \nu_p(h, p^m).$$

Lemma 5 makes possible to prove the estimates for K-sums.

Theorem 2" *Let $\{y_n\}$ be the sequence produced by recursion (1) of type (II) with $\nu_p(a) = \alpha$, $\nu_p(b) = 0$, and let $A, B \in \mathbb{Z}$. Then we have*

$$K(A, B; p^m) = \sum_{n=1}^{p^{m-\alpha}} e_{p^m}^2(Ay_n + By_n^{-1}) \ll \begin{cases} 0 & if\ 2\alpha \ge m,\ (Ab^2 + B) = 1, \\ p^{\frac{m+\alpha}{2}} & if\ 2\alpha < m,\ (Ab^2 + B) = 1. \end{cases}$$

Proof. Using Proposition 1', we after a simple calculations can obtain

$$Ay_n + By_n^{-1} = \frac{\widetilde{A}_0 + \widetilde{A}_1 n + \widetilde{A}_2 n^2}{\widetilde{B}_0 + \widetilde{B}_1 n + \widetilde{B}_2 n^2},$$

where

$\widetilde{A}_0 = (Ab^2 + B)ab^5(1 + \widetilde{A}_0' p^\alpha)y_0^2y_1^2$; $\quad \widetilde{B}_0 = b^3(1 + \widetilde{B}_0' p^\alpha)y_0^2y_1^2$;
$\widetilde{A}_1 = p^\alpha 2a_1b^3(Ab + B)(1 + \widetilde{A}_1' p^\alpha)y_0^2y_1^2$; $\quad \widetilde{B}_1 = p^\alpha 2a_1b^3(1 + \widetilde{B}_1' p^\alpha)y_0^2y_1^2$;
$\widetilde{A}_2 = p^{2\alpha}a_1^2b^{-1}(Ab^2 + B)(1 + \widetilde{A}_2' p^\alpha)y_0^2y_1^2$; $\quad \widetilde{B}_2 = p^{2\alpha}a_1(1 + \widetilde{B}_2' p^\alpha)y_0^2y_1^2$;
$\widetilde{A}_j'$, $\widetilde{B}_j'$ are some polynomials from $\mathbb{Z}[y_0, y_1, n]$.

It follows thence the assertion of theorem. □

Similarly, the result is true for the K-sum on the sequence $\{y_n\}$ produced by inversive congruential generator of second order of type (I) with $\nu_p(a) = 0$, $\nu_p(b) = \nu \geq 1$.

4 Discrepancy bound

To analyze the equidistribution and statistical independence properties of the investigated sequences of PRN's $\{x_n\}$, $x_n = \frac{y_n}{p^m}$, $n = 1, 2, \ldots$ we use the discrepancy of points $x_0, x_1, \ldots, x_{N-1}, \ldots$ and overlapping points $X_N^{(s)} = \{\ x_n,\ x_{n+1},\ \ldots,\ x_{n+s-1}\ \}$, $n = 0, 1, \ldots$, with fixed s. For given N points $X_n^{(s)}$, the discrepancy $D_N^{(s)}(X_0^{(s)}, \ldots, X_{N-1}^{(s)})$ is defined as

$$D_N^{(s)}(X_0^{(s)}, \ldots, X_{N-1}^{(s)}) = \sup_{\Delta} \left| \frac{A_N(\Delta)}{N} - vol(\Delta) \right|,$$

where the supremum is extended over all subrectangles $\Delta \subset [0,1)^s$, $A_N(\Delta)$ is the number of points among $X_0^{(s)} \ldots, X_{N-1}^{(s)}$ falling into $[0,1)^s$, and $vol(\Delta)$ is the area of Δ.

If for every $s = 1, 2, \ldots, S$, we have $D_N^{(s)}(X_0^{(s)}, \ldots, X_{N-1}^{(s)}) \to 0$ with a rise of N, we will say that the sequence of PRN's passes s-dimensional test on the pseudorandomness. In cryptographical applications a penetrations of s-serial test ($s \geq 2$) means that the sequence $\{x_n\}$ is unpredictable.

Beside discrepancy there exists other important criteria for the uniformity and the independence of PRN's. We shall restrict our attention to the discrepancy, since it is the most important measure of uniformity and independence related to PRN's. For upper estimate of the discrepancy of points we will use the following inequality from [6].

Lemma 6. *Let $q > 1$ and s be natural numbers and let $\{Y_n\}$, $Y_n \in \{0, 1, \ldots, q-1\}^s$, be a purely periodic sequence with a period τ. Then the points $X_n = \frac{Y_n}{q} \in [0,1)^s$, $n \in \{0, 1, \ldots, N-1\}$, $N \geq \tau$, have discrepancy*

$$D_N^{(s)}(X_0, X_1, \ldots, X_{N-1}) \leq \frac{s}{q} + \frac{1}{N} \sum_{h_0, h_1, \ldots, h_s} \frac{1}{\overline{h}_0 \overline{h}_1 \cdots \overline{h}_s} |S|, \qquad (13)$$

where the summation runs over all integers $h_0, h_1, \ldots, h_s$ for which $h_0 \in \left(\frac{-\tau}{2}, \frac{\tau}{2}\right]$, $h_i \in \left(-\frac{q}{2}, \frac{q}{2}\right]$, $(i = 1, \ldots, s)$, $(h_1, \ldots, h_s) \neq (0, \ldots, 0)$, $\overline{h}_i = \max(1, |h_i|)$, and

$$S := \sum_{n=0}^{\tau-1} e\left(h \cdot X_n + \frac{n h_0}{\tau}\right),$$

where $h \cdot X_n = \sum_{i=1}^{s} h_i x_i^{(n)}$ stands for the inner product of h and X_n in $\mathbb{Z}^s$.

The following lemma is a special version of Niederreiter's result [6].

Lemma 7. *The discrepancy of N arbitrary points $\mathbf{t}_0, \mathbf{t}_1, \ldots, \mathbf{t}_{N-1} \in [0,1)^2$ satisfies*

$$D_N^{(2)}(\mathbf{t}_0, \mathbf{t}_1, \ldots, \mathbf{t}_{N-1}) \geq \frac{1}{2(\pi+2)|h_1 h_2|N} \cdot \left| \sum_{k=0}^{N-1} e(\mathbf{h} \cdot \mathbf{t}_k) \right| \qquad (14)$$

for any lattice point $\mathbf{h} = (h_1, h-2) \in \mathbb{Z}^2$ *with* $h_1 h_2 \neq 0$.

Going to the estimates of a discrepancy for the sequence of PRN's produced by the generators of second order of type (I) or (II) let us remark here that required estimates of the exponential sums

$$\left|\sum_{n=0}^{N-1} e_{p^m}(hy_n)\right| \leq \begin{cases} O(m) & if\ N = \tau; \\ 4p^{\frac{m+\delta+\nu}{2}} & if\ N \leq \tau,\ \delta+\nu \leq m,\ \nu = \nu_p(h); \\ N & otherwise. \end{cases} \tag{15}$$

we can infer at once from the Corollary 1 or Corollary 1' and Lemma 3.

We need also some supporting data on upper and lower boundaries for the discrepancy of points $t_k = \frac{y_n}{q}$, $y_n \in \mathbb{Z}_q^s$, $n = 0, 1, \ldots, N-1$; $q \in \mathbb{N}$.

Lemma 8. *Let* $C_s(q)$ *be set of all nonzero point* $\mathbf{h} = (h_1, \ldots, h_s) \in \mathbb{Z}^s$, $-\frac{q}{2} < h_j \leq \frac{q}{2}$, $1 \leq j \leq s$. *For* $\mathbf{h} \in C_s(q)$, $\mathbf{y}_0, \mathbf{y}_1, \ldots, \mathbf{y}_{N-1} \in \mathbb{Z}_q^s$, $\mathbf{y} \in [0, q)^s$, $n = 0, 1, \ldots, N-1$, *we have*

$$D_N^{(s)}(\mathbf{y}_0, \mathbf{y}_1, \ldots, \mathbf{y}_{N-1}) \leq \frac{s}{q} + \frac{1}{N} \sum_{\mathbf{h} \in C_s(q)} \sum_{h_0 \in \left(-\frac{\tau}{2}, \frac{\tau}{2}\right]} \frac{1}{r(\mathbf{h}, q)} \left|\sum_{n=0}^{N-1} e_q(\mathbf{h} \cdot \mathbf{y}_n)\right|,$$

where $r(\mathbf{h}, q) = \prod_{j=1}^{s} r(h_i, q)$, $r(h, q) = \begin{cases} 1 & if\ h = 0, \\ q \sin\left(\pi \frac{|h|}{q}\right) & if\ h \neq 0, \end{cases}$

(see, [6])

Lemma 9. *The discrepancy of* N *arbitrary points* $\mathbf{y}_0, \mathbf{y}_1, \ldots, \mathbf{y}_{N-1} \in [0, 1)^s$ *suffice to inequality*

$$D_N(\mathbf{y}_0, \mathbf{y}_1, \ldots, \mathbf{y}_{N-1}) \geq \frac{1}{2^{s-1}(\pi+2)|h_1 \cdots h_s|} \cdot \frac{1}{N} \left|\sum_{n=0}^{N-1} e(\mathbf{h} \cdot \mathbf{y}_n)\right|$$

for any point $\mathbf{h} = (h_1, \ldots, h_s) \in \mathbb{Z}^s$ *under condition* $h_1 \cdot \cdots \cdot h_2 \neq 0$.

(see, [6])

For the sequence $\{y_n\}$ produced by the recursion (2) we easy infer (with help Lemma 8).

Theorem 3. *Let* $\{y_n\}$, $n = 0, 1, \ldots$, *be the sequence of PRN's of second order type (I) with the maximal period* $\tau = 3p^{m-\nu}$. *Then for discrepancy* $D_N(x_0, \ldots, x_{N-1})$ *of the sequence* $\{x_n\}$, $x_n = \frac{y_n}{p^m} \in [0, 1)^s$, *the following bound for* $N \leq \tau$

$$D_N^{(1)}(x_0, x_1, \ldots, x_{N-1}) \leq \frac{1}{p^m} + \frac{3p^{\frac{m}{2}}}{N} \left(\frac{1}{p}\left(\frac{2}{\pi} \log p^m + \frac{7}{5}\right)^2 + 1\right)$$

holds.

Proof. Since $\{y_n\}$ has a maximal period, we have $\tau = 3p^{m-\nu}$. Hence by Lemma (8)

$$D_N^{(1)}(x_0, x_1, \ldots, x_{N-1}) \leq$$

$$\leq \frac{1}{p^m} + \frac{1}{N} \sum_{|h| \leq \frac{1}{2}p^m} \sum_{|h_0| \leq \frac{1}{2}\tau} (r(h, \frac{1}{2}p^m) r(h_0, \tau))^{-1} \left|\sum_{n=0}^{\tau-1} e_{p^m}\left(hx_n + \frac{hx_0 p^m}{\tau}\right)\right| \leq$$

$$\leq \frac{1}{p^m} + \frac{1}{N}\sum_{h}\sum_{h_0}\left(r\left(h,\frac{1}{2}p^m\right)r\left(h_0,\frac{1}{2}\tau\right)\right)^{-1}\cdot\left(\left|\sum\nolimits_1\right|+\left|\sum\nolimits_2\right|+\left|\sum\nolimits_3\right|\right)$$

where

$$\sum_j = \sum_{k=0}^{p^{m-\nu}-1} e_{p^m}\left(hx_{3k+j}+nh_0p^\nu+n^2hp^{2\nu}+\cdots\right),\ \ j=0,1,2.$$

Now in view of the representations of x_{3k+j}, $j=0,1,2$, and Lemma (3), we obtain

$$D_N^1(x_0,x_1,\ldots,x_{N-1}) \leq \frac{1}{p^m} + \frac{3p^{\frac{m}{2}}}{N}\left(\frac{1}{p}\left(\frac{2}{\pi}\log p^m+\frac{7}{5}\right)^2+1\right).$$

□

Remark 1. For the case s, $2\leq s\leq 4$, we have similarly

$$D_N^s := D_N^{(s)}(x_0^{(s)},x_1^{(s)},\ldots,x_{N-1}^{(s)}) \leq \frac{s}{p^m} + \frac{1}{p^{\frac{m}{2}-\nu}}\left(1+\frac{1}{p^\nu}\left(\frac{2}{\pi}\log p^m+\frac{7}{5}\right)^s\right).$$

Theorem 4. *For every $s\in\{1,2,\ldots,p-1\}$ we have for the sequence of PRN's produced by the inversive generator type (II) of second order the following estimates*

$$D_\tau^{(s)}(x_0^{(s)},x_1^{(s)},\ldots,x_{\tau-1}^{(s)}) \leq \frac{s}{p^m} + \frac{3}{p^{\frac{m}{2}-\nu}}\left(1+\frac{1}{p^\nu}\left(\frac{s}{\pi}\log p^m+\frac{7}{5}\right)^s\right)$$

hold.

This assertion is a corollary of the representation (7) and Lemmas 3 and 7.

From Theorems 3 and 4 it follows that the sequences of PRN's $\{x_n\}$ produced by generator (2) pass the s-dimensional test ($s=1,2,3,4$) on the uniform distribution and statistical independency (unpredictability). Moreover, if we add the constant shift b to the variable shift $b(n)=b+cn+dF(n)$ with $\nu_p(c)\geq\max(\nu_p(a),\nu_p(b))$ and $\nu_p(d)\geq 2\nu_p(c)$, then all assertions of Theorems 1-4 will true.

Theorem 5. *For the sequences of PRN's produced by recursion (2) of type (I) or (II) we have*

$$\left|\overline{S}_N(h)\right| := \left|\sum_{(y_0,y_1)\in\mathbb{Z}_{p^m}^{*\,2}}\sum_{n=0}^{N-1} e_{p^m}(hy_n)\right| \leq 12N^{\frac{1}{2}}+12Np^{-\frac{m-\delta}{2}},$$

where

$$(h,p)=1,\ \ \delta=\begin{cases}\nu_p(b)\ if\ \nu_p(a)=0,\ \nu_p(b)=\nu,\\ \nu_p(a)\ if\ \nu_p(a)=\alpha,\ \nu_p(b)=0.\end{cases}$$

Theorem 6. *Let the sequence $\{y_n\}$ be produced by (2) with parameters a, b, y_0, y_1, $(a,p)=(y_0y_1,p)=1$, $\nu_p(b)=p^{\nu_0}$, $\nu_0\geq 1$. Then for every $h\in\mathbb{Z}$, $(h,p^m)=\mu\leq m$, we have*

$$\overline{S}_N(h) = \frac{1}{(\varphi(p^m))^2}\sum_{y_0,y_1\in\mathbb{Z}_{p^m}^*}|S_N(h,y_0,y_1)| \leq 12N^{\frac{1}{2}}+12Np^{-\frac{m-\nu_0}{2}}.$$

Proof. Let $\nu_p(h) = 0$, i.e. $(h,p) = 1$. By the Cauchy-Schwarz inequality we get

$$\left|\overline{S}_N(h)\right|^2 = \frac{1}{(\varphi(p^m))^2}\left|\sum_{y_0,y_1\in\mathbb{Z}_{p^m}^*}\sum_{n=0}^{N-1} e_m(hy_n)\right|^2 =$$

$$= \frac{1}{(\varphi(p^m))^2}\sum_{y_0,y_1\in\mathbb{Z}_{p^m}^*}\sum_{k,\ell=0}^{N-1} e_m(h(y_k - y_\ell)) \leq$$

$$\leq \frac{1}{(\varphi(p^m))^2}\sum_{k,\ell=0}^{N-1}|\sigma_{k,\ell}(h,-h)| = \frac{1}{(\varphi(p^m))^2}\sum_{r=0}^{\infty}\sum_{\substack{k,\ell=0\\ \nu_p(k-\ell)=r}}^{N-1}|\sigma_{k,\ell}(h,-h)| =$$

$$= \frac{1}{(\varphi(p^m))^2}\sum_{t=0}^{m-1}\sum_{\substack{k,\ell=0\\ \nu_p(k-\ell)=t}}^{N-1}|\sigma_{k,\ell}(h,-h)| + \frac{1}{(\varphi(p^m))^2}\sum_{k=0}^{N-1}|\sigma_{k,k}(h,-h)| =$$

$$= N + \frac{1}{(\varphi(p^m))^2}\sum_{t=0}^{m-1}\sum_{\substack{k,\ell=0\\ \nu_p(k-\ell)=t}}^{N-1}|\sigma_{k,\ell}(h,-h)|.$$

Using Theorem 1, we obtain

$$\left|\overline{S}_N(h)\right|^2 \leq N + \frac{1}{(\varphi(p^m))^2}\times$$

$$\times\sum_{r=0}^{m-1}\left(\sum_{\substack{k,\ell=0\\ k\not\equiv\ell \pmod 3\\ \nu_p(k-\ell)=r}}^{N-1}|\sigma_{k,\ell}(h,-h)| + \sum_{\substack{k,\ell=0\\ k\equiv\ell \pmod 3\\ \nu_p(k-\ell)=r}}^{N-1}|\sigma_{k,k}(h,-h)|\right) \leq$$

$$\leq N + \frac{1}{(\varphi(p^m))^2}\times$$

$$\times\left[4p^m\sum_{r=0}^{m-1}\frac{N^2}{p^r} + \left(\sum_{r<m-\nu_0} + \sum_{m-\nu_0\leq r\leq m-1}\right)\sum_{\substack{k,\ell=0\\ k\equiv\ell \pmod 3}}^{N-1}|\sigma_{k,\ell}(h,-h)|\right] \leq$$

$$\leq N + \frac{N}{(\varphi(p^{(m)}))^2}\times$$

$$\times\left(4Np^m + \sum_{r<m-\nu_0}\frac{N}{p^r}p^{m+\nu_0+r} + p^m\sum_{r\geq m-\nu_0}\frac{N}{p^r}\right) \leq$$

$$\leq N + N^2p^{-m}\cdot 11p^{\nu_0}(m-\nu_0).$$

Hence, for $(h,p) = 1$ we obtain

$$\left|\overline{S}_N(h)\right| \leq N^{\frac{1}{2}} + 12Np^{-\frac{m-\nu_0}{2}}.$$

□

5 Conclusion

Although the considered sequences produced by inversive congruential generators of second order do not reach the maximal period length $T = \left(p^{m-1}(p-1)\right)^2$, but due to simplicity of construction and cryptographic applicability they merit attention and further generalization.

References

1. W.-S. Chou. The period lengths of inversive congruential recursions. *Acta Arith*, 73, 4, 325–341, 1995.
2. J. Eichenauer and J. Lehn. A non-linear congruential pseudorandom number generator. *Statist. Hefte*, 27, 315–326, 1986.
3. D. E. Knuth. *The Art of Computer Programming II: seminumerical algorithms*, Addison-Wesley, 1998.
4. D. Lehmer. Mathematical methods in large-scale computing units. *Proc. 2nd Sympos. on Large Scale Digital Calculating Machinery, Harv. Univ. Press., Cambridge, Mass.*, 141–146, 1951.
5. G. Marsaglia. Random numbers fall mainly in the planes. *Proc. Nat. Acad. Sci.*, 61, 25–28, 1968.
6. H. Niederreiter. *Random Number Generation and Quasi-Monte Carlo Methods*, SIAM, Philadelphia, 1992.
7. P. Varbanets, S. Varbanets. Exponential sums on the sequences of inversive congruential pseudorandom numbers with prime-power modulus. *VoronoI's Impact on modern science, Proceedings of the 4th International Conference on Analytic Number Theory and Spatial Tessellations, Book 4, Volume 1, Kyiv, Ukraine.-September 22-28*, 112–130, 2008.
8. Sergey Varbanets. Inversive generator of the second order for the sequence of PRN's. *8th CHAOS Conference Proceedings, 26-29 May 2015, Henri Poicare Institute, Paris, France*, 877–889, 2016.
9. Pavel Varbanets and Sergey Varbanets. Inversive generator of the second order with a variable shift for the sequence of PRN's. *Annales Univ. Sci. Budapest., Sect. Comp.*, 46, 255-–273, 2017.

1 Variations on the Fermi-Pasta-Ulam chain, a survey

Ferdinand Verhulst

University of Utrecht, Department of mathematics
PO Box 80.010, 3508 TA Utrecht, The Netherlands
(E-mail: f.verhulst@uu.nl)

Abstract. We will present a survey of low energy periodic Fermi-Pasta-Ulam chains with leading idea the "breaking of symmetry". The classical periodic FPU-chain (equal masses for all particles) was analysed by Rink in 2001 with main conclusions that the normal form of the beta-chain is always integrable and that in many cases this also holds for the alfa-chain. The implication is that the KAM-theorem applies to the classical chain so that at low energy most orbits are located on invariant tori and display quasi-periodic behaviour. Most of the reasoning also applies to the FPU-chain with fixed endpoints.

The FPU-chain with alternating masses already shows a certain breaking of symmetry. Three exact families of periodic solutions can be identified and a few exact invariant manifolds which are related to the results of Chechin et al. (1998-2005) on bushes of periodic solutions. An alternating chain of 2n particles is present as submanifold in chains with k 2n particles, k=2, 3, ... The normal forms are strongly dependent on the alternating masses 1, m, 1, m,... If m is not equal to 2 or 4/3 the cubic normal form of the Hamiltonian vanishes. For alfa-chains there are some open questions regarding the integrability of the normal forms if m= 2 or 4/3. Interaction between the optical and acoustical group in the case of large mass m is demonstrated.

The part played by resonance suggests the role of the mass ratios. It turns out that in the case of 4 particles there are 3 first order resonances and 10 second order ones; the 1:1:1:...:1 resonance does not arise for any number of particles and mass ratios. An interesting case is the 1:2:3 resonance that produces after a Hamilton-Hopf bifurcation and breaking symmetry chaotic behaviour in the sense of Shilnikov-Devaney. Another interesting case is the 1:2:4 resonance. As expected the analysis of various cases has a significant impact on recurrence phenomena; this will be illustrated by numerical results.
Keywords: FPU-chain, resonance, periodic solutions, normalisation, chaos, Hamilton-Hopf bifurcation.

1.1 Introduction

Chains of oscillators arise naturally in systems of coupled oscillators and by discretisation of vibration problems of structures. In physics studying the Fermi-Pasta-Ulam (FPU) chain has been very influential for a different reason. The FPU-chain models a one-dimensional chain of oscillators with nearest-neighbour interaction only; see fig. 1.1. It was formulated to show the thermalisation of interacting particles by starting with exciting one mode with the expectation that after some time the energy would spread out over all the modes. This is one of the basic ideas of statistical mechanics. In the first numerical

experiment in 1955, 32 oscillators were used with the spectacular outcome that the dynamics was recurrent as after some time most of the energy returned to the chosen initial state. For the original report see Fermi et al. [14] and a review by Ford [15], recent references can be found in Christodoulidi et al. [10] or Bountis and Skokos [1]. Discussions can be found in Jackson [22], Campbell et al. [6] and Galavotti (ed.)[16]. Note that although studies of FPU-chains are of great interest, as models for statistical mechanics problems they are too restrictive.

Fig. 1.1. A Fermi-Pasta-Ulam chain with fixed endpoints.

1.1.1 Formulation

The original FPU-chain was designed with fixed endpoints and choosing the initial energy small. Later research showed the presence of periodic solutions and wave phenomena, also larger values of the energy were considered. Another version of the FPU-chain is the spatially periodic chain where particle 1 is connected with the last one. In this survey we will focus mainly on the periodic chain with small initial values of the energy. The Hamiltonian $H(p,q)$ for N particles is of the form:

$$H(p,q) = \sum_{j=1}^{N} \left(\frac{1}{2m_j} p_j^2 + V(q_{j+1} - q_j) \right), \tag{1.1}$$

where particle 1 is connected with particle N. The coordinate system has been chosen so that $q = p = 0$ is a stable equilibrium. For FPU-chains one considers usually potentials $V(z)$ that contain quadratic, cubic and quartic terms. Explicity

$$V(z) = \frac{1}{2}z^2 + \frac{\alpha}{3}z^3 + \frac{\beta}{4}z^4.$$

If $\beta = 0$ we call the FPU-chain an α-chain, if $\alpha = 0$ a β-chain. Physically the 2 chains are different, for an α-chain the forces on each particle are asymmetric, for a β-chain they are symmetric.
The spatially periodic chain has a second integral of motion, the momentum integral:

$$m_1\dot{q}_1 + m_2\dot{q}_2 + \ldots + m_N\dot{q}_N = \text{ constant.} \tag{1.2}$$

The momentum integral (1.2) enables us to reduce the N dof system to a $N-1$ dof Hamiltonian system by a symplectic transformation.
For low energy orbits near stable equilibrium one usually rescales $p \mapsto \varepsilon\bar{p}, q \mapsto \varepsilon\bar{q}$, divides the Hamiltonian by ε^2 and drops the bars. For the linearised system

near stable equilibrium we find:

$$\begin{cases} m_1\ddot{q}_1 + 2q_1 - q_2 - q_N & = 0, \\ m_2\ddot{q}_2 + 2q_2 - q_3 - q_1 & = 0, \\ m_3\ddot{q}_3 + 2q_3 - q_4 - q_2 & = 0, \\ \dots & = 0, \\ m_N\ddot{q}_N + 2q_N - q_1 - q_{N-1} & = 0. \end{cases} \tag{1.3}$$

The quadratic nonlinearities start with ε, the cubic ones with ε^2. The spectrum of the linear operator (the eigenvalues near stable equilibrium) determines the resonances and the nonlinear dynamics near stable equilibrium. Our survey is based on papers that make extensive use of normalisation-averaging techniques, see Sanders et al. [28], chs. 2 and 10. This involves near-identity transformations to simplify the equations of motion or the Hamiltonian itself if one studies such a system. A quadratic Hamiltonian indicated by H_2 corresponds with a linear system of differential equations; for a Hamiltonian with cubic terms near-identity transformation removes the non-resonant terms to higher order. Omitting the higher order terms the resulting normalised Hamiltonian $\bar{H} = H_2 + \bar{H}_3$ contains only the resonant terms $\bar{H}_3$ of the cubic H_3 (the index indicates the power of the polynomials). One can go on with the normalisation proces by using a near-identity transformation to remove the non-resonant terms from H_4, etc.

In general the normalised (averaged) equations that are truncated at some level of normalisation will not be integrable, although there are many exceptions. For the FPU-Hamiltonian in homogeneous polynomials we have the notation:

$$H = H_2 + \varepsilon H_3 + \varepsilon^2 H_4, \text{ and } \bar{H} = H_2 + \varepsilon\bar{H}_3 + \varepsilon^2\bar{H}_4.$$

We will describe a number of prominent cases that show different dynamics for different choices of the masses. In the original (classical) FPU problem all masses are equal which seems a natural choice. A second natural choice is to alternate the masses $m, M, m, M, \dots, m, M$; it is no restriction to assume $0 < m \leq M$. A quite different approach is to look for mass ratio's that produce interesting resonances and dynamics. We aim at summarising all these approaches for low energy chains. Of special interest in the analysis are integrals corresponding with approximate invariant manifolds of the averaged systems, periodic solutions, bifurcations and chaos.
An important conclusion will be that the classical FPU-chain contains so many symmetries that by symmetry breaking it is structurally unstable.

1.1.2 Theoretical background

There exist an enormous amount of papers on the original FPU-chain of Fermi et al. [14]. A large number of the papers consist of numerical explorations; they are often inspiring but not always satisfactorily explaining the phenomena. Apart from normalisation-averaging, symmetry considerations are important

for the qualitative results. This involves the theory of Hamiltonian systems, see for an introduction Verhulst [29] and for the more general dynamical systems context Broer et al. [2]. New results on Hamiltonian systems and symmetry are found in Bountis and Skokos [1], Efstathiou [13] and Hanßmann [18]. Basic understanding of recurrence as formulated by Poincaré [24] vol. 3, ch. 26 is essential.
A systematic study of dynamical systems with discrete symmetry was started by Chechin and Sakhnenko [7]. The authors introduce the notion of *bushes* with a bush comprising all modes singling out an active symmetry group in the system. A bush corresponds with a lower dimensional invariant manifold (or approximate invariant manifold in the sense of normalisation) giving insight in the various dynamical parts that compose the system. The theory is quite general, it was applied to FPU chains by Chechin et al. in [8] and [9].
Independently the ideas of utilising symmetries were also developed by Rink [26] and by Bruggeman and Verhulst in [4] and [5].

1.2 The classical periodic FPU-chain

In the original FPU problem one considered the so-called mono-atomic case, i.e. all masses equal; we call this the classical FPU-chain and put $m_1 = m_2 = \ldots = m_N = 1$. The recurrence of the classical FPU-chain signalled by Fermi et al. [14] was surprising at the time as this was before the time of publication of the KAM theorem (see below).
The linearised system (1.3) has the frequencies ω_j of the corresponding harmonic equations:

$$\omega_j = 2\sin\left(\frac{j\pi}{N}\right),\ j = 1, \ldots, N. \tag{1.4}$$

The implication is that we have many $1:1$ resonances, $N/2$ if N is even and $(N-1)/2$ if N is odd. Also there exist accidental other resonances like $1:2:1$.
A natural first step is to reduce the system using integral (1.2) to $N-1$ dof.
An interesting attempt to solve the recurrence problem was made by Nishida [23] by proposing to use the KAM theorem; this theorem guarantees under the right conditions the existence of an infinite number of $(N-1)$-tori containing quasi-periodic solutions near stable equilibrium. This would solve the recurrence problem, but unfortunately the spectrum is resonant and the KAM theorem can not be applied in a simple way.
The problem was for most cases solved for the spatially periodic FPU chain by Rink in [26]; his results can also be applied to the chain with endpoints fixed. We summarise the reasoning. First the system with cubic and quartic terms in the Hamiltonian is transformed by symplectic normalisation (also called Birkhoff-Gustavson normalisation) to a simpler form. If the resulting normalised Hamiltonian $\bar{H}$ is nondegenerate in the sense of the KAM theorem and if it is integrable i.e containing, in addition to integral (1.2), $N-1$ functionally independent integrals that are in involution, then the KAM theorem applies to the original Hamiltonian H. By the transformation the nonresonant terms of the cubic and quartic part are shifted to higher order. The original

system contains various discrete symmetry groups, a rotation symmetry and a reflection symmetry. These symmetries carry over to the normalised Hamiltonian system with the surprising result that the cubic terms in $\bar{H}$ vanish! From theorem 8.2 of Rink [26] we have for the classical periodic FPU chain derived from Hamiltonian (1.1) containing cubic and quartic terms:

$$\bar{H}_3 = 0. \tag{1.5}$$

The analysis in Rink [26] of $\bar{H}$ produces furthermore:

1. Assume $\alpha \neq 0$ and N is odd, then $H_2 + \varepsilon^2 \bar{H}_4$ is integrable and nondegenerate in the sense of the KAM theorem.
2. Assume $\alpha \neq 0$ and N is even, then $H_2 + \varepsilon^2 \bar{H}_4$ hast at least $(3N-4)/4$ quadratic integrals (if 4 divides N) or $(3N-2)/4$ quadratic integrals (if 4 does not divides N).
3. The normalised β-chain ($\alpha = 0$) is integrable and nondegenerate in the sense of the KAM theorem. Almost all low-energy orbits are periodic or quasi-periodic and move on invariant tori near stable equilibrium.
4. Similar results can be obtained for the classical FPU-chain with fixed endpoints.

The remaining problem is the integrability of $H_2 + \varepsilon^2 \bar{H}_4$ in the case of the even α-chain. To check this one has to carry out the normalisation to quartic terms which is quite a lot of work if N is large. We will discuss an example with $\alpha = 1, \beta = -1$.

Example 1.21
Consider a periodic Fermi-Pasta-Ulam chain consisting of four particles of equal mass m (= 1) with quadratic and cubic nearest-neighbor interaction. Periodic means that we connect the first with the fourth particle. The Hamiltonian is in this case:

$$H(p,q) = \sum_{j=1}^{4} (\frac{1}{2} p_j^2 + V(q_{j+1} - q_j)), \tag{1.6}$$

with

$$V(z) = \frac{1}{2} z^2 + \frac{1}{3} z^3 - \frac{1}{4} z^4.$$

The corresponding equations of motion were studied Rink and Verhulst [25].

The equations induced by Hamiltonian (1.6) have a second integral of motion, the momentum integral $\sum_{j=1}^{4} p_j =$ constant. This enables us to reduce the 4 dof equations of motion to 3 dof by a canonical (symplectic) transformation. From Rink and Verhulst [25] we have the reduced system:

$$\begin{cases} \ddot{x}_1 + 4x_1 &= 4x_2x_3 + 4x_1^3 + 6x_1(x_2^2 + x_3^2), \\ \ddot{x}_2 + 2x_2 &= 4x_1x_3 + x_2^3 + 3x_2(x_3^2 + 2x_1^2), \\ \ddot{x}_3 + 2x_3 &= 4x_1x_2 + x_3^3 + 3x_3(x_2^2 + 2x_1^2). \end{cases} \tag{1.7}$$

We can identify 3 families of periodic solutions, the 3 normal modes in the coordinate planes. Consider the x_2 normal mode that satisfies the equation:

$$\ddot{x}_2 + 2x_2 = x_2^3.$$

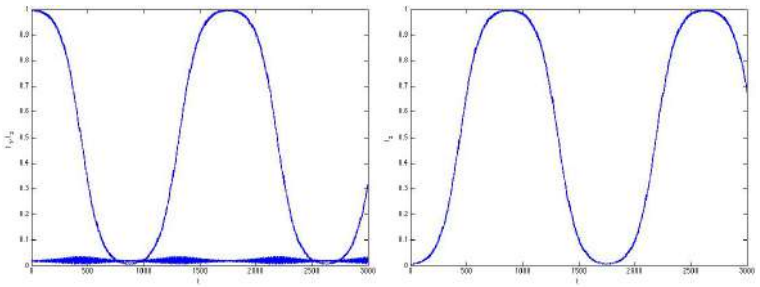

Fig. 1.2. The actions for 3000 timesteps near the unstable x_2 normal mode of system (1.7) with $\varepsilon = 0.1$, initial conditions $x_1(0) = x_3(0) = 0.1, x_2(0) = 1$ and initial velocities zero. Left the action $I_2(t) = \frac{1}{2}(\dot{x}_2^2 + 2x_2^2)$ starting near zero and increasing to values near 1; also the nonresonant $I_1(t) = \frac{1}{2}(\dot{x}_1^2 + 4x_1^2)$. Right the resonant action $I_3(t) = \frac{1}{2}(\dot{x}_3^2 + 2x_3^2))$ that exchanges energy with the x_2 mode (pictures from [31]).

In general, solutions far from stable equilibrium become chaotic, so we restrict ourselves to a neighbourhood of the origin by rescaling $x_1 = \varepsilon\bar{x}_1, x_2 = \varepsilon\bar{x}_2, x_3 = \varepsilon\bar{x}_3$ and then omitting the bars. Rescale also $\sqrt{2}t = s$. System (1.7) becomes:

$$\begin{cases} \frac{d^2x_1}{ds^2} + 2x_1 &= 2\varepsilon x_2x_3 + 2\varepsilon^2x_1^3 + 3\varepsilon^2x_1(x_2^2 + x_3^2), \\ \frac{d^2x_2}{ds^2} + x_2 &= 2\varepsilon x_1x_3 + \frac{1}{2}\varepsilon^2x_2^3 + \frac{3}{2}\varepsilon^2x_2(x_3^2 + 2x_1^2), \\ \frac{d^2x_3}{ds^2} + x_3 &= 2\varepsilon x_1x_2 + \frac{1}{2}\varepsilon^2x_3^3 + \frac{3}{2}\varepsilon^2x_3(x_2^2 + 2x_1^2). \end{cases} \tag{1.8}$$

The equation for the x_2 normal mode was studied in many introductions to the averaging method, where with initial values $x_2(0) = a, dx_2(0)/ds = 0$ we obtain the approximation:

$$\phi(s) = a\cos(s - \varepsilon^2\frac{3}{16}a^2s).$$

We transform $x_1 = y_1, x_2 = \phi(s) + y_2, x_3 = y_3$ in system (1.8) and linearising we find:

$$\begin{cases} \frac{d^2y_1}{ds^2} + 2y_1 &= 2\varepsilon\phi(s)y_3 + 3\varepsilon^2y_1\phi^2(s), \\ \frac{d^2y_2}{ds^2} + y_2 &= 0, \\ \frac{d^2y_3}{ds^2} + y_3 &= 2\varepsilon y_1\phi(s) + \frac{3}{2}\varepsilon^2y_3\phi^2(s). \end{cases} \tag{1.9}$$

The first and third equations are coupled but there is no resonance because of the basic frequencies $\sqrt{2}$ and 1; we conclude that the solutions of system (1.9) are stable. Interestingly, it was proved in [25] that near stable equilibrium the stability in linear approximation is destroyed by the nonlinearities. See fig. 1.2 for an illustration.

Example 1.22
Other examples
The relatively simple case of 3 particles was discussed by Ford [15]; the system is identified with the Hénon-Heiles system, a 2 dof Hamiltonian system in $1:1$

resonance; for a survey see Rod and Churchill [27]. This is interesting as this system has an integrable normal form for low energy values. Between the invariant tori there exists chaos but of exponentially small measure. If the energy is increased the amount of chaos increases, destroying more and more tori until the system looks fully chaotic at higher energy. Proofs are available for this behaviour, see Holmes et al. [20], except that we do not know whether at ''full chaotic behaviour" there are no tiny sets of tori left, undetected by numerics.
In Rink and Verhulst [25] the classical system with 4, 5 and 6 particles was analysed in the cases of α- and β-chains, also for mixed cubic and quartic terms. In these examples the normal forms are integrable.

1.3 The FPU-chain with alternating masses

Alternating the masses of a FPU-chain produces already a certain symmetry breaking. It is no restriction to rescale the smallest mass to 1 and have largest mass $m \geq 1$.
So we consider the periodic FPU-chain with N (even) masses that alternate: $1, m, 1, m, \ldots, 1, m$ (the case $0 < m \leq 1$ follows from symmetry considerations). The chain is related to the formulation in Galgani et al. [17] that analyses the chain and explores numerical aspects if N is large. In Bruggeman and Verhulst [5] a general analysis was started, but there are still many open questions; we summarise a number of results of this paper.
The eigenvalues $\lambda_j, j = 1, \ldots N$ of system (1.3) are with $a = 1/m$ in the case of alternating masses:

$$\lambda_j = 1 + a \pm \sqrt{1 + 2a\cos(2\pi j/N) + a^2}, j = 1, \ldots N. \tag{1.10}$$

Several observations can be made:

1. One eigenvalue equals 0 corresponding with the existence of the momentum integral (1.2).
2. If N is a multiple of 4 we have among the eigenvalues the numbers $2(a + 1), 2, 2a$.
3. For large masses m ($a \to 0$) the eigenvalue spectrum consists of 2 groups, one with size $2 + O(a)$ (the so-called optical group) and one with size $O(a)$ (the so-called acoustical group). The symplectic transformation to $N - 1$ dof mixes the modes because of the nearest-neighbour interactions, present already in the linearised system (1.3). So we cannot simply identify the dynamics of the optical group with the dynamics of the large masses.

A few qualitative and quantitative results were obtained by Bruggeman and Verhulst [5]:

1. We can identify *three explicit families of periodic solutions* characterised by the frequencies $\sqrt{2}, \sqrt{2a}, \sqrt{2(1+a)}$. The solutions are either harmonic or elliptic functions.

2. In the spirit of Chechin and Sakhenko [7] we can identify *bushes* of solutions in the following sense: the dynamics of a system with N particles will be found as a submanifold in systems with kN particles ($k = 2, 3, \ldots$). This increases the importance of studying chains with a small number of particles enormously. Note that the result is valid for large values of N, it also holds in the classical case $m = 1$.
3. First order averaging-normalisation ($m \neq 1$) produces for the α-chain only non-trivial results if $m = 2$ and $m = 4/3$. From the point of view of normalisation the case of large m ($a \to 0$) has to be treated separately.
4. An interesting discussion by Zaslavsky [32] deals with the phenomenon of delay of recurrence in Hamiltonian systems by *quasi-trapping*. This phenomenon arises for 3 and more dof if resonance manifolds, acting as subsets of the energy manifold, contain periodic solutions surrounded by invariant tori. The orbits entering such resonance manifolds may be delayed passage by staying for a number of revolutions near these tori.
   In Bruggeman and Verhulst [5] an explicit analysis and numerics of quasi-trapping is given for a number of cases with 8 particles. In the case of large mass m a second order normalisation is necessary; the recurrence is sensitive to the initial conditions.
5. For the alternating mass m large (small a) we expect different dynamics for the optical group (eigenvalues near 2) and the acoustical group (eigenvalues $O(a)$), see Galgani et al. [17]. This raises an old question: can high frequency modes transfer energy to low frequency modes and vice versa? The answer is affirmative, see the discussion below and fig. 1.3.

We summarise results for the cases $N = 4n$ and $N = 8n$.

1.3.1 Chain with 4n particles, $n = 1, 2, 3, \ldots$, [3]

A system with 4 particles is imbedded as an invariant manifold in a system with 4n particles. The momentum integral (1.2) enables reduction to 3 dof with frequencies $\sqrt{2}, \sqrt{2a}, \sqrt{2(1+a)}$. We find no 3 dof first order resonances in a system with 4 particles. The normal modes are exact periodic solutions both for the α- and the β-chain. The normal forms are in both cases integrable to second order. The recurrence of the orbits on an energy manifold depends on the initial conditions, starting near an unstable periodic orbit lengthens the recurrence times.
For the case large mass m (a small) see below.

1.3.2 Chain with 8n particles, $n = 1, 2, 3, \ldots$, [5]

A system with 8 particles is imbedded as an invariant manifold in a system with 8n particles. Using integral (1.2) produces reduction to 7 dof with frequencies:

$$\sqrt{2}, \sqrt{2a}, \sqrt{2(1+a)}, 1 + a + \sqrt{1+a^2}\,(\text{twice}), 1 + a - \sqrt{1+a^2}\,(\text{twice}).$$

The normal forms become much more complex (H_4 contains 49 terms) so we restrict the analysis to α-chains. As expected we recover the invariant manifold

associated with the first 3 eigenvalues (or frequencies) for the system *before* normalisation; we find two more 6-dimensional invariant manifolds of the exact equations. The 3 invariant manifolds have the normal mode periodic solution associated with the frequency $2a$ in common. This mode plays a pivotal part in the dynamics.
Normalisation produces $\bar{H}_3 = 0$ except if $a = 0.5, 0.75$ and if a is close to zero (large mass). The normal form flow in the 3 invariant manifolds is integrable. In the case $a = 0.75$ we find instability of the invariant manifolds, the stability in the other cases can not be decided as the eigenvalues are purely imaginary (this is a basic stability problem of Hamiltonian systems with more than 2 dof). A conclusion is that the presence of nested invariant manifolds (bushes) makes the equipartition of energy rather improbable.

1.3.3 Interactions between optical and acoustical group

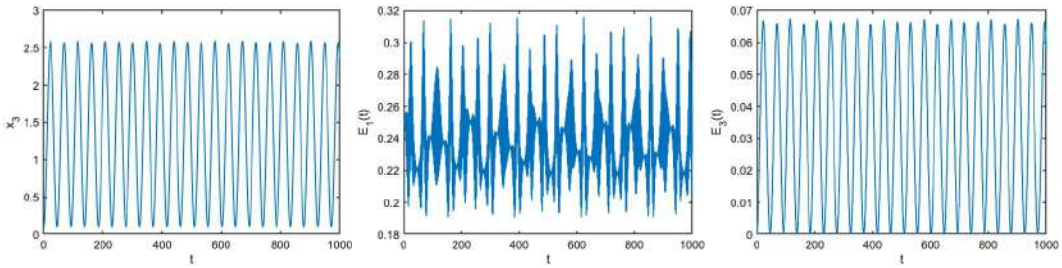

Fig. 1.3. Interaction between optical and acoustical group in invariant manifold M corresponding with 4 particles. The modes x_1, x_2 are near $1:1$ resonance. We have in system (1.11) $a = 0.01, x_1(0) = x_2(0) = 0.5, x_3(0) = 0$ and initial velocities zero. The instability of the solution in the optical group is indicated by the action $E_1(t) = 0.5(\dot{x}_1^2 + 2(1+a)x_1^2)$ (middle). Although far from resonance, the low-frequency mode x_3 is excited; figs left $x_3(t)$ and right $E_3(t) = 0.5(\dot{x}_3^2 + 2ax_3^2)$.

The eigenvalues and frequencies obtained from eq. (1.10) suggest that for mass m large we have two groups of oscillators, one with frequency size close to $\sqrt{2}$ and one with size $O(\sqrt{a})$. There are indications in Bruggeman and Verhulst [3] that in the case of a chain with 4 particles there exists significant interactions between the 2 groups. It turns out that in α-chains the acoustical group can be strongly excited by the optical group.
We will clarify this interaction phenomenon in the case of 4n particles using the 4 particles invariant manifold M that consists of the modes with frequencies $\sqrt{1+a}, \sqrt{2}, \sqrt{2a}$. This submanifold corresponds with the 4 particles system described above.
As $0 < a \ll 1$ there is actually no need for a scaling by small parameter ε in this case. The corresponding equations of motion are (see Bruggeman and

Verhulst [5]):

$$\begin{cases} \ddot{x}_1 + 2(1+a)x_1 &= 2\sqrt{a(1+a)}x_2x_3, \\ \ddot{x}_2 + 2x_2 &= 2\sqrt{a(1+a)}x_1x_3, \\ \ddot{x}_3 + 2ax_3 &= 2\sqrt{a(1+a)}x_1x_2. \end{cases} \tag{1.11}$$

The modes x_1 and x_2 are in a detuned $1:1$ resonance when choosing $0 < a \ll 1$. Consider the general position periodic solution of the $1:1$ resonance of the x_1, x_2 modes, described in Bruggeman and Verhulst [3]. A normal form approximation is $x_1(t) = r_0\cos(\sqrt{2}t + \psi_0), x_1(t) = \pm x_2(t)$; the approximation is based on the equations for these modes to order $O(a)$:

$$\ddot{x}_1 + 2x_1 = 2\sqrt{a}x_2x_3 + a\ldots, \ddot{x}_2 + 2x_2 = 2\sqrt{a}x_1x_3 + a\ldots$$

with x_3 varying on a long timescale. The asymptotic approximation with $x_1 = x_2$ leads to a forced, linear equation for $x_3(t)$:

$$\ddot{x}_3 + 2ax_3 = 2\sqrt{a}r_0^2\cos^2(\sqrt{2}t + \psi_0), \tag{1.12}$$

with particular solution:

$$x_3(t) = \frac{r_0^2}{2\sqrt{a}} - \frac{r_0^2}{8r_0^2 - 2\sqrt{a}}\cos(2\sqrt{2}t + 2\psi_0). \tag{1.13}$$

To this expression we have to add the homogeneous solution consisting of $\cos(\sqrt{2a}t)$ and $\sin(\sqrt{2a}t)$. It is remarkable that the particular solution has a large amplitude, $O(1/\sqrt{a})$, and period $\pi/\sqrt{2}$. The homogeneous solution has long period $\pi\sqrt{2}/\sqrt{a}$. We find that the "acoustical mode" x_3 is strongly excited; x_1 and x_3 are shown in fig. 1.3 in the case of large mass 100.

1.4 Resonances induced by other mass ratio's

The classical FPU-chain and the chain with alternating masses are natural models of physical chains. It is clear from dynamical systems theory that resonances and symmetries play a fundamental part in all these model chains; see for instance Poincaré [24] or Sanders et al. [28].
Take for instance the classical FPU-chain with N=6; the 6 harmonic frequencies of system (1.3) are $1, \sqrt{3}, 2, \sqrt{3}, 1, 0$. As we know, both for α- and β-chains $\bar{H}_3 = 0$ so the $1:2:1$ first order resonance is not effective because of symmetry; it might appear as a $2:4:2$ resonance at higher order. The $\sqrt{3}:\sqrt{3} = 1:1$ resonance plays a part for β-chains.

A different choice of masses that would make the frequency spectrum of system (1.3) non-resonant would always have near-resonances as the rationals are dense in the set of real numbers. This would produce detuned resonances with behaviour related to exact resonance, so even in this case the analysis of Nishida [23] would not apply although his idea turns out to be correct. Thus it makes sense to explore systematically the kind of resonances that may arise in FPU-chains. As we shall see this leads to various applications.

The exploration of possible resonances was done by Bruggeman and Verhulst [4] for the case of 4 particles leading to chains described by 3 dof. In Sanders et al. [28] ch. 10 a list of prominent Hamiltonian resonances in 3 dof is given for general Hamiltonians. In *general* for 3 dof we have 4 first order resonances (active at H_3) and 12 second order resonances (active at $H_3 + H_4$). Considering system (1.3) for the special case of the FPU chains with arbitrary positive masses, we find that the first order resonance $1:2:2$ does not arise, of the 12 seond order resonances $1:1:1$ and $1:3:3$ are missing. The importance of the resonances that do arise is partly determined by the size of sets in the parameter space of masses. We present the results from Bruggeman and Verhulst [4] where the sets in 3d-parameter space, the mass ratios of (m_1, m_2, m_3, m_4), with active resonance are indicated between brackets:

First order resonance
$1:2:1$ (4 points); $1:2:3$ (4 open curves); $1:2:4$ (12 open curves).

Second order resonances

1:1:3 (4 *points*)	1:2:5 (12 *open curves*)
1:2:6 (12 *open curves*)	1:3:4 (4 *open curves*)
1:3:5 (4 *open curves*)	1:3:6 (12 *open curves*)
1:3:7 (12 *open curves*)	1:3:9 (12 *open curves*
2:3:4 (2 *compact curves*);	2:3:6 (2 *compact curves*)

To determine the possible resonances for FPU chains with more than 4 particles is a formidable linear algebra and algebraic problem that has not been solved in generality. A general result from Bruggeman and Verhulst [4] is that for $N \geq 4$ no mass distribution will produce the N dof $1:1:\ldots:1$ resonance. We will discuss some results that are known for the $1:2:3$ and $1:2:4$ resonances with 4 particles. The second order resonances are largely unexplored for FPU-chains.

1.4.1 The 1 : 2 : 3 resonance

This resonance is of special interest as in this case for the general Hamiltonian chaos does not become exponentially small near stable equilibrium as $\varepsilon \to 0$ (see Hoveijn and Verhulst [21]). In general the normal form of the $1:2:3$ resonance is not integrable; see Christov [11]. However, symmetries may change the dynamics as is shown in systems with 4 particles, see Bruggeman and Verhulst [4] and below.

The symmetric case of 4 particles α-chains, $m_1 = m_3$
Using integral (1.2) and symplectic transformation we find the Hamiltonian:

$$H(p,q) = \frac{1}{2}\sum_{j=1}^{3}(p_j^2 + \omega_j^2 q_j^2) + \varepsilon(d_3 q_1^2 + d_{10} q_2^2 + d_6 q_3^2)q_3,\ (\omega_1, \omega_2, \omega_3) = (3, 2, 1), \tag{1.14}$$

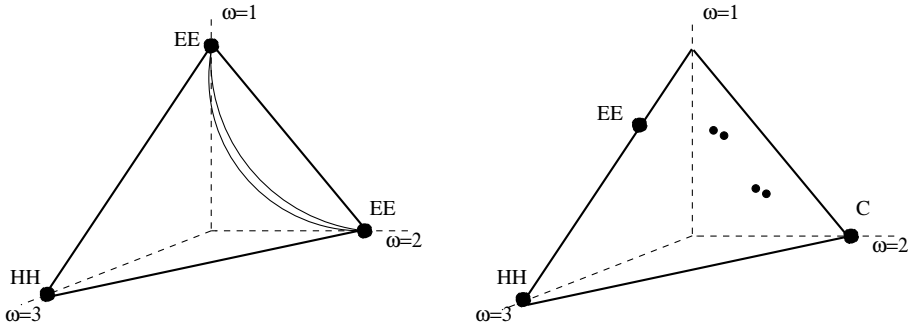

Fig. 1.4. The $1:2:3$ resonance with action simplex of the symmetric case $m_1 = m_3$ (left) and right a typical case with all masses different. Along the axes the actions form a triangle for fixed values of H_2 which is an integral of the normal forms. The frequencies $1, 2, 3$ indicate the 3 normal mode positions at the vertices. The black dots indicate periodic solutions, the indicated stability types are HH (hyperbolic-hyperbolic), EE (elliptic-elliptic) and C (complex with real and imaginary parts nonzero). The two (roughly sketched) curves connecting the 2 normal modes in the left simplex correspond for fixed energy with two tori consisting of periodic solutions, respectively with combination angle $\chi = 0$ and π. The tori break up into 4 general position periodic solutions if all masses are different.

with coefficients $d_3, d_6, d_{10} \neq 0$. The (p_1, q_1) and the (p_2, q_2) normal modes are exact periodic solutions in the 2 coordinate planes. Averaging-normalisation produces in addition the (p_3, q_3) normal mode periodic solution. We find 3 integrals of motion of the normalised system so the normal form dynamics is integrable. The normal form system contains only one combination angle $\chi = \psi_1 - \psi_2 - \psi_3$ producing for fixed energy families of periodic solutions (tori) in general position. This is a degeneration in the sense described by Poincaré [24] vol. 1, ch. 4.
The stability of the normal modes is indicated in fig. 1.4, left; the normal 2nd and 3rd modes ($\omega = 2, 1$) are stable with purely imaginary eigenvalues, the eigenvalues are coincident for the 2nd normal mode (Krein collision of eigenvalues). The first mode ($\omega = 3$) is unstable with real eigenvalues; In Bruggeman and Verhulst [4] a detailed description is given of the motion of the orbits starting near the unstable normal mode ($\omega = 3$).
We will see that the case $m_1 = m_3$ is structurally unstable, the dynamics changes drastically if all masses are different.

The case of 4 particles α-chains, all masses different
This case presents striking differences from the case with 2 masses equal, the symmetry is broken. We summarise:

1. The 3rd normal mode ($\omega = 1$) vanishes, the periodic solution shifts to the 2 dof subspace formed by the first and 3rd mode; stability EE.
2. The second normal mode becomes complex unstable (C) by a Hamiltonian-Hopf bifurcation. In this case two pairs of coincident imaginary eigenvalues (the case $m_1 = m_3$) move into the complex plane.

3. The presence of a complex unstable periodic solution fits in the Shilnikov-Devaney scenario leading to chaotic dynamics in the normal form, see Devaney [12] and Hoveijn and Verhulst [21]; the normalised Hamiltonian is not integrable in this case. Establishing chaos involves the presence of a horseshoe map. As this map is structurally stable, finding chaos in the normal form, this chaos will persist in the original system.
4. The tori consisting of periodic solutions in the case $m_1 = m_3$ break up into 4 periodic solutions at fixed energy.

1.4.2 The 1 : 2 : 4 resonance

Work in progress for the FPU-chain with 4 masses in $1 : 2 : 4$ resonance can be found in Hanßmann et al. [19]; this analysis includes detuning. We mention some of the results in the case of opposing masses equal, $m_1 = m_3$.

1. The case of 2 opposing masses equal induces a $\mathbb{Z}_2$ symmetry with as consequence that for both α- and β-chains we have $\bar{H}_3 = 0$.
2. The normal form $H_2 + \bar{H}_4$ for the α- and β-chains has 3 normal mode periodic solutions and is integrable.
3. Normalisation to H_6 breaks the symmetry, only 2 integrals of the normalised Hamiltonian could be found.

Interestingly the case of 2 adjacent equal masses produces different results; in this case $\bar{H}_3 \neq 0$, the symmetry mentioned above is broken.
The case of all masses different will be studied in a forthcoming paper.

1.4.3 An application to cell-chains

One can use low-dimensional FPU-chains as cells to form a new type of chain, see fig. 1.5. This is quite natural when thinking of interactions of molecules (a small group of connected oscillators) instead of atoms leading to a chain of connected near-neighbour interacting oscillators. A few examples of such cell-chains are discussed in Verhulst [30].

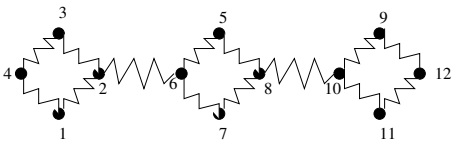

Fig. 1.5. A FPU cell-chain with 3 cells.

Consider cells consisting of a FPU-chain with 4 particles. As we have seen before the dynamics within each cell will strongly depend on the choice of the 4 masses. A second important aspect is how the cells are linked. Connecting cells by particles where stable periodic solutions dominate is expected to produce less transfer of energy than connecting by particles with more unstable periodic

solutions and more active dynamics. Also the linking of cells will detune the resonances; this effect can be stronger if the FPU-chain is structurally unstable. We will show a few examples of transfer of energy for the simplest case of two connected cells. As the systems are Hamiltonian the phase-flow will always be recurrent but if the recurrence takes a long time this will indicate active but small transfer of energy between the cells with delayed recurrence.
Hamiltonian (1.15) describes the interaction of 2 cells if $c_1 \neq 0$.

$$H(p,q) = \sum_{j=1}^{4}\left(\frac{m_j}{2}p_j^2 + \frac{1}{2}(q_{j+1}-q_))^2)\right) + \sum_{j=5}^{8}\left(\frac{m_{j-4}}{2}p_j^2 + \frac{1}{2}(q_{j+1}-q_j)^2\right) + \frac{\varepsilon}{2}c_1(q_2-q_6)^2 + H_3, \tag{1.15}$$

with

$$H_3 = \sum_{j=1}^{8}\frac{\varepsilon}{3}(q_{j+1}-q_j)^3.$$

In the experiments we start with zero initial values in the 2nd cell, $q_j(0) = v_j(0) = 0, j = 5,\ldots,8$. If $c_1 = 0$ we have non-trivial dynamics and corresponding distance $d(t)$ to the initial values only in the first cell. Explicitly:

$$d(t) = \sqrt{\sum_{j=1}^{8}[(q_j(t)-q_j(0))^2 + (v_j(t)-v_j(0))^2]}. \tag{1.16}$$

The distance $d(t)$ can be used to consider recurrence to a δ-neighbourhood of the initial values. An upper bound L for the recurrence time has been given in Verhulst [30]. Suppose we consider a bounded Hamiltonian energy manifold with N dof, energy value E_0 and Euclidean distance $d(t)$ of an orbit to the initial conditions, than we have for the recurrence time T_r to return in a δ-neighbourhood of the initial conditions an upper bound L with:

$$L = O\left(\frac{E_0^{N-1/2}}{\delta^{2N-1}}\right). \tag{1.17}$$

For one FPU-cell we have with reduction to 3 dof $L_1 = E_0^{5/2}/\delta^5$ and for 2 linked FPU-cells $L_2 = E_0^{13/2}/\delta^{13}$. Of course, starting near a stable periodic solution or if there exist extra first integrals will reduce the recurrence time enormously.

Numerical experiments
We present numerical results for 3 cases with cells consisting of 4 masses: the classical FPU-chain with equal masses in fig. 1.6 ($m = 0.1$ to have comparable timescales), the $1:2:3$ resonance case with symmetry induced by the choice $m_1 = m_3$ in fig. 1.7 and the less-balanced case of the $1:2:3$ resonance where the dynamics is chaotic, fig. 1.8. In each of the 3 cell-chains we have initial values $q_1(0) = 0.05, q_2(0) = 0.2, q_3(0) = 0.05, q_4(0) = 0.05, q_5(0) = q_6(0) = q_7(0) = q_8(0) = 0.0$, initial velocities are all zero. So we start in the first cell near the second normal mode plane.

As expected the recurrence times increase when adding one cell but most dramatically in the chaotic case. The inverse masses for fig. 1.7 are $a_1 = 0.0357143, a_2 = 0.126804, a_3 = 0.0357143, a_4 = 0.301767$ (symmetric $1:2:3$ resonance with $m_1 = m_3$) and for fig. 1.8 $a_1 = 0.00510292, a_2 = 0.117265, a_3 = 0.0854008, a_4 = 0.292231$ (chaotic $1:2:3$ resonance).
In all these recurrence experiments with for instance $\delta = 0.1$ or $\delta = 0.05$ the recurrence times are definitely lower than the corresponding upper bound L given by eq. (1.17).
The numerics used MATLAB ode 78 with abs and rel error e^{-15}.

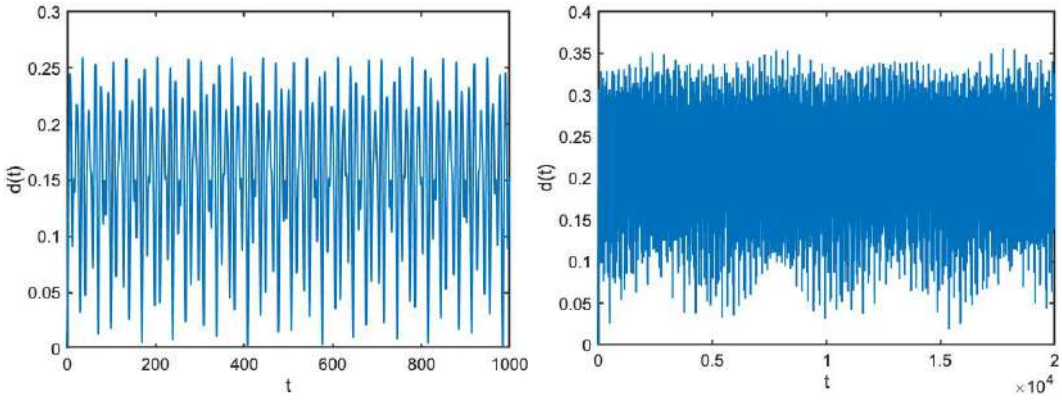

Fig. 1.6. The classical case $m = 0.1$ with strong recurrence for 1 cell (roughly 100 timesteps if $\delta = 0.05$) and delayed recurrence for 2 cells (roughly 5000 timesteps).

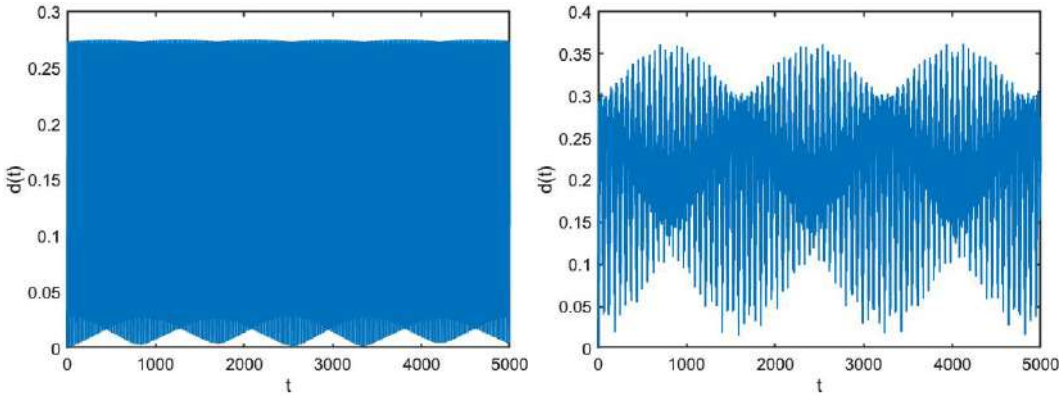

Fig. 1.7. The symmetric $1:2:3$ case $m_1 = m_3$; the normal form is integrable, we have strong recurrence. Left one cell, with $\delta = 0.01$ roughly 800 timestep;, right 2 cells with $\delta = 0.05$ roughly 1600 timesteps.

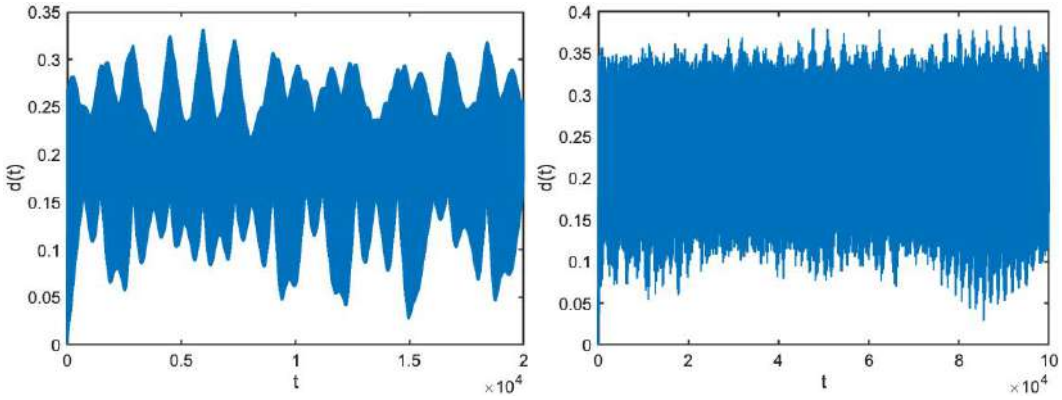

Fig. 1.8. The chaotic $1:2:3$ cell-chain with already delayed recurrence in one cell; with $\delta = 0.05$ left 15000 timesteps; right for 2 cells we have to integrate nearly 90 000 timesteps.

Acknowledgement
Comments on earlier versions of this paper by Tassos Bountis and Roelof Bruggeman are gratefully acknowledged.

References

1. T. Bountis and H. Skokos, *Complex Hamiltonian Dynamics*, Springer (2012).
2. H.W. Broer and F. Takens, (em Dynamical systems and chaos, Applied Math. Sciences 172, Springer (2011).
3. R.W. Bruggeman and F. Verhulst, *Dynamics of a chain with four particles and nearest- neighbor interaction*, in Recent Trends in Applied Nonlinear Mechanics and Physics (M. Belhaq, ed.), CSNDD 2016, pp. 103-120, doi 10.1007/978-3-319-63937-6-6, Springer (2018).
4. Roelof Bruggeman and Ferdinand Verhulst, *The inhomogenous Fermi-Pasta-Ulam chain*, Acta Appl. Math. 152, pp. 111-145 (2017).
5. Roelof Bruggeman and Ferdinand Verhulst, *Near-integrability and recurrence in FPU chains with alternating masses*, J. Nonlinear Science 29, pp. 183-206, DOI 10.1007/s00332-018-9482-x (2019).
6. D.K. Campbell, P. Rosenau and G.M. Zaslavsky (eds.), *The Fermi-Pasta-Ulam Problem. The first 50 years.* Chaos, Focus issue 15 (2005).
7. G.M. Chechin and V.P. Sakhnenko, *Interaction between normal modes in nonlinear dynamical systems with discrete symmetry. Exact results*, Physica D 117, pp. 43-76 (1998).
8. G.M. Chechin, N.V. Novikova and A.A. Abramenko, *Bushes of vibrational normal modes for Fermi-Pasta-Ulam chains*, Physica D 166, pp. 208-238 (2002).
9. G.M. Chechin, D.S. Ryabov and K.G. Zhukov, *Stability of low-dimensional bushes of vibrational modes in the Fermi-Pasta-Ulam chains*, Physica D 203, pp. 121-166 (2005).
10. Christodoulidi, H., Efthymiopoulos, Ch. and Bountis, T. [2010] *Energy localization on q-tori, long-term stability, and the interpretation of Fermi-Pasta-Ulam recurrences*, Physical Review E 81, 6210.

11. Ognyan Christov, *Non-integrability of first order resonances in Hamiltonian systems in three degrees of freedom*, Celest. Mech. Dyn. Astr. 112, pp. 149-167 (2012).
12. R.L. Devaney, *Homoclinic orbits in Hamiltonian systems*, J. Diff. Eqs. 21, pp. 431-438 (1976).
13. K. Efstathiou, *Metamorphoses of Hamiltonian systems with symmetries*, Lecture Notes Math. 1864, Springer (2005).
14. E. Fermi, J. Pasta and S. Ulam, *Los Alamos Report LA-1940*, in "E. Fermi, Collected Papers" 2, pp. 977-988 (1955).
15. J. Ford, *The Fermi-Pasta-Ulam problem: paradox turns discovery*, Physics Reports 213, pp. 271-310 (1992).
16. G. Galavotti (ed.) *The Fermi-Pasta-Ulam Problem: a status report*, Lecture Notes in Physics, Springer (2008).
17. L. Galgani, A. Giorgilli, A. Martinoli and S. Vanzini, On the problem of energy partition for large systems of the Fermi-Pasta-Ulam type: analytical and numerical estimates, Physica D 59, pp. 334-348 (1992).
18. H. Hanßmann, *Local and semi-local bifurcations in Hamiltonian dynamical systems*, Lecture Notes Math. 1893, Springer (2007).
19. H. Hanßmann, Reza Mazrooei-Sebdani and Ferdinand Verhulst, *The* $1:2:4$ *resonance in a particle chain*, arXiv nr. 2002.01263, submitted to Indagationes Mathematicae (2020).
20. P.J. Holmes, J.E. Marsden and J. Scheurle, *Exponentially small splittings of separatrices with application to KAM theory and degenerate bifurcations*, Contemp. Math. 81, pp. 213–244 (1988).
21. I. Hoveijn, I. and F. Verhulst, *Chaos in the* $1:2:3$- *Hamiltonian normal form*, Physica D, 44, pp. 397-406 1990.
22. E.A. Jackson, *Perspectives of Nonlinear Dynamics*, 2 vols., Cambridge University Press, Cambridge (1991).
23. T. Nishida, *A note on an existence of conditionally periodic oscillation in a one-dimensional anharmonic lattice*, Mem. Fac. Eng. Univ. Kyoto 33, pp. 27-34 (1971).
24. Henri Poincaré, *Les Méthodes Nouvelles de la Mécanique Céleste*, 3 vols., Gauthier-Villars, Paris (1892, 1893, 1899).
25. B. Rink and F. Verhulst, *Near-integrability of periodic FPU-chains*, Physica A 285, pp. 467-482 (2000).
26. B. Rink, *Symmetry and resonance in periodic FPU-chains*, Comm. Math. Phys. 218, pp. 665-685 (2001).
27. D.L. Rod. and R.C. Churchill, *A guide to the Hénon-Heiles Hamiltonian*, Progress in Singularities and Dynamical Systems (S.N. Pnevmatikos, ed.), pp. 385-395, Elsevier (1985).
28. J.A. Sanders, F. Verhulst and J. Murdock, *Averaging methods in nonlinear dynamical systems* 2nd ed., Appl. Math. Sciences 59, Springer, New York etc., (2007).
29. Ferdinand Verhulst, *Nonlinear differential equations and dynamical systems* 2nd ed., Springer, New York etc., (2000).
30. Ferdinand Verhulst, *Near-integrability and recurrence in FPU cells*, Int. J. Bif. Chaos 26, nr 14, DOI: 10.1142/S0218127416502308 (2016).
31. Ferdinand Verhulst, *Linear versus nonlinear stability in Hamiltonian systems*, Recent trends in Applied Nonlinear Mechanics and Physics, Proc. in Physics 199 (M. Belhaq, ed.) pp. 121-128, (2018) Springer, DOI 10.1007/978-3-319-63937-6-6.
32. G.M. Zaslavsky, *The physics of chaos in Hamiltonian systems*, Imperial College Press (2nd extended ed.) (2007).

Chaotic Mixing Experiments at High Temperature: Towards Unravelling a Large Magmatic Province

Caio M. Vicentini[1,2], Cristina P. de Campos[1], Werner Ertel-Ingrisch[1], Diego Perugini[3], Leila S. Marques[2], Donald B. Dingwell[1]

[1] Dept. of Earth and Environmental Sciences, University of Munich – DEGEO /LMU, Germany
[2] Instituto de Astronomia, Geofísica e Ciências Atmosféricas – IAG/USP, São Paulo, Brazil
[3] Dept. of Physics and Geology, University of Perugia, Italy
(E-mail: caio.vicentini@usp.br)

Abstract: The Paraná-Etendeka Magmatic Province (PEMP) is the largest outpour of magma on the Earth surface during lower Cretaceous times (~133 Ma). Basalts (~50% SiO_2, both high-Ti and low-Ti members) predominate over an estimated volume of $7 \bullet 10^5$ km^3. However, *ca.* 2.5% of the volcanic products, are chemically more evolved (>63% SiO_2). Their genesis is still under debate. This work aims a first attempt to experimentally reproduce the impact of underplating basaltic melt into a pre-existing continental crust. Mixing dynamics is thought to greatly influence the formation/contamination conditions of the high-Ti acid member (Chapecó-type). We used a chaotic mixing protocol (Journal Bearing System) at 1,350°C and following end-members: KS-700 basalt (high-Ti Pitanga-type from PEMP; η_{1350} = 8.78 Pa.s; ρ_{1350} = 2.469 g/cm³) and LMC-027 granite (syenogranite from Capão Bonito Stock; $\eta_{1350} = 1.22 \bullet 10^5$ Pa.s; ρ_{1350} = 2.292 g/cm³). Homogenized glasses from the basalt and the granitic basement were used in an 80/20 proportion, respectively. The experiment was performed during 212 min in total, *i.e.*, two periods of: (i) two clockwise rotations of outer cylinder (35 min); (ii) six anticlockwise rotations of inner cylinder (18 min). The independent and non-simultaneous movements of the two cylinders guaranteed the chaotic flow. The obtained mixed glass was cut in slices of 3 mm perpendicular to the rotation axes and two of the sections reproduced Poincaré patterns, which are theoretically expected to be resulted for this kind of dynamic mixing. With the development of stretching and folding processes, chaotic trajectories are distributed off-centered as lamellar lens-like structures in the mixed system. Vortex structures are comparable to those produced by mixing Fe-free silicate melts, however with much higher fractal dimension (D_f). These sections were preliminarily analyzed for the changes in morphology by comparing the D_f using binary images (ImageJ software). Obtained D_f's (≈ 1.79) are close to those from similar experiments with natural melts, although widespread orbicular structures found along all basaltic morphological domains are thought to enhance the complexity. Further experiments varying the granitic end-member are planned. Raman, microprobe and LA-ICP-MS investigations will be performed to compare chemical behavior of major/minor oxides and trace elements. Furthermore, numerical simulations will follow.
Keywords: Magma mixing, chaotic dynamics, journal bearing system at high-T, Paraná-Etendeka Magmatic Province, Chapecó-acidic type.

1 Introduction

The Paraná-Etendeka Magmatic Province (PEMP – Figure 1) is the second largest LIP (large igneous province) that occurs on the Earth's surface with over a $1 \bullet 10^6$ km² of area and 800,000 km³ (Frank *et al.*[1]) of expelled material. It took place about 133 My ago (Piccirillo and Melfi[2]; Janasi *et al.*[3]; Marzoli *et al.*[4]). Basalts (rocks with $SiO_2 \approx 50$ wt % in their composition) are the most common members found along the province and they are mainly divided in two groups: one with low contents of titanium ($TiO_2 < 2$ wt %; LTi), and other one with high contents ($TiO_2 \geq 2$ wt %; HTi). HTi basalts also differ from LTi due to the higher contents of P_2O_5, large-ion lithophile elements (such as Sr, Zr, Ba) and rare earth elements (as La, Ce and Lu) in general (Piccirillo and Melfi[2]; Marques *et al.*[5]; Peate *et al.*[6]). However, approximately 2.5% of the volcanic products are chemically more evolved ($SiO_2 \geq 63$ wt %), named rhyolites, and they also can be divided in two further-subgroups, according to the amount of TiO_2. Each subgroup also presents a geochemical behaviour similar to those found in the basalts (Piccirillo and Melfi[2]; Nardy *et al.*[7]). Despite the genesis of the rhyolites from PEMP being still under debate, the most accepted ideas consider these evolved members as products of basaltic evolution and interaction with other crustal rocks. Therefore, each group of basaltic rocks (LTi and HTi) would have originated rhyolites with respective low and high contents of titanium.

Figure 2 shows the underplating model used for Piccirillo and Melfi[2] to explain the genesis of Chapecó-type, where a HTi basaltic body is trapped under the crust, which is mainly composed by granitic rocks. At some point, the basalt has been remelted and interacted with the granitic basement around. Petrogenetic models tend to consider the magma chambers as static, so that the evolution of magmas is basically linear in time. However, in the last years, scientists began to compare the structures observed in volcanic environmental with the fractal geometry (De Rosa *et al.*[9], Perugini *et al.*[10], Perugini and Poli[11]), which is a characteristic of chaotic dynamic processes, and the complex dynamics inside the magma chamber started to be considered. Since then, fractal analysis and numerical simulations have been used as a tool to quantify such processes. Therefore, this work aims to an experimental approach of the genesis of high-Ti acid member of PEMP (Chapecó-type). It is a first attempt to reproduce the impact of underplating basaltic melt into a pre-existing continental crust and investigate the influence of chaotic mixing dynamics in their formation/contamination processes.

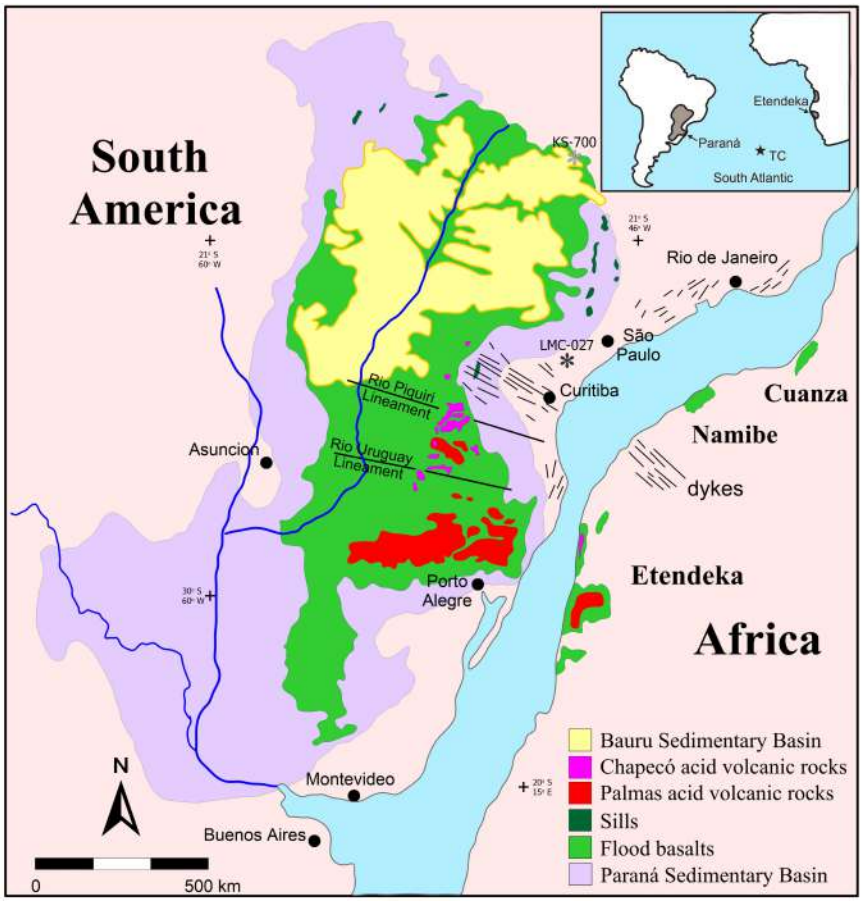

Fig. 1. Map from Paraná-Etendeka Magmatic Province – PEMP. Africa is rotated for present position of South America. Insert: TC = Tristan da Cunha island. Modified after Nardy *et al.*[7], Machado *et al.*[8] and references therein.

In order to investigate the genesis of Chapecó-acidic type, we chose an experimental approach, which is based on previously obtained results from chaotic mixing experiments with geological materials at high temperatures. Therefore, the development and construction of the first experimental apparatus succeeded, being able to reproduce the chaotic dynamics according a specific protocol of motion at high temperature (De Campos *et al.*[12]). It mimics the processes that would govern the magma chambers, in where the mixing process occurs. Results with synthetic end-members showed similar patterns comparing to those theoretically expected (*e.g.*: Poincaré sections). Using the same device, Perugini *et al.*[13] generated a hybrid sample from synthetic end-members and correlated the chemical analysis with numerical simulations considering that the particles have been submitted to a chaotic field motion. The comparison demonstrated that the patterns fit, meaning that a chaotic mixing process could

explain what is observed in nature. Finally, Morgavi *et al.*[14] performed the same experiment using natural end-members and finding different geometrical patterns compared to those obtained from synthetic end-members. Furthermore, the chemical analysis showed that the elementary mobility is different to the linear behaviour expected.

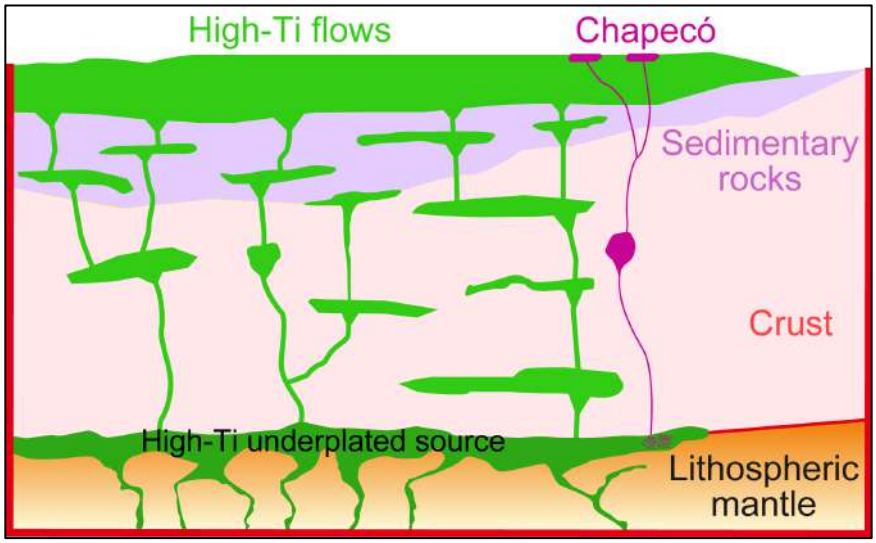

Fig. 2. Model for the underplating scenario of Chapecó-type genesis.

2 Methods

The chaotic mixing device is based on the Journal Bearing System (JBS; Swanson and Ottino[15]) that is able to generate a chaotic flow using a certain protocol of motion. Our apparatus scheme is shown in Figure 3. It is basically consisted by two independent motors. The lower motor moves a base where an Al_2O_3-rod (alumina: AL23) is fixed and allows positioning the crucible inside the hot spot of a high temperature furnace. The upper motor fixes an off-centered spindle also made from alumina and sheathed by a Pt foil in its extremity that will be positioned inside the sample. The geometry of JBS is determined basically by: (i) the ratio of the radii of the two cylinders, $r = R_{in}/R_{out} = 1/3$; (ii) the eccentricity ratio to the outer cylinder $\varepsilon = \delta/R_{out} = 0.3$, where δ is the distance between the centers of the inner and outer cylinders (R_{in} and R_{out}). The system was designed to enable independent rotations of inner and outer cylinders at variable speeds, directions and stirring protocols and to place the apparatus in the hot spot region of a well-calibrated high-temperature oven. The motors for both (inner and outer) cylinder movements are controlled by a central mixing system, which enables independent control of rotation direction, rotation speed and number of rotations (De Campos *et al.*[12]).

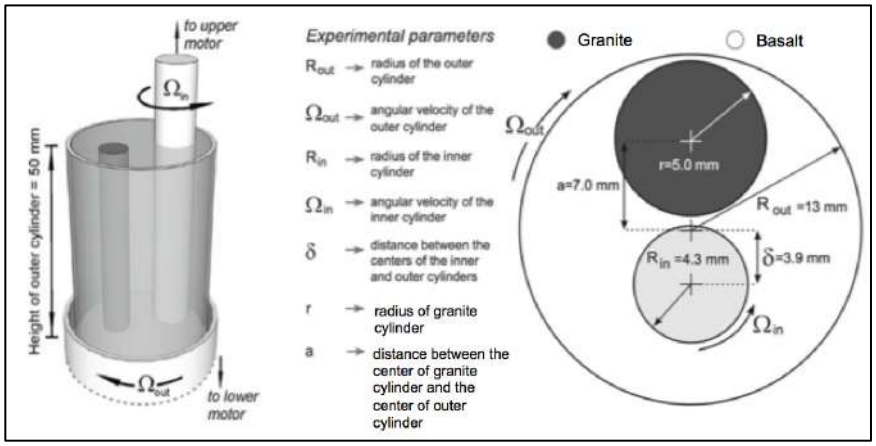

Fig. 3. Schematics of the experimental apparatus. Extracted from De Campos *et al.*[12] and Morgavi *et al.*[14].

The protocol used to generate the chaotic streamlines is: (i) two clockwise rotations of outer cylinder (35 min); (ii) six anticlockwise rotations of inner cylinder (18 min); (iii) two clockwise rotations of outer cylinder (35 min); (iv) six anticlockwise rotations of inner cylinder (18 min). It totalizes 212 min of non-simultaneous and independent movements, which guarantees the chaotic flow. This choice was made based on Morgavi *et al.*[14] that performed the experiment during ½, 1 and 2 protocols and demonstrated that the mixing efficiency at this time is sufficient to preserve the structures.

The end-members used in our experiment were: (i) a HTi *Pitanga*-type basalt from PEMP (mafic); (ii) a basement syenogranite from *Capão Bonito* Stock (felsic). The experimental temperature was 1350°C and it was chosen taking in to account the lowest value that still allows the interaction between the melts, once at low temperatures the viscosity increases and in some point no interaction would be possible. Estimated temperatures in nature where this interaction happens are lower than that, however there are other factors not considered in the experiment such as volatiles content and pressure that may greatly change the viscosity. In our case, melts are free of volatiles. At 1350°C, measured viscosity and calculated density for basalt was η_{1350} = 8.78 Pa.s; ρ_{1350} = 2.469 g/cm³, while to granite was η_{1350} = $1.22 \bullet 10^5$ Pa.s; ρ_{1350} = 2.292 g/cm³, which leads to a viscosity ratio of approximately $1.4 \bullet 10^4$. For the preparation, the end-members were pulverized and heated to produce a glass. Melts have been homogenized with a viscometer following the procedure described by Morgavi *et al.*[14]. The dry-bubble-free glasses were inserted into a Pt_{80}-Rh_{20} crucible with 25 mm of diameter, 50 mm of length and 1 mm thick in a proportion of 80% of basalt and 20% of granite. After positioning the crucible in the device, the oven is turned on and it heats up during approximately 40 minutes to all parts accommodate. During this time the temperature increases gradually until 1350°C is reached and then the mixing protocol starts. At the end, the chaotic mixing device is turned off and hybrid glass is cooled at room temperature.

After cooling, the sample was drilled out. The obtained core was cut perpendicular to the rotation axis into several pieces with approximately 3 mm length for further analysis. It is important to notice that De Campos *et al.*[12], Perugini *et al.*[13] and Morgavi *et al.*[14] used the inverse proportion (*i.e.*, 80% of felsic end-member with 20% of mafic inside) due to the fact the higher viscous material would stabilize the less viscous one at high temperatures. In principal, it would avoid any movement of the small cylinder before the protocol starts, although during the experiment the interaction expected between the end-members and the resultant patterns would not have been affected.

3 Results and Discussion

The initial cooling rate observed was approximately 86.5°C/min, which is concordant with previous reports (De Campos *et al.*[12]; Morgavi *et al.*[14]). Two sections of the sample core presented morphological aspects theoretically expected and similar to Poincaré sections. These have been polished for microscopic further geochemical analysis as shown in Figure 4.

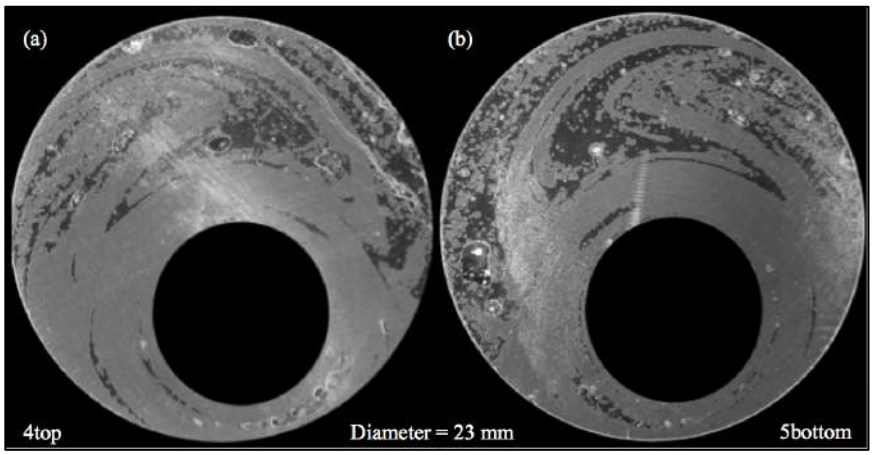

Fig. 4. Representative sections of chaotic mixing patterns after one protocol. Dark grey = granit; light grey = basalt.

The sections exhibit complex patterns of non-centered lamellar structures consisting of alternation of lens-like filaments in the mixed system. Around the inner cylinder these filaments are more or less concentric. At the top part it is observed a complex morphology composed by filaments strongly stretched and folded defining a lobate and banded structure pointing to the right side (4top; 5bottom is an adjacent face, therefore it points to opposite direction). The left side shows the felsic end-member thinning and forming a tail that almost connects to the concentric part described before. Comparing the morphology with those obtained for synthetic sample experiments the same vortex structures are observed (Figure 5).

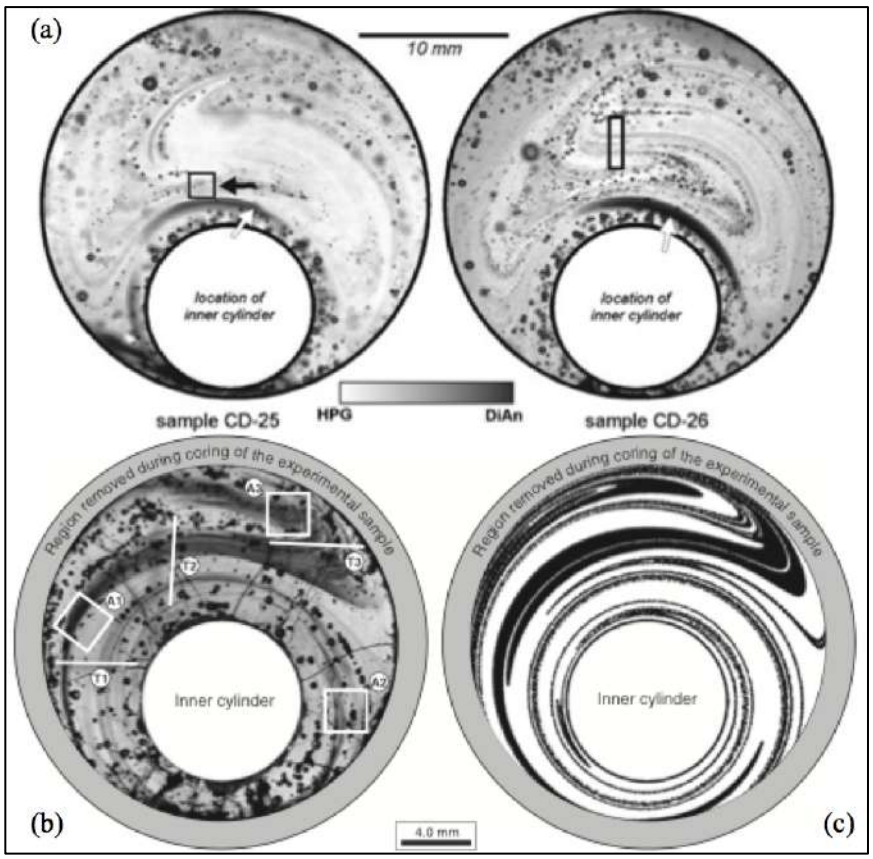

Fig. 5: Previous results by: (a) De Campos *et al.*[12]; (b,c) Perugini *et al.*[13]. Dark grey = mafic end-member; light grey = felsic end-member.

It is important to notice that synthetic samples prepared by De Campos *et al.*[12] and Perugini *et al.*[13] are iron free (composition: SiO_2, Al_2O_3, MgO, CaO, Na_2O and K_2O) and their experiments were executed at 1400°C, which facilitated the mixing process. At this temperature the authors calculated a viscosity of $1.55 \bullet 10^3$ Pa.s to felsic and 1.4 Pa.s to mafic end-member, corresponding to a viscosity ratio of *c.a.* $1.1 \bullet 10^3$, and densities of 2.26 and 2.52 g/cm^3 respectively. The same morphological response to mixtures with different chemical and physical properties could indicate that this mechanism is sufficiently robust. Perugini *et al.*[13] also numerically simulated the trajectory of the particles (Figure 5c) and, despite the differences due to the initial proportion (felsic = 65%; mafic = 35%), similar structures appears in the simulation such as the off-centered lamellar structures, the lobate and banded portion at the top and the concentric filaments around the inner cylinder. The

agreement between experiment and numerical results corroborates to the importance of this mechanism on the genesis of this rocks.
Nonetheless, the comparison with natural material from Morgavi *et al.*[14] permits to observe the discrepant patterns (Figure 6). It seems the principal mafic body dropped inside the felsic one at the right part, while the upper region suffered more influence of stretching and folding processes. Measured viscosity of the rhyolite was $5.6 \bullet 10^4$ Pa.s and of basalt was 7.2 Pa.s, corresponding to a viscosity ratio of *c.a.* $7.8 \bullet 10^3$, and the calculated densities were 2.33 and 2.98 g/cm^3 respectively. The discrepancies between the final morphology of natural and synthetic materials were initially thought to appear due to the presence of iron, that plays an important role in the melt structure, especially because of its two possible valences (Fe^{2+} and Fe^{3+}). Nevertheless, there are other factors that apparently influence the melt interaction taking into account the physical parameters of two experiments using natural samples show no relevant differences.

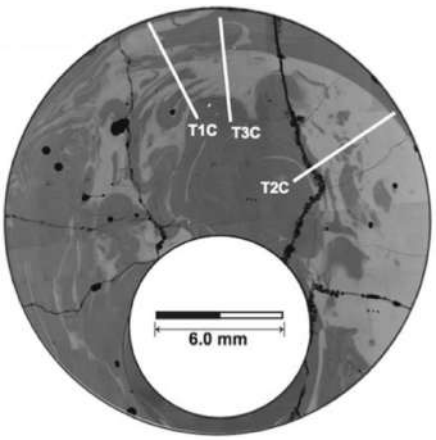

Fig. 6. Previous result by Morgavi *et al.*[14]. Dark grey = rhyolite; light grey = basalt.

Fig. 7. 4top: 8x zoom from Carl Zeiss Discovery V8.0 microscope. Object field = 2.9 mm. Dark grey = granite; light grey = basalt.

One of the most interesting features observed in the mixed glass presented in the Figure 7 are the orbicular structures along the two end-members. They are more evident on the granitic portion though. It is notice such feature was not reported on previous works using synthetic or natural materials (De Campos *et al.*[12]; Perugini *et al.*[13]; Morgavi *et al.*[14]).
In order to estimate the fractal dimension of both sections its photos were transformed in binary images using the *ImageJ* software developed by Rasband[16] (Figure 8) and the fractal coefficient D_f was calculate using the box-counting method, developed by Mandelbrot[17]. D_f values are substantially sensitive to the input (*i.e.*, the image) once even some blurred portions and

anomalous pixels can be interpreted as interest features by the software. Therefore, a simple protocol was adopted to provide the best estimative. It implicated in changing its brightness to highlight the contrast between the end-members, transforming in binary images and using tools (*Erode* and *Dilate*) to remove some anomalous pixels and to highlight the relevant ones.

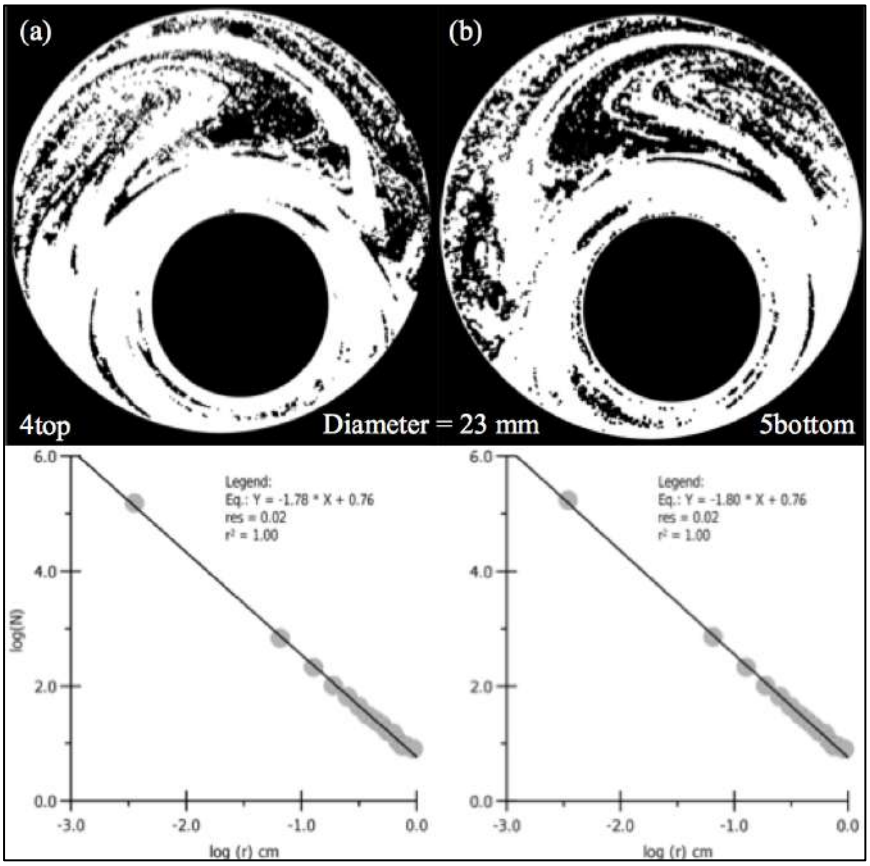

Fig. 8. Binary images used to calculate D_f (*ImageJ*) and respective curves built by box-counting method.

After this procedure the calculated D_f's were 1.78 (4top) and 1.80 (5bottom). The values are consistently higher than $D_f = 0.91$ obtained by De Campos *et al.*[12], for a mixture composed by synthetic samples, and similar to other results obtained to natural occurrences that takes place in the intervals: $1.01 < D_f < 1.84$ (De Rosa *et al.*[9]); $1.67 < D_f < 1.92$ (Perugini *et al.*[10]); $1.39 < D_f < 1.62$ (Guimarães *et al.*[18]). D_f's reported are consider an initial estimative indicating the experiment reproduced the patterns expected by a natural chaotic dynamic process. More precise calculations will be further obtained improving the quality of digitalized sections.

4 Conclusions

Chaotic mixing processes are thought to be a sophisticated explanation for natural melts interaction that have to be approached carefully. Therefore, at this stage is possible to summarize some conclusions:

1. The experiment showed very good primarily results. Compared to the morphological features previously obtained by Morgavi *et al.*[14], results from this study are better than expected, with the generation of Poincaré sections. It is evident this line of investigation should be maintained;
2. According to the results, inserting a cylinder of a more viscous material (granite) inside a less viscous material (basalt) did not affect the experimental stability at high temperatures (1350°C). The heating procedure adopted is thought to be vital to this fact and allows to invert the end-members proportion;
3. The patterns produced by chaotic dynamics are in concordance with those theoretically expected. This was noticed on the appearance of similar morphological elements in comparison with numerical simulations performed under similar conditions (Perugini *et al.*[13]);
4. Orbicular structures were identified for the first time on this type of experiment;
5. The fractal coefficients ($D_f \approx 1.79 \pm 0.01$) are in agreement with those values reported. Based on geological cases previous reported (*e.g.*: De Rosa *et al.*[9], Perugini *et al.*[10] and Guimarães *et al.*[18]) this first estimative could stand that the chaotic mixing has a role on petrogenesis of Chapecó-acidic type of PEMP.

Following investigation steps are still under development:

- Geochemical behavior of major/minor oxides and trace elements (microprobe and Laser Ablation-ICP-MS analysis);
- Numerical simulations to compare the theoretical response of the system;
- Raman analysis of the orbicular structures to study the nature and changes of the glass structure;
- Further chaotic mixing experiments varying the granitic end-member in order to test other candidates as contaminants for the Chapecó-type genesis. As a consequence, the impact of chemical and physical variations on morphological aspects under the same experimental conditions can be evaluated (*i.e.*, temperature and duration).

5 Acknowledgements

This study was financed in part by the Coordenação de Aperfeiçoamento de Pessoal de Nível Superior - Brasil (CAPES) – process: 88887.363370/2019-00 (CAPES – DAAD project 57389574 “Large Igneous Province Paraná-Etendeka”).

References

1. H.T. Frank, M.E.B. Gomes and M.L.L. Formoso. Review of the areal extent and the volume of the Serra Geral Formation - Paraná Basin, South. Pesquisas em Geociências, 36, 1, 49- 57, 2009.
2. E.M. Piccirillo and A.J. Melfi. The Mesozoic flood volcanism of the Paraná Basin: petrogenetic and geophysical aspects. São Paulo, Brazil. IAG, University of São Paulo (ed.) 600p, 1988.
3. V.A. Janasi, V.A. Freitas and L.H. Heaman. The onset of flood basalt volcanism, Northern Paraná Basin, Brazil: A precise U–Pb baddeleyite/zircon age for a Chapecó-type dacite. Earth. Plan. Sci. Letters, 302, 147–153, 2011.
4. A. Marzoli, L. Melluso, V. Morra, P.R. Renne, I. Sgrosso, M. D'Antonio, L. Duarte Morais, E.A.A. Morais and G. Ricci. Geochronology and petrology of Cretaceous basaltic magmatism in the Kwanza basin (western Angola), and relationships with the Paraná-Etendeka continental flood basalt province. Journal of Geodynamics, 28, 341-356, 1999.
5. L.S. Marques, E.M. Piccirilo, A.J. Melfi, P. Comin-Chiaramonti and G. Bellieni. Distribuição de terras raras e outros elementos traços em basaltos da Bacia do Paraná. Geochim. Brasil., 3, 33–50, 1989.
6. D.W. Peate, C.J. Hawkesworth and M.S.M. Mantovani. Chemical stratigraphy of the Paraná lavas, South America: classification of magma types and their spatial distribution. Bulletin of Volcanology, 55, 119-139, 1992.
7. A.J.R. Nardy, F.B. Machado and M.A.F. Oliveira. As rochas vulcânicas mesozoicas ácidas da Bacia do Paraná: litoestratigrafia e considerações geoquímico-estratigráficas. Rev. Bras. de Geoc., 38, 1, 178-195, 2008.
8. F.B. Machado, E.R.V. Rocha-Júnior, L.S. Marques, A.J.R. Nardy, L.V. Zezzo and N.S. Marteleto. Geochemistry of the Northern Paraná Continental Flood Basalt (PCFB) Province: implications for regional chemostratigraphy. Braz. J. Geol., 48, 2, 2018.
9. R. De Rosa, P. Donato, and G. Ventura. Fractal analysis of mingled/mixed magmas: an example from the Upper Pollara eruption (Salina Island, southern Tyrrhenian Sea, Italy). Lithos, 65, 299–311, 2002.
10. D. Perugini, G. Poli and R. Mazzuoli. Chaotic advection, fractals and diffusion during mixing of magmas: evidence from lava flows. J. Volcanol. Geotherm. Res., 124, 255–279, 2003.
11. D. Perugini, and G. Poli. Analysis and numerical simulation of chaotic advection and chemical diffusion during magma mixing: petrological implications. Lithos, 78, 43–66, 2004.
12. C.P. de Campos, D. Perugini, W. Ertel-Ingrisch, D.B. Dingwell and G. Poli. Enhancement of magma mixing efficiency by chaotic dynamics: an experimental study. Contrib. to Mineral. Petrol., 161, 863–881, 2011.
13. D. Perugini, C.P. de Campos, W. Ertel-Ingrisch, and D.B. Dingwell. The space and time complexity of chaotic mixing of silicate melts: implications for igneous petrology. Lithos, 155, 326–340, 2012.
14. D. Morgavi, D. Perugini, C.P. de Campos, W. Ertel-Ingrisch and D. Dingwell. Time evolution of chemical exchanges during mixing of rhyolitic and basaltic melts. Contributions to Mineralogy and Petrology, 166, 615–638, 2013.
15. P.D. Swanson and J.M. Ottino. A comparative computational and experimental study of chaotic mixing of viscous fluids. J. Fluid. Mech., 213, 227–249, 1990.
16. Rasband WS. ImageJ. U. S. National Institutes of Health, 2016. Software free available on http://rsb.info.nih.gov/nih-image

17. B.B. Mandelbrot. The Fractal Geometry of Nature. W.H. Freeman, New York, 1982.
18. L.F. Guimarães, C.P. de Campos, V.A. Janasi, E.F. Lima and D.B. Dingwell. Flow and fragmentation patterns in the silicic feeder system and related deposits in the Paraná-Etendeka Magmatic Province, São Marcos, South Brazil. Journal of Volcanology and Geothermal Research, 358, 149–164, 2018.

Self-similar chaotic processes in dynamical systems of nonlinear stochastic maps

George Vostrov[1,a], Andrii Khrinenko[1,b], Roman Opiata[1,c]

[1] Department of Applied Mathematics and Information Technologies, Odessa National Polytechnic University, Odessa, Ukraine.
[a] E-mail: vostrov@gmail.com
[b] E-mail: khrinenko@stud.opu.ua
[c] E-mail: roma.opyata@gmail.com

Abstract. The subject of research is cyclic processes that arise in recursive nonlinear maps under the influence of external probabilistic or stochastic factors. A wide range of nonlinear maps are considered, both continuous and containing discontinuity points. It is proved that any cyclic trajectory of considerable length always contains fragments with chaos properties, which are defined as properties of maps as well as properties of numbers from the domain of their definition. The laws are established for the transition of a dynamic system from one chaotic state to another chaotic state, depending on the properties of nonlinear maps.
Keywords: nonlinear maps, dynamical systems, self-similarity.

1 Introduction

Emergence of a book by famous authors with the name “Many-sided Chaos” is not accidental [1]. There is no doubt that the concept of “chaos” is associated with dynamic processes taking place in a certain space. In the literature [2], deterministic and stochastic chaos is defined as two general forms. However, the systematic use of the term “chaos” often leads to an incorrect analysis of its properties [3]. This fact is due to the fact that the nature of all chaotic processes is diverse and in some sense has many faces. Despite this, chaotic processes of completely different nature are often subject to general laws [4]. The study of such universal, in a certain sense, laws of chaotic processes of different nature is an actual and interesting problem of modern concept of chaos. Despite the fact that the deterministic and stochastic forms of chaos are very different from the point of view on mechanisms of its origin, from the point of view of their mathematical models it can be stated about certain patterns of interweaving of their properties in one frame.

The stochastic model of chaos is certainly based on the concept of randomness. Any random variable ξ, in the simplest case with a uniform probability distribution law over a finite interval (a, b), with a large number of tests, potentially allows to get a chaotic sequence of arbitrarily large length. Unfortunately, this is only a theoretical possibility. At present moment, random generators with a uniform distribution law are absent, and, consequently, with any other probability distribution law. Moreover, as shown in [5], none of the mathematical models of algorithmic computability makes it possible to obtain a binary sequence that could be called random in the exact mathematical sense.

The same result was obtained in [6] on the basis of another mathematical analysis of algorithms for constructing binary random sequences. It follows that absolute non-deterministic chaos, i.e. stochastic chaos at this stage in the development of research cannot be obtained by physical methods.

Assuming that this is "potentially" possible, the question arises as to what conditions a numerical sequence must satisfy in order to be considered as random. This question also applies to its binary representation. It is proved that absolutely random, and therefore chaotic sequence should not have any internal predicted structures. When solving problems of dynamical systems modeling [7], analyzing and processing data, and especially in the case of Big Data, when analyzing random processes [8], non-stationary time series and many other areas of pure and applied mathematics, random number generators with a given probability distribution law are needed. It follows that algorithmic models of random number generators are needed based on the theory of recursive functions, which allow us to model "absolute chaos" with maximum approximation to a given probability distribution law.

At present, it is not possible to construct random number generators based on the theory of recursive functions that could simultaneously simulate "absolute chaos" with a given distribution law. But the condition on the distribution law already violates the requirement that there are no internal properties in the generated sequences that reduce the level of randomness to some extent. It is necessary to construct pseudorandom number generators [9], but at the same time one has to admit the existence in the generated sequences of numbers of internal controlled patterns that minimize distortion of the results of modeling limited chaos. This means that we have to move to deterministic chaos [10]. The basis of such mathematical constructions is the theory of recursive functions and the theory of effective computability associated with it [10].

Such class of recursive functions is very extensive. It includes features of high computational complexity. Uncontrolled use of the theory of recursive functions can lead to a significant limitation on the speed of obtaining pseudorandom numbers. Therefore, we have to choose such classes of recursive functions that play a dual role. On the one hand, they are models of dynamical systems of a certain class, and on the other hand, their cyclic fixe points make it possible to generate their trajectories in such a way that they can be used to construct pseudorandom number generators. To solve this problem, it is could be promising to use maps on the set of integers or rational numbers, which on the one hand are models of deterministic dynamical systems, and on the other hand, the recursive sequences generate with these maps can be used to construct pseudorandom number generators.

In this regard, it seems perspective to start such studies with maps of the "tent" class in symmetric and asymmetric form, logistic map and algebraic maps that are based on the theory of residues modulo prime. The use of primes is interesting since in modern state of mathematical science there are still major blind spots in knowledge of its nature, although their logarithmic distribution law is established.

$$\pi(x) = \int_2^x \frac{dt}{ln\, t} + O\left(x\bar{e}^{c\sqrt{lnx}}\right),$$

where $\pi(x)$ is the number of primes $p \leq x$, however, the exact behavior of the function $f(x) = \pi(x) - Li(x)$, where $Li(x) = \int_2^x \frac{dt}{ln\, t}$ not studied. There is an assumption that the function $f(x)$ has a fractal structure. Until now the dynamics of changes in the distance between primes is unknown in number theory. Estimation of increase in the distance between primes based on the following expression:

$$p_{n+1} - p_n \geq \frac{\ln x \ln\ln x \ln\ln\ln\ln x}{\ln\ln\ln x},$$

shows that the distance between primes is continuously increasing. However, this expression does not at all follow how the properties of adjacent primes differ. Despite their simplicity, the properties of $p_{n+1} - 1$ and $p_n - 1$ can be very different, and this must be taken into account in the modern theory of the discrete logarithm, modern cryptography and in the modern theory of pseudorandom number generators.

The answers to these questions can be obtained to a certain extent by studying dynamic chaotic processes modeled by simple maps abovementioned classes at their cyclic fixed points determined by primes $p \in \mathcal{P}$. At the same time, it is important to choose such primes from the set of all primes $\mathcal{P}$ that allow obtaining of cyclic trajectories of large length and complex structure. At points given by primes $p \in \mathcal{P}$, rational numbers of the form q/p where p and q are primes allow to study the properties of dynamical systems determined on the given maps.

2 Self-similar processes inside the trajectories of nonlinear chaotic maps

Maps of the set of natural, integer, rational, real, complex numbers onto or into itself by means of nonlinear maps are always associated with the representation of such maps using recursive, primitively recursive, and therefore computable functions. Any such map defines a dynamic system, which is usually associated with some dynamic processes of a very different nature. As proven by well-known authors mathematical models of such processes can be built in arithmetic systems of various levels of complexity. The study of such mathematical models always includes an analysis of the trajectories of cyclic fixed points. As proved by Sharkovsky, the existence of a cycle of length three implies the existence of an iterative cycle in a dynamical system with a trajectory of any length, i.e. while the relation:

$$3 > 5 > 7 > 9 > \cdots > 2 \cdot 3 > 2 \cdot 5 > \cdots > 1.$$

It follows that there is an iterative cycle of a fixed point of any length. The existence of long cycles leads to the need to analyze their properties, since these properties are properties of a dynamical system. Information about the properties of iterable maps is important for control of dynamical systems, analysis of their properties in order to make decisions aimed at studying the

behavior of systems under various conditions. As proven in many monographs, scientific articles [10, 12] studies of the properties of dynamical systems based on the analysis of their trajectories are associated with significant difficulties due to the chaotic properties of the trajectories. The term "chaos" is interpreted by different authors in very different ways. This fact is not paradoxical since the nature of dynamic systems differs significantly from dynamic processes in biology, medicine, and economics. However, it can be assumed that there are some properties that are common to any models of dynamical systems. These properties are related to the mathematical form of the system representation and the properties of numbers, which determine the conditions for the occurrence of a cyclic trajectory of a fixed point.

Let examine the class of algebraic dynamical systems, which is surprisingly connected with nonlinear dynamical systems and represented by very simple nonlinear maps. Consider the set of all primes $\mathcal{P}$ and the residue group (Z/pZ) which is a cyclic group associated with each prime $p \in \mathcal{P}$. Natural numbers a are usually called the primitive root of a prime p and, therefore, the group $(Z/pZ)^*$ if the next condition is satisfied:

$$\begin{cases} a^{p-1} \equiv 1(mod\ p) \\ a^{\frac{p-k}{k}} \not\equiv 1(mod\ p) \end{cases}, (1)$$

for any divisor $k > 1$ of numbers $p - 1 = \prod_{i=1}^{n} p_i^{\alpha_i}$. These are necessary and sufficient conditions for verifying that a is the primitive root of p and it follows from Fermat's little theorem. The validation of these conditions is based on the calculation of a recursive sequence:

$$x_0 = 1, x_n = ax_n(mod\ p)\ (2)$$

to those. until the condition $x_m = ax_{m-1}(mod\ p) = 1$ is satisfied at the m −th step of the iteration. If $m = p - 1$, then a is the antiderivative root of p. Otherwise, the number a is a generating element of the number p of some subgroup of the group (Z/pZ). And any number a is a classifier of the set of all primes $\mathcal{P}$ into classes:

$$\mathcal{P}(a,1), \mathcal{P}(a,2), \dots, \mathcal{P}(a,i), \dots\ (3)$$

According to condition:

$$\mathcal{P}(a,i) = \{p|(p-1)card_a(p) = ind_a(p) = i\},$$

where $card_a(p)$ is the minimum recursion length (2) at which 1 modulo p is achieved, since $card_a(p)$ always divides $p - 1$, then $ind_a(p)$ determines the number of adjacency classes of the subgroup of the group $(Z/pZ)^*$. Obviously, if $card_a(p) = p - 1$, then a is the primitive root of the group $(Z/pZ)^*$, and if $card_a(p) < p - 1$, then a is a generating element of the cyclic subgroup of this group and its order is $card_a(p)$, and the number of adjacency classes is $ind_a(p)$. Thus, the set $\mathcal{P}(a,1)$ contains all primes p for which a is a primitive root, $\mathcal{P}(a,i)$ contains all primes p for which a is a generating element with index $ind_a(p) = i$. The infinity of the set of all primes $\mathcal{P}$ determines the existence of cyclic recursion (2) of arbitrarily large length for all classes and especially for the class $\mathcal{P}(a,1)$. In this case, four classes of problems arise:

1. $x \equiv a^m(mod\ p)$ - defined a, p, m, find x;
2. $c \equiv a^x(mod\ p)$ - defined a, p, c, find x;

3. $c \equiv x^m (mod\ p)$ - defined c, p, m, find x;
4. $c \equiv a^m (mod\ x)$ - defined a, c, m, find $x \in \mathcal{P}$.

The first problem is solved relatively simply by the method of repeated squaring. The second problem is the discrete logarithm problem, which belongs to the class of problems of high complexity, and it is possible that to the class of algorithmically unsolvable problems. The third and fourth task is much more complicated since the literature does not describe attempts to solve them. Closely related to the solution of the second problem is modern cryptography and modern methods for constructing pseudorandom number generators [8]. And also along with the first problem these problems has relation to the problem of chaos analysis. For convenience, we consider the case when a is a primitive root $p \in \mathcal{P}$ and the number p has a larger order, for example, $p > 10^{200}$. Recursion (2) for any such type is a permutation of the set of numbers $\{2,3, \dots, p-2\}$, where the number $p-1$ is not included since $a^{p-1} \equiv 1(mod\ p)$.

The prime p has $\varphi(p-1) = \prod_{i=1}^{m} p_i^{\alpha_i - 1}(p_i - 1)$ (Euler function) of primitive roots $(a_1, a_2, \dots, a_{\varphi(p-1)})$ and for each of which there exists a permutation in which the order of numbers from 2 to $p-2$ differs from the order of any other primitive root. In order to solve all problems associated with the discrete logarithm, it is necessary to possess information at least some degree on the order of the placement of numbers in chaos that is generated by recursion (2) for each a_i from the set of all primitive roots.

Definition. Let $p \in \mathcal{P}$ be a prime such that $p - 1 = \prod_{i=1}^{k} p_i^k$ and a is its primitive root, then in the trajectory of the recursive function (2) $x_{n+1} = ax_n (mod\ p)$ and the index $n = kp_i$ for all $p_1, \dots, p_k$ will be called basic indices. With respect to the set of indices of trajectories of recursion on the base a for a prime number $p \in \mathcal{P}$ and set of its primitive roots $\{a_1, \dots, a_{q(p-1)}\}$ next theorem is true.

Theorem. For any prime number $p \in \mathcal{P}$ such that $p - 1 = \prod_{i=1}^{k} p_i^{\alpha_i}$ and any primitive root of it, the set of all primitive roots $\{a_1, \dots, a_{q(p-1)}\}$ at the base points of the trajectories (2) there cannot be numbers from the set of all its primitive roots.

The validity of the theorem follows from the fact that during operations at base points of primitive roots there cannot be created a conflict situation among them in accordance with Fermat's little theorem and set theory.

Thus, the structure of the trajectories is constructed to a certain extent, taking into account the self-similarity of the trajectories of all primitive roots of a given prime number. This theorem confirms that in deterministic chaos, the properties of the map functions and the properties of a number from the region of the trajectories of recursive fixed points to some extent affect the structure of chaos.

Consider the case of dynamical system maps that are defined by simple functions of the "tent" class [10]. Despite their simplicity, as shown in [12], their behavior, both of dynamical systems and of sources of chaos formation, is far from simple. Consider two types of maps of this class:

$$x_{n+1} = \begin{cases} 2x_n, & x_n < \frac{1}{4}; \quad (5) \\ 1 - 2x_n, & \frac{1}{2} > x_n \geq \frac{1}{4}. (6) \end{cases}$$

The graphic representation of these maps is elementary. Consider the behavior of these maps on a set of numbers of the form $x = 1/p$ under the condition $p \in \mathcal{P}$. This choice of the set of initial conditions is chosen due to two considerations. Firstly, the analysis of dynamic processes and the chaos accompanying them can be compared with the algebraic map of residues modulo prime (2), and secondly, the study of the properties of dynamic processes by elements of such a set of initial values allows us to study their dependence on the properties of primes without taking into account decomposition $p - 1 = \prod_{i=1}^{k} p_i^{\alpha_i}$ and the properties resulting from it. In addition, since such a rational number $0 < m/n < 1$ is expressed through decomposition into simple factors, knowing the laws of the influence of the $1/p$ properties on the dynamics and chaos features, we can switch to composite numbers of the form m/n.

Maps (5) and (6) were studied in papers where the study of map (2) led to the construction of a generalized Artin hypothesis and its solution [8, 9, 11]. Based on the results of these studies, interesting conclusions can be drawn. Note that the logistic map:

$$x_{n+1} = 4x_n(1 - x_n) \quad (7)$$

As an object of numerous studies [10] on a set of numbers of the form $1/p$, it behaves in a certain sense "similarly" to maps (5) and (6). By analogy it is ment the congruence of these maps, which was studied in [13] for maps (5) and (7). The congruence of the two mappings $f(x)$ and $g(x)$ on the set $[0,1]$ suggests that there is a one-to-one correspondence between their cyclic fixed points for which the lengths of the cyclic trajectories of the congruent points coincide, but the topological structure is different. The author of the congruence method in [13] described a method for proving the congruence of maps on a distinguished set from the domain of definition of maps.

Based on the results of modeling the processes of formation of classes $\mathcal{P}(a, i)$ for any $a \neq i \& \pm 1$ and $i \epsilon \{1,2, \dots, n, \dots\}$, theorems on congruence of maps, analysis of trajectories of maps (2), (5), (6) it is not difficult to prove the validity of the following statements.

Statement 1. The map (5) is congruent to the map (2) for $a = 4$ on the set of all primes $p \in \mathcal{P}$, but for any prime number their trajectories in the chaos structure do not coincide.

This statement means that, on the basis of map (5), we obtain the same system of primes in the generalized Artin hypothesis as on the basis of map (2), although map (2) is discrete and map (5) is continuous. As shown in [12], the display paths (2) represent a sequence of self-similar successive fragments of the trajectory located at a regular distance from each other and interconnected by successive fragments of chaotic behavior. A fragment of such a structure of cyclic trajectories of fixed points $1/p$ is shown in Figure 1 where solid line

represents sequence fragments with high degree of similarity and dashed line represent chaotic behavior of the map.

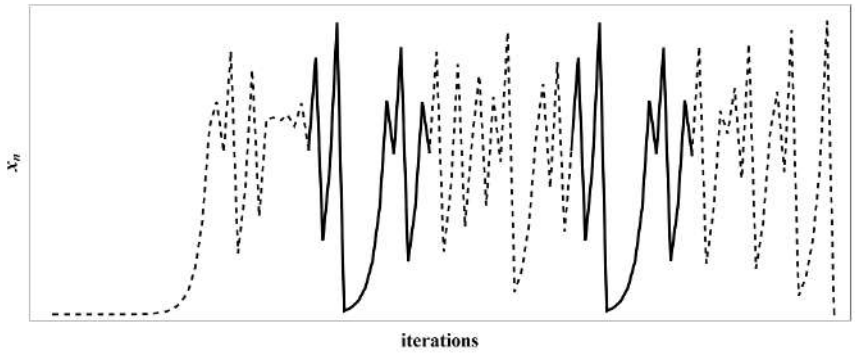

Fig. 1. Sequence with self-similar successive fragments

It should be noted that a completely non-algebraic function of the "tent" type allows one to solve a problem from number theory related to the discrete logarithm problem, modern cryptography and problems of constructing pseudorandom number generators, and, on the other hand, stimulates a deeper analysis of the trajectories of cyclic fixed points of dynamical systems in order to identify areas where chaotic behavior approaches its non-deterministic models. A similar analysis of the map (6) allows us to prove the following statement.

Statement 2. The map (6) is congruent to the map (2) with $a = 2$ on the set of all primes p∈P, but their trajectories do not coincide in structure for any p.

From this statement it follows that map (6) forms a system of classes of primes of the form:

$$\mathcal{P}(2,1), \mathcal{P}(2,2), \dots, \mathcal{P}(2,i), \dots$$

This means that $\mathcal{P}(2,1) = \{p \epsilon \mathcal{P} | (p-1)/card_2(p) = ind_2(p) = 1\}$, i.e. these are all prime numbers for which the number $a = 2$ is their primitive root. The class $\mathcal{P}(2,i)$ consists of the set of all primes p for which in the group $(Z/pZ)^*$ a subgroup with index i has the number $a = 2$ by its generating element. Thus, maps of the "tent" type with an appropriate choice of parameter allow to solve problems of modern number theory. In addition, it follows from statements 1 and 2 that the properties of dynamical systems fundamentally depend on the properties of the functions that determine them and on the properties of the number of some fundamental sequences from the domain of their definition.

Conclusions

An analysis of the chaos structure in the cyclic trajectories of fixed points of dynamical systems reveals formation patterns of their trajectories based on the properties of the maps that determine the dynamical system. The parameters of the maps determine the classification of numbers from the domain of their definition whose properties are functions of the properties of parameters.

Various studies in this direction allow us to deepen an understanding of the mechanisms of chaos formation and its dynamical structure.

References

1. E. Mishchenko, V. Sadovnichy. Many-sided chaos. Moscow, 2012.
2. C. Skiadas, I. Dimotikalis. Chaotic Systems: Theory and Applications, World Scientific, 2010.
3. C. Skiadas, C. Skiadas. Handbook of Applications of Chaos Theory. Chapman & Hall/CRC, 2016.
4. P. Cvitanović, R. Artuso, R. Mainieri, G. Tanner and G. Vattay, "Chaos: Classical and Quantum" Niels Bohr Institute, Copenhagen 2016
5. Schöll E., and Heinz Georg. Schuster. Handbook of Chaos Control. Wiley-VCH, 2014.
6. H. Rogers. Theory of recursive functions and effective computability. Cambridge, Mass.: MIT Press, 2011.
7. V. Uspenskii, A. Semenov and A. Shen'. "Can an individual sequence of zeros and ones be random?". Russian Math. Surveys, 45:1 (1990), 121–189 pp.
8. R. Crandall and C. Pomerance. Prime Numbers. New York, NY: Springer Science+Business Media, Inc., 2005.
9. Y. Manin and A. Panchishkin. Introduction to Modern Number Theory. Berlin, Heidelberg: Springer-Verlag Berlin Heidelberg, 2005.
10. B. Hasselblatt and A. Katok. A First Course in Dynamics: with a Panorama of Recent Developments. Cambridge: Cambridge University Press, 2003.
11. Computer Data Analysis and Modeling: Stochastics and Data Science : Proc. of the Twelfth Intern. Conf. Minsk : BSU, 2019. 319-325 pp.
12. G. Vostrov and A. Khrinenko, "Sequence internal structure formation during pseudorandom generation", Electrical and Computer Systems, vol. 29, no. 105, pp. 164-168, 2018.
13. J. Rauch, "Conjugation of Logistic and Tent Maps", 2014.

Stabilization in the Instability Region Around the Triangular Libration Points for the Restricted Three-Body Problem

Asher Yahalom[1] and Natalia Puzanov[2]

[1] Ariel University, Ariel 40700, Israel
Princeton University, Princeton, New Jersey 08543, USA
(E-mail: asya@ariel.ac.il)
[2] Ariel University, Ariel 40700, Israel
(E-mail: puzanovn@ariel.ac.il)

Abstract. Stabilized restricted three-body problem in which the motion of third body is planar and circular is presented. The instability region of triangular libration points is stabilized by feedback control in integral form.
Keywords: Three-body problem, triangular libration points, stabilization, control function.

1 Introduction

We consider the plane elliptic restricted three-body problem. The differential equations of this problem in the Nechville coordinates (ξ, η) have the form [1,3,4]:

$$\begin{cases} \xi'' - 2\eta' = \rho(\xi - \mu + \frac{\mu-1}{(\xi^2+\eta^2)^{\frac{3}{2}}}\xi - \frac{\mu}{[(\xi-1)^2+\eta^2]^{\frac{3}{2}}}(\xi-1)) \\ \eta'' + 2\eta' = \rho(\eta + \frac{\mu-1}{(\xi^2+\eta^2)^{\frac{3}{2}}}\eta - \frac{\mu}{[(\xi-1)^2+\eta^2]^{\frac{3}{2}}}\eta) \end{cases} \tag{1}$$

where

$$\rho = \frac{1}{1+\epsilon\cos t},\ \mu = \frac{m_1}{m_0+m_1},$$

ϵ is the eccentricity of the Keplerian orbit ($0 \le \epsilon < 1$), t is the true anomaly, m_0 and m_1 are the masses of actively gravitating bodies; thus $0 < \mu < 1$. Those equations are derived in the appendix.

The system (1) has five constant solutions - libration points: straight-line L_1, L_2 , and triangular L_4 and L_5. In the plane of the variables (ξ, η) of the system (1), the straight-line libration points lie on the line $\eta = 0$, and the triangular libration points have the coordinates:

$$L_4\left(\frac{1}{2}, \frac{\sqrt{3}}{2}\right),\ L_5\left(\frac{1}{2}, -\frac{\sqrt{3}}{2}\right). \tag{2}$$

13^{th} *CHAOS Conference Proceedings, 9 - 12 June 2020, Florence, Italy*
C. H. Skiadas (Ed)

We will be interested in questions related to the stability of triangular libration points.

Fig.1 [6] describes the regions of stability and instability of the system (1) for small values of μ. The shaded area corresponds to stability region in parameter space.

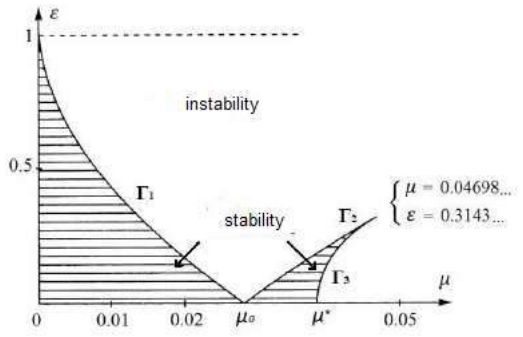

Fig.1 The stability region of triangular libration points.

Here

$$\mu^* = \frac{1}{2} - \frac{\sqrt{69}}{18} = 0.038520...., \;\; \mu_0 = \frac{1}{2} - \frac{\sqrt{2}}{3} = 0.028595.... \tag{3}$$

Numerous studies addressing the regions of stability of the system (1) and the behavior of the solutions of this system near the boundaries of these regions of stability are due to the importance of these questions for celestial mechanics. However, so far no attempts have been made to stabilize system (1) in the region of instability of the libration point.

We will pass from system (1) to equivalent normal system by introduction of new variables $u_1 = \xi, u_2 = \eta$, $u_3 = \xi'$, $u_4 = \eta'$

$$\begin{cases} u_1' = u_3, \\ u_2' = u_4, \\ u_3' = 2u_4 + \rho(u_1 - \mu + \frac{\mu-1}{(u_1^2+u_2^2)^{\frac{3}{2}}}u_1 - \frac{\mu}{[(u_1-1)^2+u_2^2]^{\frac{3}{2}}}(u_1-1)) \\ \\ u_4' = -2u_3 + \rho(u_2 + \frac{\mu-1}{(u_1^2+u_2^2)^{\frac{3}{2}}}u_2 - \frac{\mu}{[(u_1-1)^2+u_2^2]^{\frac{3}{2}}}u_2) \end{cases} \tag{4}$$

We thus have a system of the form:

$$u' = F(u, \epsilon, \mu, t), \;\; u \in R^4 \tag{5}$$

$F(u, \epsilon, \mu, t)$ is the vector function defined by the right part of system (4). Libration points of system (1) correspond to constant solutions of system (5). In particular triangular libration points L_4 and L_5 correspond to following

constant solutions of system (5)

$$v_4 = \begin{bmatrix} \frac{1}{2} \\ \frac{\sqrt{3}}{2} \\ 0 \\ 0 \end{bmatrix} \qquad v_5 = \begin{bmatrix} \frac{1}{2} \\ -\frac{\sqrt{3}}{2} \\ 0 \\ 0 \end{bmatrix} \tag{6}$$

The behaviour of system (5) is the same in neighborhoods of libration points v_4 and v_5. For definiteness we will study behaviour of system (5) in neighborhood of libration point v_4.

Carrying out in (4) the substitution $X = u - v_4$, we arrive at the equivalent system.

$$\begin{cases} X'(t) = Z(t), \\ Y'(t) = W(t), \\ Z'(t) = 2W(t) + \rho \left[\left(X(t) + \frac{1}{2} \right) - \mu + \frac{\mu - 1}{\left[\left(X(t) + \frac{1}{2} \right)^2 + \left(Y(t) + \frac{\sqrt{3}}{2} \right)^2 \right]^{\frac{3}{2}}} \left(X(t) + \frac{1}{2} \right) - \right. \\ \qquad \left. \frac{\mu}{\left[\left(X(t) - \frac{1}{2} \right)^2 + \left(Y(t) + \frac{\sqrt{3}}{2} \right)^2 \right]^{\frac{3}{2}}} \left(X(t) - \frac{1}{2} \right) \right] \\ W'(t) = -2Z(t) + \rho \left[\left(Y(t) + \frac{\sqrt{3}}{2} \right) + \frac{\mu - 1}{\left[\left(X(t) + \frac{1}{2} \right)^2 + \left(Y(t) + \frac{\sqrt{3}}{2} \right)^2 \right]^{\frac{3}{2}}} \left(Y(t) + \frac{\sqrt{3}}{2} \right) - \right. \\ \qquad \left. \frac{\mu}{\left[\left(X(t) - \frac{1}{2} \right)^2 + \left(Y(t) + \frac{\sqrt{3}}{2} \right)^2 \right]^{\frac{3}{2}}} \left(Y(t) + \frac{\sqrt{3}}{2} \right) \right] \end{cases} \tag{7}$$

The libration point v_4 of the system (5) corresponds to an equilibrium point $X = 0$ of the system (7). System (7) can be represented as

$$X' = A(\epsilon, \mu, t)X + a(X, \epsilon, \mu, t), \qquad X \in R^4 \tag{8}$$

in which $A(\epsilon, \mu, t) = F'_X(0, \epsilon, \mu, t)$ is the Jacobi matrix of the vector function $F(X, \epsilon, \mu, t)$ calculated at the point $X = 0$, and $a(X, \epsilon, \mu, t)$ is a nonlinearity which begins with terms quadratic in X. At $\epsilon = 0$ (a circular case) the system (7) is autonomous.

The matrix $A(\epsilon,\mu,t)$ is equal to

$$A(\epsilon,\mu,t)=\begin{bmatrix} 0 & 0 & 1 & 0\\ 0 & 0 & 0 & 1\\ \frac{3}{4}\rho & 3\frac{\sqrt{3}}{4}(1-2\mu)\rho & 0 & 1\\ 3\frac{\sqrt{3}}{4}(1-2\mu)\rho & \frac{9}{4}\rho & -2 & 0 \end{bmatrix} \tag{9}$$

To investigate our problem it suffices to consider the linear equation:

$$X'=A(\epsilon,\mu,t)X. \tag{10}$$

Since for $0\le\epsilon<1$ the equality

$$\rho=\frac{1}{1+\epsilon\cos t}=1-\epsilon\cos t+\epsilon^2 cos^2 t-\epsilon^3 cos^3 t+.... \tag{11}$$

is correct then the matrix (9) can be represented in the form:

$$A(\epsilon,\mu,t)=A_0(\mu)+(-\epsilon\cos t)A_1(\mu)+... \tag{12}$$

where

$$A_0(\mu)=\begin{bmatrix} 0 & 0 & 1 & 0\\ 0 & 0 & 0 & 1\\ \frac{3}{4} & 3\frac{\sqrt{3}}{4}(1-2\mu) & 0 & 1\\ 3\frac{\sqrt{3}}{4}(1-2\mu) & \frac{9}{4} & -2 & 0 \end{bmatrix} \tag{13}$$

and for $\mu=\mu_0=\frac{1}{2}-\frac{\sqrt{2}}{3}$

$$A_0=A_0(\mu_0)=\begin{bmatrix} 0 & 0 & 1 & 0\\ 0 & 0 & 0 & 1\\ \frac{3}{4} & \frac{\sqrt{6}}{2} & 0 & 2\\ \frac{\sqrt{6}}{2} & \frac{9}{4} & -2 & 0 \end{bmatrix}, \tag{14}$$

The linear approximation (10) for the planar case is:

$$X'=A_0(\mu_0)X. \tag{15}$$

has the following simple eigenvalues:

$$\lambda_{1,2}=\pm\frac{1}{2},\qquad \lambda_{3,4}=\pm\frac{\sqrt{3}}{2} \tag{16}$$

In accordance with the Fig.1, system (7) is not stable at $\mu=\mu_0$, $\epsilon=0$ ($\rho=1$).

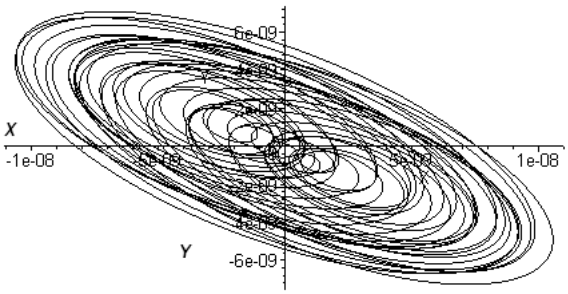

Fig.2 The phase portrait of the solution of the system (7) for $\rho = 0$ in the (X, Y) plane with initial conditions: $X(0) = Y(0) = Z(0) = W(0) = 0$ for interval $200 \leq t \leq 500$.

2 Exponential stabilization of triangular libration points in instability region by feedback delay control in integral form.

We introduce the feedback delay control $V(t)$ in the form, in which all the history of the process W(t) is taken into account [5].

$$V(t) = \int_0^t e^{-\beta(t-s)} W(s) ds, \tag{17}$$

We apply stabilization by the feedback delay control signal to the system (7) assuming that the control signal $V(t)$ acts only in the first equation.

$$
\begin{cases}
X'(t) = Z(t) - \alpha \int\limits_0^t e^{-\beta(t-s)} W(s) ds, \\
Y'(t) = W(t), \\
Z'(t) = 2W(t) + \rho \left[\left(X(t) + \frac{1}{2} \right) - \mu + \frac{\mu - 1}{\left[\left(X(t) + \frac{1}{2} \right)^2 + \left(Y(t) + \frac{\sqrt{3}}{2} \right)^2 \right]^{\frac{3}{2}}} \left(X(t) + \frac{1}{2} \right) - \right. \\
\left. \frac{\mu}{\left[\left(X(t) - \frac{1}{2} \right)^2 + \left(Y(t) + \frac{\sqrt{3}}{2} \right)^2 \right]^{\frac{3}{2}}} \left(X(t) - \frac{1}{2} \right) \right], \\
W'(t) = -2Z(t) + \rho \left[\left(Y(t) + \frac{\sqrt{3}}{2} \right) + \frac{\mu - 1}{\left[\left(X(t) + \frac{1}{2} \right)^2 + \left(Y(t) + \frac{\sqrt{3}}{2} \right)^2 \right]^{\frac{3}{2}}} \left(Y(t) + \frac{\sqrt{3}}{2} \right) - \right. \\
\left. \frac{\mu}{\left[\left(X(t) - \frac{1}{2} \right)^2 + \left(Y(t) + \frac{\sqrt{3}}{2} \right)^2 \right]^{\frac{3}{2}}} \left(Y(t) + \frac{\sqrt{3}}{2} \right) \right],
\end{cases}
\tag{18}
$$

where α and β the parameters needed to achieve the point $(X, Y, Z, W) = (0, 0, 0, 0)$ at which the system becomes exponentially stable. In accordance with the Leibnitz rule for differentiation under the integral sign, of the form $\frac{d}{dy} \int_{a(y)}^{b(y)} f(x, y) dt$ we get the expression for $V'(t)$. Thus we can rewrite the system (18) in a form of the system of ordinary differential equations [2]:

$$
\begin{cases}
X'(t) = Z(t) - \alpha V(t), \\
Y'(t) = W(t), \\
Z'(t) = 2W(t) + \rho \left[\left(X(t) + \frac{1}{2} \right) - \mu + \frac{\mu - 1}{\left[\left(X(t) + \frac{1}{2} \right)^2 + \left(Y(t) + \frac{\sqrt{3}}{2} \right)^2 \right]^{\frac{3}{2}}} \left(X(t) + \frac{1}{2} \right) - \right. \\
\qquad \left. \frac{\mu}{\left[\left(X(t) - \frac{1}{2} \right)^2 + \left(Y(t) + \frac{\sqrt{3}}{2} \right)^2 \right]^{\frac{3}{2}}} \left(X(t) - \frac{1}{2} \right) \right], \\
W'(t) = -2Z(t) + \rho \left[\left(Y(t) + \frac{\sqrt{3}}{2} \right) + \frac{\mu - 1}{\left[\left(X(t) + \frac{1}{2} \right)^2 + \left(Y(t) + \frac{\sqrt{3}}{2} \right)^2 \right]^{\frac{3}{2}}} \left(Y(t) + \frac{\sqrt{3}}{2} \right) - \right. \\
\qquad \left. \frac{\mu}{\left[\left(X(t) - \frac{1}{2} \right)^2 + \left(Y(t) + \frac{\sqrt{3}}{2} \right)^2 \right]^{\frac{3}{2}}} \left(Y(t) + \frac{\sqrt{3}}{2} \right) \right], \\
V'(t) = W(t) - \beta V(t).
\end{cases}
\tag{19}
$$

In the linear approximation, system (19) can be represented as

$$X' = JX, \tag{20}$$

where J is Jacobi matrix for the right side of the system (19)

$$
J = \begin{bmatrix}
0 & 0 & 1 & 0 & -\alpha \\
0 & 0 & 0 & 1 & 0 \\
\frac{3}{4} & \frac{\sqrt{6}}{2} & 0 & 2 & 0 \\
\frac{\sqrt{6}}{2} & \frac{9}{4} & -2 & 0 & 0 \\
0 & 0 & 0 & 1 & -\beta
\end{bmatrix}
\tag{21}
$$

$$det(J-\lambda I)=\begin{vmatrix} -\lambda & 0 & 1 & 0 & -\alpha \\ 0 & -\lambda & 0 & 1 & 0 \\ \frac{3}{4} & \frac{\sqrt{6}}{2} & -\lambda & 2 & 0 \\ \frac{\sqrt{6}}{2} & \frac{9}{4} & -2 & -\lambda & 0 \\ 0 & 0 & 0 & 1 & -\lambda-\beta \end{vmatrix} \tag{22}$$

Characteristic equation is

$$-\left(\lambda^5+\beta\lambda^4+\lambda^3+\Big(\beta+\frac{\sqrt{6}}{2}\alpha\Big)\lambda^2+\Big(-\frac{3}{2}\alpha+\frac{3}{16}\Big)\lambda+\frac{3}{16}\beta\right)=0 \tag{23}$$

According to the Hurwitz criterion for a 6-th order system all roots of the characteristic equation (23) have negative real parts if and only if

$$\begin{aligned} &a_1=\beta>0\\ &a_2=1>0,\\ &a_3=\beta+\frac{\sqrt{6}}{2}\alpha>0,\\ &a_4=-\frac{3}{2}\alpha+\frac{3}{16}>0,\\ &a_5=\frac{3}{16}\beta>0,\\ &a_1a_2-a_3=-\frac{\sqrt{6}}{2}\alpha>0,\\ &(a_1a_2-a_3)(a_3a_4-a_2a_5)-(a_1a_4-a_5)^2=\\ &\qquad\qquad\frac{3}{32}\alpha^2\Big(-24\beta^2+8\sqrt{6}+24\alpha-3\Big)>0. \end{aligned} \tag{24}$$

From (24) we obtain:

$$\begin{aligned} &-\frac{1}{24}<\alpha<0,\\ &\frac{\sqrt{6}}{6}-\frac{\sqrt{6+144\alpha}}{6}<\beta<\frac{\sqrt{6}}{6}+\frac{\sqrt{6+144\alpha}}{6} \end{aligned} \tag{25}$$

Numerical integration of the system (19) illustrated in Fig.3.

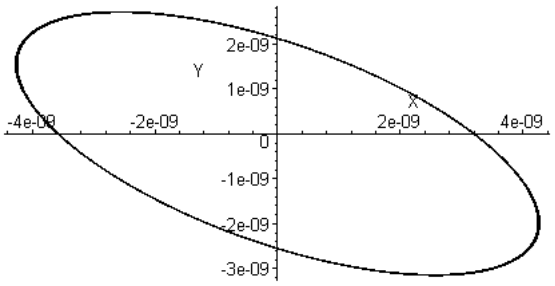

Fig.3 The phase portrait of the solution of the system (19) for $\rho = 0$ in the (X, Y) plane with initial conditions: $X(0) = Y(0) = Z(0) = W(0) = V(0) = 0$ for interval $200 \leq t \leq 500$ with control parameters: $\alpha = -0.029, \beta = 0.5$.

3 Conclusion

Comparison of figures (2) and (3) show quite clearly the effect of stabilization on a planetary orbit. The dramatic change from a chaotic orbit to a regular elliptic orbit is quite apparent. This is achieved by adding an additional degree of freedom which stabilizes the orbit (see equation (19)), this approach seems quite general and may be used for many chaotic systems.

Appendix: Derivation of Nechville differential equations for bounded, restricted three-body problem

We define our problem as follows: Two bodies (M_0 and M_1) revolve around their center of mass G under the influence of their mutual gravitational attraction and a third body M_2 which attracted by the previous two but not influence in their motion, movies on the plane defined by the two revolving bodies (Fig.4). The restricted problem of three bodies is to describe the motion of this third body (M_2).

The masses of bodies M_0 and M_1 are arbitrary but these bodies have such internal mass distributions that they may be considered point masses. The mass of third body M_2 does not influence the motion of M_0 and M_1.

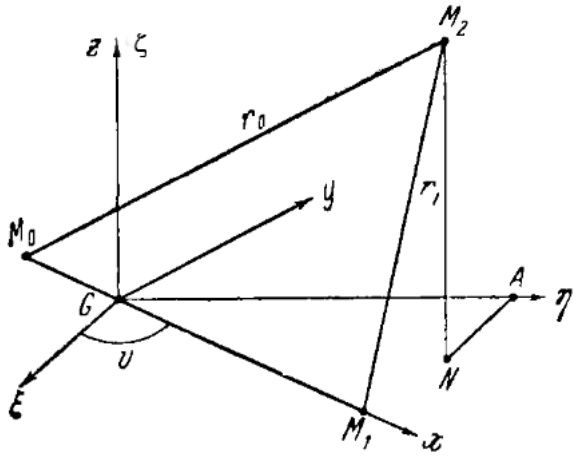

Fig.4

Let $G\xi\eta\zeta$ is a coordinate system, in the plane $(\xi\eta)$ in which the point M_1 moves.

The equation of motion of M_2 ("zero" mass) in inertial (fixed) rectangular coordinate system $(\xi\eta\zeta)$ are

$$\ddot{\xi} = -\frac{\partial U}{\partial \xi}, \quad \ddot{\eta} = -\frac{\partial U}{\partial \eta}, \quad \ddot{\zeta} = -\frac{\partial U}{\partial \zeta}, \tag{26}$$

where

$$U = f\Big(\frac{m_0}{r_0} + \frac{m_1}{r_1}\Big), \tag{27}$$

f is constant of gravitation; m_0 and m_1 are masses of bodies M_0 and M_1, and mutual distances are determined by formulas:

$$\begin{cases} r_0^2 = (\xi - \xi_0)^2 + (\eta - \eta_0)^2 + \zeta^2 \\ r_1^2 = (\xi - \xi_1)^2 + (\eta - \eta_1)^2 + \zeta^2 \\ \zeta_0 = \zeta_1 = 0, \end{cases} \tag{28}$$

where ξ_0, η_0 and ξ_1, η_1 are coordinates of points M_0 and M_1 in the system $G\xi\eta\zeta$.

These coordinates are determined by obvious formulas.

$$\begin{cases} (m_0 + m_1)\xi_0 = -m_1 r\cos v, \quad (m_0 + m_1)\eta_0 = -m_1 r \sin v, \\ (m_0 + m_1)\xi_1 = +m_0 r\cos v, \quad (m_0 + m_1)\eta_1 = +m_0 r \sin v. \end{cases} \tag{29}$$

Values of r and v are known functions of time defined by the Keplerian motion formulas. $r = \overline{M_0 M_1}$; v is the angle of vector r with the positive direction of the axis $G\xi$ (the true anomaly).

Orbit of point M_1 in the plane $G\xi\eta$ is ellipse with focus at the point M_0. It is determined by the equation.

$$r = \frac{p}{1 + \epsilon\cos v} \tag{30}$$

where p is a focal parameter, ϵ is the eccentricity of the Keplerian orbit ($0 \leq \epsilon < 1$), v is the true anomaly.

The expression for the kinetic energy of the point M_2 is

$$T = \frac{1}{2} m_2 (\dot{\xi}^2 + \dot{\eta}^2 + \dot{\zeta}^2) \tag{31}$$

Let us move in equations (26) from the fixed axis system $G\xi\eta\zeta$ to the rotating one around $G\zeta$ axis, so that the new abscissa passes through the points M_0 and M_1. Denoting the coordinates of the point M_2 in the new coordinate system: x, y, z we have

$$\begin{cases} \xi = x\cos v - y\sin v, \\ \eta = x\sin v + y\cos v \\ \zeta = z, \end{cases} \tag{32}$$

where v is the same angle as in formula (29), i.e. true anomaly of the Keplerian movement. Whence by means of differentiation on time one find derivatives

$$\begin{cases} \dot{\xi} = \dot{x}\cos v - \dot{y}\sin v - \dot{v}(x\sin v - y\cos v) \\ \dot{\eta} = \dot{x}\sin v + \dot{y}\cos v + \dot{v}(x\cos v - y\sin v) \\ \dot{\zeta} = \dot{z}. \end{cases} \tag{33}$$

The expression for the kinetic energy (31) in the new coordinates will take the form

$$T = \frac{1}{2}m_2(\dot{x}^2 + \dot{y}^2 + \dot{z}^2 + (2\dot{v}(x\dot{y} - y\dot{x}) + \dot{v}^2(x^2 + y^2). \tag{34}$$

Expressions for partial derivatives of kinetic energy take the form

$$\begin{cases} \dfrac{\partial T}{\partial \dot{x}} = m_2(\dot{x} - \dot{v}y), \quad \dfrac{\partial T}{\partial x} = m_2\dot{v}(\dot{y} + \dot{v}x), \\ \dfrac{\partial T}{\partial \dot{y}} = m_2(\dot{y} + \dot{v}x), \quad \dfrac{\partial T}{\partial y} = m_2\dot{v}(-\dot{x} + \dot{v}y), \\ \dfrac{\partial T}{\partial \dot{z}} = m_2\dot{z}, \quad \dfrac{\partial T}{\partial z} = 0. \end{cases} \tag{35}$$

Substituting these expressions into the Lagrange equation

$$\frac{d}{dt}\left(\frac{\partial T}{\partial \dot{q}_j}\right) - \frac{\partial T}{\partial q_j} = \frac{\partial U}{\partial q_j}, \ (j = 1, 2, 3). \tag{36}$$

We will get the equations of motion of a point M_2 in the rotating axes

$$\begin{cases} \ddot{x} - 2\dot{v}\dot{y} - \dot{v}^2x - \ddot{v}y = \dfrac{\partial U}{\partial x} \\ \ddot{y} + 2\dot{v}\dot{x} - \dot{v}^2y + \ddot{v}x = \dfrac{\partial U}{\partial y} \\ \ddot{z} = \dfrac{\partial U}{\partial z} \end{cases} \tag{37}$$

where U is defined by (27) but the distances r_0 and r_1 taking into account (32) are given by the formulas

$$\begin{cases} r_0^2 = (x - x_0)^2 + y^2 + z^2 \\ r_1^2 = (x - x_1)^2 + y^2 + z^2 \\ x_0 = -\dfrac{m_1 r}{m_0 + m_1} \\ x_1 = -\dfrac{m_0 r}{m_0 + m_1}. \end{cases} \tag{38}$$

Further since

$$r^2\dot{v} = c = const \tag{39}$$

where c is area integral in the orbit plane, we have

$$\dot{v} = \frac{c}{p^2}(1 + e\,cos\,v)^2; \ \ddot{v} = -\frac{2c^2e}{p^4}(1 + e\,cos\,v)^4 \tag{40}$$

In equations (37), we make a transition to a pulsating coordinate of system $G\tilde{\xi}\tilde{\eta}\tilde{\zeta}$ using formulas

$$x = \rho\tilde{\xi},\ y = \rho\tilde{\eta},\ z = \rho\tilde{\zeta} \tag{41}$$

where

$$\rho = \frac{r}{p} = \frac{1}{1 + e\,cos\,v}, \tag{42}$$

and following Nechville [5] we input a new independent variable, namely the true anomaly v of the body M_1.

Then, as is simply to verify, we have

$$\begin{cases} \dot{x} = (\rho'\tilde{\xi} + \rho\tilde{\xi}')\dot{v} \\ \ddot{x} = (\rho''\xi + 2\rho'\xi' + \rho\xi'')\dot{v}^2 + (\rho'\xi + \rho\xi')\dot{v}\dot{v}' \end{cases} \tag{43}$$

(hatchs denote differentiation by variable v). Similarly, we can obtain formulas for two other coordinates.

Substituting the expressions for the old coordinates and their derivatives and the expressions for $\dot{v}$ and $\ddot{v}$ from (40) into equation (37), we obtain as a result, instead of system (37), the following

$$\begin{cases} \tilde{\xi}'' - 2\tilde{\eta} = \dfrac{\partial\Omega}{\partial\tilde{\xi}} \\ \tilde{\eta}'' - 2\tilde{\xi} = \dfrac{\partial\Omega}{\partial\tilde{\eta}} \\ \tilde{\zeta}'' = \dfrac{\partial\Omega}{\partial\tilde{\zeta}} \end{cases} \tag{44}$$

where

$$\Omega = \rho\left[\tfrac{1}{2}(\tilde{\xi}^2 + \tilde{\eta}^2 + e\tilde{\zeta}^2\cos v) + p^3\left(\tfrac{1-\mu}{\tilde{r}_1} + \tfrac{\mu}{\tilde{r}_2}\right)\right],$$

$$\tilde{r}_1 = \sqrt{(\tilde{\xi} - \tilde{\xi}_1)^2 + \tilde{\eta}^2 + \tilde{\zeta}^2},\ \tilde{r}_2 = \sqrt{(\tilde{\xi} - \tilde{\xi}_2)^2 + \tilde{\eta}^2 + \tilde{\zeta}^2}, \tag{45}$$
$$\tilde{\xi}_1 = -p\mu,\ \tilde{\xi}_2 = -p(1-\mu),$$
$$\mu = m_1/(m_0 + m_1),\ 1 - \mu = m_0/(m_0 + m_1).$$

References

1. G. N. Duboshin, Celestial Mechanics. Analytical and Qualitative Methods (Nauka, Moscow, 1978) [in Russian].
2. Ya.Goltser and A.Domoshnitsky. Bifurcation and stability of integro-differential equations, Nonlinear Analysis.Theory, Methods and Applications, 47 (2001), pp.953-967.
3. C. Marchal, The Three-Body Problem, Elsevier, Amsterdam, 1990.
4. A. P. Markeev, Libration Points in Celestial Mechanics and Astrodynamics (Nauka, Moscow, 1978) [in Russian].
5. V. Nechville, Sur une forme nouvelle des equations differentielles due probleme restreint elliptique, Compt. Rend., 182 (1926).

6. M.G. Yumagulov, O.N. Belikova and N.R. Isanbaeva, Bifurcation near Boundaries of Regions of Stability of Libration Points in the Three-Body Problem, Astronomy Reports, Vol. 62, No.2, (2018) pp.144-153 .

Influence of M-Current on Dopamine Modulation of Weak PING Gamma Rhythm

Denis Zakharov[1] and Boris Gutkin[2]

[1] Centre for Cognition and Decision Making, National Research University Higher School of Economics, Myasnitskaya St. 20, Moscow, Russia
Institute of Biology and Biomedicine, Lobachevsky State University of Nizhni Novgorod, Gagarin Ave. 23, Nizhny Novogorod, Russia
(E-mail: dgzakharov@hse.ru)

[2] Centre for Cognition and Decision Making, National Research University Higher School of Economics, Myasnitskaya St. 20, Moscow, Russia
Group of Neural Theory, LNC INSERM U960, École Normale Supérieure PSL* University, 29 rue d'Ulm, Paris, France
(E-mail: boris.gutkin@ens.fr)

Abstract. The human brain demonstrates electrical oscillations of various frequency ranges that are associated with a number of cognitive tasks. Here we will focus on the so-called weak (clustered) gamma rhythm (20-80 Hz). Typically, in the cortex, gamma oscillations appear in neuronal networks consisting of excitatory pyramidal cells and inhibitory interneurons. This is the Pyramidal INterneuronal Gamma (PING) rhytm. The weak clustered gamma oscillations are a specific case of PING when the pyramidal cells fire in several internally synchronous clusters producing a "collective" rhythm by alternating the cluster firing. We will analyse how characteristics of the cluster states (mainly the number of clusters) depend on the intrinsic ionic currents of the PY cells (AHP- and m-currents). Since different number of clusters mean different level of PING oscillations coherence, our work links the intrinsic cellular properties of the constitutent neurons to the coherence of the gamma rhythm.
Keywords: PING gamma rhythm, weak gamma rhythm, cluster synchronization, spike frequency adaptation, M-current.

1 Introduction

During performance of cognitive tasks, the brain demonstrates electrical activity of various frequency ranges (Buzsáki[1]). One such prominent oscillation is the gamma rhythm (20-80 Hz). It is observed during a wide variety of cognitive tasks, such as working memory, coding and information processing (Akam et al.[2]). In comparison with the other oscillations, gamma has a higher frequency, is comparatively much more irregular, sparse and locally distributed (Dickson et al.[3]). It is well known that typically this rhythm is generated in the networks consisting of two neuronal populations of interneurons (IN) and pyramidal (PY) cells (Bartos et al.[4]). There are two basic mechanisms of gamma oscillations generation in such networks. The first is INterneuronal Gamma (ING) rhythm which are produced in the IN population (Ermentrout and Buhl[5]). In this case the PY population has negligible influence on the IN neurons and, in fact, mirrors the IN population activity. In the second mechanism, the gamma oscillations are a result of recurrent interactions

between both populations. This is so called Pyramidal-INterneuronal Gamma (PING) gamma rhythm (Whittington et al.[6]). In addition, it is possible to to construct either strong or weak gamma rhythms. In the first case, both populations have almost the same firing rate and regularly fire together with a small time lag. To take into account the experimental features of the gamma and the observed large difference between intrinsic frequencies of the PY cells and IN neurons, one potentially likely mechanism is that alternatively firing of synchronous PY clusters generates the gamma oscillations (see, for example, Börgers and Kopell[7], Kilpatrick and Ermetrout [8] and Krupa et al.[9]). This is a weak clustered gamma rhythm. Each PY cell, in this case, fires with the frequency, which is lower than gamma frequency, whereas the gamma oscillations are formed by collective activity of the PY clusters. The number of clusters in a cluster state and the number of PY cells in the each cluster determine coherence of the gamma oscillations while making them sparse and irregular. In Krupa et al.[9] it was shown that the maximum number of clusters dramatically depends on the intrinsic neuronal parameters and coupling strength of interpopulation coupling, especially inhibitory ones. In particular, Krupa et al. found that the spike frequency adaptation of PY cells has a significant influence on the cluster formation process. This was confirmed by parametric modulation studies of the network parameters on the changes in cluster states (Zakharov et al.[10,11]). For instance, it was shown that modulation of the spike frequency adaptation is the most effective in increasing of cluster number under an increase of the spike frequency adaptation parameters and a decrease, for a negative modulation of the spike frequency adaptation. The strength of the inhibitory interpopulational coupling, in turn, also substantially influenced on the cluster modulation. Higher connection strengths stabilized the cluster states with a lower number of clusters.

In this paper, we expand on Krupa et al.[9] and focus in the influence of the intrinsic parameters of the PY cells on the cluster formation process in a PING network and therefore, on the coherence of the oscillations. In particular, we take into account both spike frequency adaptation (AHP-current) and the M-current. The former is a slow spike-dependent hyperpolarizing current (biophysically speaking it is a calcium-dependent slow potassium current), the latter is voltage a voltage-dependent slow hyperpolarizing K-current. The M-current has a significant impact on the dynamics of the PY cells, controls the intrinsic cellular excitability and synaptic responses of the pyramidal neurons [see, for example, Marrion[12] and Peng et al[13]]. This current is slowly activated when the membrane potential is depolarized towards voltage levels where the spike producing currents activate, and repolarizes the neuron back to the rest state reducing neuronal excitability In addition, the M-current has no inactivation and may play a critical role for neuronal excitability, especially near the rest state. It was previously shown that the addition of this current even in the canonical theta-neuron model with adaptation results in a change of excitability type (from 1st type to 2nd one) Gutkin et al.[14]. For the hippocampal PY cells it was shown experimentally and theoretically (within the framework of Morris-Lecar equations) that the M-current, as well as shunting

inhibition, can lead to the same change of excitability type and thereby significantly change dynamics of the PY cells (Prescott et al.[14-16]).

2 Influence of AHP- and M-currents on PY cell activity

To describe the PY neuron activity, we use the modified the Miles-Traub equations with adaptation from Krupa et al.[9] with the addition of the M-current :

$$\begin{aligned}
\frac{dv_e}{dt} &= I_{app} - g_L(v_e - E_L) - g_K n^4 (v_e - E_K) \\
&\quad - g_{Na} m_{inf,Na}(v_e)^3 F_h(n)(v_e - E_{Na}) \\
&\quad - g_{Ca} m_{inf,Ca}(v_e)(v_e - E_{Ca}) - g_{AHP}\frac{[Ca]}{[Ca]+1}(v_e - E_K) \\
&\quad - g_M w_e (v_e - E_K), \\
\frac{d[Ca]}{dt} &= -\varepsilon_{Ca} I_{Ca} - \frac{[Ca]}{\tau_{Ca}}, \\
\frac{dn}{dt} &= \alpha_n(v_e)(1-n) - \beta_n(v_e)n, \\
w_e &= \varepsilon(w_{inf}(v_e) - w_e)/\tau_M(v_e) \\
m_{inf,Na}(v_e) &= \frac{\alpha_m(v_e)}{\alpha_m(vv_e)+\beta_m(v_e)}, \\
m_{inf,Ca}(v_e) &= \frac{1}{1+e^{-(v_e+25)/2.5}},
\end{aligned} \qquad (1)$$

where the first equation is the current balance equation giving the dynamics of v_e the membrane potential of a PY cell, [Ca] is the calcium concentration, n, $m_{inf,Na}$, $m_{inf,Ca}$ and w_e are the voltage-dependent gating variables for the various cross-membrane currents; E_x are the reversal potentials of the various ionic species. This is a biophysical neuronal model containing on the right hand side of the first equation a combination of the ionic currents: an applied current I_{app}, a leak current I_L, a fast potassium current I_K, a sodium current I_{Na}, calcium current I_{Ca}, a slow after-hyperpolarization (AHP) current I_{AHP}, and M-current I_M respectively. The AHP current is a calcium-activated slow potassium current that effectively results in the spike frequency adaptation of a PY cell. Gating functions of the currents describes by the following equations:

$$\begin{aligned}
&\alpha_n(v_e) = 0.32\frac{v+52}{1-e^{-\frac{v+52}{5}}}, \quad \beta_n(v_e) = 0.5\,0.28e^{-\frac{v_e+57}{40}}; \\
&\alpha_m(v_e) = 0.32\frac{v_e+54}{1-e^{-\frac{v_e+54}{4}}}, \quad \beta_m(v_e) = 0.28\frac{v_e+27}{e^{\frac{v_e+27}{5}}-1}; \\
&w_{inf}(v_e) = \frac{1}{1+e^{--\frac{v_e+35}{10}}}, \quad \tau_m(v_e) = \frac{400}{3.3e^{\frac{v_e+35}{20}}+e^{-\frac{v_e+35}{20}}};
\end{aligned} \qquad (2)$$

$F_h(n) = \max\{1 - 1.25n, 0\}$.

We choose the g_{AHP} and g_M as control parameters and fix the other parameters of the PY model in the following way:
$I_{app}=4\ \mu A$, $g_{Na}=100\ ms/cm^2$, $g_K=80\ ms/cm^2$, $g_{Ca}=1\ ms/cm^2$, $E_{Na}=50\ mV$, $E_K=-100\ mV$, $E_{Ca}=120\ mV$, $E_L=67\ mV$, $\tau_{Ca}=80\ ms$, $\varepsilon_{Ca}=0.01\ cm^2/(ms\ \mu A)$.

Our analysis shows that both AHP- and M-currents can effectively change the frequency of the PY cell firing but there is a qualitative difference between their influence. The M-current changes the bifurcation scenario that govern the onset of the repetitive firing (Fig. 1). If the conductance of this current is zero, the transition from the rest state (stable equilibrium) to the active one (stable limit cycle) is through the bifurcation of saddle-node in invariant circle (SNIC, Fig. 1A), whereas for sufficiently large positive values of the conductance the limit cycle appears through the saddle-node bifurcation of limit cycles (Fig. 1B). In the first case, the limit cycle has zero frequency at the bifurcation point. It means that the PY cell has the 1st type of excitability and is able to generate spike trains with arbitrary small frequencies. In the second case, it is born with a finite frequency and, thus, the neuron has a minimum frequency and can fire only in a certain frequency band. It corresponds to the 2nd type of excitability. This is confirmed by the Infinitesimal phase response curves (iPRC) which were plotted for both cases in Fig. 2. The AHP-current decreases the frequency of the PY cell but keeps iPRC positive (Fig. 2A). The M- current also increases the frequency but at the same time changes the iPRC to the 2nd type. The change of excitability type can significantly change the neurocomputational properties of the PY cells and has influence on their synchronization properties.

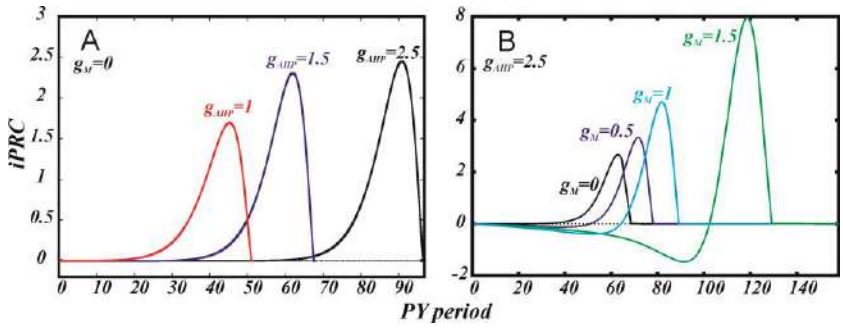

Fig. 1. Infinitesimal phase response curves (iPRC) for the different values of g_{AHP} (A, $g_M=0$) and for the different values of g_M (B, $g_{AHP}=2.5$). The frequency spike adaptation current keeps the 1st type of excitability ($g_M=0$), whereas the M-current ($g_M>0$) changes it to 2nd type.

Both conductances of the AHP and M-currents decrease the firing rate of the PY cell the diagram showing the dependence of the frequency on both parameters has a well-expressed diagonal structure (Fig. 3). The lowest firing rate is

observed in the upper right corner. We would like to note that the increase of spike frequency adaptation by the AHP does not lead to activity suppression for biologically relevant values, making this parameter to be effective for firing rate control of the PY cells. In contrast, the PY cells can demonstrate activity only for the certain interval of the conductance of the M-current, its increase leads to the disappearance of the stable limit cycle through the saddle-node bifurcations of limit cycles.

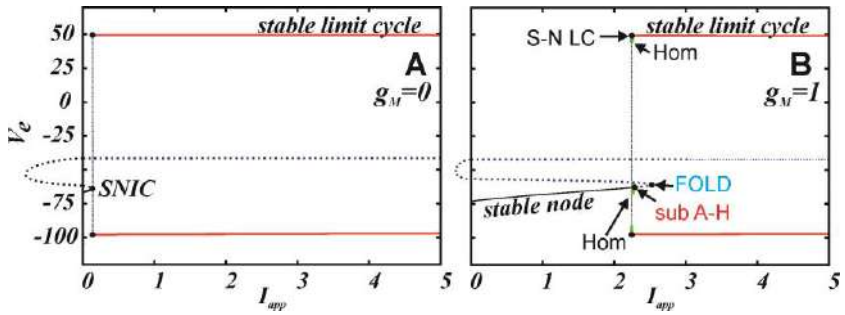

Fig. 2. One parametric bifurcation diagrams for $g_M=0$ (A) and $g_M=1$ (B) ($g_{AHP}=2.5$). If $g_M=0$ the stable equilibrium, corresponding the rest state of the neuron (the solid black curve), disappears through the SNIC bifurcation. In addition, it results in the birth of the stable limit cycle corresponding to the active state of the neuron. For values of the parameter $g_M>0$ the stable equilibrium loses stability through the subcritical Andronov-Hopf bifurcation (A-H). An unstable limit cycle, which was also born due to the bifurcation, disappears flipping to the saddle separatrix loop (Hom, the homoclinic bifurcation) and appears once more due to another homoclinic bifurcation for the smaller value of I. In contrast to the previous case, the stable limit cycle is born by the saddle-node bifurcation of limit cycles.

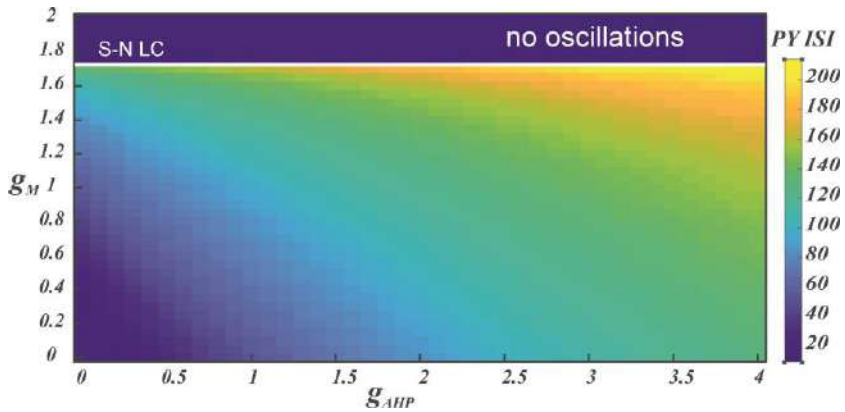

Fig. 3. Dependence of the PY cell period on the control parameter plane (g_{AHP},g_M) ($I_{app}=4$). The period increases with growth of both control parameters.

Increase of g_M leads to the disappearance of the stable limit cycle through the saddle-node bifurcation (S-N LC).

3 Influence of AHP- and M-currents on cluster formation

To describe the generation of the PING rhythm, the network model should consist of two interacting populations of neurons of the PY cells and IN neurons. Since we do not focus on the intrinsic properties of the interneurons, following the approach in Krupa et al.[9], we may describe the population of the IN neurons we need a minimal yet relevant model of a spiking neuron. Thus, we chose the quadratic Integrate-and-fire (QIF) model:

$$\frac{dv_i}{dt} = I_{int} - 2v_i(v_i - 1), \quad \text{reset: if } v_i \geq 1, v_i \to 0, \tag{3}$$

where v_i is a membrane potential of a IN neuron, $I_{int}=0.52$ is a parameter determining the excitability of the IN neurons. We note that the QIF neuron is the canonical model for type I excitability and spike generation (SNIC driven spiking).

In the IN population, the neurons interact with each other and with the PY cells via inhibitory synapses (GABA synapse, gamma-aminobutyric acid). In contrast, the PY cells have projections only to the IN neurons via fast excitatory synapses (AMPA-synapses, α-amino-3-hydroxy-5-methyl-4-isoxazolepropionic acid). All existing couplings have an all-to-all topology. Thus, the network model has the following form:

$$\begin{aligned} \frac{dv_{e,j}}{dt} &= \sum_j I_{ionic,j} - g_{ei}\left(\frac{1}{N_i}\sum_{k=1}^{N_i} s_{i,k}\right)(v_{e,j} - E_{rev}^{ei}), j = \overline{1, N_e}, \\ \frac{dv_{i,l}}{dt} &= f(2v_{i,l}, I_{int}) - g_{ie}\left(\frac{1}{N_e}\sum_{k=1}^{N_e} s_{e,k}\right)(v_{i,l} - E_{rev}^{ie}) \\ &\quad - g_{ii}\left(\frac{1}{N_i}\sum_{k=1}^{N_i} s_{i,k}\right)(v_{i,l} - E_{rev}^{ii}), \end{aligned} \tag{4}$$

where $v_{i,l}$ and $v_{i,j}$ are the membrane potential of the l-th IN neuron and j-th PY cell respectively. The neurons interact through chemical synapses: g_{ie} is the conductance of the inhibitory synapses located on the PY cells, g_{ei} and g_{ii} are the conductances of the excitatory and inhibitory synapses located on the IN neurons. Parameters E^{ei}_{rev}, E^{ie}_{rev} and E^{ii}_{rev} determine the reversal potentials of the synapses. The synaptic variables $s_{i,k}$ and $s_{e,j}$ have values between 0 and 1. They are set to 1 after each spike of the kth IN neuron and the j^{ht} PY cell E-cell and decay exponentially with time constant τ_i and τ_e. The parameter g_l, that controls intrinsic frequency of the PY cells, was uniformly distributed in the

interval *[0.075,0.125]*. As in Krupa et al.[9] the IN population contains 20 IN neurons, the PY population has 200 neurons.The coupling parameters were set in the following way: $g_{ei}=0.2$, $g_{ii}=10$, $\tau_i=9$, $\tau_e=2$, $E^{ei}_{rev}=-80$ *mV*, $E^{ie}_{rev}=6.5$ and $E^{ii}_{rev}=-0.25$.

In agreement with the frequency distribution on Fig. 3, the diagrams on Fig. 4 have almost the same diagonal structure of the cluster states with different number of clusters (Fig. 4). Typically, simultaneous growth of the M-current conductance and the spike frequency adaptation AHP parameter leads to greater number of clusters. Because of much higher frequency of IN neurons, the PY cells split into several alternatively firing clusters and form a cluster state. Examples of the different cluster states are presented in Fig. 5. I may be one (Fig. 5A), two (Fig. 5B), three (Fig. 5C), four (Fig. 5D) and five cluster states, cluster states with "skipping" PY cells activity each three periods of IN neurons (Fig. 5E). It is important to note that each point at each diagram in the Fig. 4 is a result of network evolution from the randomly generated initial conditions. The network is multistable, thus, for the same parameter set but for different initial conditions, it is possible to get various cluster state with either the same or the different number of clusters. For instance, in the lower right corners of the diagrams in Fig 4C,D there is a 2-cluster state (Fig. 5F) that coexists with some 2- and 3-cluster states. This is a result of the PING mechanism of gamma rhythm generation for which the interaction between the network populations can make their frequency multiples and form a state with a number of clusters determined by the ratio between the frequencies of IN and PY populations.

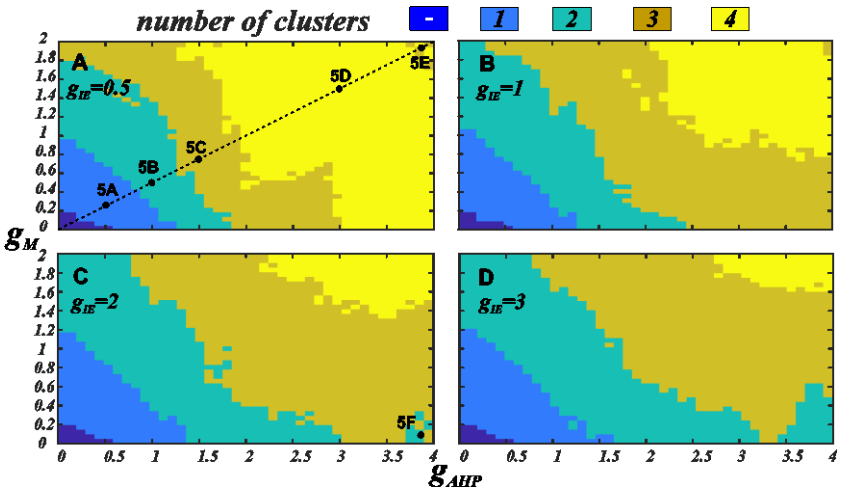

Fig. 4. Number of clusters in the cluster states for the different strengths of the interpopulational inhibitory connections. Each point on these diagrams corresponds to the number of clusters in a state to which the system has evaluated from randomly generated initial conditions. The diagrams demonstrate the well-expressed diagonal layered structure according with the

changes of the PY cells period (Fig. 3). Simultaneous growth of m-current and spike frequency adaptation leads to greater number of clusters. In contrast, increasing inhibition results in smaller number of clusters. The black circles in the diagrams correspond to the rasterplots in fig. 5. We draw your attention that here there is a multistability between different cluster states with either the same or the different numbers of clusters. For example in the region labeled 5F it is possible to get (depending on initial conditions) either 2, 3 or 4 clusters in the cluster state.

Interestingly we note that changing of excitability type of the PY cells by the M-current from type I to type II, leads to an increase in region of activity of the PY population. At first we note, that an individual PY cell with $g_L=0.1$ does not fire for the $g_M>1.7$ (see Fig. 3). In the PY population in our network, the parameter g_L is distributed in the interval [0.05, 0.15]. Thus, it is possible to suggest that some PY cells stop to fire before this critical value of g_M, the others above it. In contrast, all PY cells fire at least for g_M which is approximately higher two (Fig. 4). Taking into account the absence of excitatory connections between the PY cells, it is possible to conclude that such behavior (that cannot be predicted directly from single cell analysis) is likely due to inhibitory synaptic influence of the IN neurons and a generation of rebound spikes.

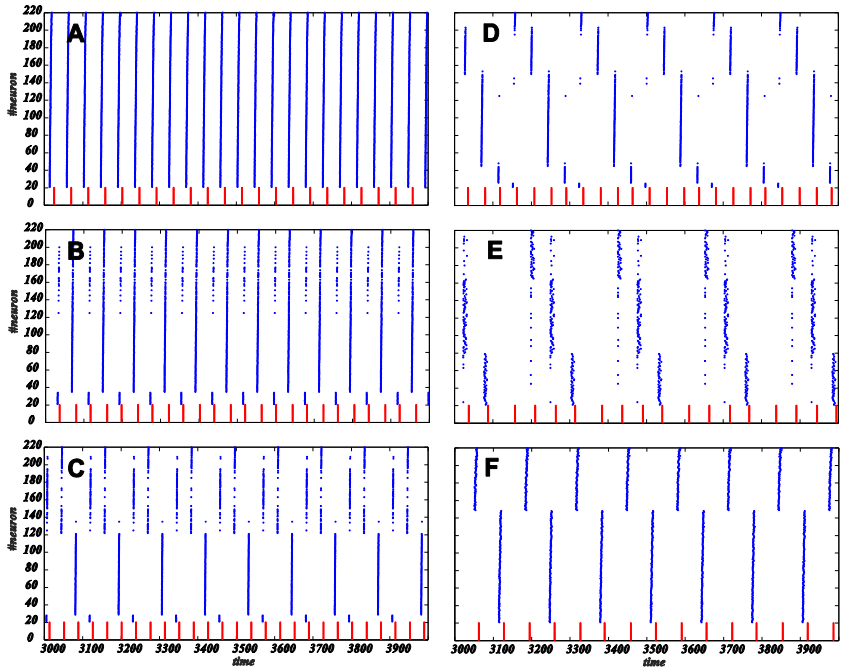

Fig. 5. Rasterplots showing different possible cluster states in the PY population for the different values of conductances of AHP and M-currents: one cluster for $g_{AHP}=0.5, g_M=0.25$ (A), two clusters for $g_{AHP}=1, g_M=0.5$ (B), three clusters for

$g_{AHP}=1.5,g_M=0.75$ (C), four clusters for $g_{AHP}=3,g_M=1.5$ (D), three cluster state with "skipping" PY cells activity each three periods of IN neurons for $g_{AHP}=3.9,g_M=1.95$ (E) and two clusters for $g_{AHP}=3.9,g_M=0.1$ (F). All panels labels coincide with letters titled the points on the diagrams in the Fig. 4A,B.

The inhibitory couplings from the IN neurons to the pyramidal cells have a stabilizing effect on the network. Stronger inhibition leads to lower numbers of clusters in the cluster states and, thus, increase coherence of the gamma. In particular, the size of three and especially four clusters regions decreases. It is important for investigation of modulation of such cluster states by endogenous neuromodulators (dopamine, acetylcholine and others). For example, the positive dopamine modulation can increase the PY cells inhibition and decrease the spike frequency adaptation and, vice versa, the negative dopamine modulation decreases the inhibitory connections and increases the spike frequency adaptation (see, for example, Zakharov et al.[10,11] and cited papers). Depending on initial point in the diagrams in Fig. 4, it is possible to control the efficiency of the positive and negative dopamine modulation.

Conclusions

In this paper, we consider process of cluster formation in a PING network producing the weak (clustered) gamma rhythm. We have shown that the M-current significantly changes the dynamical properties of the PY cells. The M-current changes excitability type of the PY cells and decreases the region of their activity in the parameter space. In addition, the M-current, as well as AHP-current, effectively changes the frequency of the neuron and can effectively affect the cluster formation. In particular, due to the frequency drop with the increase of these currents, the color plots in the Fig 5, showing the dependence of number of clusters in the cluster states, have the well-expressed diagonal layered structure. By changing PY cell excitability to 2nd type, the M-current also promotes the population activity of the PY cells within the PING network. In comparison with papers of Prescott et al.[14-16] we used more realistic model of the PY cell that also takes into account transport of Ca^{2+} ions. It allows us to describe spike frequency adaptation more accurately and use this model for simulation of action of endogenous neuromodulators in the brain.

In our previous studies, we have shown that DA modulation of the AHP-current can effectively change the cluster number in the cluster states of the weak PING networks and thus the coherence of their collective activity that can significantly affect information processing and decision-making. Thus, we expect that a joint modulation of AHP- and M-currents will be able to do it more efficiently. From the biological point of view, it can happen in the cases of simultaneous action of dopamine, which can affect the AHP-current (Pedarzani et al.[18]), and acetylcholine, which can decrease the M-current by, for

example, muscarinic receptors (Marrion[12]), or due to acetylcholine modulation, which can influence both currents (Nicoll[19]).

ACKNOWLEDGMENT
This work was supported by the HSE Basic Research Program and the Russian Academic Excellence Project '5-100'. D.Z. acknowledges support of Russian Science Foundation Grant No. 18-11-00294 (numerical simulations). BSG acknowledges partial support from ANR project “ERMUNDY”.

References

1. G. Buzsáki, Rhythms of the Brai, New York: Oxford University Press, 2006.
2. T. Akam, D.M. Kullmann. Oscillatory multiplexing of population codes for selective communication in the mammalian brain, Nat Rev Neurosci, 15,111–22, 2014.
3. C. T. Dickson, G. Biella, M. de Curtis. Evidence for Spatial Modules Mediated by Temporal Synchronization of Carbachol-Induced Gamma Rhythm in Medial Entorhinal Cortex, Journal of Neuroscience, 20, 7846-54, 2000.
4. M. Bartos, I. Vida, P. Jonas. Synaptic mechanisms of synchronized gamma oscillations in inhibitory interneuron networks, Nat Rev Neurosci, 8, 1, 45–56, 2007.
5. B. Ermentrout and E.H. Buhl. Inhibition-based rhythms: experimental and mathematical observations on network dynamics, Int. J. Psychophysiol, 38, 315-336, 2000.
6. M.A.Whittington, R.D. Traub, N. Kopell, B. Ermentrout, and E.H. Buhl. Inhibition-based rhythms: experimental and mathematical observations on network dynamics, Int. J. Psychophysiol., 38, 315-336, 2000.
7. C. Börgers, N. Kopell. Synchronization in Networks of Excitatory and Inhibitory Neurons with Sparse, Random Connectivity, Neural Computation, 15, 509–538, 2003.
8. Z.P. Kilpatrick, B. Ermetrout. Sparse Gamma Rhythms Arising through Clustering in Adapting Neuronal Networks, PLoS Computational Biology, 7, e1002281, 2011.
9. M. Krupa, S. Gielen, and B. Gutkin. Adaptation and shunting inhibition leads to pyramidal/interneuron gamma with sparse firing of interneurons, J. Comput. Neurosci., 37, 357–76, 2014.
10. D. Zakharov, V. Tyutin, M. Krupa, B. Gutkin. Modulation of synchronous gamma rhythm clusters, Cybernetics and Physics, 8, 185-188, 2019.
11. D. Zakharov, M. Krupa, B. Gutkin. Modelling dopaminergic modulation of clustered gamma rhythms, Communications in Nonlinear Science and Numerical Simulation, 82, 105086, 2020.
12. N.V. Marrion. Control of m-current, Annu. Rev. Physiol, 59, 483–504, 1997.
13. H. Peng, X-L. Bian, F.-C. Ma, K.-W. Wang. Pharmacological modulation of the voltage-gated neuronal Kv7/KCNQ/M-channel alters the intrinsic excitability and synaptic responses of pyramidal neurons in rat prefrontal cortex slices, Acta Pharmacologica Sinica, 38, 1248–1256, 2017.
14. B. S. Gutkin, G. B. Ermentrout, A. D. Reyes. Phase-Response Curves Give the Responses of Neurons to Transient Inputs, Journal of Neurophysiology, 94, 1623–1635, 2005.

15. S. A. Prescott. Nonlinear Interaction between Shunting and Adaptation Controls a Switch between Integration and Coincidence Detection in Pyramidal Neurons, Journal of Neuroscience, 26, 9084–9097, 2006.
16. S. A. Prescott, S. Ratté, Y. De Koninck, T. J. Sejnowski. Pyramidal Neurons Switch From Integrators In Vitro to Resonators Under In Vivo-Like Conditions, Journal of Neurophysiology, 100, 3030–3042, 2008.
17. S. A. Prescott, Y. De Koninck, T. J. Sejnowski. Biophysical Basis for Three Distinct Dynamical Mechanisms of Action Potential Initiation, PLoS Computational Biology, 4, e1000198, 2008.
18. P. Pedarzani, and J.F.Storm. Dopamine modulates the slow Ca2+-activated K+-current IAHP via cyclic AMP-dependent protein kinase in hippocampal neurons, Journal of Neurophysiology, 74, 2749–53, 1995.
19. R. A. Nicoll. The coupling of neurotransmitter receptors to ion channels in the brain, Science, 241, 545–551, 1988.